LASER FLASH PHOTOLYSIS STUDIES OF HALOGEN ATOM REACTIONS OF ATMOSPHERIC INTEREST

A Dissertation
Presented to
The Academic Faculty

by

Patrick L. Laine

In Partial Fulfillment
of the Requirements for the Degree
Doctor of Philosophy in the
School of Earth and Atmospheric Sciences

Georgia Institute of Technology
December 2011

Laser Flash Photolysis Studies of Halogen Atom Reactions of Atmospheric Interest

Approved by:

Dr. Paul H. Wine, Advisor
School of Chemistry and Biochemistry
School of Earth and Atmospheric Sciences
Georgia Institute of Technology

Dr. Greg Huey
School of Earth and Atmospheric Sciences
Georgia Institute of Technology

Dr. Athanasios Nenes
School of Earth and Atmospheric Sciences
School of Chemical and Biomolecular Engineering
Georgia Institute of Technology

Dr. Rodney Weber
School of Earth and Atmospheric Sciences
Georgia Institute of Technology

Dr. Thomas Orlando
School of Chemistry and Biochemistry
Georgia Institute of Technology

Date Approved: October 1, 2011

To my incredible family

ACKNOWLEDGEMENTS

I have received support, financial and personal, from numerous sources over the last four years. Funding for this work has been provided by the National Aeronautics and Space Administration. I also was fortunate enough to warrant partial support from an Oak Ridge Associated Universities fellowship during a portion of my time at Georgia Tech.

I would like to extend my profound thanks to many people, for without each of them I most certainly wouldn't be where I am today. I would like to express my gratitude to my advisor Dr. Paul Wine for providing me the opportunity to participate in the research in his group, and for his enduring guidance and support in my studies. He has taught me many valuable lessons and showed me how to become a careful and thorough scientist. I also need to extend my gratitude to Dr. J. Michael Nicovich, who helped me through the inevitable pitfalls I encountered in the laboratory. I also want to extend my appreciation to Michael Henley at USAFRL for believing in me that I could complete this task. I want to recognize the efforts of Dr. Mike McKee of Auburn University who provided all the theoretical information which helped to compliment my experimental data.

I would like to acknowledge my thesis committee members, Drs. Greg Huey, Rodney Weber, Athanasios Nenes, and Thomas Orlando for their valuable time and helpful advice provided to me during my graduate student career. I also would like to thank several former and current Georgia Tech graduate students who I have had the pleasure of working with during the past four years especially, Anne Case, Venus

Dookwah-Roberts, Dow Huskey, Zhijun Zhao, Arsineh Hecobian, and Katie Olsen. Additionally, I have to extend thanks to undergraduate students Yoon Sohn and Garrett Dowdy for their contributions in the lab.

Last but most certainly not least, I would like to extend my gratitude to my incredible family. I have been truly blessed with the two best parents, the two best brothers, the two best kids, and the best wife I could ever ask for. Words cannot possibly describe how important all of you are to me. I want to thank my parents for their unending generosity, love, and support. I could never have been in this position without you. Not much about this process was easy, but coming home each and every day to two absolutely beautiful kids who enthusiastically screamed "Daddy!" as I arrived home has constantly reminded me of the purpose behind this endeavor. Of course, keeping those kids healthy and happy was the primary job of my amazing wife. Jennifer, I love you! And without your unending love, energy, and support over the last 5 years I would be lost. Thank you!

TABLE OF CONTENTS

LIST OF TABLES

LIST OF FIGURES

SUMMARY

The Earth's atmosphere is a large photochemical reactor consisting primarily of N_2 (~78%) and O_2 (~21%) with Ar and water vapor being the next most abundant constituents. All of the remaining gases in the atmosphere are referred to as 'trace gases', and they play a critical role in understanding climate change, urban air quality, ozone production and depletion, and in determining the overall 'health' of the atmosphere. These trace components are present in our atmosphere with mixing ratios, i.e., mole fractions, ranging from sub parts per trillion to several hundred parts per million. One class of trace constituents that play a critical role in atmospheric chemistry are free radicals. Free radicals are highly reactive, often initiating the oxidation of natural and anthropogenic atmospheric species, thereby often controlling the fate and lifetimes of these species. The research comprising this dissertation focuses on laboratory studies of the kinetics and mechanisms of free radical (atomic halogen) reactions that can impact the levels of important trace atmospheric species. In the studies reported herein, laser flash photolysis (LFP) was coupled with time resolved atomic resonance fluorescence (RF) spectroscopic detection of Cl or Br atoms to investigate halogen atom chemistry. The research addresses three groups of reactions: Cl atom reactions with alkyl bromides, Cl and Br-initiated oxidations of small (C_2-C_6) alkenes, and Cl reactions with CH_3SCH_3 (DMS, dimethylsulfide) and CH_3SeCH_3 (DMSe, dimethylselenide).

The alkyl bromide reactions were experimentally unique in that we were able to deduce kinetics of the Cl atom reaction with bromoethane, *n*-bromopropane, and 1,2-dibromoethane by monitoring the appearance of the Br product by LFP-RF. The Br is formed via elimination that occurs essentially instantaneously following β-H abstraction

by the Cl atom. All three of the bromoalkanes investigated are emitted into the atmosphere primarily from anthropogenic sources and all three have been identified by the World Meteorological Organization (WMO) as very short-lived (lifetime less than 6 months) source gases with significant ozone depletion potentials (ODPs). Additionally, the bromoalkanes mentioned above have been of interest as model compounds for larger partially halogenated organics found in the atmosphere, and they have been considered as potential replacement compounds for chlorofluorocarbons (CFCs) that have been banned as a result of the Montreal Protocol. Brominated very short-lived compounds are thought to contribute 20-25% of total stratospheric bromine. Thus, there is considerable interest in understanding the atmospheric chemistry of even the most short-lived organic bromine compounds. Temporal profiles of Br atoms provided important kinetic and mechanistic insight for the reactions over a wide range of temperature and pressure. Temperature-dependent rate coefficients are determined for the alkyl bromides of interest for the first time, and the potential importance of the Cl reaction as an atmospheric degradation pathway for each alkyl bromide is qualitatively assessed.

The studies of halogen atom reactions with alkenes focused on formation of weakly-bound adducts where kinetics of adduct formation and dissociation as well as non-adduct forming channels were evaluated. The elementary steps in the Br initiated oxidation of the alkenes 2-methyl-1,3-butadiene (isoprene), 2,3-dimethyl-2-butene (tetramethylethylene, TME), and 1,3-butadiene have been investigated. The experimental kinetic database for these reactions is quite sparse. The kinetic results reported herein, suggests that Br reaction with the above olefins is much faster than previously thought. Analysis of the temperature dependence of the "approach to

equilibrium" kinetic data in conjunction with electronic structure calculations allows for determination of enthalpy and entropy changes associated with each addition reaction. Where possible, both forward addition and reverse dissociation channels as well as H-abstraction pathways were characterized. The enthalpy change associated with the addition reaction to give the Br−isoprene and Br−1,3-butadiene adducts has been determined for the first time and the bond dissociation enthalpy obtained for the Br−TME adduct is in reasonable agreement with the only other previously reported value. It should be noted that in the case of isoprene and 1,3-butadiene, there are multiple possible adducts that could be formed. In order to help clarify which adducts are more or less likely to be formed, we rely on electronic structure calculations (see Chapter 5) to aid in our overall understanding of the adduct forming channels. Furthermore, for the Br reactions with the three alkenes above, atomic Br kinetics have been monitored directly both in the absence and in the presence of O_2 which allowed, for the first time, determination of rate coefficients for the elementary steps in the overall complex mechanism including determination of the Br−olefin + O_2 rate coefficient.

Also included in this group of reactions is the chlorine reaction with isoprene. In addition to the well-known fact that isoprene is emitted into the atmosphere from vegetation, a potentially significant marine source of isoprene has received considerable attention. Chlorine has long been thought to exist primarily in marine environments, however, recent findings also suggest a significant Cl production rate in the middle of the continental United States. There are numerous room temperature kinetic studies for the Cl + isoprene reaction in the literature, however, there is only one temperature dependent study reported. Current recommended 298 K rate coefficients for isoprene reactions

suggest the Cl reaction is ~ 4x faster than the analogous OH reaction. If indeed this is the case, the Cl reaction could play a non-neglibible role in isoprene oxidation in atmospheric locales where Cl concentrations are relatively high. In addition, the C−Cl bond strength in $Cl-C_5H_8$ is obtained from direct measurements of the forward and reversible addition rate coefficients. Our results are compared with the literature data, and the potential importance of Cl-initiated oxidation as an atmospheric sink for isoprene is assessed.

The final group of reactions investigated involves reactions of Cl with DMS and DMSe. DMS and DMSe are the most prevalent sulfur and selenium compounds emitted to the atmosphere from the oceans. The oxidation of DMS has been studied extensively due to the interest in the possible role of DMS oxidation in the formation of sulfate aerosols, however, DMSe oxidation processes have hardly been studied at all. And, DMSe oxidation products are likely to be less volatile than the analogous DMS species. Selenium is an essential nutrient for many plants and animals; however, there is a fine line between enough and excess selenium which can be toxic. Most studies suggest that atmospheric deposition is an important source of Se contamination, and it is therefore critical to evaluate the source emissions and fate of Se in the atmosphere. Since the majority of atmospheric Se exists in the form of DMSe, determination of the kinetics and oxidation mechanisms of DMSe will go a long way towards understanding the global biogeochemical cycle of Se.

Both reversible addition and H-abstraction pathways have been characterized, and the first experimental determination of bond strength of the gas-phase DMS−Cl and DMSe−Cl adducts have been obtained.

CHAPTER 1

INTRODUCTION

The Earth's atmosphere is a large photochemical reactor consisting primarily of N_2 (~78%) and O_2 (~21%) with Ar and water vapor being the next most abundant constituents. All of the remaining gases in the atmosphere are referred to as 'trace gases', and these minor components play a critical role in understanding climate change, urban air quality, ozone production and depletion, and in determining the overall 'health' of the atmosphere. Important trace components are present in our atmosphere with mixing ratios, i.e., mole fractions, ranging from sub parts per trillion to hundreds of parts per million. One class of trace constituents that play a critical role in atmospheric chemistry are free radicals. Free radicals are highly reactive, often initiating the oxidation of natural and anthropogenic atmospheric species, thus often controlling the fate and lifetimes of these species.

A majority of atmospheric gas phase transformations and some condensed phase transformations are initiated by free radical reactions. Although this thesis focuses on gas phase processes, it should be noted that aqueous-phase and multi-phase processes also play a significant role in atmospheric chemistry. Many atmospheric trace gases are highly soluble in water, and these species can undergo aqueous phase reactions once taken up into cloud water. The uptake of soluble pollutants into clouds followed by subsequent rainout is an important pathway for the removal of trace species from the atmosphere, although, most clouds evaporate before they ever produce rain. Upon evaporation, some chemical species are returned to the gas phase, albeit in a chemically more oxidized form than upon initial uptake into the aqueous phase. The oxidized species are typically less volatile than their reduced precursors which can lead to particle growth. Particles play a critical role in atmospheric chemistry by scattering and

absorbing atmospheric radiation, altering cloud properties, and acting as a medium through which chemical transformations can occur that do not occur in the gas phase. A notable example of the latter case is the role of polar stratospheric clouds (PSCs) in the formation of the Anarctic ozone hole.

Gas phase chemical reactions play an integral role in understanding climate change, urban air quality, ozone production and depletion, and in determining the overall "well being" of our atmosphere. Many gas phase processes are initiated by radical species including hydroxyl (OH), nitrate (NO_3), halogen atoms (Cl, Br, I), and halogen oxides (ClO, BrO, IO). These radicals are typically highly reactive because they contain an unpaired electron in the outer shell. This high reactivity ensures the radical species remain in low abundance in the atmosphere, but they still play a crucial role in regulating the Earth's radiative balance and in the chemical properties of the atmosphere. With the current high level of interest in stratospheric ozone depletion events as well as tropospheric ozone production and global warming, it is important to understand the chemistry behind these atmospheric processes. When analyzing these processes, it is necessary to consider the vertical layers of the atmosphere. We consider the two main layers of the (lower) atmosphere, the troposphere and the stratosphere. The troposphere extends from ground level up to the tropopause at ~10 km, while the stratosphere extends from the tropopause to the stratopause at ~50 km. Greater than 99.9% of the mass of the atmosphere is contained in this lowest 50 km of altitude [*Seinfeld and Pandis, 2006*].

The most abundant oxidants in the atmosphere are O_2 and O_3, however, these molecules are generally not very reactive (except with some radicals). Approximately 90% of atmospheric ozone resides in the stratosphere where it serves to block harmful UV radiation ($\lambda < 290$ nm) from reaching the Earth's surface; thus the central interest in the study of stratospheric processes involves the chemical mechanisms that control ozone levels, particularly ozone destruction by catalytic cycles involving HO_x, NO_x, and halogen species. While ozone is the single most important chemical species in

stratospheric chemisty, it is the hydroxyl radical that is widely accepted to be the most important species in tropospheric chemistry. Ozone acts as both a toxicant and as a greenhouse gas (ie. absorbs and emits radiation) in the troposphere, however, tropospheric ozone does have some positive effect. OH is primarily generated from photolysis of ozone, and thus exists in relatively high concentrations in the day (~ 10^6 molecule cm^{-3}). Because of its high reactivity towards many pollutants, the OH radical is often referred to as the detergent of the troposphere. At the same time, OH initiated oxidation reactions are also critical in leading to ozone formation.

While OH is considered the primary oxidant in the troposphere, many other species such as NO_3, O_3, Cl, Br, ClO, and BrO can play a role in controlling the lifetimes of both natural and anthropogenic species. NO_3 tends to undergo rapid photolysis during the day and can therefore only accumulate at night. NO_3 reactions are typically slower than the analogous OH reactions, but typical 12 hour nighttime average NO_3 concentrations can be very high (~ 10^8 molecule cm^{-3}). Compounds emitted from the Earth's surface such as hydrocarbons or sulfur compounds, react with OH or NO_3 radicals in addition to other less abundant radical species such as halogens and halogen oxides. Knowledge of the kinetics of important free radical reactions helps to determine the lifetime of atmospheric trace species. Such information is important for evaluating quantities such as global warming potentials (GWPs) and ozone depletion potentials (ODPs) for trace gases of interest.

Consider the following general scheme where Y represents the reactive species mentioned above, RH represents the species subject to oxidation, and R / Y−RH represent the radical product resulting from the initial oxidation step.

$$Y + RH \rightarrow HY + R \qquad (1.1)$$

$$Y + RH \leftrightarrow Y{-}RH \rightarrow \text{Products} \qquad (1.1a)$$

The initial oxidation step can be either H-abstraction (1.1) or addition by Y (1.1a). Halogen atoms can be especially important in the marine boundary layer where their concentrations are typically highest.

The initial oxidation steps mentioned above are followed by radical products that undergo further chemical processes.

$$R + O_2 \rightarrow RO_2 \quad (1.2)$$

$$RO_2 + NO \rightarrow RO + NO_2 \quad (1.3)$$

$$NO_2 + h\nu \rightarrow NO + O \quad (1.4)$$

$$O + O_2 \rightarrow O_3 \quad (1.5)$$

These radical interconversions are omnipresent in the atmosphere and display persistent effects on the chemical evolution of atmospheric species. The radical reactions are only terminated when two radicals react with each other to form a stable species. Characterizations of the above processes contributes to our overall understanding of critical societal and scientific issues including ozone production and destruction, oxidation capacity of the troposphere, and climate change.

Over the past several decades, radical reactions of the general type described above have been the subject of many laboratory and theoretical studies, and the kinetic information for these reactions has been accumulated and compiled for model use [*Atkinson et al.*, 2004; 2006; 2007; 2008; Crowley *et al.*, 2010; *Sander et al.*, 2011]. Knowledge of such kinetic information allows for the concentrations of the major radicals in the atmosphere to be modeled with reasonable accuracy, although disagreements do often appear. Such models can also be helpful for predicting future trends in climate change, stratospheric ozone depletion, and air quality.

This dissertation reports studies of a series of potentially important atmospheric halogen atom (Cl and Br) reactions with various compounds known to exist in the atmosphere. These reactions can be separated into four classes, (i) Cl reaction with a series of bromo-alkanes that have been identified by the World Meteorological Organization (WMO) [WMO, 2007] as short lived source gases with potentially significant ozone depletion potentials (Ch. 3), (ii) Cl initiated oxidation of isoprene (Ch. 4), (iii) Br atom reactions with olefins involving the formation of weakly bound Br adducts (Ch. 5), and (iv) Cl atom reactions with the most abundant natural sulfur and selenium compounds found in the atmosphere (dimethyl sulfide (DMS) and dimethyl selenide (DMSe)) (Ch. 6). Results from the reactions studied provide new knowledge regarding the significance of these reactions in atmospheric chemistry. A brief introduction to the chemistry of these classes of compounds as well as their roles in the atmosphere and the motivation behind the work is given below, following an initial introduction to the role of halogen atoms in the atmosphere.

Halogen Atoms

Halogen atoms in the stratosphere

Chlorine and bromine were first suggested as a significant contributor to the depletion of stratospheric ozone in the mid 1970's [*Molina and Rowland, 1974; Stolarski and Cicerone, 1974; Wolfsy et al., 1975*]. A majority of stratospheric chlorine and bromine is thought to be anthropogenic in origin [*WMO, 2010*]. Chlorine and bromine atoms exist in the stratosphere as the result of transport of long-lived anthropogenic chlorofluorocarbons (CFCs), hydrochlorofluorocarbons (HCFCs), and halons from the troposphere [*WMO, 2010*]. Natural sources are primarily methyl halides emitted into the

troposphere from the oceans and transported to the stratosphere [*WMO, 2010*]. Key catalytic cycles for destroying ozone that involve halogen atoms include the following

$$Cl + O_3 \rightarrow ClO + O_2 \quad (1.6)$$

$$ClO + O \rightarrow Cl + O_2 \quad (1.7)$$

$$\text{Net: } O_3 + O \rightarrow 2O_2$$

$$Cl + O_3 \rightarrow ClO + O_2 \quad (1.8)$$

$$ClO + HO_2 \rightarrow HOCl + O_2 \quad (1.9)$$

$$HOCl + h\nu \rightarrow OH + Cl \quad (1.10)$$

$$OH + O_3 \rightarrow HO_2 + O_2 \quad (1.11)$$

$$\text{Net: } 2O_3 \rightarrow 3O_2$$

$$Br + O_3 \rightarrow BrO + O_2 \quad (1.12)$$

$$BrO + HO_2 \rightarrow HOBr + O_2 \quad (1.13)$$

$$HOBr + h\nu \rightarrow OH + Br \quad (1.14)$$

$$OH + O_3 \rightarrow HO_2 + O_2 \quad (1.15)$$

$$\text{Net: } 2O_3 \rightarrow 3O_2$$

Because the stratospheric O_3 / O ratio decreases dramatically with increasing altitude [*Jacob, 1999*], catalytic cycles where the net reaction is $O_3 + O \rightarrow 2\ O_2$ are most important in the mid and upper stratosphere, whereas catalytic cycles where the net reaction is $2\ O_3 \rightarrow 3\ O_2$ are most important in the lower stratosphere.

One important example of how chlorine affects stratospheric chemistry is the formation of the Antarctic ozone hole. In this region, massive ozone depletion can be attributed to the following efficient heterogeneous processes on the surfaces of polar stratospheric clouds (PSC) as follows [*Crutzen and Arnold, 1986; Leu, 1988a; 1988b; McElroy et al., 1986; Molina et al., 1987; Solomon et al., 1986; Tolbert et al., 1987; Tolbert et al., 1988a; 1988b*]:

$$HCl + ClONO_2 \rightarrow HNO_3 + Cl_2 \quad (1.16)$$

$$H_2O + ClONO_2 \rightarrow HNO_3 + HOCl \quad (1.17)$$

$$H_2O\,(g) + N_2O_5\,(g) \rightarrow 2\,HNO_3 \quad (1.18)$$

$$HCl\,(g) + HOCl\,(g) \rightarrow H_2O + Cl_2 \quad (1.19)$$

$$H_2O + BrONO_2 \rightarrow HNO_3 + HOBr \quad (1.20)$$

$$HCl + BrONO_2 \rightarrow HNO_3 + BrCl \quad (1.21)$$

$$HCl\,(g) + HOBr\,(g) \rightarrow H_2O + BrCl \quad (1.22)$$

Reactions 1.16 and 1.17 proceed very slowly in the gas phase but these reactions occur rapidly on PSC surfaces. Photochemically labile halogen species such as Cl_2, BrCl, HOCl, and HOBr accumulate during dark winter and photolyze rapidly upon exposure to spring sunlight, thus releasing large amounts of reactive Cl and Br atoms which facilitate ozone destruction via the following catalytic cycles.

$$2\,(Cl + O_3 \rightarrow ClO + O_2) \quad (1.23)$$

$$ClO + ClO + M \rightarrow ClOOCl + M \quad (1.24)$$

$$ClOOCl + h\nu \rightarrow Cl + Cl + O_2 \quad (1.25)$$

Net: $2O_3 \rightarrow 3O_2$

$$Br + O_3 \rightarrow BrO + O_2 \quad (1.26)$$

$$Cl + O_3 \rightarrow ClO + O_2 \quad (1.27)$$

$$BrO + ClO \rightarrow Cl + Br + O_2 \quad (1.28)$$

Net: $2O_3 \rightarrow 3O_2$

Iodine atoms could potentially catalyze ozone destruction via cycles similar to those described above for Cl and Br. In fact, because iodine resovoir species such as HOI and $IONO_2$ are inefficient at sequestering IO_X radicals, iodine is potentially a very efficient catalyst for ozone destruction. However, since all iodine source compounds photolyse rapidly in the troposphere, the influence of iodine on stratospheric ozone levels is generally thought to be negligible.

Halogen atoms in the troposphere

While the effect of reactive halogen species on stratospheric chemistry, ozone destruction, in particular, has been largely understood for some time, the impact of halogen chemistry on the oxidation capacity of the troposphere is much more complex. Chlorine chemistry in the troposphere differs from that in the stratosphere in two primary ways: (i) the source compounds that photolyze to produce Cl atoms in the stratosphere are stable toward photolysis by radiation that penetrates into the troposphere; (ii) the majority stratospheric Cl atoms react with ozone, while in the troposphere most Cl atoms are destroyed by reaction with organics. As a result, ClO_x radicals are ineffective at catalyzing ozone destruction in the troposphere. However, Cl atoms are the most reactive

of all atmospherically important halogen atoms as they can react with tropospheric trace gases via both H-abstraction and addition pathways. Cl reactions with organic compounds are typically much faster, i.e., rate coefficients are larger by an order of magnitude or more, than the corresponding OH reactions [*Sander et al., 2011; Atkinson et al., 2006*]. Hence, in the event that Cl concentrations are greater than ~ 1 % of OH concentrations, Cl would be able to effectively compete with OH for reaction with many organics in the troposphere.

Several field studies in both tropical and mid-latitude marine environments [*Wingenter et al., 1996; Wingenter et al., 2005*] as well as in arctic regions [*Ariya et al., 1999; Boudries and Bottenheim, 2000; Jobson et al., 1994*] suggest tropospheric Cl chemistry plays a role in controlling concentrations and lifetimes of nonmethane hydrocarbons (NMHCs). Kinetic information for the oxidation of hydrocarbons by OH and Cl have been used to deduce average Cl concentration by time series observations of NMHCs, while simultaneously solving for air mass mixing and OH concentrations [*Wingenter et al., 1996; Wingenter et al., 2005*]. A similar approach was utilized in order to deduce average [Cl] over a few days [*Ariya et al., 1999; Boudries and Bottenheim, 2000; Jobson et al., 1994*]. Inferred [Cl] were all in the range of 10^4–10^5 atoms cm^{-3} (~1-10% of OH levels), which supports results from the Cl precursor measurements stated above.

Cl atoms in the MBL exist primarily as the result of photolysis of photo-labile compounds such as Cl_2, ClNO, or $ClNO_2$, which are produced from heterogeneous reactions either in the bulk or on the surface of aqueous particles [*Knipping et al., 2000; Laskin et al., 2006; Raff et al., 2009; Finlayson-Pitts, 2010*]. Measurements of these

source compounds can provide information about Cl atom levels. A photochemical model has been employed along with results of field measurements of [Cl_2*] (including Cl_2 and HOCl) in Miami, FL to deduce Cl atom concentrations of 10^4–10^5 atoms cm^{-3} [*Pszenny et al., 1993*]. In addition, atmospheric pressure chemical ionization mass spectrometry was employed in an effort to deduce concentrations of molecular chlorine (Cl_2) near Long Island, NY [*Spicer et al., 1998*] and in Irvine, California [*Finley and Saltzman, 2006*]; both studies conclude peak Cl concentrations were in excess of 1×10^5 atoms cm^{-3}. Gas phase species such as OH, $ClONO_2$, N_2O_5, NO_2, and HNO_3 have also been shown to contribute to heterogeneous processes which produce gas phase Cl atoms.

The oceans represent the largest natural source of halogenated compounds, although it is worth noting that recent findings suggest a significant Cl production rate ($ClNO_2$) even in the middle of the continental United States far removed from sea salt sources [*Thornton et al., 2010*]. Sea salt contains 55.7 % Cl, 0.19% Br, and 0.00002 % I by weight [*Seinfeld and Pandis, 2006*]. There is evidence that suggests a net flux of Cl and Br from marine aerosol to the gas phase [*Seinfeld and Pandis, 2006; Finlayson-Pitts, 2010*]. However, for I atoms, the I content in marine aerosol is typically ~ 1000 times greater than that present in seawater, which stems from an enhanced level of organic I compounds in the surface organic layer of the ocean [*Carpenter, 2003*].

In addition to the heterogeneous chemistry addressed above, pure gas phase processes also can contribute to generate Cl atoms. Gas phase HCl, a product of the Cl hydrogen abstraction reaction, reacts with OH to yield Cl atoms.

$$HCl + OH \rightarrow Cl + H_2O \qquad (1.29)$$

Other less abundant gas phase processes that generate Cl atoms include the result of the ClO reaction with NO or HO_2.

Similar to the case with chlorine, the source compounds that photolyze to generate Br atoms in the stratosphere are stable toward photolysis by radiation that penetrates into the troposphere. Unlike Cl which is reactive towards most hydrocarbons Br atom reactions with saturated hydrocarbons proceed slowly via hydrogen abstraction and are thought to be of negligible importance in the atmosphere. Br does react with aldehydes, olefins, and HO_2 radicals, but the typical fate of atomic Br involves reaction with O_3 and subsequent production of BrO as seen in (1.26).

The Br addition reactions with unsaturated organics lead to formation of a bromoalkyl radical, although the C−Br bond in a given bromoalkyl radical is much weaker than the C−Cl bond in the corresponding chloroalkyl radical. The effective rate coefficients for Br + olefin reactions under tropospheric conditions depend on the addition rate coefficient and on the competition between bromoalkyl radical unimolecular decomposition and bromoalkyl radical reaction with O_2. These effective rate coefficients can have complex dependences on temperature, pressure, and $[O_2]$, but appear to approach gas kinetic rates under conditions where the O_2 reaction dominates the competition for removal of the bromoalkyl radical adduct [*Laine et al., 2011a*].

The primary result of the fact that Br atoms are less reactive with organics than Cl atoms is that Br atoms can participate in catalytic cycles that destroy tropospheric ozone. The most important catalytic cycle under typical tropospheric conditions is the BrO + HO_2 cycle, reactions (12-15). Analagous to the case for Cl, heterogeneous reactions are required to maintain significant levels of BrO_x radicals. Lab studies have shown that

BrO_x can be produced in the troposphere by the heterogeneous process described above [*Kirchner et al., 1997; Abbatt, 1994; Abbatt and Nowak, 1997; Fickert et al., 1999; Huff and Abbatt, 2000, 2002; Adams et al., 2002*]. The reaction sequence below (1.30-1.32) has been proposed [*Vogt et al., 1996*] and supported by both laboratory studies [*Fickert et al., 1999*] and field measurements [*Foster et al., 2001*] which have shown that both BrCl and Br_2 are produced from the snow pack.

$$HOBr + Cl^- + H^+ \rightarrow H_2O + BrCl \quad (1.30)$$

$$BrCl + Br^- \rightarrow Br_2Cl^- \quad (1.31)$$

$$Br_2Cl^- \rightarrow Br_2 + Cl^- \quad (1.32)$$

$$\text{Net: } HOBr + H^+ + Br^- \rightarrow H_2O + Br_2$$

It should be noted that the HOBr in reaction (1.30) is produced from reaction (13). Also of note, reaction (1.32) is a heterogeneous reaction, and (1.30-1.31) occur in the aqueous phase. Additionally, when there isn't sufficient Br^- to react with BrCl (1.31), then BrCl can escape into the gas phase where it is rapidly photolysed to yield both reactive Cl and Br.

Recent research has shown atomic halogens can also be produced near the sea surface via photosensitized oxidations of halide anions (X^-, where X = Cl, Br, or I) by chlorophyll and carbonyls [*Jammoul et al., 2009*; *Reeser et al., 2009*]. These formed photo-labile compounds are unreactive at night, thus allowing for accumulation prior to undergoing rapid photolysis and subsequent production of large concentrations of X atoms. Therefore, [X] is expected to be at its highest concentrations in the marine boundary layer (MBL) after sunrise, consistent with field measurements [*Liao et al.,*

2011a; 2011b]. Modeling investigations have suggested that inclusion of chlorine chemistry resulting from sea salt reactions has a significant effect on projected ozone levels in coastal urban areas [*Chang et al., 2002*; *Knipping and Dabdub, 2003*].

A similar sequence (shown below) is thought to be the dominant source of reactive halogen atoms during polar boundary layer ozone depletion events [*Fan and Jacob, 1992; McConnell et al., 1992; Platt and Janssen, 1995; Platt and Lehrer, 1996; Tang and McConnell, 1996; Wennberg, 1999; Simpson et al., 2007*].

$$HOBr + Br^- + H^+ \rightarrow H_2O + Br_2 \quad (1.33)$$

$$Br_2 + h\nu \rightarrow 2Br \quad (1.34)$$

$$Br + O_3 \rightarrow BrO + O_2 \quad (1.35)$$

$$BrO + HO_2 \rightarrow HOBr + O_2 \quad (1.36)$$

$$\text{Net: } H^+ + Br^- + HO_2 + O_3 \rightarrow Br + H_2O + 2O_2$$

As can be seen from the net reaction above, the reaction sequence is 'autocatalytic'. The mechanism of (1.33) has been the subject of numerous laboratory studies. It is a multiphase reaction, for example, gaseous HOBr is taken up into brine solution where it reacts and is followed by release of gaseous Br_2 [*Fickert et al., 1999; Huff and Abbatt, 2000; 2002; Adams et al., 2002*]. The sequences shown above (1.30-1.32 and 1.33-1.36) are often referred to as the 'bromine explosion'. The result of this 'explosion' is very high BrO_x levels which contribute to the following catalytic cycle:

$$2\,(Br + O_3 \rightarrow BrO + O_2) \quad (1.37)$$

$$BrO + BrO \rightarrow 2Br + O_2 \qquad (1.38)$$

Net: $2O_3 \rightarrow 3O_2$

Reaction (1.38) can also proceed to yield $Br_2 + O_2$, however, Br_2 is rapidly photolyzed to give 2Br.

An estimated concentration of 1.4×10^7 atoms cm^{-3} was obtained for [Br] during an Arctic boundary layer ozone depletion event where ozone was reduced to below 1ppbv, which accounts for the additional removal of some highly reactive compounds (acetylene) via mechanisms other than OH and Cl reactions. The above-mentioned field data suggest that Cl and Br reactions make significant contributions to the oxidation of many organic compounds in atmospheric locales where halogen atoms are prevalent, i.e., in marine and polar environments.

It had been previously found that reaction (1.29) is an insignificant source for Cl atoms [*Finlayson-Pitts, 2003*]. However, recent model studies [*Keene et al., 2007*; *Pechtl and von Glasow, 2007*] have suggested the reaction initiates the production of Cl_2 in the marine boundary layer and sustains Cl steady state concentrations at relatively high levels via the following scheme:

$$HCl + OH \rightarrow Cl + H_2O \qquad (1.29)$$

$$Cl + O_3 \rightarrow ClO + O_2 \qquad (1.39)$$

$$ClO + HO_2 \rightarrow HOCl\,(g) + O_2 \qquad (1.40)$$

$$HOCl\,(g) \rightarrow HOCl\,(aq) \qquad (1.41)$$

$$HOCl\,(aq) + Cl^-\,(aq) + H^+\,(aq) \rightarrow Cl_2\,(g) + H_2O \qquad (1.42)$$

HOCl and Cl_2 accumulate at night and rapidly release Cl atoms after sunrise, resulting in high concentrations of Cl in the morning.

$$Cl_2 + h\nu \rightarrow Cl + Cl \quad (1.43)$$

$$HOCl + h\nu \rightarrow Cl + OH \quad (1.10)$$

In addition, recent laboratory and theoretical research demonstrates that heterogeneous reaction of N_2O_5 with HCl (in competition with H_2O) may represent a significant source of tropospheric $ClNO_x$ species that can rapidly photolyze under daytime conditions to produce Cl atoms [Raff *et al., 2009*].

$$HCl\,(g) + N_2O_5\,(g) \rightarrow HNO_3\,(l) + ClNO_2\,(g) \quad (1.44)$$

Similarly, photolysis of other photo-labile chlorine containing compounds that originate from heterogeneous reactions involving sea salt aerosols also produce Cl atoms in marine environments [*Finlayson-Pitts et al., 1989*; *Finlayson-Pitts, 2003*].

$$NaCl\,(s) + N_2O_5\,(g) \rightarrow NaNO_3\,(s) + ClNO_2\,(g) \quad (1.45)$$

$$NaCl\,(s) + ClONO_2\,(g) \rightarrow NaNO_3\,(s) + Cl_2\,(g) \quad (1.46)$$

$$ClNO_2 + h\nu \rightarrow Cl + NO_2 \quad (1.47)$$

$$Cl_2 + h\nu \rightarrow Cl + Cl \quad (1.48)$$

Analogous to Cl production, heterogeneous reactions on sea salt surface can also occur in the marine boundary layer to produce Br atoms [*Finlayson-Pitts, 2003*; *Frinak and Abbatt, 2006*]. Molecular bromine (Br_2) is found most commonly as the result of

heterogeneous reactions of sea salt bromide occurring in snow-pack, sea ice, or marine aerosols *[Tang et al., 1996; Vogt et al., 1996]*.

$$NaBr\ (s) + N_2O_5\ (g) \rightarrow NaNO_3\ (s) + BrNO_2\ (g) \quad (1.49)$$

$$BrNO_2 + h\nu \rightarrow Br + NO_2 \quad (1.50)$$

or

$$Br^-\ (aq) + OH\ (aq) \leftrightarrow HOBr^-\ (aq) \quad (1.51)$$

$$HOBr^-\ (aq) + H^+\ (aq) \rightarrow Br\ (aq) + H_2O \quad (1.52)$$

$$Br\ (aq) + Br^-\ (aq) \leftrightarrow Br_2^-\ (aq) \quad (1.53)$$

$$Br_2^-\ (aq) + Br_2^-\ (aq) \leftrightarrow Br_3^-\ (aq) + Br^-\ (aq) \quad (1.54)$$

$$Br_3^-\ (aq) \leftrightarrow Br_2\ (g) + Br^-\ (aq) \quad (1.55)$$

It has also been suggested that micro algae in the Arctic emits the photolabile species, bromoform ($CHBr_3$), yielding Br radicals during the polar sunrise *[Sturges et al., 1992; Sturges et al., 1993a,b]*. Additionally, theoretical studies have led to the conclusion that high concentrations of Br are possible in the lower arctic environment *[Barrie et al., 1988; Platt et al., 1995; Ramacher et al., 1997]*.

Br atoms are then regenerated from a variety of reactions, similar to (1.56-1.60) shown below (X, Y = Cl, Br, or I)

$$X + O_3 \rightarrow XO + O_2 \quad (1.56)$$

$$XO + h\nu \rightarrow X + O \quad (1.57)$$

$$XO + XO \rightarrow 2X + O_2 \quad (1.58a)$$

$$\rightarrow X_2 + O_2 \quad (1.58b)$$

$$XO + YO \rightarrow X + Y + O_2 \quad (1.59a)$$

$$\rightarrow \quad XY + O_2 \qquad (1.59b)$$

$$\rightarrow \quad OXO + Y \qquad (1.59c)$$

$$XO + YO + M \rightarrow XOOY \qquad (1.59d)$$

$$XO + NO \rightarrow NO_2 + X \qquad (1.60)$$

Typical springtime Arctic daytime j-values, i.e., first-order photolysis rate coefficients, for (1.53) are 3×10^{-5} s^{-1}, 4×10^{-2} s^{-1}, and 0.2 s^{-1} for X = Cl, Br, I, respectively [*Simpson et al., 2007*]. The BrO + NO reaction occurs with a rate coefficient of ~2 x 10^{-11} cm^3 $molecule^{-1}$ s^{-1}, but NO levels are typically too low in these regions to impact BrO levels significantly [*Atkinson et al., 2007*]. Hence, the fate of BrO is dominated by photolysis (1.53) at low ozone, ie., Br/BrO is highest, while at high ozone during the day Br/BrO will be lowest. The formation of X_2 and XY in reactions 1.54b and 1.55b will rapidly lead to 2X and X + Y via photolysis. Once halogen atoms are released by any of the steps above (1.53-1.56) the next most common step is for the halogen atom to react again with ozone. The probabilities are >99% for I, up to 99% for Br, and up to 50% for Cl [*Simpson et al., 2007*]. This supports data from studies showing significant amounts of IO and BrO have been observed in the polar boundary layer, while previous research shows the same cannot be said for ClO in this region [*Platt, 1995; Simpson et al., 2007*]. In polluted environments [XO] / [X] ~ 10 – 100 for Cl and [XO] / [X] ~ 1 − 10 for Br and I [*Simpson et al., 2007; Zeng, 2005*].

In the Arctic springtime, a strong correlation is found between the sudden loss of ozone at ground level and the concurrent increase of filterable bromine species (HBr, $BrONO_2$, Br, BrO, HOBr, and particulate Br), implying that the tropospheric ozone depletion is heavily influenced by Br catalytic cycles [*Barrie et al., 1988; Bottenheim et*

al., 1990; Yang et al., 2005]. Furthermore, a strong peak in both I and Br containing aerosol concentrations has been observed during this time period [*Bottenheim et al., 1990; Barrie et al., 1994*]. These investigations, in addition to others [*Vogt et al., 1999; O'Dowd and Hoffmann, 2005*] imply that interhalogen couplings involving I atoms could be important in regulating the reactive halogen budget in regards to ozone destruction. Reverting back to the XO + XO self reaction leading to OXO formation (R1.54), the case where X = I is interesting because (i) the IO self reaction is much faster than the BrO or ClO self reactions [*Sander et al., 2011*] and (ii) OIO photolysis to give I + O_2 is possible (strong absorption bands between 480 and 620 nm), thus making the IO + IO self reaction a potentially major ozone depletion cycle [*Ingham et al., 2000; Ashworth et al., 2002*].

$$IO + IO \rightarrow 2I + O_2 \quad (1.61a)$$

$$\rightarrow I_2 + O_2 \quad (1.61b)$$

$$\rightarrow OIO + I \quad (1.61c)$$

$$IO + IO + M \rightarrow I_2O_2 + M \quad (1.61d)$$

The photolysis of tropospheric iodine species is of potential importance with regard to influencing ozone budget and NO_x balance [*Carpenter, 2003; Chameides and Davis, 1980*]. Further evidence suggests that iodine in the marine boundary layer has an influence on ozone destruction, the oxidizing capacity of the troposphere, denoxification, and particle formation [*Hoffmann et al., 2001; O'Dowd et al., 2002*; *Pechtl et al., 2006; Carpenter, 2003*]. Inorganic iodine (i.e., reactive iodine) comes primarily from methyl iodide (CH_3I), diiodomethane (CH_2I_2), and chloroiodomethane (CH_2ICl) which is emitted from microalgae with some evidence of an open ocean source [*Carpenter, 2003;*

Finlayson-Pitts, 2010]. The potential significance of I atom chemistry, in regards to many of the processes discussed above is currently unclear.

Halogen atoms and tropospheric O_3 formation

The primary oxidant in the troposphere has long been thought to be the OH radical, which subsequently leads to ozone formation as seen from the reaction sequence 1.1-1.5. Halogen atom reactions can also serve as oxidants of many trace species, through much the same pathway shown in reactions 1.1-1.5. Cl atoms can react readily with hydrocarbons via H-abstraction or addition if the hydrocarbon is unsaturated. Br atoms can also add to the double bond in much the same way as Cl, however, H-abstraction by Br is typically less favorable, and I atoms are generally less reactive than Br. The largest uncertainty associated with tropospheric halogen chemistry and its role in ozone formation lies in the difficulty associated with directly measuring halogen atoms in the troposphere. Attempts have been made in an effort to deduce tropospheric concentrations of Cl and Br atoms in a number of studies [*Ariya et al., 1999; Boudries and Bottenheim, 2000; Finley and Saltzman, 2006; 2008; Jobson et al., 1994; Lawler et al., 2009; Wingenter et al., 1996; Wingenter et al., 2005*]. Because of the difficulties in directly detecting these halogen atoms, the standard procedure in determining tropospheric Cl and Br concentrations is to employ indirect methods. For example, measurements of the concentration-time behaviour of hydrocarbons during O_3 depletion events have provided strong evidence that their oxidation is strongly dependent on both chlorine and bromine chemistry [*Jobson et al., 1994; Sauer et al., 1999; Wingenter et al., 2005*]. In fact Br atom concentrations have been estimated to be as high as 6×10^7 atoms cm^{-3} [*Boudries and Bottenheim, 2000*]. Additional measurements by a completely

different technique estimate Br atom concentration as high as 5 x 10^7 atoms cm^{-3} (inferred from differential optical absorption spectroscopy (DOAS) measurements of the BrO radical concentration) [*Platt and Janssen, 1995*].

A great example of the effectiveness of this approach in assessing the halogen atom abundance on a global scale is the method employed by Singh *et al*. [*1996*]. These researchers inferred a global average Cl atom concentration by analyzing the concentrations of tetrachloroethylene (C_2Cl_4) in various environments and interpreting the results using a 2-D model. The emission inventory of C_2Cl_4 is known with high accuracy, as tropospheric C_2Cl_4 is primarily of industrial origin although a small ocean source has been suggested [*Singh et al., 1996*]. Knowledge of its emission inventory and the Cl atom kinetics (the Cl reaction with C_2Cl_4 is over 300 times faster than that with OH [*Nicovich et al., 1996*]) allows for reliable Cl concentration estimates on a global scale. An upper limit of Cl concentrations of 1×10^3 atoms cm^{-3} was calculated as a global average [*Singh et al., 1996*]. Additional confidence stems from the fact that OH radical kinetics are sufficient to balance the C_2Cl_4 budget.

Finley and Saltzman [*2008*] also measured the concentrations of Cl_2 and Br_2 along the Pacific coast off southern California. They estimated the 24-hour mean concentrations of Cl and Br atoms to be 7.7×10^3 and 6.1×10^4 atoms cm^{-3}, respectively, using a photochemical box model. In a very recent field observation, Lawler *et al.* [*2009*] measured the Cl_2 concentrations in the eastern tropical Atlantic and simulated a 24-hour mean Cl concentration of 3.5×10^4 atoms cm^{-3}.

Halocarbons

Halogenated alkanes are present in the atmosphere as a result of both natural and anthropogenic processes, however, the majority of brominated alkyl bromides are of natural origin being emitted from the ocean. Notable exceptions include ethyl bromide, *n*-propyl bromide (*n*-C_3H_7Br) and 1,2-dibromoethane (CH_2BrCH_2Br). Ethyl bromide is primarily used in organic synthesis as an ethylating agent, *n*-propyl bromide is an organic solvent used primarily for cleaning metal surfaces, while 1,2-dibromoethane is primarily used as a fumigant. Another source of tropospheric halogen compounds involve use of replacement compounds for fully halogenated CFCs that can be chemically degraded in the troposphere. Many alkyl bromides are considered very short-lived substances, which are defined as those having atmospheric lifetimes comparable to, or less than, average tropospheric transport time scales of approximately six months [*Law et al., 2007*]. Brominated very short-lived compounds are thought to contribute 20-25% (or ~ 5 ppt) of total stratospheric bromine [*Law et al., 2007*]. As mentioned earlier, while stratospheric levels of bromine are considerably lower than those of chlorine, ozone depletion potentials (ODPs) for organic bromine compounds are much higher than for analogous organic chlorine compounds. Thus, there is considerable interest in understanding the atmospheric chemistry of even relatively short-lived organic bromine compounds. The potential for any halogenated source gas to destroy ozone is ultimately decided by the altitude at which species is destroyed in the atmosphere. The primary tropospheric sink for most halocarbons including the bromoethane, bromopropane, and 1,2-dibromoethane is reaction with OH radicals [see for example, *Brioude et al., 2010*]. Direct photolysis is a major player in the destruction of iodine containing compounds.

If the Cl rate coefficients are significantly (> 10 times) faster than the OH rate coefficients, and the Cl concentrations are near 4 x 10^4 atoms cm^{-3} [*Wingenter et al., 2005*], which is typical for the marine boundary layer, then inclusion of the Cl reaction can reduce the estimated tropospheric lifetimes of the alkyl bromide in question. In Chapter 3 the results from studies of the Cl reaction with three alkyl bromides are presented and the potential effect on the atmospheric lifetimes and ODPs of each bromoalkane is assessed. Furthermore, branching ratios for β-hydrogen abstraction are evaluated to provide mechanistic information.

Alkenes ($C_2 – C_6$)

Alkenes exist in our atmosphere as the result of both natural and anthropogenic processes. One primary source of anthropogenic emissions includes gasoline fuels and other automobile exhaust emissions [*Seinfeld and Pandis, 2006*]. These small unsaturated organics make up roughly 10 % of non-methane-hydrocarbon (NMHC) concentration in many U.S. cities [*Lurmann and Main, 1992; Chameides et al., 1992*]. It is well-established that isoprene is the single most important NMHC emitted from terrestrial sources. In addition, a potentially significant marine source of isoprene has received considerable recent attention [*Liss, 2007; Liakakou et al., 2007; Sinha et al., 2007; Arnold et al., 2009; Gantt et al., 2009; 2010*]. Alkenes are unique in that they can be oxidized by hydrogen abstraction or by addition to the double bond, thus increasing their overall reactivity and, in turn, leading to increased potential for ozone formation in urban (high NO_x) environments.

The reaction scheme below illustrates the steps leading to ozone formation via oxidation of hydrocarbons (R). The initial step is oxidation, via OH, O_3, NO_3, or a halogen atom, to form the hydrocarbon radical species (R·), followed by:

$$R\cdot + O_2 + M \rightarrow RO_2 + M \qquad (1.2)$$

The hydrocarbon radical (R·) above can be formed as the result of either H-abstraction or addition to a double bond; however, in cases where an adduct is formed the adduct dissociation reaction will compete with the O_2 reaction above. The fate of the peroxy (RO_2) radical varies with the identity and size of R. For example:

$$CH_3 + O_2 \rightarrow CH_3O_2 \rightarrow HCHO + OH \qquad (1.62)$$

HCHO is the result of the alkoxy radical reaction with O_2 ($CH_3O + O_2$). In all but the remote troposphere, alkylperoxy radicals (RO_2) react with NO to form alkoxy radicals (RO):

$$RO_2 + NO \rightarrow NO_2 + RO \qquad (1.3)$$

Alkoxy radicals undergo more complex chemistry than peroxy radicals. These radicals (RO) can react with O_2, undergo isomerization, undergo decomposition, and react with NO or with NO_2. For larger alkyl radicals (C > 2) stable alkyl nitrates can be formed:

$$RO_2 + NO + M \rightarrow RONO_2 + O_2 \qquad (1.63)$$

In an atmosphere devoid of NO, RO_2 will likely react with HO_2:

$$RO_2 + HO_2 \rightarrow ROOH + O_2 \qquad (1.64)$$

The fate of the ROOH product of reaction (1.70) is dominated by either reaction with OH or by photolysis.

Production of NO_2 is considered the most significant source of anthropogenically produced ozone [*Finlayson-Pitts and Pitts, 2000*]. This entire process is critical in controlling the oxidizing capacity of the atmosphere. The initial H-abstraction reaction preceding reaction (1.2) is typically accepted to be dominated by the hydroxyl radical, however, in some locales chlorine atoms can play a significant role. In the case of bromine, H-abstraction by Br is often slow and unimportant in the atmosphere. However, Br reactions with unsaturated hydrocarbons can be much more complex. These reactions typically proceed rapidly via addition of the Br atom to the double bond and, depending on the local Br atom concentration and subsequent chemistry of the Br-containing adduct, could play a significant role in atmospheric chemisty.

Reactions of atomic halogens with olefins are thought to play a potentially significant role in the chemistry of marine atmospheric environments, often times with rate coefficients approaching the collision-controlled regime, particularly at low temperatures. Weakly-bound radical-molecule adducts could potentially play an important role in cold atmospheric environments because at lower temperatures unimolecular decomposition is slower, i.e., less able to compete with adduct reaction with O_2. In the Arctic troposphere, for example, bromine atom initiated oxidation of olefins could potentially represent an important loss process for bromine (and for many alkenes) depending on the local alkene concentration, Br atom concentration, and subsequent chemistry of the Br-containing adduct.

In Chapters 4 and 5 we report studies of the halogen initiated oxidation of isoprene, 2,3-dimethyl-2-butene, and 1,3-butadiene under atmospheric conditions. The results are compared with prior literature when appropriate. The kinetic data are used to assess the potential importance of the halogen atom reaction as a loss process for each alkene relative to the reactions with OH, NO_3, and O_3.

Sulfur and Selenium (DMS and DMSe)

Anthropogenic sulfur emissions exceed natural emissions by about a factor of ten in industrialized nations such as the United States [*Andreae, 1990; Bates et al., 1992; 1994; Spiro et al., 1992*]. However, since the ocean covers nearly 70 % of the Earth's surface biogenic emissions can represent a significant fraction (15-20 % in the Northern Hemisphere and 50-60 % in the Southern Hemisphere) of the overall sulfur budget on a global scale [*Andreae, 1990; Bates et al., 1992; 1994*]. Roughly half of all biogenic sulfur is emitted from the oceans in the form of dimethyl sulfide (DMS, CH_3SCH_3). DMS is believed to stem from the decomposition of dimethyl sulfoniopropionate produced by marine organisms such as phytoplankton [*Andreae, 1990*], and its concentrations have been found to be highly variable in marine environments. DMS concentrations depend on diurnal and seasonal variations, as well as depth and location in seawater [*Andreae and Barnard, 1984; Turner and Liss, 1985; Andreae and Raemdonck, 1983*]. Research yielding DMS concentrations in the atmosphere along with Henry's law constants for DMS in seawater lead to oceanic DMS concentrations in large excess of those that would be in equilibrium with atmospheric levels. Hence, the result of this lack of equilibrium is a net flux of DMS from the ocean to the atmosphere [*Seinfeld and Pandis, 2006*].

The atmospheric chemistry of DMS has been well studied because of its potential importance in regulating global climate. [*Barnes et al.*, 2006 and references therein; *Daykin and Wine*, 1990; *Hynes et al.*, 1986; *Ingham et al.*, 1999; *Jefferson et al.*, 1994; *Stickel et al.*, 1992; *Wine et al.*, 1993; *Zhao et al.*, 1996]. The atmospheric oxidation reactions initiated by OH and Cl can proceed via both H-abstraction and addition pathways. The DMS–OH adduct can react with O_2 in competition with adduct decomposition, thus efficiently destroying DMS in the atmosphere [*Williams et al., 2007; Barone et al., 1995; Hynes et al., 1986*]. However, the DMS–Cl adduct does not react with O_2 at a measurable rate, and the likely atmospheric fate includes thermal decomposition back to the DMS and Cl, reaction with NO_x, and possibly photolysis to yield unknown products [*Enami et al.*, 2004; *Urbanski and Wine*, 1999].

The H-abstraction product, CH_3SCH_2, readily reacts O_2 which yields the peroxy radical, $CH_3SCH_2(OO)$. Under atmospheric conditions, the sulfur peroxy radical is subject to reaction with NO to give CH_3S (+H_2CO) [*Urbanski et al., 1997*], or reaction with HO_2 (similar to alkyl radical reactions) that could lead to production of an important intermediate for the end products SO_2, methane sulfonic acid (MSA), and eventually H_2SO_4. These less-volatile sulfur oxidation products such as H_2SO_4 can lead to new particle formation, which in the marine boundary layer can lead to formation of cloud condensation nuclei (CCN). CCN lead to formation of stratus clouds, and above the ocean, roughly half of the sky is covered by stratus clouds which play a crucial role in governing planetary albedo. The three primary sources of aerosols in the marine boundary layer are sea salt, non-sea-salt-sulfate (nss), and entrainment of free tropospheric aerosol [*Barnes et al., 2006*]. The oxidation of DMS in the gas phase

represents the primary component of nss-aerosol [*Charlson et al., 1987; Andreae et al., 1994; Ayers et al., 1996*]. The CLAW hypothesis postulates that emission of DMS from the oceans may have a significant impact on Earth's radiation budget and possibly on climate regulation [*Charlson et al., 1987*]. The question that still remains unsettled today is to the extent that DMS plays in controlling levels of aerosol in the marine boundary layer [*Barnes et al., 2006*]. Understanding the kinetics of DMS reactions is important towards that end.

Similar to its analog DMS, dimethyl selenide (DMSe, CH_3SeCH_3) is found to be the most abundant volatile Se species in the atmosphere and in surface seawater, although other Se containing species have been measured including dimethyl diselenide (DMDSe, $CH_3SeSeCH_3$), methyl selenyl sulfide (DMSeS, CH_3SeSCH_3), and methane selenol (MeSeH, CH_3SeH) [*Amouroux and Donard,* 1996; *Amouroux et al.*, 2001]. Because of physiochemical and geochemical similarities between Se and S species, the atmospheric chemistry of DMSe is often compared with DMS. It is thought that DMSe is produced via a similar pathway to DMS in cocolithophorid, the most widespread species of plankton in the ocean [*Amouroux et al., 2001*]. In fact, the concentrations of DMSe and DMS in marine environments are found to be strongly correlated. However, DMSe is in much less abundance than DMS with a molar ratio of $\sim 10^{-4}$; therefore, DMSe chemistry has not been studied nearly to the extent that DMS chemistry has.

The atmosphere is a transient reservoir of selenium, which is subjected to a variety of physical, chemical, and photochemical processes. Selenium levels are found to be highly variable in time and space. According to recent evaluations of the global Se budget, approximately 13,000 − 19,000 tons of Se is cycled through the troposphere

annually. Selenium is an essential nutrient for many plants and animals; however, there is a fine line between enough and excess selenium which can be toxic [*Wilber, 1980; Amouroux et al., 2001*]. Lack of enough Se has been recognized in some parts of China as the cause for Keshan disease, an endemic cardiomyopathy, and Kashin-Beck disease, a deforming arthritis [*Fordyce et al., 2000; Rayman, 2000*].

Although it has been established that dimethyl selenide, in particular, does not undergo photolysis in the troposphere, suggesting that its atmospheric removal is dominated by reactions with hydroxyl radicals, nitrate radicals, and/or ozone [*Atkinson et al., 1990*]. The reactions of halogen atoms (as well as halogen monoxides) with DMSe may also be of importance. Because oxidized selenium compounds are quite non-volatile, DMSe oxidation products may play a role in the formation or growth of aerosols, and condensed phase chemistry is expected to be an important component of atmospheric selenium transformation chemistry. Considerable levels of Se in particulate form (up to 3 ng m^{-3}) have been observed by a number of field studies at different sites around the world [*Beavington et al., 2004; Eldred, 1997; Kagawa et al., 2003; Mosher and Duce, 1987*]. Aerosol formation by selenium species is certainly of less significance to global climate modification than aerosol formation by sulfur species due to the scarcity of selenium in the atmosphere. Interest in the atmospheric chemistry of selenium focuses more on understanding the influence of oceanic emission, atmospheric transport, and atmospheric transformation on selenium levels and speciation observed in terrestrial environments than on climate impacts.

DMSe oxidation products are likely to be less volatile than the analogous DMS species. Most studies suggest that atmospheric deposition is an important source of Se

contamination, and it is therefore critical to evaluate the source emissions and fate of Se in the atmosphere. Since the majority of atmospheric Se exists in the form of DMSe, determination of the kinetics and oxidation mechanisms of DMSe will go a long way towards understanding the global biogeochemical cycle of Se.

The atmospheric transport, transformation and removal of Se has been reviewed by several investigators [*Ross, 1984; Wen and Carignan, 2007*]. Only a few papers describing lab studies of potentially important reactions in the atmospheric oxidation of DMSe have appeared in the literature and as a result, the atmospheric chemistry of selenium remains poorly understood.

In chapters 6 we report studies of chlorine atom reactions with DMS and DMSe. The results are compared with prior literature when appropriate. The kinetic data are used to determine the importance of the halogen atom reaction as a loss process for DMS and DMSe relative to the reactions with OH, NO_3, and O_3; thermodynamic information is also obtained.

The radical reactions studied in this work are halogen reactions with a series of Cl reactions with alkyl bromides (Chapter 3), Cl + isoprene (Chapter 4), Br reactions with isoprene, tetramethyl ethylene and 1,3-butadiene (Chapter 5), Cl + dimethyl sulfide and dimethyl selenide (Chapter 6). Laser flash photolysis (LFP) was used to generate radical species and was coupled with time resolved atomic resonance fluorescence (RF) spectroscopic detection of Cl or Br. The experimental technique employed is described in detail in Chapter 2. Most of the subject reactions were studied over a range of temperature and pressure towards the evaluation of kinetic and mechanistic information,

which has been used to assess the potential importance of the reactions in the atmosphere. Chapter 7 provides a summary of the results as well as suggestions for future work.

CHAPTER 2

EXPERIMENTAL TECHNIQUES

Experimental Approach

All of the atom-molecule reactions discussed throughout this thesis were initiated by ultraviolet laser flash photolysis (LFP) of a particular radical precursor resulting in direct production of the desired free radical. LFP was then coupled with time resolved resonance fluorescence (RF) spectroscopic detection of halogen atoms, (Cl and Br) and atom temporal profiles of the atomic species (either the radical reactant or a product) were monitored under pseudo first-order conditions with the concentrations of the reactant species (molecule) in large excess over that of the atomic reactant. A flowing gas mixture consisting of a reactant gas, suitable photolytic precursor(s), and buffer gas (N_2 or He) was passed through a reaction cell. The LFP-RF apparatus and some general experimental methods employed in this work are discussed in detail below, while the experimental details specific to each study including preparation and measurement of the reagent chemicals are presented separately in the appropriate chapters devoted to individual studies.

The LFP-RF technique has been employed in our laboratory in numerous studies of the kinetics of reactions involving halogen atoms [*Bilde et al., 1997; Jefferson et al., 1994; Nicovich et al., 1995; Nicovich et al., 1996; Nicovich et al., 2006; Piety et al., 1998; Strekowski et al., 2004; Wine et al., 1985; Laine et al., 2011a; 2011b*]. A schematic of the apparatus is shown in Figure 2.1. Its major components include a temperature-controlled

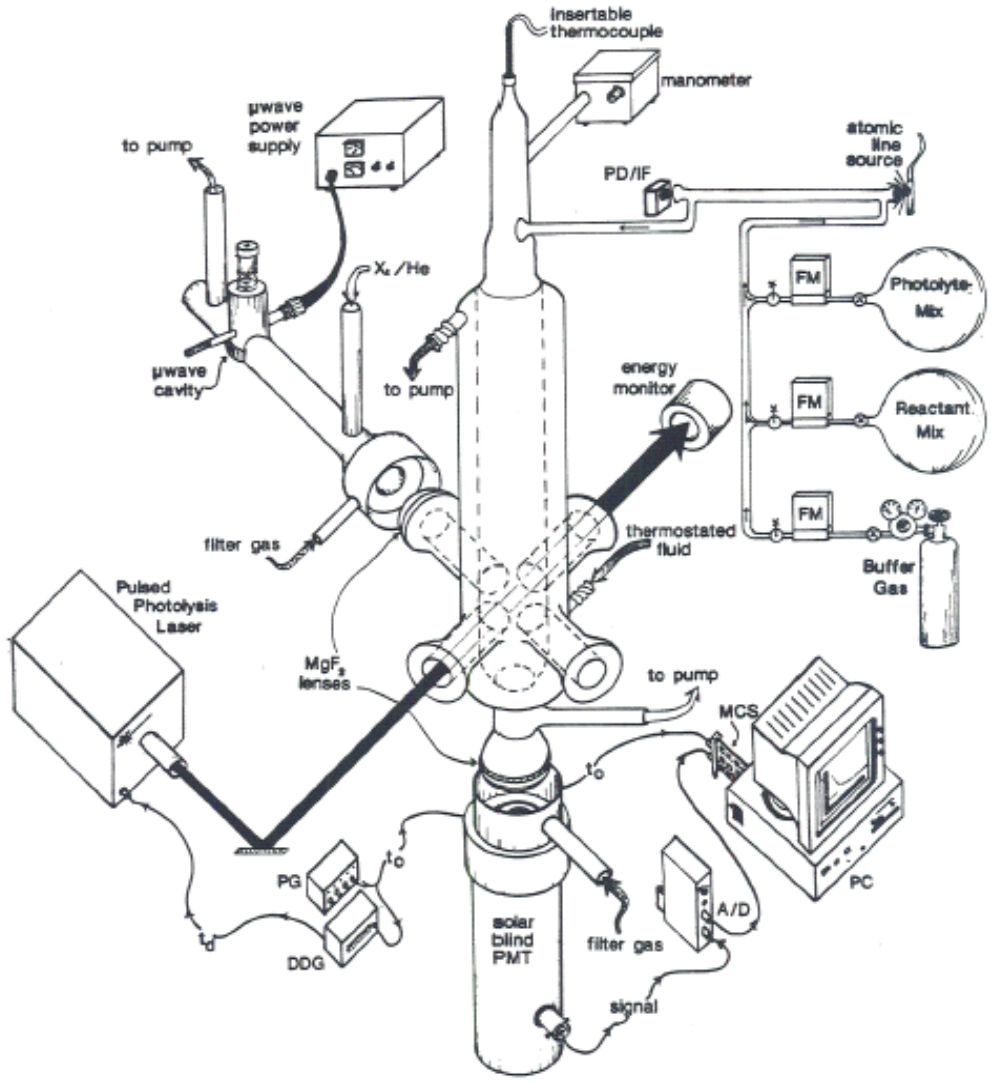

Figure 2.1 Schematic diagram of the LFP–RF apparatus. PG: pulse generator; DDG: digital delay generator; A/D: amplifier/Discriminator; PMT: photomultiplier; FM: mass flow meter; PD/IF: photodetector/interference filter; MCS: multichannel scalar. The figure was generated by J. M. Nicovich and P. H. Wine of Georgia Institute of Technology and appears on p.146 of Finlayson Pitts and Pitts [2000].

reaction cell, a photolysis laser, an atomic resonance lamp, a solar blind photomultiplier tube (PMT), and the appropriate detection electronics.

Two different jacketed Pyrex reaction cells, both with internal volumes of 150 cm^3, were used in all LFP–RF experiments where $T \leq 436$ K. The second reaction cell is different from the one shown in Figure 2.1 in that it is specially designed to minimize the throughput path of resonance radiation; a diagram of this cell, which allows vacuum-UV Br fluorescence to be observable in the presence of significant concentrations of O_2, is shown in Figure 2.2. The jacketed cells were maintained at a constant temperature by circulating either ethylene glycol (for $T > 298$ K) or a 2:1 ethanol-methanol mixture (for $T < 298$ K) from a thermostated bath through the outer jacket. Copper-constantan (Type T) or chromel-alumel (Type K) thermocouples were inserted into the reaction zone through a vacuum seal, allowing the measurement of gas temperature under the precise pressure and flow rate conditions of the experiment. The temperature variation in the reaction zone, that is, the volume from which fluorescence could be detected, was less than ± 3 K at the temperature extremes of the studies.

For all experiments at $T > 436$ K, an all pyrex reaction cell with an internal volume of approximately 200 cm^3 was resistively heated by using electrically insulated nichrome wire windings wrapped around the outer surface. The wire heaters were covered with ceramic felt and layers of stainless-steel radiation shields. Air-cooled jackets on the arms of the reaction cell allowed the O-ring joints to be kept near 298 K. The temperature of the gas mixture inside the reaction zone was measured using a chromel-alumel thermocouple inserted through a vacuum seal. The temperature gradient

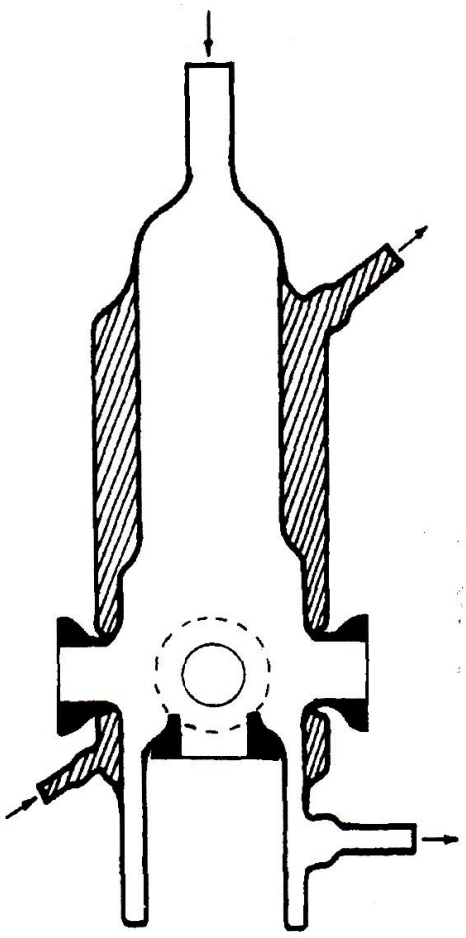

Figure 2.2 Diagram of the reaction cell specially designed to minimize the throughput path of resonance radiation. The figure was taken from [*Nicovich et al.*, 1990].

between in the top and bottom of the reaction zone (~1.5cm) was approximately ± 3 K and was found not to be a significant source of uncertainty.

Atomic species were produced by laser flash photolysis of suitable photolytic precursors. Photolysis of Cl_2CO at $\lambda < 270$ nm or photolysis of Cl_2 at 300 nm $< \lambda <$ 400 nm is most commonly employed for generation of Cl atoms in laboratory studies. The wavelengths employed in this study include 248 nm and 266 nm photolysis of Cl_2CO or CF_2Br_2 and 355 nm photolysis of Cl_2 or Br_2. Generally, Cl_2CO is a friendlier photolyte for Cl atom generation than Cl_2 because Cl_2 reacts with the alkyl radicals produced by the hydrogen abstraction reactions between Cl and organic compounds, thus, regenerating Cl atoms. The Cl kinetics can be influenced by these recycled Cl atoms. We employed Cl_2CO in the studies of Cl reactions with bromoethane, *n*-bromopropane, isoprene, and dimethyl selenide. However, in the study of Cl + 1,2-dibromoethane, strong absorption of dibromoethane at $\lambda < 300$ nm precluded the use of Cl_2CO, so Cl_2 photolysis at 355 nm was used to generate Cl atoms. Sufficient variations were conducted to ensure the kinetic data were not affected by secondary chemistry.

Br atom chemistry was also investigated. The most common method for Br atom production was CF_2Br_2 photolysis at 248 or 266 nm, however, Br_2 photolysis at 355 nm was employed on some occasions, but Br_2 presents problems similar to those associated with the use of Cl_2 as mentioned above.

An atomic resonance lamp, situated perpendicular to the photolysis laser, excited resonance fluorescence in the probed atoms. The resonance lamp consisted of an electrodeless microwave discharge through about 1 Torr of a flowing mixture containing a trace of atom precursor (X_2) in He, e.g., X = Cl or Br. The flow of the X_2 / He mixture

and pure He into the lamp were controlled by separate needle valves which allowed the total pressure and the X_2 concentration to be independently adjusted for the optimum signal-to-noise ratio. A commercial microwave generator (Opthos, MPG 4M) coupled to an Evenson cavity was used to excite a discharge in the lamp, which produced high energy atomic species that emit vacuum UV radiation at their atomic transition wavelengths, 135–140 nm for Cl atoms and 138 nm and 145-165 nm for Br atoms. The low energy lines for Br (163 nm) allow us to detect these atoms in the presence of O_2. This emission was coupled out of the lamp through an MgF_2 window and into the reaction cell through an MgF_2 lens. In cases where Cl detection was employed, the region between the resonance lamp and the reaction cell was purged with N_2 to minimize the absorption of vacuum UV resonance radiation by O_2 and H_2O. In experiments where Br detection was employed, before entering the reaction cell the lamp output passed through a flowing gas filter containing 75−150 Torr-cm of methane. The methane filter prevented radiation at wavelengths shorter than 140 nm (including impurity emissions from excited oxygen, hydrogen, and nitrogen atoms) from entering the reaction cell but transmitted the strong bromine lines at $\lambda > 140$ nm. The atoms in the reaction cell absorbed the radiation and relaxed to ground states by fluorescence, which was collected by a CaF_2 lens and imaged onto the photocathode of a solar blind photomultiplier. The CaF_2 lens eliminated detection of emissions at wavelengths shorter than 125 nm (Lyman-α emission, for example). The region between the reaction cell and the photomultiplier was also purged with N_2. Fluorescence intensities were found to vary linearly with atom concentration up to levels several times higher than any employed in the kinetic experiments. Signals were processed using photon counting techniques in conjunction

with multichannel scaling. A preamplifier/discriminator (Advanced Research Instruments Corporation, F-100T) and an amplifier (California Avionics Laboratories, Inc.) were used to minimize background noise and optimize the photon counting signal to noise ratio. The multichannel scaler sweep was triggered prior to the photolysis laser to allow a pre-flash baseline to be obtained. For each experiment, signals from a large number of laser shots were averaged to obtain a temporal profile with adequate signal-to-noise for quantitative kinetic analysis.

It is worth noting that the resonance fluorescence detection scheme is sensitive to both ground state ($^2P_{3/2}$) and spin-orbit excited state ($^2P_{1/2}$) Cl and Br atoms. Approximately 0.5 Torr CO_2 was added to each reaction mixture in order to rapidly deactivate any spin-orbit excited halogen atoms. The fraction of excited Cl($^2P_{1/2}$) produced by the ultraviolet photo-dissociation of phosgene is reported to be ~15% at 235 nm [*Maul et al., 1995*]. Rate coefficients for quenching of Cl($^2P_{1/2}$) by N_2, Cl_2CO, and CO_2 are reported to be (in units of cm^3 $molecule^{-1}$ s^{-1}), 5.0×10^{-15} [*Tyndall et al., 1995*], 3.0×10^{-10} [*Chichinin, 1993*], and 9.0×10^{-12} [*Chichinin, 1996*] respectively. For typical Cl_2CO concentrations ($1.5–7.0 \times 10^{13}$ molecules cm^{-3}) and pressures employed in this study, equilibration of the spin-orbit states via collision with CO_2, N_2 and Cl_2CO occurred on a time scale that was short compared to the time scale for chemical reactions under a majority of the experimental conditions employed ($< 10^{-4}$ s^{-1}). The fraction of excited Br($^2P_{1/2}$) produced by the ultraviolet photo-dissociation of CF_2Br_2 is reported to be ~45% at 265 nm [*Park et al., 2001*]. Rate coefficients for quenching of Br($^2P_{1/2}$) by N_2 and CO_2 are reported to be (in units of cm^3 $molecule^{-1}$ s^{-1}) $(2.5 - 14) \times 10^{-15}$ [*Donovan and Husain, 1966; Johnson et al., 1996*] and 1.5×10^{-11} [*Peterson, et al. 1975*],

respectively. Equilibration of the spin-orbit states via collision with CO_2 occurred on a time scale that was short compared to the time scale for chemical reactions ($> 8 \times 10^{-5}$ s) under a majority of the experimental conditions employed. The rapid deactivation of excited state halogen atoms avoided any problems associated with the difference in detection sensitivities for the two atomic halogen electronic states. In addition, it can be safely assumed that all the data reported in this study were representative of an equilibrium mixture of halogen atom spin-orbit states.

Gas Flow System

All experiments were carried out under "slow flow" conditions, with a linear flow rate (2-6 cm s^{-1}) sufficient to replenish the reaction mixture between photolysis laser pulses. The gases were introduced into the reaction cell from their respective containers (high pressure tanks or Pyrex bulbs) through Teflon or stainless steel tubing. All gas flows were measured by calibrated mass flow meters (MKS Instruments, model 0258B) connected to a shut-off valve and a needle valve. A capacitance manometer pressure gauge attached to the inlet port of the reaction cell provided the pressure measurement for the reaction cell. After passing through the reaction cell and/or the downstream photometry cell, the gas flow was exhausted through a throttle valve by a mechanical pump. A liquid nitrogen cold trap was used prior to the pump to remove toxic and corrosive gases in the flow as well as prevent the pump oil from diffusing back into the reaction cell.

The reagent gases were flowed from Pyrex bulbs, and reagent gas concentrations in the flowing gas mixtures were calculated using the following equation:

$$[X] = \frac{F_x \chi P}{F_{total} k_B T} \tag{2-I}$$

where F_x is the flow rate of the reagent gas, F_{total} is the flow rate of the total gas, χ is the mole fraction of the reagent gas in the bulb (refer to 2-II), P is pressure (Torr), T is temperature (K), and k_B is the Boltzmann constant (1.035×10^{-19} Torr cm^3 K^{-1}).

Bulb Concentration Determination

The mole fraction of a reagent gas in its storage bulb was measured by photometry methods at 298 K in a high vacuum gas handling system. A fraction of the bulb mixture was introduced into a vacuum sealed cylindrical Pyrex cell (35 − 200 cm long) with the pressure measured by capacitance manometers (0–1000 Torr and 0–10 Torr). A penray lamp was used as the light source and a photo-multiplier tube (PMT) with an interference band pass filter mounted in front of the PMT photocathode was used as the detector, or in some instances, a SPEX 1681 0.22 m monochromator was used in place of a band pass filter. The PMT current output was monitored by a digital picoammeter. The mole fraction of the absorbing gas was determined by recording the light intensity (current) as a function of pressure in the absorption cell and employing Beer's law,

$$\chi = \frac{k_B T \ln(\frac{I_0}{I})}{\sigma(\lambda) l P}. \tag{2-II}$$

In equation (2-II) I_0 is the initial current (no absorbing gas in the cell), I is the measured current in the presence of absorbing gas, $\sigma(\lambda)$ is the absorption cross-section of the gas at

wavelength λ (cm^2), *l* is the path length of the absorption cell (cm), P is pressure (Torr), T is temperature (K), and k_B is the Boltzmann constant (1.035×10^{-19} Torr cm^3 K^{-1}). The bulb fraction of a reagent gas was usually measured multiple times during the course of the experiments; the agreement of different measurements was very good (<5%).

Absorption Cross-section Measurements

Accurate absorption cross-sections have been obtained during the course of the experiments in an effort to increase the confidence of the concentration measurements. The absorption cross-section measurements were conducted in the same gas handling system as the bulb fraction measurements. The pure reagent sample, usually a liquid, was transferred to a vial fitted with a high-vacuum stopcock and introduced into a vacuum sealed cylindrical Pyrex absorption cell that was 1 inch (2.54 cm) in length. The pressure was measured by capacitance manometers (0–1000 Torr and 0–10 Torr). An appropriate Penray® lamp (213.9 nm (Zn), 228.8 nm (Cd), 254 nm (Hg)) was placed at one side of the absorption cell as the light source and a PMT with a corresponding interference band pass filter or monochromator mounted in front of the PMT photocathode was placed at the other side as the detector. The absorption cross-section of a given compound can be derived as below (Beer's law).

$$\sigma(\lambda) = \frac{k_B T \ln(\frac{I_0}{I})}{lP}(cm^2) \qquad \text{(2-III)}$$

where I_0 is the initial current (no absorbing gas in the cell), I is the measured current, *l* is the path length of the absorption cell (2.54 cm), P is pressure (Torr), T is temperature (K),

and k_B is the Boltzmann constant (1.035×10^{-19} Torr cm^3 K^{-1}). In order to ensure that sample photolysis did not affect cross section measurements the following steps were taken (i) numerous absorption measurements were taken for each sample over a wide range of pressures and (ii) the light source was blocked at times when readings were not taken. No dependence on the cross section was observed with either time or with pressure.

CHAPTER 3

KINETIC AND MECHANISTIC STUDY OF THE REACTIONS OF ATOMIC CHLORINE WITH BROMOETHANE, 1-BROMOPROPANE, AND 1,2-DIBROMOETHANE

Introduction

Halogenated alkanes are present in the atmosphere as a result of both natural and anthropogenic processes. The bromoalkanes (R-Br) ethyl bromide (CH_3CH_2Br), n-propylbromide ($CH_3CH_2CH_2Br$), and 1,2-dibromoethane (CH_2BrCH_2Br) are emitted into the atmosphere primarily from anthropogenic sources [*Brasseur et al., 1999*] and all three have been identified in a recent World Meteorological Organization (WMO) report as very short-lived (lifetime less than 6 months) source gases with significant ozone depletion potentials (ODPs) [*Law et al., 2006*]. Brominated very short-lived compounds are thought to contribute 20-25% of total stratospheric bromine [*Law et al., 2006*]. Although stratospheric levels of bromine are considerably lower than levels of chlorine, ODPs for organic bromine compounds are much higher than for analogous organic chlorine compounds. Hence, there is considerable interest in understanding the atmospheric chemistry of even relatively short-lived organic bromine compounds. The brominated alkanes investigated herein (CH_3CH_2Br, $CH_3CH_2CH_2Br$, CH_2Br-CH_2Br) are also of interest as model compounds for larger partially halogenated organics found in the atmosphere, and they have been considered as potential replacement compounds for

chlorofluorocarbons (CFCs) that have been banned as a result of the Montreal Protocol [*Wuebbles et al., 1998*].

The primary tropospheric sink for most alkyl bromides including the three of interest in this study is widely accepted to be reaction with OH radicals [*Brioude et al., 2010*]. It has been reported that levels of Cl atoms in the marine boundary layer can be 1-10% of OH levels [*Wingenter et al., 2005*], and recent findings suggest a significant Cl production rate even in the middle of the continental United States.[*Thornton et al., 2010*] Recent laboratory and theoretical research demonstrates that heterogeneous reaction of N_2O_5 with HCl may represent a significant source of tropospheric $ClNO_x$ species that can rapidly photolyze under daytime conditions to generate Cl atoms [*Raff et al., 2009*]. Hence, it appears that Cl + R-Br reactions could be significant tropospheric sinks for R-Br in cases where the Cl + R-Br reaction is considerably faster than the corresponding OH + R-Br reaction.

In this study, the kinetics of Cl reactions with the three alkyl bromides of interest are investigated as a function of temperature and pressure.

$$Cl + CH_3CH_2Br \rightarrow \text{products} \quad (3.1)$$

$$Cl + CH_3CH_2H_2Br \rightarrow \text{products} \quad (3.2)$$

$$Cl + CH_2BrCH_2Br \rightarrow \text{products} \quad (3.3)$$

Rate coefficients for reactions of OH with the above alkyl bromides are reasonably well established over the relevant atmospheric temperature regime [*Sander et al., 2011; Howard et al., 1976; Xing et al., 1992; Qiu et al., 1992; Donaghy et al., 1993; Teton et al., 1996; Nelson et al., 1997; Herndon et al., 2001; Gilles et al., 2002; Kozlov et al.,*

2003]. However, there is very little published data for the corresponding Cl reactions. One room-temperature competitive kinetics study has been reported for reactions 1 and 2, [*Donaghy et al., 1993*] and one product study for reaction 1 at T = 226-298 K in 1 atm air has also been reported.[*Orlando et al., 2002*] The limited available data suggest that reactions 1 and 2 are substantially faster at room temperature than their corresponding OH reactions. In addition to the experimental results cited above, computational studies are reported that address the kinetics of OH + CH_2BrCH_2Br,[*Cohen and Benson,* 1987] the mechanism of Cl + $CH_3CH_2CH_2Br$,[*Rosado-Reyes et al., 2008*] and the OH-initiated oxidations of all three R-Br compounds of interest.[*Rosado-Reyes et al., 2008; Martinez-Aviles et al., 2007; Martinez-Aviles et al., 2008a; 2008b; Christiansen and Fransisco, 2009*]

In this study, we employ monitoring of Br appearance temporal profiles to obtain kinetic information as well as some product branching information for the title reactions. Our study represents the first temperature-dependent kinetics study of Cl reactions with the alkyl bromides of interest. Temperature-dependent rate coefficients and Br yields, which provide information about branching ratios for H abstraction at the β position, are reported. The potential importance of reaction with Cl as an atmospheric degradation pathway for the R−Br compounds of interest is qualitatively assessed.

Experimental Details

The experimental approach involves production of Cl by laser flash photolysis (LFP) of suitable precursors in conjunction with time-resolved monitoring of Br atom appearance by atomic resonance fluorescence (RF) spectroscopy. The descriptions of the

apparatus and the technique can be found in Chapter 2 and only details particular to the studies of Cl + R-Br reactions are discussed below.

Chlorine atoms were produced by the following methods

$$Cl_2CO + h\nu\ (266\ nm) \rightarrow 2Cl + CO \qquad (3.4)$$

$$Cl_2 + h\nu\ (355\ nm) \rightarrow 2Cl \qquad (3.5)$$

Reactions (3.1) and (3.2) were studied using 266 nm photolysis of Cl_2CO/R-Br/N_2 mixtures. Both CH_3CH_2Br and $CH_3CH_2CH_2Br$ are transparent at 266 nm, whereas CH_2BrCH_2Br absorbs significantly at this wavelength (σ = 1.1 x 10^{-20} cm^2 $molecule^{-1}$) [*Uthman et al., 1978*]. As a result, reaction (3.3) was studied using 355 nm photolysis of Cl_2 as the chlorine atom source. Fourth harmonic radiation from a Quanta Ray model DCR-3 Nd:YAG laser served as the 266 nm light source, and third harmonic radiation from the same laser served as the 355 nm light source. The maximum repetition rate was 10 Hz, the pulse width was ~6 ns, and laser fluence ranges in units of mJ cm^{-2} $pulse^{-1}$ were 3-12 at 266 nm and 15-40 at 355 nm. Chlorine atom concentrations produced by the laser flash were typically in the range (3-7) × 10^{11} atoms cm^{-3}.

The alkyl bromides, Br_2, and photolytes flowed into the reaction cell from 12 L bulbs containing dilute mixtures in nitrogen while CO_2, helium, and additional nitrogen flowed directly from their storage cylinders. The fraction of R-Br in each R-Br/N_2 mixture was checked frequently by UV photometry at 213.9 nm (Zn Penray® lamp). Absorption cross sections used to convert measured absorbances to concentrations were measured as part of this study; in units of 10^{-19} cm^2 $molecule^{-1}$, they were found to be 21.0 for CH_2Br-CH_2Br (21.035), 4.93 for $CH_3CH_2CH_2Br$ (5.017), and 4.08 for

CH_3CH_2Br (4.5036), where the numbers in parentheses are literature values for the cross sections. Our reported 213.9 nm cross sections are in excellent agreement with the literature values forCH_2BrCH_2Br [*Zhang et al., 1990*] and $CH_3CH_2CH_2Br$ [*Kozlov et al., 2003*]. Our measured CH_3CH_2Br cross section, however, is ~10% lower than the value extracted from a published low-resolution undigitized spectrum [*Meller et al., 1991*]. As mentioned above, we used our measured cross sections (in conjunction with absorbance, pressure, and temperature measurements) to evaluate the mole fraction of each alkyl bromide in each storage bulb.

The gases and liquids used in this study had the following stated minimum purities: N_2 (UHP, 99.999%), He (UHP, 99.999%), CO_2 (Instrument grade, 99.99%), Cl_2 (Research grade, 99.999%), Cl_2CO (99.0%), Br_2 (99.5þ%), CH_3CH_2Br (99.0%), $CH_3CH_2CH_2Br$ (99.0%), and CH_2BrCH_2Br (99.0%). All R-Br samples were obtained from Sigma Aldrich. For Cl_2, Cl_2CO, and CO_2, the stated purity refers to the liquid phase in the high-pressure gas cylinder. For the alkyl bromides, stated purity refers to liquid samples. The gases N_2, He, CO_2, and Cl_2CO were used as supplied, while the alkyl bromides and Br_2 were degassed repeatedly at 77 K and then stored in pyrex vials fitted with high vacuum stopcocks. Photometric measurements at 405 nm (Hg Penray® lamp light source) showed the mole fraction of Br_2 in the R-Br samples to be less than 5×10^{-5} in all cases.

Results and Discussion: Kinetics

All experiments were carried out under pseudo-first order conditions with [R-Br] >> $[Cl]_0$. Bimolecular rate coefficients, $k_i(T,P)$ (i = 3.1-3.3), were determined by measuring pseudo first-order Br appearance rates as a function of R-Br concentration. Atomic Br is

generated via rapid elimination of Br from the radical produced when Cl abstracts hydrogen at the β position. At the temperatures and pressures employed in this study, the CH_2CH_2Br product of reaction 3.1, the CH_3CHCH_2Br product of reaction 3.2, and the only possible H-abstraction product of reaction 3.3 all eliminate Br rapidly enough that the rate-limiting step in Br generation is the Cl + R-Br reaction; evidence from the literature that supports this conclusion is discussed below.

Experiments were performed over a wide range of temperatures (221-569 K) and at total pressures ranging from 25 to 100 Torr N_2. The fate of Cl atoms is controlled by reaction with R-Br, loss by reaction with background impurities, and loss by diffusion from the detector field of view.

$$Cl \rightarrow \text{Reaction with background impurities and/or loss by diffusion from the detector field of view.} \qquad (3.6)$$

Reaction mixtures used to study reactions 3.1 and 3.2 contained (4.5-12) × 10^{14} Cl_2CO per cm^3. The 0.5 Torr CO_2 added to deactivate $Br(^2P_{1/2})$ also effectively deactivates $Cl(^2P_{1/2})$; the rate coefficient for collisional deactivation of $Cl(^2P_{1/2})$ by CO_2 is known to be (1.2 (± 0.3) × 10^{-11} cm^3 $molecule^{-1}$ s^{-1} [*Sotnichenko et al.,* 1988; *Matsumi et al.,* 1997; *Chichinin,* 1996]. Therefore, it can be safely assumed that all the data reported in this study are representative of equilibrium mixtures of Cl and Br spin-orbit states.

The temporal profile of Br fluorescence following the laser flash can be well described by the following expression

$$S_t / S_0 = \{k_a / (k_d - k_a)\}A\{\exp(-k_a t) - \exp(-k_d t)\} + B \exp(-k_d t) \qquad (3\text{-I})$$

In eq 3-I, S_t is the fluorescence signal at time t after the laser flash, S_0 is the signal at time zero, i.e., immediately after the flash, k_a represents the pseudo-first-order rate coefficient for Br appearance (which is equal to the pseudo-first-order rate coefficient for Cl disappearance), k_d is the rate coefficient for Br decay (assumed to be first order), A represents the magnitude of the Br signal that would be obtained from the Cl + R-Br reaction if there were no competing losses of Br, and B represents the Br signal generated at t = 0 via photolysis of R-Br. Equation 3-I is the standard textbook integrated rate equation describing the time evolution of the intermediate in consecutive first order reactions [*Pilling and Seakins, 2005*] except for the last term, which arises when the concentration of the intermediate (Br) is not zero at time zero. For reactions 3.1 and 3.2, where there are parallel pathways only one of which leads to Br formation, the parameter A is proportional not only to $[Cl]_0$ but also to the ratio k_{ia}/k_i (i = 3.1 or 3.2),where k_{ia} is the rate coefficient for the β-H abstraction channel that results in rapid elimination of Br.

Each observed Br temporal profile was fit to the double exponential eq 3-I using a nonlinear least-squares method to obtain values for k_a, k_d, A, and B. The first-order decay rate coefficient k_d is found to be much smaller than the first-order appearance rate coefficient k_a in all experiments; hence, the assumption that k_d is first order, while not strictly correct, does not compromise the accuracy of the analysis for obtaining k_a and A, the fit parameters of primary interest. The value of the parameter B in eq 3-I was only a few percent of the value of A in all cases, except in preliminary experiments where 266 nm photolysis of Cl_2CO was employed to study reaction 3.3. In that case the value of B was as large as 50-60% of the value of A due to CH_2BrCH_2Br photolysis. For this reason, all reported data for reaction 3.3 were obtained employing 355 nm LFP of Cl_2 as the

atomic chlorine source. Reaction mixtures used to study reaction 3 contained (2.2-11) × 10^{13} Cl_2 per cm^3.

Measured Br pseudo-first-order appearance rates, k_a, were found to increase linearly as a function of [R-Br], ranging from 1500 to 12 800 s^{-1} over the range of [R-Br] employed. No systematic trend in obtained kinetic parameters was observed as a result of variations in $[Cl_2CO]$, $[Cl]_0$, laser fluence, or laser repetition rate. Typical Br appearance temporal profiles observed as a function of $[CH_3CH_2CH_2Br]$ concentration are shown in Figure 3.1. As mentioned above, each bimolecular rate coefficient, $k_i(T,P)$ (i = 3.1-3.3), was obtained from the variation of k_a with [R-Br]. Figure 3.2 shows plots of k_a vs $[CH_3CH_2Br]$ at three temperatures. As expected, when reactivity is dominated by hydrogen abstraction, rate coefficients for reactions (3.1) and (3.3) are found to be independent of pressure (see Tables 3.1 and 3.3). Rate coefficients for reaction 3.2 are presumably also independent of pressure, although in this case all data were collected at a pressure of 50 Torr.

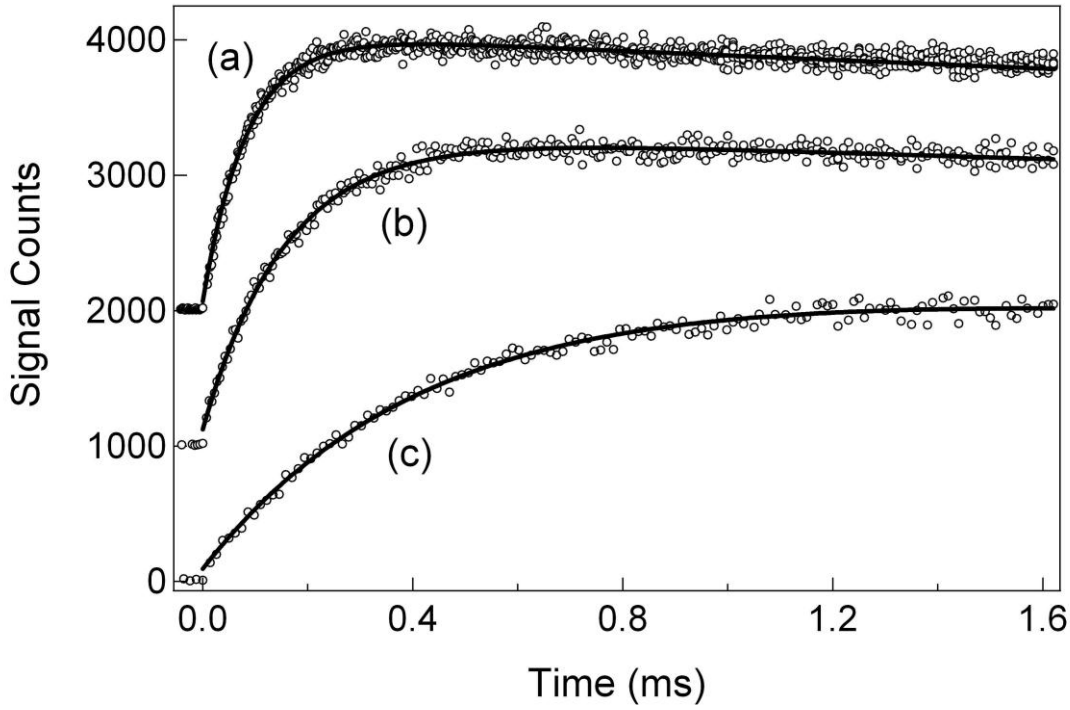

Figure 3.1 Appearance temporal profiles observed following LFP of $Cl_2CO/CH_3CH_2CH_2Br/N_2$ mixtures. T = 296 K and P = 50 Torr. Concentrations in units of 10^{11} per cm^3: $[Cl_2CO]$ = 9260; $[Cl]_0$ = 7; $[CH_3CH_2\text{-}CH_2Br]$ = (a) 2230, (b) 1110, (c) 419. Solid lines are obtained from nonlinear least-squares fits to eq 3-I, which give the following best-fit parameters: $k_a(s^{-1})$ = (a) 12 500, (b) 6270, and (c) 2320; $k_d(s^{-1})$ = (a) 74, (b) 55, (c) 61; A = (a) 1980, (b) 2230, (c) 2130; B = (a) 39, (b) 67, (c) 97. To optimize the quality of the information presented, traces a and b are offset upward by 1000 and 2000 counts, respectively, and only data obtained in the first 1.6 ms after the laser flash are shown. Data were actually collected for 2000 channels with the multichannel scalar dwell time set at (a) 2, (b) 5, and (c) 12 μs.

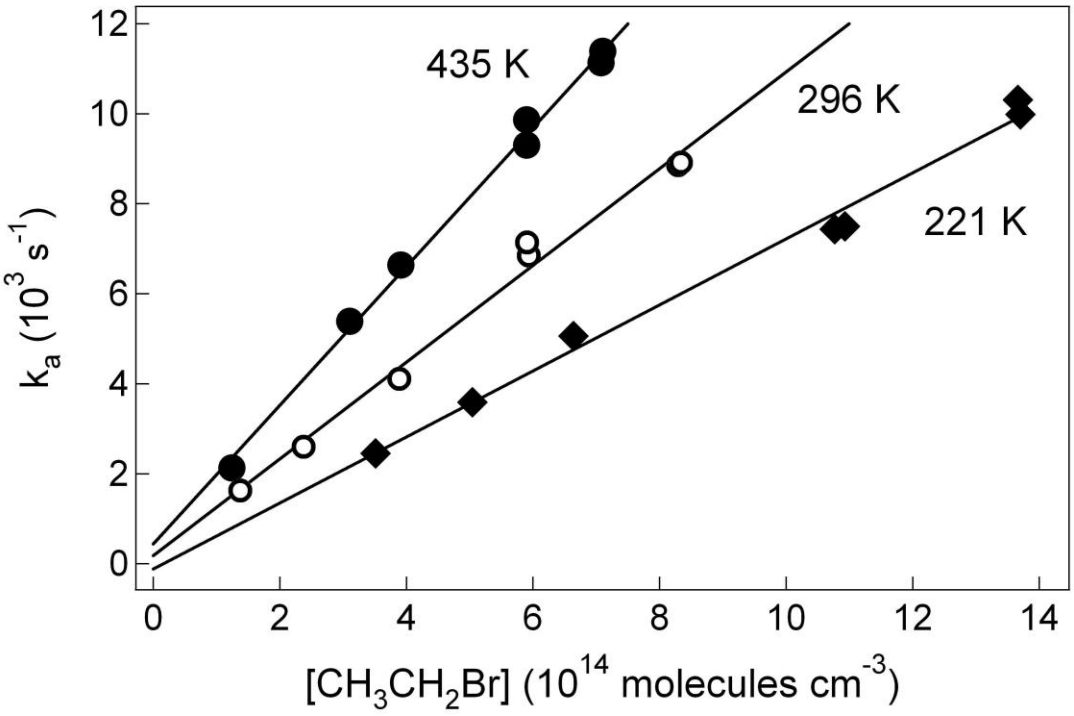

Figure 3.2 Plots of k_a vs [CH_3CH_2Br] for data obtained at P = 50 Torr over a range of T. Solid lines are obtained from linear least-squares analyses, and their slopes give the following values for $k_{3.1}(T)$ in units of 10^{-12} cm^3 $molecule^{-1}$ s^{-1}: 7.34 ± 0.64 at 221 K, 10.8 ± 1.1 at 296 K, and 15.4 ± 0.9 at 435 K; uncertainties are 2σ, precision only.

Kinetic data for reactions (3.1-3.3) are summarized in Tables 3.1-3.3, and plots of *ln* k_i vs 1/T for all three reactions, along with previously reported 298 K rate coefficients, are shown in Figure 3.3. The following Arrhenius expressions are obtained from linear least-squares analyses of the *ln* k_i vs 1/T data for reactions 3.1 and 3.2 (units are cm^3 $molecule^{-1}$ s^{-1})

$k_{3.1}(T) = (3.73 \pm 0.50) \times 10^{-11} \exp[(-378 \pm 44) / T]$ $(221\ K \leq T \leq 435\ K)$

$k_{3.2}(T) = (5.14 \pm 0.78) \times 10^{-11} \exp[(21 \pm 42) / T]$ $(221\ K \leq T \leq 436\ K)$

Uncertainties in the above expressions are 2σ, precision only, and represent the uncertainties of the Arrhenius parameters; these uncertainties cannot be used in a straightforward way to obtain uncertainties in reported rate coefficients, which are discussed below. The observed temperature dependence for reaction 3.2 is so weak that the temperature-independent rate coefficient $k_{3.2} = (5.5 \pm 1.0) \times 10^{-11}$ cm^3 $molecule^{-1}$ s^{-1} is also an adequate representation of the data. While the temperature dependences observed for reactions (3.1 and 3.2) are well described by Arrhenius expressions, the plot of ln $k_{3.3}$ vs 1/T shows significant curvature. The data for reaction 3.3 have been fit to a modified Arrhenius expression, which reproduces the data quite well (units are cm^3 $molecule^{-1}$ s^{-1}; temperature range is 244-569 K)

$$k_{3.3}(T) = (2.79 \pm 0.30) \times 10^{-17} T^2 \exp[(-184 \pm 52)/T$$

In the above expression, the T exponent is fixed at 2; however, if this exponent is treated as an adjustable parameter, the bestfit value retrieved from the analysis is very close to 2,

i.e., 2.004. Uncertainties in the above expression for $k_{3.3}(T)$ are 2σ and represent precision only.

Table 3.1. Summary of Kinetic Data for the Cl + CH_3CH_2Br Reaction[a]

T	P	N[b]	$[Cl_2CO]$	$[Cl]_0$	$[CH_3CH_2Br]_{max}$	k'_{max}	$k_{3.1} \pm 2\sigma$ [c]
221	50	7	6500	5	13700	10300	7.34 ±0.65
250	50	7	6500	5	12000	9950	8.01±0.40
296	25	10	9500	7	10100	10100	9.99±0.26
296	50	7	9000	6	8340	8910	10.8±1.1
296	100	6	4000-9500	2-6	9960	10200	9.80±0.68
360	50	8	8200	5	8500	11100	13.6±0.5
435	50	7	5600	4	7100	11400	15.4±0.9

[a] Units: T (K); P (Torr); Concentrations (10^{11} per cm^3); k' (s^{-1}); $k_{3.1}$ (10^{-12} cm^3 $molecule^{-1}$ s^{-1}). [b] N = no. of experiments = no. of Br temporal profiles measured. [c] Uncertainties are precision only.

Table 3.2. Summary of Kinetic Data for the Cl + $CH_3CH_2CH_2Br$ Reaction[a,b]

T	N[c]	$[Cl_2CO]$	$[Cl]_0$	$[CH_3CH_2CH_2Br]_{max}$	k'_{max}	$k_{3.2} \pm 2\sigma$[d]
221	8	7000-8500	5	2250	12800	54.9±1.1
243	7	11000	7	1680	9700	58.1±2.5
296	7	9000	6	2280	12 700	56.6±1.0
358	8	5500-8000	4-6	1810	9560	52.0±1.2
436	7	3900	3	1360	7520	55.1±1.4

[a] Units: T (K); Concentrations (10^{11} per cm^3); k' (s^{-1}); $k_{3.2}$ (10^{-12} cm^3 $molecule^{-1}$ s^{-1}). [b] The pressure was 50 Torr in all experiments. [c]N= no.of experiments = no. of Br temporal profiles measured. [d] Uncertainties are precision only.

Table 3.3. Summary of Kinetic Data for the Cl + CH_2BrCH_2Br Reaction[a]

T	P	N[b]	$[Cl_2]$	$[Cl]_0$	$[CH_2Br\text{-}CH_2Br]_{max}$	k'_{max}	$k_{3.3} \pm 2\sigma$[c]
244	50	5	490	7	10 700	1050	0.855±0.040
260	50	5	490	6	33 100	3390	0.966±0.075
296	50	5	360	4	27 400	3720	1.28±0.08
296	50	5	1100	10	29 600	4380	1.43±0.07
296	100	5	370	5	29 600	4100	1.29±0.08
296	50	5	240	6	29 600	4140	1.38±0.23
296	25	5	410	4	27500	3960	1.31±0.16
296	50	9	400	2-16	29 500	4500	1.37±0.15
355	50	5	360	4	26 400	5400	1.96±0.17
420	50	5	370	4	21 500	6370	2.80±0.18
442	50	5	260	3	16 900	6570	3.73±0.35
512	50	5	380	5	16 100	7670	4.67±0.27
525	50	5	220	3	13 900	7800	5.56±0.18
529	50	4	610	3	17 700	9630	5.31±0.34
533	50	3	260	4	7440	4860	6.47±0.54
569	50	5	360	4	6040	4210	6.28±0.30

[a]Units: T (K); P (Torr); Concentrations (10^{11} cm^{-3}); k' (s^{-1}); $k_{3.3}$ (10^{-12} cm^3 $molecule^{-1}$ s^{-1}). [b]N = no. of experiments = no. of Br temporal profiles measured. [c]Uncertainties are precision only.

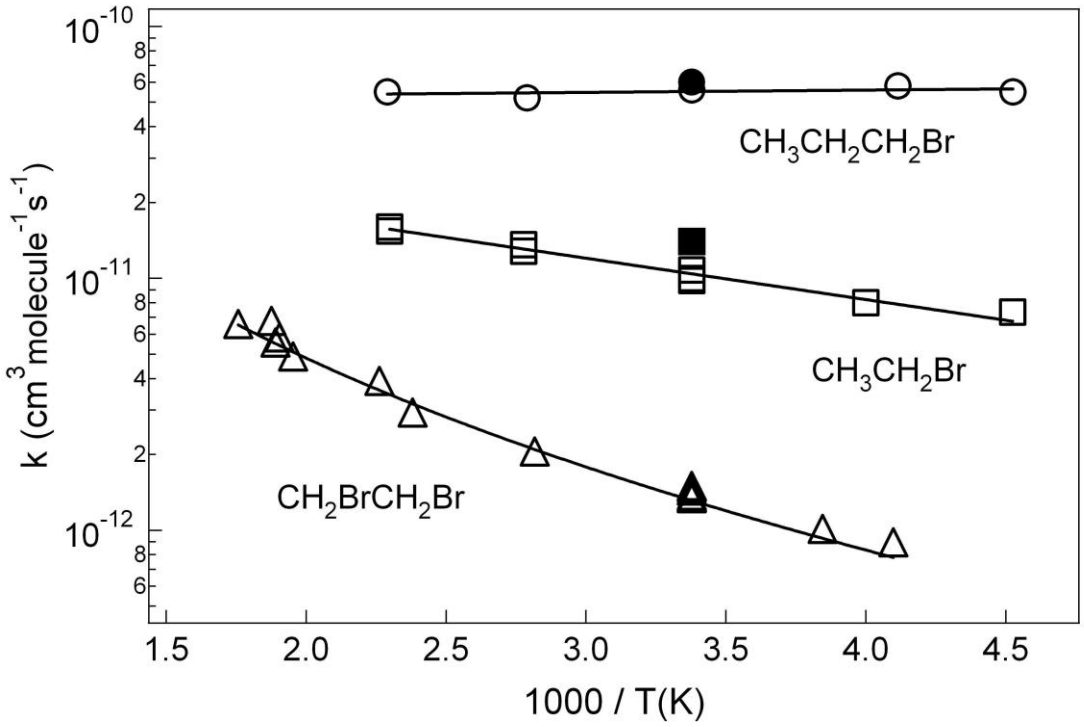

Figure 3.3 Arrhenius plots for Cl reactions with CH_3CH_2Br, $CH_3CH_2CH_2Br$, and CH_2BrCH_2Br. Solid lines are obtained from least-squares analyses which give the expressions reported in the text. Filled data points are values for 298 K rate coefficients reported in Donaghy *et al.* [*1993*].

Results and Discussion: Br Yields

Br Atom Yields (Branching Ratios for β-Hydrogen Abstraction)

By comparing product Br signal strengths with those obtained when Cl removal is dominated by reaction with Br_2 (where the Br yield is known to be unity), temperaturedependent branching ratios for abstraction of the β-hydrogen are obtained for reactions (3.1 and 3.2).

$$Cl + Br_2 \rightarrow Br + BrCl \qquad (3.7)$$

Yields were determined by comparison of the magnitude of the Br signal resulting from the Cl + R-Br reaction with the magnitude of the signal resulting from the Cl + Br_2 reaction. One critical step in obtaining accurate yield data is construction of calibration curves that correct for absorption of resonance radiation by R-Br and Br_2. The method for obtaining the calibration curves consisted of photolyzing CF_2Br_2 at 266 nm to generate a readily reproducible $[Br]_0$. Signal levels were then obtained as a function of [R-Br] (or $[Br_2]$), and plots of signal/$[Br]_0$ vs [R-Br] (or $[Br_2]$) were constructed covering the range of [R-Br] (or $[Br_2]$) used in the yield experiments. As expected, the signal strength fell exponentially as a function of [R-Br] (or $[Br_2]$). The data obtained as described above allow evaluation of the signal strength that would be observed in the limit of zero [R-Br] (or $[Br_2]$); comparison of such signal strengths in the limits where (i) essentially all Cl reacts with R-Br and (ii) essentially all Cl reacts with Br_2 allows the Br yield from Cl + R-Br to be evaluated. At the concentration levels employed in the yield measurements, signal attenuation was negligible for Br_2 and $CH_3CH_2CH_2Br$ but was significant for CH_3CH_2Br.

Br yields were obtained from multiple “back to back” experiments where the order in which the Cl + R-Br and Cl + Br_2 reactions were carried out was varied in order

to minimize the likelihood of systematic errors. Experiments employed photolysis mixtures containing 25-100 Torr N_2, 0.5 Torr CO_2, Cl_2CO (~90), and either CH_3CH_2Br (42-140), $CH_3CH_2CH_2Br$ (9.7-24), or Br_2 (1.7-6.8); numbers in parentheses are concentrations in units of 10^{13} molecules cm^{-3}. Typical back-to-back temporal profiles obtained with Cl consumption dominated by (i) Br_2 and (ii) $CH_3CH_2CH_2Br$ are shown in Figure 4. Since signal corrections are negligible for both Br_2 and $CH_3CH_2CH_2Br$, the yield is obtained directly from the ratio $A_{CH3CH2CH2Br}/A_{Br2}$, where the parameter A is defined in eq 3-I. Yield data for reactions (3.1 and 3.2) are summarized in Table 3.4, and Arrhenius-type plots of ln yield vs 1/T are shown in Figure 3.5.

On the time scale of our LFP experiments, reactions (3.1-3.3) are expected to result in Br atom formation only following abstraction of a hydrogen atom from a carbon adjacent to one containing a bromine atom, i.e., following abstraction of a β-hydrogen.

$Cl + CH_3CH_2Br \rightarrow HCl + [\bullet CH_2CH_2Br]$

$\rightarrow HCl + CH_2{=}CH_2 + Br$ (3.1a)

$\rightarrow HCl + CH_3C\bullet HBr$ (3.1b)

$Cl + CH_3CH_2CH_2Br \rightarrow HCl + [CH_3C\bullet HCH_2Br]$

$\rightarrow HCl + CH_3CH{=}CH_2 + Br$ (3.2a)

$\rightarrow HCl + CH_3CH_2C\bullet HBr$ (3.2b)

$\rightarrow HCl + C\bullet H_2CH_2CH_2Br$ (3.2c)

$Cl + CH_2BrCH_2Br \rightarrow HCl + [C\bullet HBrCH_2Br]$

$\rightarrow HCl + CH_2{=}CHBr + Br$ (3.3)

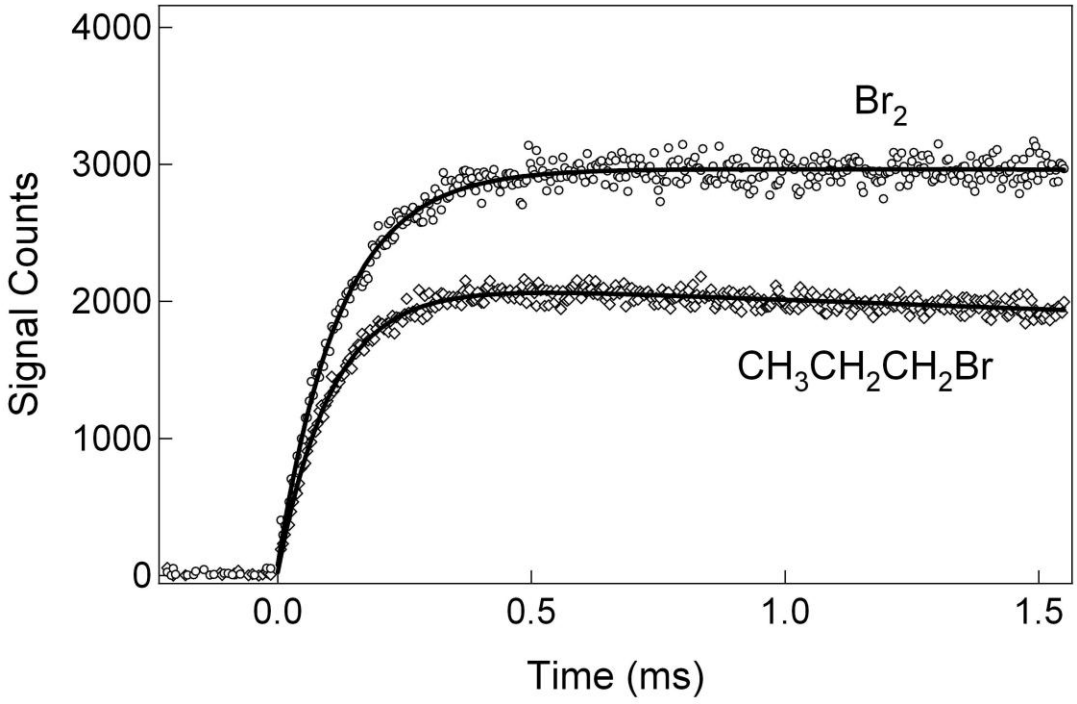

Figure 3.4 Typical Br appearance temporal profiles observed in experiments designed to measure $k_{3.2a}/k_{3.2}$. T = 296 K and P = 50 Torr. Concentrations in units of 10^{11} per cm^3: $[Cl_2CO]$ = 9030; $[Cl]_0$ = 7; $[CH_3CH_2CH_2Br]$ = 1650; $[Br_2]$ = 317. Solid lines are obtained from nonlinear least-squares fits to eq 3-I, which give the following best-fit parameters. For Cl + Br_2: k_a = 8050 s^{-1}, k_d = 7 s^{-1}, A = 2900, B = 55. For Cl + $CH_3CH_2CH_2Br$: k_a = 9380 s^{-1}, k_d = 57 s^{-1}, A = 2110, B = 35.

Table 3.4. Summary of Br Yield Data for Reactions 3.1 and 3.2.

$[Br_2]^a$	$[R\text{-}Br]^a$	SCF[b]	T(K)	N[c]	Br yield ± 2σ[d]
		R-Br = CH_3CH_2Br (3.1)			
4.25-4.80	110-140	1.22-1.30	221	4	0.33 ±0.05
3.60-3.96	98-120	1.18-1.25	250	4	0.29 ± 0.03
2.85-6.75	58-100	1.10-1.29	296	6	0.41 ± 0.08
2.60-3.60	50-80	1.14-1.30	360	4	0.45 ± 0.06
2.95-3.85	42-55	1.17-1.20	435	4	0.50 ± 0.08
		R-Br = $CH_3CH_2CH_2Br$ (3.2)			
2.50-4.50	13.0-22.0	1.00	221	4	0.91 ± 0.11
2.92-4.82	16.8-24.0	1.00	243	4	0.85 ± 0.08
3.15-3.91	16.5-22.5	1.00	296	4	0.77 ± 0.06
2.40-3.24	13.0-18.0	1.00	358	4	0.64 ± 0.10
1.74-2.71	9.7-13.5	1.00	436	4	0.62 ± 0.12

[a] Units are 10^{13} molecules cm^{-3}. [b]SCF = Signal correction factor that accounts for loss of RF signal due to absorption of resonance radiation by the R-Br reactant. [c]N = no. of experiments where one experiment represents back-to-back measurements of Br temporal profiles with (i) virtually all Cl consumed by reaction with Br_2 and (ii) virtually all Cl consumed by reaction with R-Br. [d] Uncertainties represent precision only.

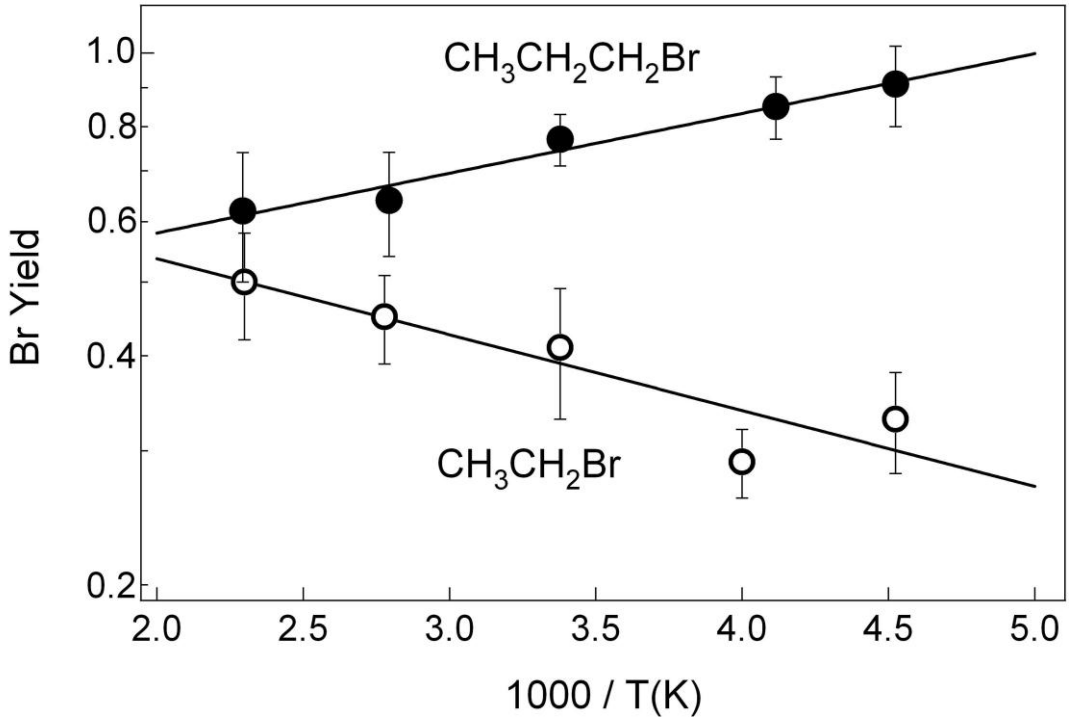

Figure 3.5 Arrhenius-type plots of Br yield (= k_{ia}/k_i, i = 3.1, 3.2) vs 1/T. Solid lines are obtained from linear least-squares analyses which yield the Arrhenius-type expressions reported in the text. Error bars are 2σ, precision only.

Over the range of temperatures and pressures employed in this study, the radical species shown in brackets in reactions (3.1a, 3.2a, and 3.3) above are expected to dissociate essentially instantaneously on the experimental time scale. Bond dissociation enthalpies at 298 K for CH_2CH_2Br and CH_3CHCH_2Br are reported in the literature to be 29± 4 [*Bedjanian et al., 1999; Ferrell, 1998*] and 32 ± 6 kJ/mol [*Bedjanian et al., 1998*], respectively. No experimental data appear to be available for the bond dissociation enthalpy of $CHBrCH_2Br$, but the presence of the electron-withdrawing Br atom on the olefin product of dissociation suggests that this radical will be less strongly bound than CH_2CH_2Br. Ferrell measured the rate coefficient (k_{uni}) for unimolecular decomposition of CH_2CH_2Br over the temperature range 163-184 K in 20 Torr N_2, and the following Arrhenius expression reproduces Ferrell's data quite well: $k_{uni}=6.56 \times 10^{10} \exp(-2950/T)$ s^{-1} [*Ferrell, 1998*]. Extrapolation of Ferrell's Arrhenius expression to 221 K, the lowest temperature employed to acquire kinetic data in this study, suggests that k_{uni}(221 K, 20 Torr N_2) > 10^5 s^{-1}. On the basis of analysis of competitive kinetics experiments in 700-760 Torr N_2 + O_2 over the temperature range 226-298 K, along with an assumed temperature-independent value of 7.5×10^{-12} cm^3 $molecule^{-1}$ s^{-1} for the $CH_2CH_2Br + O_2$ rate coefficient at atmospheric pressure, Orlando and Tyndall report $k_{uni} = 1 \times 10^{12} \exp(-2800/T)$ s^{-1} [*Orlando and Tyndall, 2002*]. Extrapolation of Orlando and Tyndall's Arrhenius expression to 221 K suggests that k_{uni}(221K, 730 Torr N_2) ≈ 3×10^6 s^{-1}. Comparison of the literature values for k_{uni} with our measured Br pseudo-first-order appearance rates (see Tables 3.1-3.3) leads to the conclusion that the rate-limiting step in the formation of Br is the Cl + R-Br reaction under all experimental conditions employed in this study.

As mentioned above, ArrheniusArrhenius-type plots of *ln* (Br yield) vs 1/T are shown in Figure 3-5, where the Br yield can be equated to the branching ratio for β-hydrogen abstraction, which is equal to 1.00 for reaction (3.3) and equal to k_{ia}/k_i (i = 3.1, 3.2). The solid lines in Figure 3.5 are obtained from least-squares analyses which yield the following expressions:

$$k_{3.1a} / k_{3.1} = (0.85 \pm 0.28) \exp[(-230 \pm 102)/T]$$

$$k_{3.2a} / k_{3.2} = (0.40 \pm 0.05) \exp[(181 \pm 34)/T]$$

Uncertainties in the above expressions are 2σ, precision only, and represent the uncertainties of the Arrhenius-type parameters; these uncertainties cannot be used in a straightforward way to obtain uncertainties in reported yields, which are discussed below.

The Br yield results demonstrate that $k_{3.1a}/k_{3.1}$ increases with increasing temperature while $k_{3.2a}/k_{3.2}$ decreases with increasing temperature. This result makes sense when one considers that it is one of the most strongly bound hydrogen atoms that must be abstracted to generate Br atoms from reaction (3.1) whereas it is one of the least strongly bound hydrogen atoms that must be abstracted to generate Br atoms from reaction (3.2). For example, recent electronic structure calculations at the CCSD(T)/6-311++G(2df,2p) level of theory obtain 0 K enthalpy changes for reactions (3.2a, 3.2b, and 3.2c) of −25, −14, and −4 kJ/mol, respectively [*Rosado-Reyes et al., 2008*]. The least exothermic pathway (3.2c) is the only one for which a positive energy barrier along the reaction coordinate is predicted [*Rosado-Reyes et al., 2008*].

Uncertainty Estimates for Rate Coefficients and Br Yields

Interference from secondary chemistry is insignificant in this study. The employed atom concentrations are low enough (< 7×10^{11} atoms cm^{-3} in nearly all experiments) that contributions from radical-radical side reactions cannot exert a significant influence on measured values for the parameters of primary interest, k_a and A. Ultra-high-purity N_2 was used as the bath gas, and while background Cl loss rates were not measured directly, the intercepts of all k_a vs [R-Br] plots were within ± 2σ of the expected value for $k_{3.6}$ (~ 100 s^{-1}). One major potential systematic uncertainty lies in the determination of the R-Br concentration in the reaction mixture; we estimate this uncertainty to be ± 10% with little dependence on temperature, pressure, or the identity of R-Br. Since the precision of all measured rate coefficients is good (2σ ≤ 10%), we conservatively estimate the accuracy of each reported bimolecular rate coefficient to be ± 15% (2σ) as long as reactions with impurities in the R-Br sample can be ruled out as a source of systematic error. Unfortunately, since numerous possible alkane, alkene, haloalkane, and haloalkene impurities react rapidly with atomic chlorine, only for the very fast reaction (3.2) is it clear that impurity reactions are of negligible importance. For the moderately fast reaction (3.1), impurity reactions could result in measured values for $k_{3.1}(T)$ being faster than the true value, though probably not by more than about 20%. To accommodate this possibility, we report the asymmetric error limits (2σ) +15/−25% for reaction (3.1). For the relatively slow reaction (3.3), significant contribution to observed kinetics from impurity reactions is possible. Hence, we feel that our measured values for $k_{3.3}$ plus 15% should be considered upper limits for $k_{3.3}(T)$, i.e.

$$k_{3.3}(T) \leq 3.2 \times 10^{-17} T^2 \exp(-184/T)$$

Even though only upper limit values for $k_{3.3}(T)$ can be reported with confidence, it will be shown in at the end of this chapter that the obtained upper limits are significant with regard to assessing the potential role of reaction (3.3) in tropospheric chemistry.

The precision of reported branching ratios k_{ia}/k_i (i = 3.1, 3.2) is not as good as that of the $k_i(T)$ values. Examination of the results reported in Table 3.4 show that 2σ precision uncertainties in measured branching ratios vary over the range 8-19%. For reaction (3.1), additional sources of uncertainty arise from (i) the need to correct the signal for absorption of resonance radiation by the CH_3CH_2Br reactant and (ii) the potential effect of minor but not completely negligible impurity reactions on the measured yields. Allowing for additional poorly characterized sources of systematic error, we feel that a reasonable estimate of the accuracy of the reported Br yields (2σ) is ± 35% for reaction 3.1 and ± 25% for reaction 3.2.

Literature Comparison

To our knowledge, there are no kinetics studies of reaction (3.3) and no temperature-dependent kinetics studies of any of the reactions (3.1-3.3) reported in the literature. The only published kinetics study of reactions (3.1 and 3.2) is the 298 K relative rate study of Donaghy et al. [*Donaghy et al., 1993*], where $k_{3.1}$ and $k_{3.2}$ were measured relative to an assumed rate coefficient of 6.2×10^{-11} cm^3 $molecule^{-1}$ s^{-1} for the Cl + ethane reference reaction. The *currently* recommended value for the Cl + ethane rate coefficient, 5.7×10^{-11} cm^3 $molecule^{-1}$ s^{-1}, is based on nine independent determinations that all report values within the range $(5.3\text{-}6.1) \times 10^{-11}$ cm^3 $molecule^{-1}$ s^{-1} [*Sander et al., 2011*]. Scaling the reported rate coefficients of Donaghy *et al.* downward by the factor 5.7/6.2 gives the following 298 K rate coefficients in units of 10^{-11} cm^3 $molecule^{-1}$ s^{-1}: $k_{3.1} = 1.28 \pm 0.37$

and $k_{3.2} = 5.6 \pm 1.7$; these values agree within combined uncertainties with the values $k_{3.1} = 1.04$ (+ 0.16 / −0.26) and $k_{3.2} = 5.47 \pm 0.82$ obtained from the Arrhenius expressions and error analyses reported in this study. It is worth noting that the technique employed by Donaghy *et al*., while potentially subject to interferences from secondary consumption of R-Br or ethane, is not subject to systematic errors that could result from the presence of reactive impurities in the R-Br sample. Hence, the fact that our measured room-temperature value for $k_{3.1}$ is more than 20% lower than the value reported by Donaghy *et al.* is at least suggestive that impurity reactions are not a significant source of systematic error in our study of reaction (3.1).

Orlando and Tyndall observed products of reaction (3.1) in a chamber study [*Orlando and Tyndall, 2002*]; yields of $CH_2=CH_2$, presumably formed via reaction (3.1a), were measured as a function of $[O_2]$. Comparison of our measured yields with those reported by Orlando and Tyndall in the limit of zero $[O_2]$ shows excellent agreement for the temperature dependence of $k_{3.1a}/k_{3.1}$ and reasonable agreement for the magnitude of $k_{3.1a}/k_{3.1}$. On the basis of our reported Arrhenius-type expressions and estimates of accuracy, we report $k_{3.1a}/k_{3.1}$ values that drop from 0.39 ± 0.14 at 298 K to 0.34 ± 0.12 at 250 K. Orlando and Tyndall report $CH_2=CH_2$ yields (at zero $[O_2]$) that drop from 0.29 at 298 K to 0.23 at 250 K (error limits are not reported). It is worth noting that the yields we report represent the ratio of Br formed to Cl lost under conditions where essentially all Cl is consumed by CH_3CH_2Br, whereas the yields reported by Orlando and Tyndall represent the ratio of $CH_2=CH_2$ formed to CH_3CH_2Br lost under conditions where essentially all CH_3CH_2Br is consumed by Cl.

Computational studies have been reported by Francisco and co-workers that address the OH-initiated atmospheric oxidation pathways for all three alkyl bromides of interest in this study [*Rosado-Reyes et al., 2008; Martinez-Aviles et al., 2007; Martinez-Aviles et al., 2008a; 2008b; Christiansen and Fransisco, 2009*]. One of the computational studies also addresses the thermochemistry and kinetics of reaction 3.2 [*Rosado-Reyes et al., 2008*]. As mentioned earlier, Francisco and co-workers find that channel (3.2a) is the most energetically favorable (exothermic by 25 $kJmol^{-1}$) while channel (3.2c) is the least energetically favorable (exothermic by 4 $kJ\ mol^{-1}$), and they also find that only channel (3.2c) has a positive energy barrier (~ 2 $kJ\ mol^{-1}$) along the reaction coordinate. They conclude that reaction (3.2) "should proceed via the abstraction of R and β hydrogen atoms," i.e., via channels (3.2b and 3.2a). The results reported in this study suggest that at temperatures of interest for atmospheric chemistry, i.e., $T < 310$ K, $k_{3.2a}/k_{3.2} > 0.7$. Hence, our results are consistent with the theoretical predictions of Francisco and co-workers.

Implications for Atmospheric Chemistry

The ODPs of alkyl bromides depend strongly on their tropospheric lifetimes. It is widely assumed that chemical loss of CH_3CH_2Br, $CH_3CH_2CH_2Br$, and CH_2BrCH_2Br in the troposphere is dominated by their reactions with the OH radical. Brioude *et al.* employed a sophisticated modeling scheme to evaluate the yearly averaged global lifetimes of CH_3CH_2Br and $CH_3CH_2CH_2Br$ following emission into the atmosphere from four different terrestrial regions: Europe, midlatitude North America, East Asia, and the Indian subcontinent [*Brioude et al., 2010*]. Lifetimes of CH_3CH_2Br ranged from 40 to 66 days, while lifetimes of $CH_3CH_2CH_2Br$ ranged from 11 to 27 days. For both alkyl

bromides, the shortest lifetime was for emission from the Indian subcontinent and the longest lifetimewas for emission from Europe. Chemical removal by reaction with OH and by photolysis was considered in the Brioude *et al.* analysis, but chemical loss by reaction with Cl atoms was not considered; reaction with OH was found to be the dominant chemical loss process for both CH_3CH_2Br and $CH_3CH_2CH_2Br$.

Table 3.5. Comparison of Rate Coefficients for OH and Cl Reactions with CH_3CH_2Br, $CH_3CH_2CH_2Br$, and CH_2BrCH_2Br at Atmospheric Temperatures

	k_{OH} (10^{-13} cm^3 $molecule^{-1}$ s^{-1})[a]		k_{Cl}/k_{OH}[b]	
R-Br	297 K	220 K	297 K	220 K
CH_3CH_2Br	3.4	1.6	31	42
$CH_3CH_2CH_2Br$	9.9	6.7	56	84
CH_2BrCH_2Br	2.5	1.3	<6	<5

[a] Rate coefficients for OH reactions with CH_3CH_2Br and $CH_3CH_2CH_2Br$ are taken from Sander et al., 2011. The 297 K rate coefficient for the OH + CH_2BrCH_2Br reaction is taken from Howard and Evenson [1976], while the 220 K rate coefficient is based on the 297 K experimental value from Howard and Evenson [1976] and the theoretical temperature dependence reported in Cohen and Benson [1987]. [b] Rate coefficients for Cl reactions with CH_3CH_2Br, $CH_3CH_2CH_2Br$, and CH_2BrCH_2Br are obtained from the Arrhenius or upper limit modified Arrhenius expressions reported in this study.

The reactivities of Cl and OH with the alkyl bromides of interest are summarized in Table 3.5. The contribution of Cl to the tropospheric degradation of alkyl bromides is difficult to evaluate because (unlike OH) tropospheric concentrations of Cl cannot currently be measured directly and atmospheric Cl production rates are highly variable in space and time and not readily quantifiable in model simulations. As discussed earlier, there is growing evidence that supports significant Cl fluxes through the troposphere in both marine and terrestrial environments [*Brioude et al., 2010; Wingenter et al., 2005; Thornton et al., 2010; Raff et al., 2009*]. Assuming an average Cl concentration of 4 ×

10^4 atoms cm^{-3}, which appears to be appropriate for the marine boundary layer [*Wingenter et al., 2005*], a mean Earth surface temperature of 288 K, and rate coefficients obtained from the results reported in this study, the following lifetimes for R-Br removal by Cl are obtained: 29 days for CH_3CH_2Br, 5.3 days for $CH_3CH_2CH_2Br$, and $\geq$ 260 days for CH_2BrCH_2Br. Rate coefficients for reactions of Cl atoms with CH_3CH_2Br and $CH_3CH_2CH_2Br$ are substantially faster than the corresponding OH rate coefficients (factors of 30-90 depending on temperature and the identity of R-Br), so it seems likely that the Cl reaction makes a significant contribution to the tropospheric degradation of these compounds. As a result, the ozone depletion potentials of CH_3CH_2Br and $CH_3CH_2CH_2Br$ may be significantly smaller than current estimates suggest. The rate coefficient for the reaction of Cl atoms with CH_2BrCH_2Br is at most a factor of 5-6 faster than the corresponding OH reaction at tropospheric temperatures, so reaction with Cl is probably only a very minor contributor to the tropospheric degradation of this alkyl bromide.

CHAPTER 4

TEMPERATURE-DEPENDENT KINETICS ASSOCIATED WITH THE CHLORINE ATOM INITIATED OXIDATION OF ISOPRENE

Introduction

It is well-established that isoprene is the single most important biogenic hydrocarbon both in terms of magnitude of emissions from terrestrial sources and in terms of its high reactivity [*Brasseur et al., 1999; Harley et al., 1999*]. Isoprene emissions from vegetation (primarily trees) total ~ 500 TgC yr^{-1} while anthropogenic emissions from all nonmethane hydrocarbons (NMHC) total ~ 100 TgC yr^{-1} [*Guenther et al., 2006*]. Furthermore, the isoprene flux into the atmosphere is larger than that of any NMHC [*Guenther et al., 2006*] and, unlike methane, the chemistry of isoprene in the atmosphere is highly complex involving many reaction steps and many unique oxidation products [*Sander et al., 2011; Atkinson et al., 2006*]. Since isoprene is primarily emitted from terrestrial vegetation during photosynthesis its emissions overlap in time with high OH radical concentrations. Hence, OH radicals are thought to be the dominant initiator of isoprene oxidation during daytime hours. Nitrate radicals (NO_3) are thought to play a significant role at night in polluted environments and O_3 is thought to dominate at night in clean environments [*Wine and Nicovich, 2012; Atkinson and Arey, 2003; Brown et al., 2009*]. However, recent work indicating potentially significant marine source of isoprene has received considerable attention [*Liss, 2007; Liakakou et al., 2007; Sinha et al., 2007; Arnold et al., 2009; Gantt et al., 2009; 2010*], and since Cl atoms in the marine boundary

layer can be 1-10% of OH levels, [*Jobson et al., 1994; Wingenter et al., 1999; Wingenter et al., 2005*] the gas phase reactions of isoprene with atomic chlorine could represent an effective atmospheric oxidation processe for isoprene [*Atkinson and Arey, 2003*].

Chlorine has long been thought to exist primarily in marine environments, however, significant levels of $ClNO_2$ have recently been observed in the middle of the continental United States [*Thornton et al., 2010*]. Recent laboratory and theoretical research has shown the heterogeneous reaction of N_2O_5 with HCl may represent a significant source of $ClNO_x$ species that can readily photolyze in the daytime troposphere to generate Cl atoms [Raff *et al.,* 2009]. At 298 K, currently recommended rate coefficients for isoprene reactions with OH, NO_3, O_3, and Cl are 1000, 7.3, .00013, and 4100×10^{-13} cm^3 $molecule^{-1}$ s^{-1}, respectively [*Sander et al., 2011*]. If indeed the Cl rate coefficient is 4 times faster than the OH reaction, the Cl reaction could play a non-neglibible role in isoprene oxidation in atmospheric locales where Cl concentrations are high enough.

In this study, we focus on the reaction of atomic chlorine with isoprene over a wide range of temperature and pressure.

$$Cl + H_2C{=}C(CH_3)CH{=}CH_2 \rightarrow HCl + H_2C{=}C(CH_2)CH{=}CH_2 \qquad (4.1a)$$

$$Cl + H_2C{=}C(CH_3)CH{=}CH_2 \leftrightarrow C_5H_8Cl \qquad (4.1b, -4.1b)$$

Cl + isoprene has been the subject of numerous room temperature studies performed by a variety of different techniques, and the kinetic database for this reaction contains a wide range of values for the 298 K rate coefficient [*Ragains and Finlayson-Pitts, 1997; Notario et al., 1997; Fantechi et al., 1998; Bedjanian et al., 1998; Stutz et al., 1998;*

Finlayson-Pitts et al., 1999; Canosa-Mas et al., 1999; Suh and Zhang, 2000; Albaladejo et al., 2003; Orlando et al., 2003]. The four reported 298 K HCl yields are in excellent agreement even though they were all obtained under very different conditions of pressure and bath gas, i.e., 1 Torr He [*Bedjanian et al., 1998*], 10 Torr He [*Suh and Zhang, 2000*], 740 Torr Air [*Fantechi et al., 1998*], and 760 Torr N_2 [*Ragains et al., 1997*]. In addition, there has only been one temperature dependent study (233 – 320 K) on the Cl + isoprene reaction [*Bedjanian et al., 1998*]. Figure 4.1 shows the major reactions that occur in the reaction of Cl atoms with isoprene in NO_x free air.

In this study, we couple 266 nm laser flash photolysis of Cl_2CO with monitoring of atomic Cl by time-resolved atomic resonance fluorescence spectroscopy to investigate Cl + isoprene kinetics over a wide range of temperature and pressure. Our results add to the ubiquitous 298 K kinetic database and, more importantly, they supplement the very limited temperature dependent kinetic database. In addition we report the first experimental determination of the C−Cl bond strength in the Cl−isoprene radical adduct. The potential importance of reaction with Cl as an atmospheric degradation pathway for isoprene is assessed at the end of the chapter.

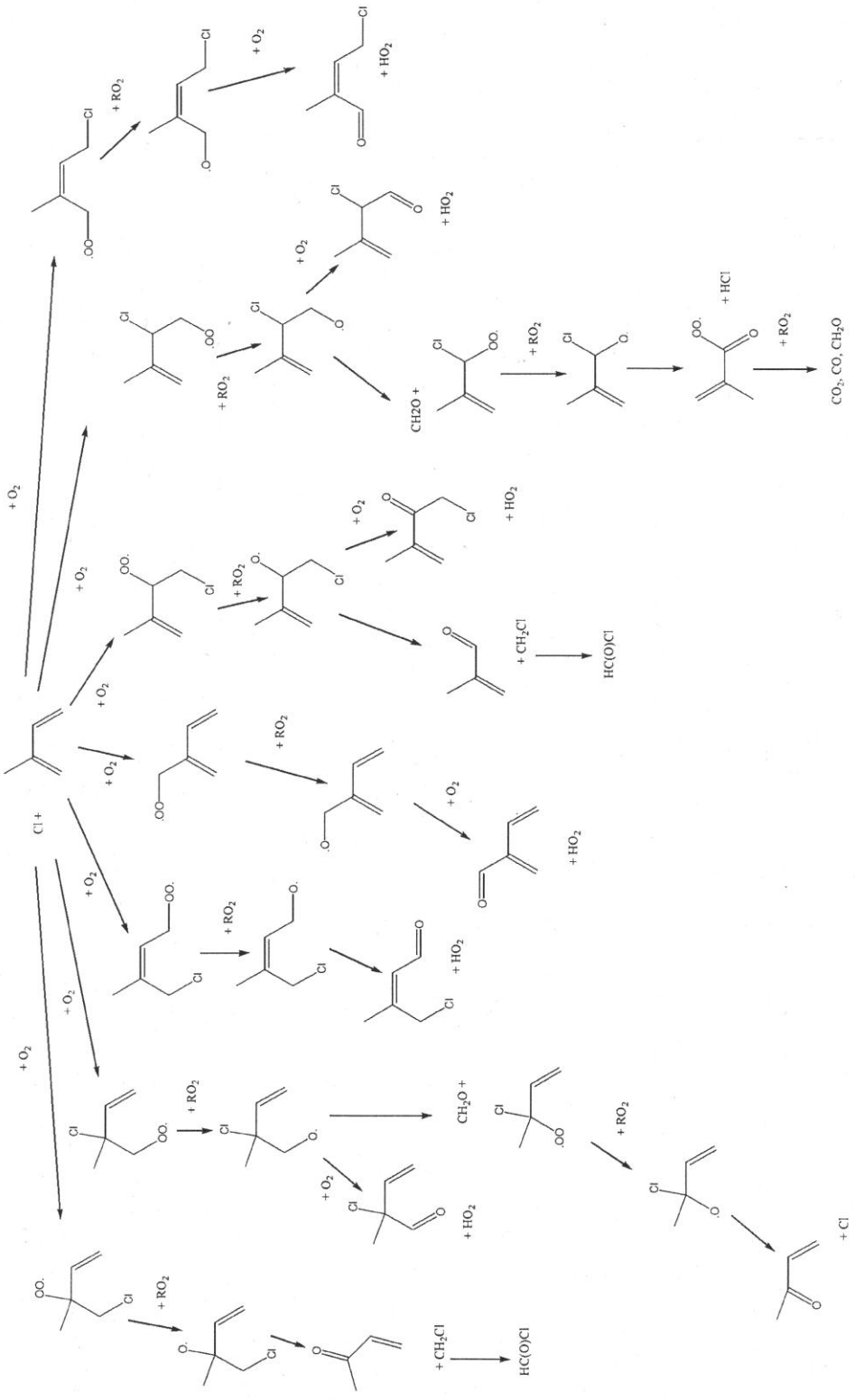

Figure 4.1 The major reactions associated with oxidation of isoprene by atomic Cl in NO_x free air. Scheme taken from Orlando *et al.*, 2003.

Experimental Details

The studies of Cl + isoprene were conducted by coupling laser flash photolysis of Cl_2CO/N_2 mixtures with time-resolved atomic resonance fluorescence spectroscopic detection of chlorine atoms. The descriptions of the apparatus and the technique can be found in Chapter 2 and only details particular to this study are discussed below.

Chlorine atoms were generated by 266 nm LFP of Cl_2CO using fourth harmonic radiation from a Quanta Ray Model DCR-3 Nd:YAG laser as the photolytic light source.

$$Cl_2CO + h\nu\ (266\ nm) \rightarrow CO + 2Cl \qquad (4.2)$$

The photolysis laser can deliver up to 60 mJ $pulse^{-1}$ at a repetition rate of up to 10 Hz; the pulse width is 6 ns. Fluences employed in this study ranged from 2.5 to 10 mJ cm^{-2} $pulse^{-1}$. Chlorine atom concentrations produced by the laser flash were typically in the range $(1-4) \times 10^{11}$ atoms cm^{-3}.

The isoprene and Cl_2CO flowed into the reaction cell from 12 L bulbs containing dilute mixtures in nitrogen while carbon dioxide, helium, and additional nitrogen flowed directly from their storage cylinders. The contents of each bulb were measured frequently by UV photometry at 228.8 nm using a Cd Penray® lamp as the light source. The isoprene absorption cross section needed to convert absorbance to concentration was measured during the course of this study and found to be 9.36×10^{-18} cm^2.

The gases used in this study had the following stated minimum purities: N_2 (99.999%, Air Gas), He (99.999%, Air Gas), CO_2 (99.99 %, Air Gas), and Cl_2CO (99.0%, Matheson Trigas). For Cl_2CO and CO_2 the stated purity refers to the liquid phase in the high-pressure gas cylinder. The liquids used in this study had the following

stated minimum purities: isoprene (>99.0 %, TCI America (stabilized with *tert*-butyl-catechol, TBC)). N_2, He, and CO_2 were used as supplied, while isoprene, Cl_2CO, and CF_2Br_2 were degassed repeatedly at 77 K, then diluted in N_2 and stored in pyrex bulbs before use.

Results and Discussion

All experiments were carried out under pseudo-first-order conditions with isoprene in large excess over $[Cl]_0$. Thus, in the absence of secondary reactions that enhance or deplete the Cl concentration, the Cl temporal profile following the laser flash would be described by the relationship:

$$\ln\{[X]_0/[X]_t\} = \ln\{S_0/S_t\} = (k_{4.1}[C_5H_8] + k_{4.3})t = k't \qquad (4\text{-I})$$

In eq (4-I), S_0 is the Cl fluorescence signal at a time immediately after the laser fires and S_t is the Cl fluorescence signal at time t, $k_{4.1}$ is the overall rate coefficient for loss of Cl by all irreversible Cl + isoprene reaction channels, and $k_{4.3}$ is the rate coefficient for the following reaction:

$$Cl \rightarrow \text{Reaction with background impurities and/or loss by diffusion from detector field of view} \qquad (4.3)$$

The bimolecular rate coefficients of interest, $k_{4.1}(P, T)$, are determined from the slopes of k' vs $[C_5H_8]$ plots for data obtained at constant T and P. The dominant observed reaction pathway varies as a function of temperature. Hence, the following discussion of the observed kinetics of Cl + isoprene considers high and low temperature regimes separately.

Kinetics at 201 K ≤ T ≤ 320 K

Well-behaved pseudo-first-order Cl atom kinetics were observed in studies carried out over the temperature range 201 – 320 K, i.e., Cl temporal profiles were exponential and observed first order decay rates were found to increase linearly with increasing isoprene concentration but were independent of laser photon fluence and [$COCl_2$]; these kinetic observations are consistent with the behavior predicted by equation (4-I). This evidence strongly supports the contention that reactions (4.1) and (4.3) are the only processes affecting the post-laser-flash Cl temporal profile. Typical data are shown in Figures 4.2 and 4.3, and measured bimolecular rate coefficients $k_{4.1}(P,T)$ are summarized in Table 1. An Arrhenius plot describing T dependence of the reaction from 201 – 320 K is shown in Figure 4.4. The following best fit Arrhenius expression is derived from a linear least-squares analysis of the *ln* $k_{4.1}$ versus T^{-1} data:

$$k_{4.1}(T) = (3.48 \pm 0.26) \times 10^{-10} \exp[(+6 \pm 20)/T)] \text{ cm}^3 \text{ molecule}^{-1} \text{ s}^{-1} \qquad (4\text{-II})$$

Uncertainties in the above expression are 2σ and represent the precision of the Arrhenius parameters. The largest systematic uncertainty lies in the reagent concentration in the reaction mixture, which we estimate to be uncertain by a maximum of ± 10%. Since the precision of the overall rate coefficients reported herein is good (2σ ≤ 10%), we conservatively estimate the accuracy of each reported value for $k_{4.1}(T)$ to be ± 15% at the 95% confidence level. The observed T dependence of $k_{4.1}(T)$ is so small that the temperature independent rate coefficient, $k_{4.1} = (3.55 \pm 0.53) \times 10^{-10}$ cm^3 molecule^{-1} s^{-1} is a very adequate representation of the experimental results.

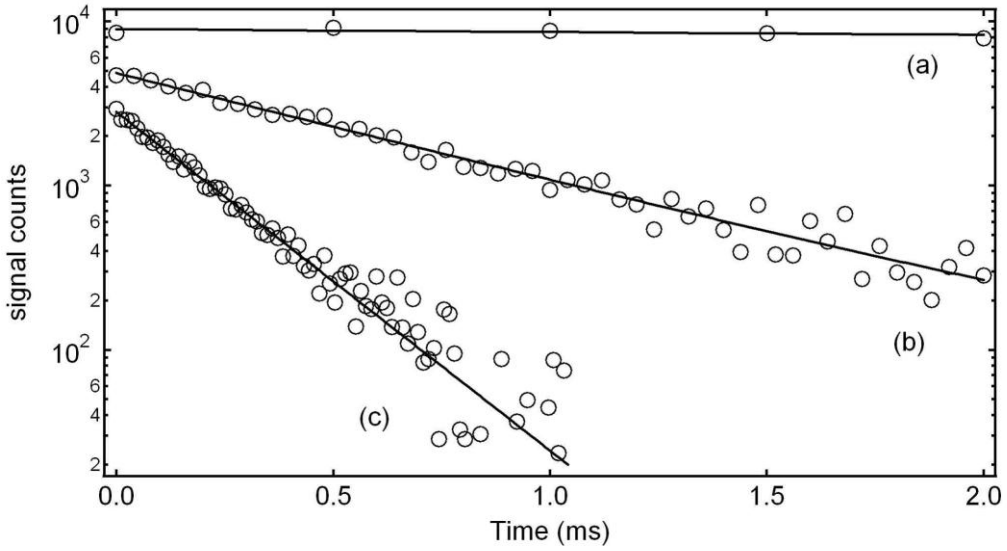

Figure 4.2 Typical Cl atom temporal profiles observed in our studies of the Cl + isoprene reaction at 201 K ≤ T ≤ 320 K. Experimental conditions: T = 296 K, P = 50 Torr, $[Cl_2CO] = 3 \times 10^{14}$ molecule cm^{-3}, [Cl] = 2×10^{11} atoms cm^{-3}, [isoprene]: (a) 0, (b) 0.41, (c) 1.3 x 10^{13} molecule cm^{-3}. Decay rates (k_a) are 43 s^{-1} (a), 1480 s^{-1} (b), and 4528 s^{-1} (c). Data are separated by 1000 signal counts for clarity. Data was collected for 500 channels with the multi channel scalar dwell time set to 500 μs (a), 40 μs (b), 12 μs (c).

Table 4.1. Kinetic data for Cl + isoprene from 201 - 320 K.[a]

T	P	# exp.	Cl_2CO	Cl_0	$C_5H_{8\,max}$	k'_{max}	$k_{4.1} \pm 2\sigma$
201	55	5	2000	3	140	4860	3.60 ± 0.23
215	50	5	2000	2	120	4420	3.59 ± 0.33
233	55	6	3000	3	200	7210	3.49 ± 0.19
254	50	5	2000	2	110	4060	3.63 ± 0.02
273	55	5	2000	3	180	6660	3.63 ± 0.26
296	3	4	2000	1	64	2710	3.85 ± 0.27
296	50	4	3000	2	160	5800	3.58 ± 0.23
296	300	4	4000	3	130	4670	3.70 ± 0.39
297	10	10	4000	4	160	5840	3.70 ± 0.12
298	50	8	4000	3	170	6000	3.50 ± 0.12
320	50	5	2000	2	97	3500	3.51 ± 0.27

[a] Concentrations (cm^{-3}): $COCl_2$, Cl_0, C_5H_8 (10^{11}); Units: $k_{4.1}$(10^{-10} $cm^3 molecule^{-1} s^{-1}$), $k'(s^{-1})$.

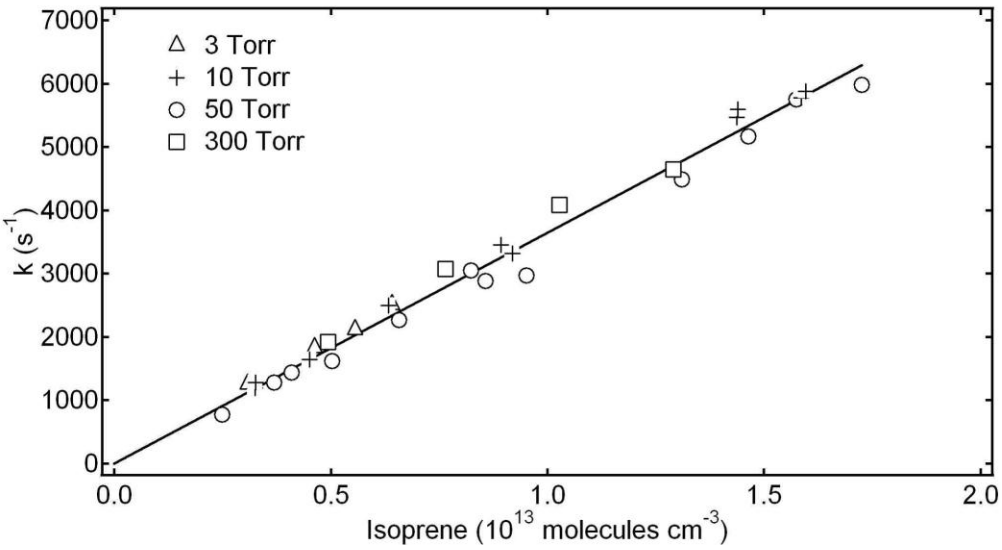

Figure 4.3 Plots of k′ versus [isoprene] for reaction 4.1 at 297 K. The solid line is obtained from a linear least-squares analysis and lead to the T and P-independent bimolecular rate coefficient reported in the text. Background loss rates were subtracted from k′ to give the data shown. Those loss rates decareased with increasing pressure at 297 K from 3 – 300 Torr as follows: 209 s^{-1}, 64 s^{-1}, 43 s^{-1}, 21 s^{-1}. Individual rate coefficients over the wide range of conditions are reported in Table 4.1.

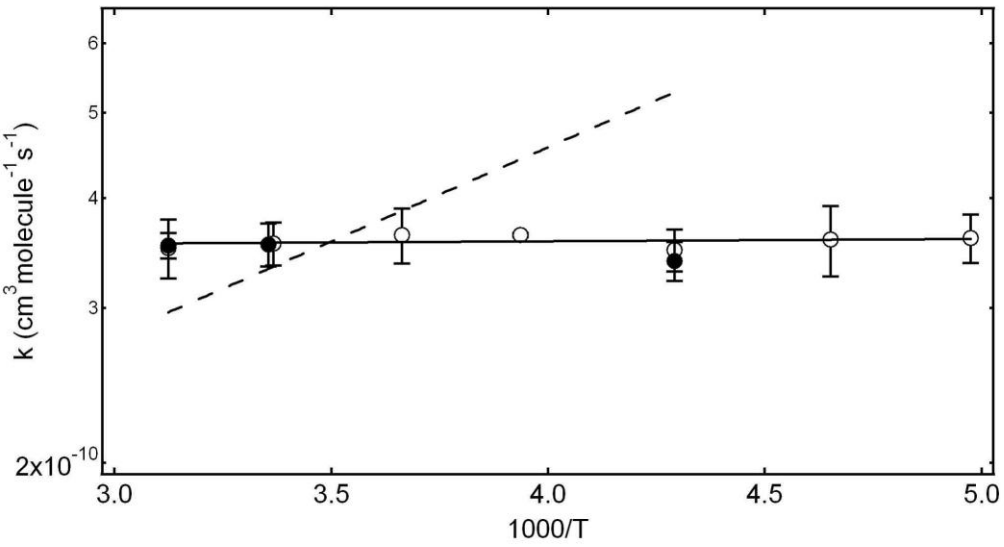

Figure 4.4 Arrhenius plot for the Cl + Isoprene reaction from 201 – 320 K. The open symbols represent data obtained by Cl_2CO photolysis at 266 nm and the closed symbols represent data obtained by Cl_2 photolysis at 355 nm. The lines are obtained from linear least squares analyses which weights each data point equally. The best fit Arrhenius expression obtained is (units are cm^3 $molecule^{-1}$ s^{-1}): $k_{4.1} = (3.48 \pm 0.26) \times 10^{-10}$ $\exp((+6 \pm 20)/T)$. The dotted line represents data reported by Bedjanian *et al.* [*1998*]

High Temperature Studies

Experiments were conducted at elevated temperatures (488 K ≤ T ≤ 635 K) where evidence for reversible adduct formation, i.e., double exponential Cl decay, was observed. This observation strongly suggests that over the temperature range 201−320 K, a stable adduct is formed via reaction (4.1b), i.e., reaction (–4.1b) is extremely slow over this temperature range. As we continued to increase temperature to T > 690 K, exponential decays were once again observed. The high temperature (T > 690 K) data are strongly indicative of a case where reaction (–4.1b) is too fast to observe on the time scale of our experiments, i.e., at this temperature we are observing only the H-abstraction reaction (4.1a). We will address the non-exponential decays after discussing results from the experiments at T ≥ 690 K.

Kinetics at T ≥ 690 K

Well-behaved pseudo-first-order Cl atom kinetics were observed in studies carried out at 690 ≤ T ≤ 719 K, i.e., Cl temporal profiles were exponential and observed first order decay rates were found to increase linearly with increasing [isoprene]. These kinetic observations are consistent with eq (4-I), and observed decay rates were independent of laser photon fluence. Furthermore, bimolecular rate coefficients obtained from the slopes of k′ vs [isoprene] plots were found to be independent of pressure over the range 50 – 250 Torr. The observational evidence in conjunction with observed behavior at lower temperatures strongly supports the contentions that (i) the dominant pathway for Cl + isoprene reaction at T > 690 K is H-abstraction and (ii) reactions (4.1a) and (4.3) are the only processes which significantly affect the post-laser-flash Cl atom

time history. Typical high temperature data are shown in Figure 4.5, and measured bimolecular rate coefficients, $k_{4.1a}(P,T)$, are summarized in Table 4.2.

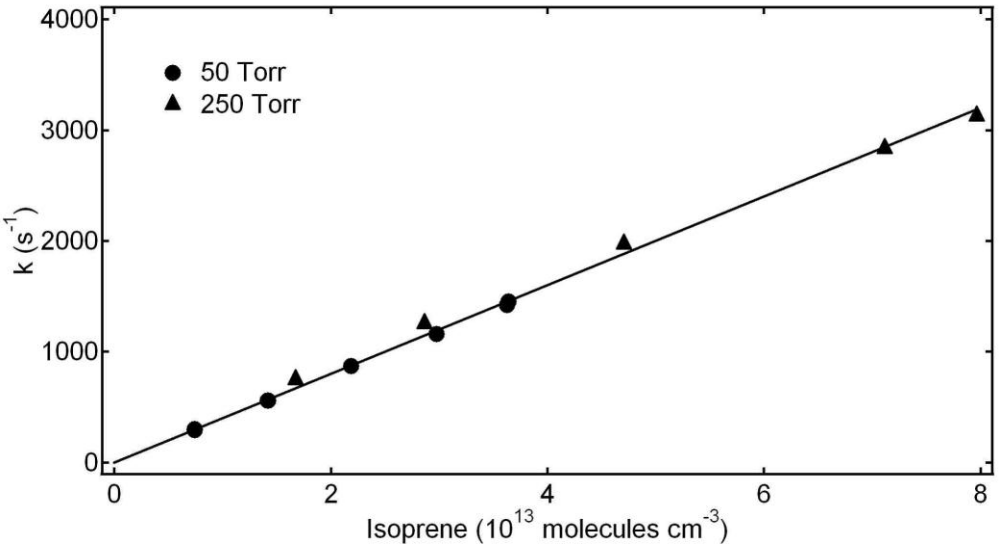

Figure 4.5 Plots of k′, the pseudo-first order Cl atom decay rate, versus [isoprene] at 719 K. The solid line is obtained from a linear least squares analysis and the resulting bimolecular rate coefficients, i.e., the slope of the fit to the data, is (in cm^3 $molecule^{-1}$ s^{-1}) 3.91×10^{-11}. Background loss rates were subtracted from k′ to give the data shown. Background loss rates for the 719 K data were 101 s^{-1} at 50 Torr and 25 s^{-1} at 250 Torr. Uncertainties are 2σ and represent precision only.

Table 4.2. Kinetic data for reaction (4.1a) from 690 - 719 K. [a]

T	P	# exp.	$[Cl_2CO]$	$[Cl]_0$	$[C_5H_8]_{max}$	k'_{max}	$k_{4.1a} \pm 2\sigma$ [b]
690	50	6	1700	1.0	400	1740	4.09 ± 0.06
719	50	8	1700	0.3-1.2	360	1550	3.94 ± 0.05
719	250	5	2300	1.5	800	3150	3.89 ± 0.18

[a] Units: T (K); P (Torr); $k'(s^{-1})$; $[COCl_2]$, $[C_5H_8]$, $[Cl]_0$ $(10^{11}$ $cm^{-3})$; $k_{4.1a}$ $(10^{-11}$ $cm^3 molecule^{-1} s^{-1})$. [b] Uncertainty is precision only.

The 719 K value for $k_{4.1a}$ is found to be $(3.91 \pm 0.08) \times 10^{-11}$ cm^3 $molecule^{-1}$ s^{-1} independent of P from 50 to 250 Torr; uncertainty is 2σ, precision only. Since the precision of the $k_{4.1a}(T,P)$ values tabulated in Table 4.2 is quite good ($2\sigma < 5$ %), we conservatively estimate the accuracy of each reported value for $k_{4.1a}(T)$ to be ± 15 %. Since $k_{4.1a}(T)$ could only be experimentally determined over a very narrow temperature range, we have obtained a "guesstimated" Arrhenius expression for the H-abstraction reaction based on known A factors found in the literature for reactions of Cl with small hydrocarbons such as ethane, *n*-propane, propylene, and *n*-butane [*Sander et al., 2011; Pilgrim and Taatjes, 1997; Tyndall et al., 1997*]. We used the estimated A factor (2×10^{-10} cm^3 $molecule^{-1}$ s^{-1}) to compute E_a/R based on our 719 K value for $k_{4.1a}$. The "guesstimated" expression is as follows:

$$k_{4.1a}(T) \approx 2 \times 10^{-10} \exp(-1340 / T) cm^3 \text{ molecule}^{-1} s^{-1} \qquad \text{(4-III)}$$

The "guesstimated" Arrhenius expression is used in the analysis of kinetic data obtained over the temperature range 488−635 K (see below).

Kinetics at 488 K ≤ T ≤ 635 K

Over the temperature range 488 – 635 K, kinetic evidence for reversible addition of Cl to isoprene was observed. The relevant kinetic scheme for analysis of this data includes reactions (4.1a), (4.1b), −(4.1b), (4.3), and (4.4).

$C_5H_8Cl \rightarrow$ Loss by processes that do not regenerate Cl atoms (4.4)

The rate equations for the above reaction scheme can be solved analytically, and predict a double exponential functional form for the Cl decay:

$$[S]_t/[S]_0 = [(Q + \lambda_1)\exp(\lambda_1 t) - (Q + \lambda_2)\exp(\lambda_2 t)] / (\lambda_1 - \lambda_2) \quad \text{(4-IV)}$$

In equation (4-IV), S_t and S_0 are the resonance fluorescence signal levels at times t and 0, and

$$Q = k_{-4.1b} + k_{4.4} \quad \text{(4-V)}$$

$$-(\lambda_1 + \lambda_2) = Q + k_{4.3} + (k_{4.1a} + k_{4.1b})[C_5H_8] \quad \text{(4-VI)}$$

$$\lambda_1\lambda_2 = Q(k_{4.3} + k_{4.1a}[C_5H_8]) + k_{4.4}k_{4.1b}[C_5H_8] \quad \text{(4-VII)}$$

Typical observed Cl temporal profiles are shown in Figure 4.6. Such temporal profiles were fit to the double exponential equation (4-IV) using a non-linear least squares method to obtain values for the fitted parameters S_0, Q, λ_1, and λ_2.. Rearrangement of equations (4-V) – (4-VII) gives the relationships for the rate coefficients of interest:

$$k_{4.1b} = -(Q + k_{4.3} + k_{4.1a}[C_5H_8] + \lambda_1 + \lambda_2) / [C_5H_8], \quad \text{(4-VIII)}$$

$$k_{4.4} = \{\lambda_1\lambda_2 - Q(k_{4.3} + k_{4.1a}[C_5H_8]\} / k_{4.1b}[C_5H_8], \quad \text{(4-IX)}$$

$$k_{-4.1b} = Q - k_{4.4} \quad \text{(4-X)}$$

The background Cl atom loss rate ($k_{4.3}$) was directly measured by observing the RF decay in the absence of isoprene at each temperature and pressure. At 50 Torr, $k_{4.3}$ varied from ~ 40 s^{-1} at 488 K to 80 s^{-1} at 635 K. At 200 Torr and 488 K, $k_{4.3}$ was found to be 25 s^{-1}.

Temperature dependent rate coefficients for the H-abstraction pathway, $k_{4.1a}(T)$, were obtained by using the Arrhenius expression described earlier in this chapter.

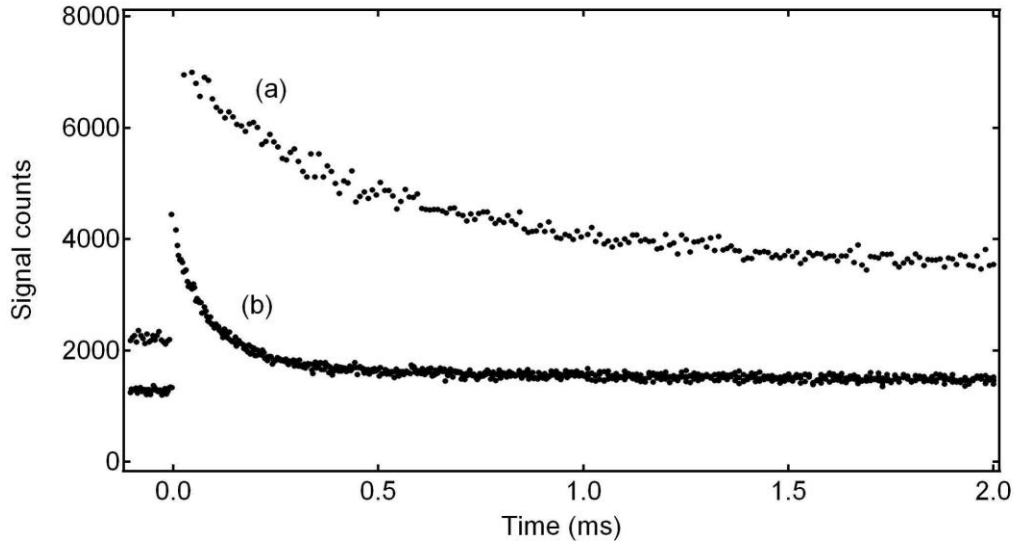

Figure 4.6 Typical Cl atom temporal profiles observed at 488 K ≤ T ≤ 635 K. Note the appearance of a pre triggered baseline. Experimental conditions: T = 561 K, P = 50 Torr N_2, [C_5H_8] (in units of 10^{13} molecule cm^{-3}) = (a) 0.99 and (b) 4.9. Solid lines are obtained from non-linear least-square fits to equation (ii) and give the following best fit parameters (also shown in Table 2): (a) So = 2779, Q = 1398, λ_1 = -2843, λ_2 = −249 and (b) So = 2672, Q = 1802, λ_1 = −10128, λ_2 = −393. Trace (a) has been scaled upwards by a factor of 2 for clarity.

Experimental conditions and results of all of the equilibration kinetics experiments are summarized in Table 4.3. The values of the equilibrium constants given in Table 4.3 have been derived from the following relationship

$$K_P = k_{4.1b} / (k_{-4.1b}RT) = K_c / (RT) \quad \text{(4-XI)}$$

Since the precision of multiple determinations of $k_{4.1b}$ and $k_{-4.1b}$ is quite good, we estimate that the absolute accuracies of reported $k_{4.1b}$, $k_{-4.1b}$, and K_P values are ± 15%, ± 25%, and ± 30%, respectively, over the full range of temperature and pressure spanned by the results given in Table 4.3. A plot of ln K_P vs 1/T, i.e., a van't Hoff plot, is shown in Fig. 4.7. A linear least-squares analysis of the data gives the following expression:

$$ln\ K_P = -(10.3 \pm 0.8) + (13700 \pm 400)/T \quad \text{(4-XII)}$$

It should be noted, that the derived values for K_P are dependent on the choice of $k_{4.1a}(T)$, i.e., as can be seen from equations (4-VI and 4-VII) the fit parameters provide the sum of the H abstraction and addition channels ($k_{4.1a} + k_{4.1b}$). The expression above (4-XII) was obtained assuming that $k_{4.1a}(T) = 2.0 \times 10^{-10} \exp(-1340/T)$. Potential uncertainty in $K_P(T)$ associated with the uncertainty in $k_{4.1a}(T)$ is discussed below.

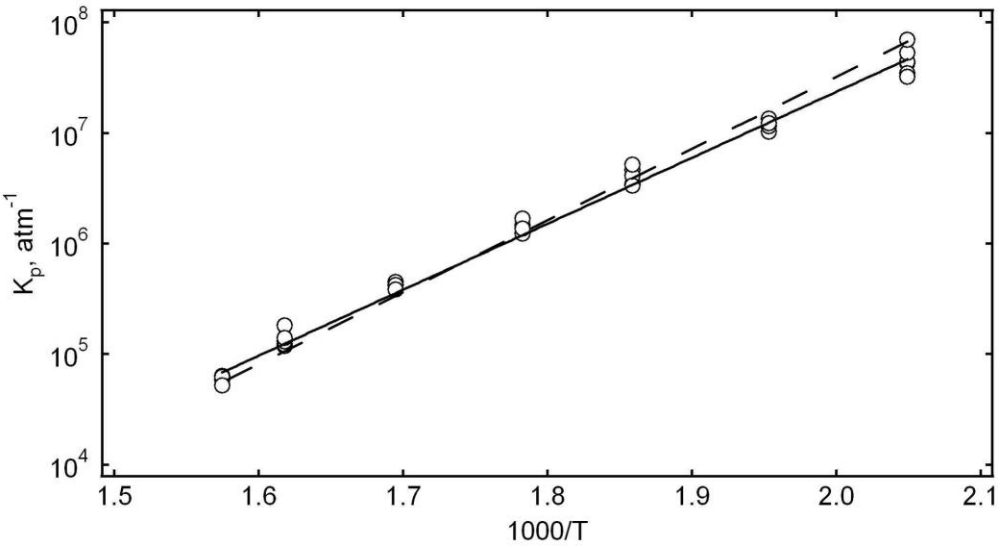

Figure 4.7 van't Hoff plot for the reaction Cl + isoprene at 488 K ≤ T ≤ 635 K. The solid line is obtained from a least squares analysis of ln K_P vs 1/T data for isoprene and gives the following second-law thermochemical parameters for the reaction: $\Delta H = -113.6$ kJ/mol and $\Delta S = -86$ J/mol/K. The dashed line represents results from the third law analysis. The van't Hoff plot shown here assumes $k_{4.1a}(T) = 2.0 \times 10^{-10} \exp(-1340/T)$.

Table 4.3. Results of the Cl + isoprene + N_2 ↔ Cl−isoprene + N_2 equilibration kinetics experiments.[a]

T	P	Q	$-\lambda_1$	$-\lambda_2$	$[C_5H_8]$	$[COCl_2]$	$[Cl]_0$	$k_{4.1b}$	$k_{4.4}$	$k_{-4.1b}$	K_P
488	50	202	4246	114	151	2140	1.44	2.47	107	95	38.9
		626	8918	536	320	2150	1.39	2.50	533	93	40.3
		267	7862	158	284	2130	1.25	2.47	149	118	31.4
		150	1591	80	550	2100	1.24	2.44	75	76	48.4
	200	316	10883	253	348	2530	1.49	2.85	249	67	64.3
		243	5738	109	180	2430	1.30	2.84	99	145	29.5
512	50	411	2600	179	101	2100	1.52	2.04	164	247	11.9
		432	1910	177	70	2090	1.40	2.08	173	259	12.1
		846	14428	518	580	2090	1.46	2.18	493	353	9.27
		346	11085	72	459	2100	1.24	2.08	-42	388	8.05
		531	6296	244	238	2070	1.11	2.26	223	307	11.0
538	50	658	2486	163	102	1400	1.02	1.61	109	549	4.00
		1200	12205	416	506	2090	1.40	1.96	332	868	3.08
		879	4776	247	191	2070	1.16	1.86	186	694	3.66
		1173	9577	398	408	2040	1.26	1.86	315	857	2.96
		657	1919	153	65	2020	1.14	1.80	118	539	4.56
561	50	1707	5061	347	209	1970	1.27	1.45	199	1507	1.26
		1398	2844	249	99	1980	1.22	1.35	165	1233	1.44
		2141	12631	514	602	1960	1.00	1.52	276	1865	1.07
		1802	10128	393	494	2090	1.12	1.45	170	1632	1.17
590	50	4998	6316	365	936	1790	1.20	1.42	410	4588	.385
		4564	10601	805	450	1760	1.13	1.19	329	4235	.350
		4168	7041	601	244	1750	1.08	1.09	295	3873	.349
		4837	12318	860	554	2150	1.21	1.18	278	4559	.322
618	50	11754	19679	1793	786	1820	1.12	1.24	3631	8123	.183
		12782	20792	1743	736	1760	1.09	0.991	658	12124	.097
		11154	15371	1288	462	1730	1.07	0.858	653	10501	.097
		8739	10263	824	243	1690	1.04	.0632	887	7852	.096
		11279	12825	648	168	1750	1.08	0.969	1201	10078	.114
635	50	15661	17275	985	280	1830	1.22	0.582	1157	14504	.046
		13650	16475	1638	559	1830	1.23	0.454	282	13368	.039
		25024	34270	2201	794	1780	1.19	1.10	808	24216	.052
		19981	25861	2233	803	1780	1.19	0.666	472	19509	.039

[a] Units: T (K); P (Torr); Q, λ_1, λ_2, $k_{4.4}$, $k_{-4.1b}$ (s^{-1}); [isoprene], $[COCl_2]$, $[Cl]_0$ (10^{11} cm^{-3}); $k_{4.1b}$ (10^{-10} cm^3 $molecule^{-1}$ s^{-1}); K_P (10^6 atm^{-1}); S_0 not shown in Table, but $2000 \le S_0 \le 4000$ in all experiments.

Cl−Isoprene thermochemistry

Both second and third law methods have been employed to evaluate the thermochemistry of Cl−isoprene. In the second law approach, the enthalpy and entropy changes associated with the Cl−Isoprene formation (4.1b) are evaluated from the van't Hoff plot shown in Figure 4.7. Since

$$ln\ K_P = (\Delta_r S / R) - (\Delta_r H / RT), \qquad \text{(4-XIII)}$$

the enthalpy change is obtained from the slope of the van't Hoff plot while the entropy change is obtained from the intercept. As mentioned earlier, and as can be seen from equations (4-VI and 4-VII) the second law results are dependent on the values of $k_{4.1a}(T)$ used in the data analysis. The fit parameters only yield the sum of the H abstraction and addition channels ($k_{4.1a} + k_{4.1b}$). There are several different approaches that could be employed for estimating $k_{4.1a}(T)$. After careful consideration of all possible values for $k_{4.1a}(T)$, the analysis was performed using two limiting cases, (i) $k_{4.1a}(T) = 2.0 \times 10^{-10}$ exp(−1340/T) and (ii) $k_{4.1a}(T) = 3.91 \times 10^{-11}$ cm^3 $molecule^{-1}$ s^{-1} (measured value at 719 K) independent of temperature. These analyses yield second law values (seen in Table 4.5) for $\Delta_r H$ of −113.6 and −116.6 kJ/mol, respectively. Assuming the average of the two limiting cases yields the second law results shown in Table 4.5. At 561 K, near the midpoint of the experimental 1/T range, this second-law analysis gives the results $\Delta_r H = -115 \pm 8$ kJ mol^{-1} and $\Delta_r S = -90 \pm 15$ J mol^{-1} K^{-1}, where uncertainties are 2σ and represent precision only.

In addition to the second-law analysis, we have carried out a third-law analysis, where the value of K_p at 561 K obtained from the van't Hoff analysis, $(1.26 \pm 0.38) \times 10^6$ atm^{-1} has been employed in conjunction with a calculated entropy change to determine $\Delta_r H(561)$. To evaluate $\Delta_r S$ for reaction (4.1b), absolute entropies as a function of temperature were obtained from the JANAF table for Cl [Chase et al., 1985], and calculated using *ab initio* vibrational frequenies and moments of inertia for isoprene and for the Cl−isoprene adduct. Relevant parameters used in the calculations of absolute entropies and heat capacity corrections are summarized in Table 4.4.

Electronic structure calculations were carried out by our collaborator, Michael L. McKee of Auburn University. The geometry of the isoprene and Cl−isoprene adduct were determined by the G4 method [*Curtiss et al., 2007*] using the Gaussian09 program [*Frisch et al., 2009*]. The G4 method is a composite of several calculations and includes an extrapolation procedure and a spin-orbit correction for the chlorine atom (5.6 kJ mol^{-1} for Cl). The average absolute deviation from experiment for the G3/05 test set (454 experimental energies, 34 of which are for radicals) is only 3.5 kJ mol^{-1}. There are two potentially stable Cl−isoprene adducts, the C1−adduct is found to be 6.8 kJ/mol more stable than the C4−adduct. Both structures are shown in Figure 4.8.

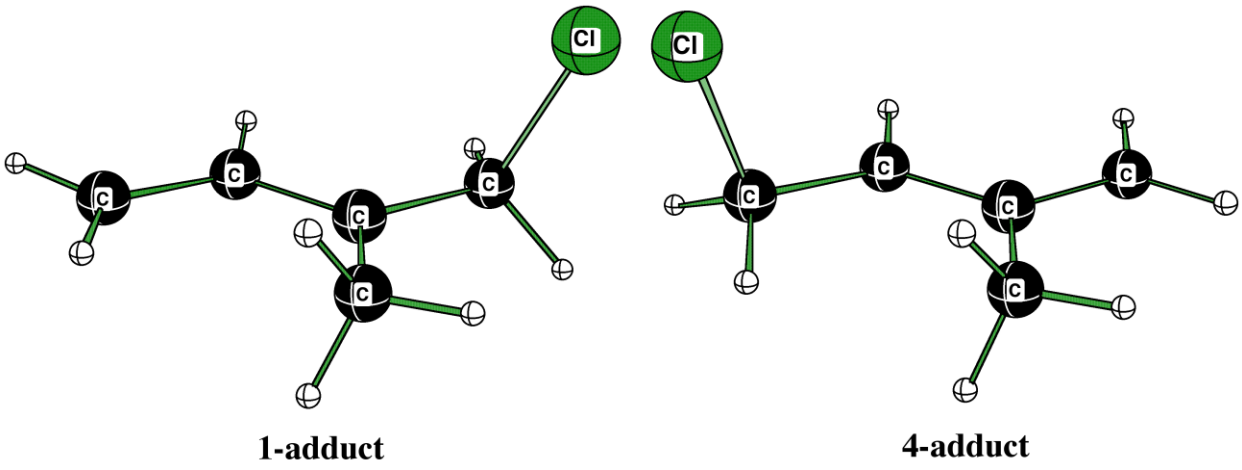

Figure 4.8. Optimized structure and geometries of the Cl−isoprene complexes. The "best" C1 (left) and C4 (right) adducts are shown for C_5H_8Cl. C−Cl bond lengths are 1.86 and 1.87 Angstroms for the C-1 and C-4 adducts, respectively. Provided by Mike L. McKee.

Table 4.4. Summary of parameters used in calculations of absolute entropies and heat capacity corrections for the Cl reaction with isoprene.

	Cl	isoprene	Cl−isoprene [c]
g_0	4	1	2
g_1	2		
$\Delta\varepsilon/cm^{-1}$ [a]	882.36		
σ		1	1
Rot. Constants/GHz[b]		8.5477, 4.1750, 2.8544	5.4537, 1.4668, 1.3064
Vib. Frequencies/cm^{-1}[b]		164, **209**, 277, 413, 426, 533, 649, 794, 796, 930, 937, 965, 1012, 1041, 1074, 1091, 1328, 1330, 1411, 1435, 1462, 1481, 1503, 1669, 1708, 3029, 3080, 3121, 3140, 3148, 3158, 3230, 3237	**54**, 64, 149, 240, 293, 374, 395, 542, 569, 648, 778, 813, 909, 983, 994, 1033, 1048, 1147, 1247, 1257, 1263, 1378, 1409, 1459, 1471, 1484, 1502, 1530, 3017, 3064, 3088, 3133, 3139, 3159, 3166, 3254

[a] Δε ≡ energy splitting between the lowest two electronic states; neither of the di-alkenes in question here has low-energy excited states and the adducts are assumed to have none. [b] Calculated values at the B3LYP/6-31G(2d,p) level of theory. [c] Frequencies are for the C1 adduct.

At 561 K, our third law analysis gives the results $\Delta_r S = -105 \pm 10$ J mol^{-1} K^{-1} and $\Delta_r H = -124.4 \pm 7.1$ kJ mol^{-1}; the uncertainties we report reflect an estimate of our imperfect knowledge of the input data needed to calculate absolute entropies (particularly the low frequency $Cl-C_5H_8$ vibrations and the potential for a small contribution from the C4 adduct) as well as the estimated uncertainty in the experimental value for K_P at 561 K. In arriving at the above uncertainty in $\Delta_r S$, we assume that the frequencies in the three lowest frequency $Cl-C_5H_8$ vibrations could differ from the values given in Table 4.9 by ± 25 cm^{-1}. Appropriate heat capacity corrections have been employed to obtain $\Delta_r H$ values at 298 K and 0 K; the results are summarized in Table 4.6. The thermochemical parameters determined from the second- and third-law analyses are in reasonable agreement; however, the uncertainties associated with the third law values are smaller. Hence, we feel it appropriate to report the third law results as the experimentally determined values for $\Delta_r H$: In units of kJ/mol, $\Delta_r H_{298} = -124.5 \pm 7.2$, $\Delta_r H_0 = -123.1 \pm$

7.2 where uncertainties are accuracy estimates at the 95% confidence level. Theoretical bond strengths are also tabulated in Table 4.5 and agree reasonably well with the experimental values. The dashed line in Figure 4.6 is generated from equation (4-XII) using the 561 K third law values for $\Delta_r S$ and $\Delta_r H$. The mathematical expression represented by the dashed line in Figure 4.6 is

$$ln\ K_P\ (atm^{-1}) = -12.6 + 14900 / T \qquad \text{(third-law analysis)} \qquad (4\text{-XIV})$$

The values for $\Delta_r H$ obtained above can be used in conjunction with literature values for the standard enthalpies of formation of Cl [*Chase et al., 1985*] and isoprene [*Fraser and Prosen, 1955*] to deduct a value for the standard enthalpy of formation of Cl−isoprene at 298 K, $\Delta_f H_{298} = 72.6$ kJ/mol.

Table 4.5. Thermochemical parameters for the reaction Cl + isoprene ↔ Cl−isoprene.

T /K	Method	$-\Delta_r H$ (kJ mol^{-1})	$-\Delta_r S$ (J mol^{-1} K^{-1})	$\Delta_f H$ (C_5H_8−Cl)[a] (kJ mol^{-1})
561	Second law	116.0 ± 8.0 [b]	92 ± 15.0	
	Third law	124.4 ± 7.1 [c]	105 ± 10	
0	Second law	114.7 ± 8.0 [b]		
	Third law	123.1 ± 7.2 [c]		
	G4 theory [d]	127.1 ± 3.5 [e]		
298	Second law	116.1 ± 8.0 [b]		
	Third law	124.5 ± 7.2 [c]	105 ± 10	72.6 ± 6
	G4 theory [d]	128.5 ± 3.5 [e]		

[a]Values are based on third law results; [b] Uncertainty is 2σ, precision only; [c] Uncertainty is estimated accuracy at 95 % confidence level; [d] The level of optimization is B3LYP/6-31G(2df,p); [e] Uncertainty represents average deviation between experiment and theory for a test set of 454 chemical species, 34 of which were radicals.

At temperatures where the adduct was very stable we could measure $k_{4.1b}(T)$. From 201 to 320 K, we observe temperature independent rate coefficients for the total rate of reaction of Cl to isoprene, $k_{4.1}(T)$. We have successfully measured $k_{4.1b}(T)$ by conducting experiments at temperatures where the adduct falls apart immediately on the timescale of our experiments ($> 10^5$ s^{-1}). Measurement of $k_{4.1a}(T)$ required heating to high T ($T \geq 690$ K), so we were unable to experimentally determine $k_{4.1a}(T)$. Direct observation of adduct formation/dissociation kinetics were observed from 488 – 635 K for the reactions above (4.1b/−1b). The data obtained can be compared with other published studies of Cl + isoprene and expands the temperature range studied for reaction. Furthermore, the bond dissociation enthalpy is experimentally obtained for Cl−isoprene adduct for the first time.

Literature Comparisons

Our observed independence of $k_{4.1}$ on P (for $P \geq 3$ Torr) is consistent with the literature [*Ragains and Finlayson-Pitts, 1997; Notario et al., 1997; Fantechi et al., 1998; Bedjanian et al., 1998; Stutz et al., 1998; Finlayson-Pitts et al., 1999; Canosa-Mas et al., 1999; Suh and Zhang, 2000; Albaladejo et al., 2003; Orlando et al., 2003; Xing et al., 2009*], and our 298 K value for $k_{4.1}$, $3.55 \pm 0.53 \times 10^{-10}$ cm^3 $molecule^{-1}$ s^{-1}) is near the low end of the range of reported values in the literature However, our observed T independence of $k_{4.1}$ (Table 4.1 and Fig. 4.3) is not consistent with the only reported temperature dependent rate coefficient [*Bedjanian et al., 1998*]. While Bedjanian et al. observe a 298 K rate coefficient that is in excellent agreement with our 298 K value, they report a substantial negative activation energy over the range 233-320 K. There are no

reported bond strengths with which to compare our measured bond strength for Cl−isoprene.

Implications for Atmospheric Chemistry

The gas phase rate coefficients measured in this study can be employed to compare the potential importance of Cl as an atmospheric sink for isoprene with contributions from other atmospheric species that are known to also be reactive toward isoprene, i.e., OH, NO_3, and O_3. Cl atom concentrations generally peak at dawn which is much earlier than OH. The peak Cl concentration has been predicted to be approximately an order of magnitude larger than the simultaneous OH concentration [*Brauers et al., 1996*]. Because of this, combined with the fact that the 298 K Cl + isoprene reaction is so fast (3.55×10^{-10} cm^3 $molecule^{-1}$ s^{-1}) the reaction could compete with OH as an effective loss pathway for isoprene under some atmospheric conditions. The calculated atmospheric lifetime of isoprene based solely on oxidation by OH, where [OH] = 1×10^6 molecules cm^{-3} [*Seinfeld and Pandis, 2006*] is 3 hrs. Estimates of the peak concentrations of atomic chlorine in the marine boundary layer vary from 10^3–10^5 cm^{-3} [*Spicer et al., 1998; Pszenny et al., 1993; Singh and Kasting, 1998*]. If Cl concentrations are as high as 1×10^5 atoms cm^{-3}, the lifetime for isoprene removal by Cl would be roughly 8 hrs. This would make the Cl a non-negligible player in isoprene oxidation, especially at dawn when OH is < 10^5 molecules cm^{-3} [*Prinn et al., 2001*]. More conservatively, assuming an average Cl concentration of 4 x 10^4 atoms cm^{-3}, which appears to be appropriate for the marine boundary layer [*Wingenter et al., 2005*] and the rate coefficient reported in this study, the atmospheric lifetime for isoprene removal by Cl is approximately 20 hrs.

The contribution of Cl to isoprene destruction is difficult to evaluate because (i) atmospheric Cl concentrations are highly variable in space and time and (ii) the atmospheric fate of Cl−isoprene is uncertain. Since (i) Cl levels in the MBL are thought to be the highest encountered in the unpolluted troposphere and (ii) it is likely that, as in the case of Cl–C_6H_6 [*Sokolov et al.*, 1998], a significant fraction of Cl–isoprene loss in the atmosphere results in regeneration of isoprene, the above scenario only represents the maximum possible contribution from the Cl + isoprene reaction. While it is difficult to assess the overall importance of the Cl reaction as discussed above, it appears unlikely that Cl represents a significant loss process for isoprene in the atmosphere as it simply cannot compete with the OH reaction except for possibly at dawn.

CHAPTER 5

KINECTIC STUDIES OF BROMINE ATOM REACTIONS WITH ISOPRENE, 2,3-DIMETHYL-2-BUTENE AND 1,3 BUTADIENE

Introduction

Reactions of atomic bromine with olefins are thought to play a significant role in the chemistry of marine atmospheric environments, particularly in polar regions during ozone depletion events [*Jobson et al., 1994; Solberg et al., 1994*]. In comparison with other radical species such as Cl, OH and NO_3, the kinetic data base for the reactions of Br atoms with unsaturated hydrocarbons is quite sparse [*Bierbach et al., 1996; Barnes et al., 1989; Wallington et al., 1989; Anthony and Roscoe, 2004*]. The reactions of Br atoms with saturated hydrocarbons proceed slowly via hydrogen abstraction, and are thought to be of negligible importance in the atmosphere. However, Br reactions with unsaturated hydrocarbons can be more complex. These reactions typically proceed rapidly via addition of the Br atom to the double bond and, depending on the local Br atom concentration and subsequent chemistry of the Br-containing adduct, could play a significant role in atmospheric chemisty.

The bromoalkyl radicals formed via Br + olefin addition reactions typically have relatively weak C−Br bonds such that under atmospheric conditions radical unimolecular decomposition occurs in competition with the radical + O_2 reaction. As a result, the rates of Br initiated oxidations of olefins under atmospheric conditions typically display

complex temperature and pressure dependences [*Bierbach et al., 1996; Barnes et al., 1989; Bedjanian et al., 1998; Sauer et al., 1999; Ramacher et al., 2001*].

In this chapter, we focus on the reactions of atomic bromine with a series of unsaturated hydrocarbons, tetramethylethylene (TME, 2,3-dimethyl-2-butene), 1,3-butadiene, and isoprene (2-methyl-1,3-butadiene).

$$Br(^2P_{3/2}) + (CH_3)_2C{=}C(CH_3)_2 \rightarrow HBr + (CH_3)_2C{=}C(CH_3)(CH_2) \quad (5.1a)$$

$$Br(^2P_{3/2}) + (CH_3)_2C{=}C(CH_3)_2 + M \leftrightarrow (CH_3)_2C(Br)C(CH_3)_2 + M \quad (5.1b, -5.1b)$$

$$(CH_3)_2C(Br)C(CH_3)_2 + O_2 + M \rightarrow (CH_3)_2C(Br)C(OO)(CH_3)_2 + M \quad (5.2)$$

$$Br(^2P_{3/2}) + H_2C{=}CHCH{=}CH_2 \rightarrow HBr + Products \quad (5.3a)$$

$$Br(^2P_{3/2}) + H_2C{=}CHCH{=}CH_2 + M \leftrightarrow H_2C(Br){=}CHCH{=}CH_2 + M \quad (5.3b, -5.3b)$$

$$H_2C(Br){=}CHCH{=}CH_2 + O_2 + M \rightarrow H_2C(Br){=}CH(OO)CH{=}CH_2 + M \quad (5.4)$$

$$Br + H_2C{=}C(CH_3)CH{=}CH_2 \rightarrow HBr + H_2C{=}C(CH_2)CH{=}CH_2 \quad (5.5a)$$

$$Br + H_2C{=}C(CH_3)CH{=}CH_2 + M \leftrightarrow C_5H_8Br + M \quad (5.5b, -5.5b)$$

$$C_5H_8Br + O_2 + M \rightarrow C_5H_8BrOO + M \quad (5.6)$$

Various factors led the motivation behind the study of Br + olefin reactions depicted in the scheme above. Our interest in the Br + TME reaction (5.1a, 5.1b/−5.1b, 5.2) stems, in part, from its chemical uniqueness. The C−H bonds in TME are unusually weak; hence, unlike most organic molecules, hydrogen abstraction from TME by atomic bromine is exothermic and occurs with a large rate coefficient even at low atmospheric temperatures [*Bedjanian et al., 2000*]. Furthermore, donation of electron density to the double bond from the methyl groups results in increased stability for the C−Br bond in

the Br−TME adduct compared to the CH_2CH_2Br radical formed from Br addition to ethylene which has an experimentally determined C−Br bond strength of 29 kJ/mol [*Ferrell, 1998*]. Additionally, TME has been observed in the atmosphere (primarily in automobile exhaust plumes) with mixing ratios as high as 1 ppbv (parts per billion by volume) [*McEwen, 1966*].

Isoprene is the most abundant NMHC in our atmosphere as described in Chapter 4 of this dissertation. In addition to the well-known fact that isoprene is emitted into the atmosphere from vegetation, a potentially significant marine source of isoprene has received considerable recent attention [*Moore et al., 1994; Liss, 2007; Liakakou et al., 2007; Sinha et al., 2007; Arnold et al., 2009; Gantt et al., 2009; 2010*]. In order to gain a complete understanding of the lifetime of isoprene under a variety of atmospheric conditions, it is important to investigate Br + isoprene kinetics. 1,3−butadiene is known to be a human carcinogen, and exists in the atmosphere from various anthropogenic sources. Three quarters of the manufactured 1,3−butadiene is used in synthetic rubber production for tires [*ATSDR, 1992a*].

As mentioned previously, published kinetic data on Br + olefin reactions are limited. Bierbach *et al.* [*1996*] report the following effective rate coefficients from a relative rate study at 298 K and 1000 mbar synthetic air where the loss of each alkene by reaction with Br was monitored: isoprene 7.42×10^{-11}; 1,3-butadine 5.75×10^{-11}; TME 2.82×10^{-11} $cm^3\,molecule^{-1}\,s^{-1}$. However, the process studied by Bierbach *et al.* is not an elementary reaction.

It is worth noting that Bierbach *et al.* [*1996*] obtained their Br kinetics results by measuring the chain of rate coefficient ratios Isoprene : 1,3-butadiene : TME : *trans*-2-

butene : propylene : acetaldehyde with an assumed absolute rate coefficient of 3.6×10^{-12} cm^3 $molecule^{-1}$ s^{-1} for the Br + acetaldehyde reaction; the only reaction in the sequence for which an absolute rate determination has been reported [*Atkinson et al., 2006; Sander et al., 2011*]. Ideally, relative rate experiments are carried out under conditions where both the reactant compound and the reference compound react at similar rates, i.e., rate coefficients within a factor of three or so, but the limited kinetic database for Br reactions forced the researchers [*Bierbach et al., 1996*] to employ a stepwise method to determine kinetics for the above-mentioned alkenes. This study will help to expand the kinetic database for Br + alkene reactions.

In addition to the relative rate study mentioned above, there is one additional study on the kinetics of the Br + TME reaction in the literature. Bedjanian *et al.* [*2000*] in a discharge flow study at P = 1 Torr He and 233 K ≤ T ≤ 320 K obtained the Arrhenius expression $k_{5.1a} = 2.4 \times 10^{-11} \exp(-75/T)$ for the H-abstraction reaction which corresponds to approximately 1.5 times slower than the effective rate coefficient reported by Bierbach *et al.* [*1996*]. Bedjanian *et al.* also determined the temperature dependence of the product of the equilibrium constant for Br−TME formation/dissociation (i.e., $k_{5.1b} / k_{-5.1b}$) and the rate coefficient for Br−TME reaction with Br_2, from which they deduced the enthalpy change associated with Br−TME formation to be −(41 ± 9) kJ/mol.

In this study, we couple 266 nm laser flash photolysis of CF_2Br_2 with monitoring of Br by time-resolved atomic resonance fluorescence spectroscopy to investigate Br + isoprene, TME, and 1,3-butadiene kinetics over a wide range of temperature, pressure, and $[O_2]$. The results allow rate coefficients for elementary steps in the overall mechanism for the Br-initiated oxidation of each olefin to be evaluated more directly than

in earlier studies. In addition, the C−Br bond strength in each of the Br−alkene adducts is obtained from direct measurements of ($k_{5.1b}/k_{-5.1b}$), ($k_{5.3b}/k_{-5.3b}$), and ($k_{5.5b}/k_{-5.5b}$), respectively. Observations of perturbation to "approach to equilibrium" kinetics upon addition of O_2 to reaction mixtures allows for the evaluation of the O_2 reaction with the Br−alkenes to give the rate coefficients, $k_{5.2}$, $k_{5.4}$, and $k_{5.6}$, respectively. Our ability to monitor Br kinetics directly both in the absence and presence of O_2 allows the rate coefficients for some elementary steps in the overall complex mechanisms to be determined for the first time. Our results are compared with the literature data described above, and the potential importance of Br-initiated oxidation as an atmospheric sink for each of the alkenes is assessed.

Experimental Details

The studies of Br reaction with a series of alkenes was conducted by coupling laser flash photolysis of CF_2Br_2/N_2 mixtures with time-resolved atomic resonance fluorescence spectroscopic detection of bromine atoms. The descriptions of the apparatus and the technique can be found in Chapter 2 and only details particular to this study are discussed below.

Bromine atoms were generated by 266 nm laser flash photolysis of CF_2Br_2 using fourth harmonic radiation from a Quanta Ray model DCR-3 Nd:YAG laser as the photolytic light source:

$$CF_2Br_2 + h\nu(266\ nm) \rightarrow CF_2Br + Br \qquad (5.7)$$

The maximum laser repetition rate was 10 Hz, the pulse width was ~ 6 ns, and the laser fluence ranged from 3 to 20 mJ cm^{-2} $pulse^{-1}$. The laser energy was measured by a

thermopile calorimeter energy meter upon exit of the laser beam from the reaction cell. Bromine atom concentrations produced by the laser flash were typically in the range of (1 - 6) × 10^{11} atoms cm^{-3}. The absorption cross-section for CF_2Br_2 at 266 nm is 7.50 × 10^{-20} cm^2 [*Sander et al., 2011*] and the quantum yield for Br production from CF_2Br_2 is unity [*Park et al., 2001*].

Two different reaction cells were used during the course of the Br + alkene experiments. The reaction cell shown in Figure 2.2 was used for the majority of experiments; however, the reaction cell shown in Figure 2.1 was employed for high temperature Br + isoprene experiments.

The reagent and photolyte were flowed into the reaction cell from 12 L bulbs containing dilute mixtures in nitrogen while CO_2, He, and additional N_2 flowed directly from their storage cylinders. The mole fraction of each alkene in the dilute bulbs was checked frequently by UV photometry at 228.8 nm using a Cd Penray® lamp. The photometric measurements were carried out on a separate high vacuum gas handling system using a monochromator to isolate the 228.8 nm Cd emission line. The absorption cross sections at 228.8 nm have been measured as part of this study and determined to be 2.07 × 10^{-18} cm^2 $molecule^{-1}$ for TME, 9.36 × 10^{-18} cm^2 for isoprene, and 1.30 × 10^{-18} cm^2 for 1,3-butadiene.

The gases used in this study had the following stated minimum purities: N_2 (99.999%, Airgas), He (99.999%, Airgas), CO_2 (99.99%, Airgas), Cl_2CO (99.0%, Matheson Trigas). For Cl_2CO and CO_2 the purity refers to liquid in a high pressure cylinder. The liquids used in this study had the following stated minimum purities: CF_2Br_2 (97%, Aldrich), 1,3-butadiene (≥99%, Aldrich (contains TBC)) isoprene ((>99.0

%, TCI America (stabilized with TBC)), and TME (Aldrich, 98%). N_2, CO_2, and He were used as supplied, while the TME, isoprene, and 1,3-butadiene were degassed repeatedly at 77 K, then diluted in N_2 and stored in a pyrex bulb before use.

Results and Discussion

All experiments were carried out under pseudo-first-order conditions with the alkene in large excess over $[Br]_0$. Thus, in the absence of secondary reactions that enhance or deplete the Br concentration, the Br temporal profile following the laser flash would be described by the relationship

$$ln\{[Br]_0 / [Br]_t\} = ln\{S_0 / S_t\} = (k_{5.i}[alkene] + k_{5.8})t = k't \quad (i = 1,3,5) \qquad (5\text{-I})$$

In equation (5-I), S_0 is the Br fluorescence signal at a time immediately after the laser fires, S_t is the Br fluorescence signal at time t, $k_{5.i}$ is the overall rate coefficient for loss of Br by all *irreversible* Br + alkene reaction channels, and $k_{5.8}$ is the rate coefficient for the following reaction:

$$Br \rightarrow \text{Reaction with background impurities and/or loss by diffusion from detector field of view} \qquad (5.8)$$

The bimolecular rate coefficients of interest, $k_{5.i}(P,T)$ (i = 1,3,5) are determined from the slopes of k′ vs [alkene] plots obtained at constant T and P.

Br + TME at 274 K ≤ T ≤ 420 K

Well-behaved pseudo-first order Br atom kinetics were observed in studies carried out over the temperature range 274 – 420 K, i.e., Br temporal profiles were exponential

and observed first order decay rates were found to increase linearly with increasing [TME] but were independent of laser photon fluence and [CF_2Br_2]; these kinetic observations are consistent with the behavior predicted by equation (5-I). Furthermore, bimolecular rate coefficients obtained from the slopes of k′ vs [TME] plots were found to increase slightly with increasing temperature and were independent of pressure over the range 25 – 700 Torr. The observational evidence strongly supports the contentions that (i) the dominant pathway for Br + TME reaction is H-abstraction and (ii) reactions (5.1a) and (5.8) are the only processes that significantly affect the post-laser-flash Br time history. Typical Br + TME data are shown in Figures 5.1 and 5.2, and measured bimolecular rate coefficients, $k_{5.1a}(P,T)$, are summarized in Table 5.1. An Arrhenius plot for reaction (5.1a) is shown in Figure 5.3. The following best fit Arrhenius expression is derived from a linear least-squares analysis of the *ln* $k_{5.1a}$ versus T^{-1} data:

$$k_{5.1a}(T) = (3.84 \pm 0.84) \times 10^{-11} \exp[(-169 \pm 61) / T] \text{ cm}^3 \text{ molecule}^{-1} \text{ s}^{-1}$$

The range of temperatures where irreversible Br + TME kinetics were observed was 274 K ≤ T ≤ 420 K.

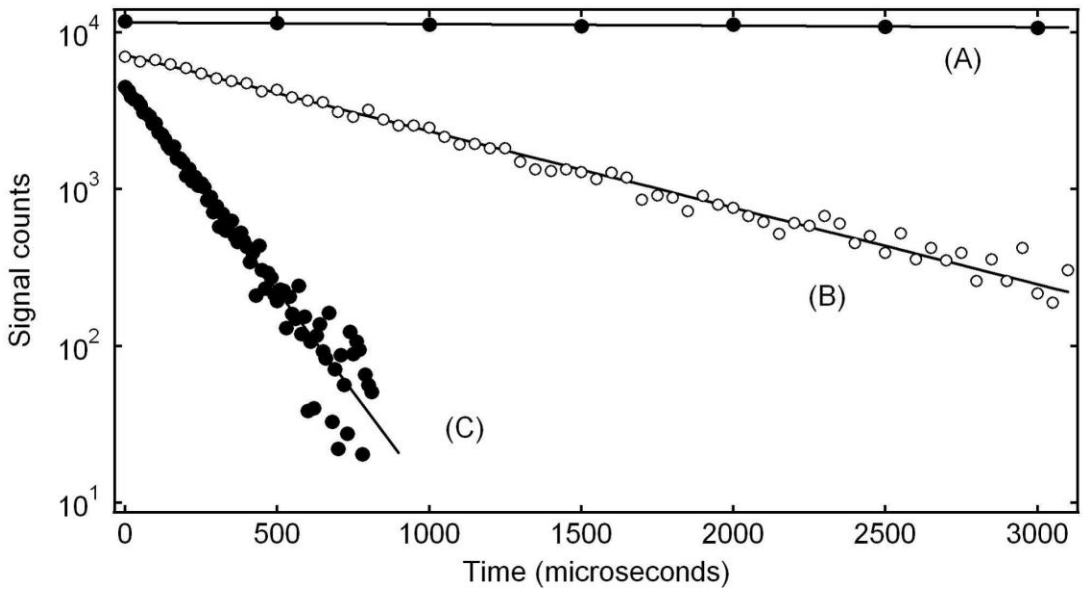

Figure 5.1. Typical resonance fluorescence temporal profiles observed in kinetics studies of Br + TME at 298 K. Experimental conditions: P = 25 Torr; [TME] (10^{13} molecule cm^{-3}) = (A) 0, (B) 4.31, and (C) 27.6; number of laser shots averaged = (A) 50, (B) 1000, and (C) 5000. Solid lines are obtained from least-squares analyses and give the following pseudo-first-order decay rates in units of s^{-1}: (A) 25, (B) 1180, and (C) 6090. For clarity, traces are scaled by the following factors: (A) 1.5, (B) 3, (C) 1.7.

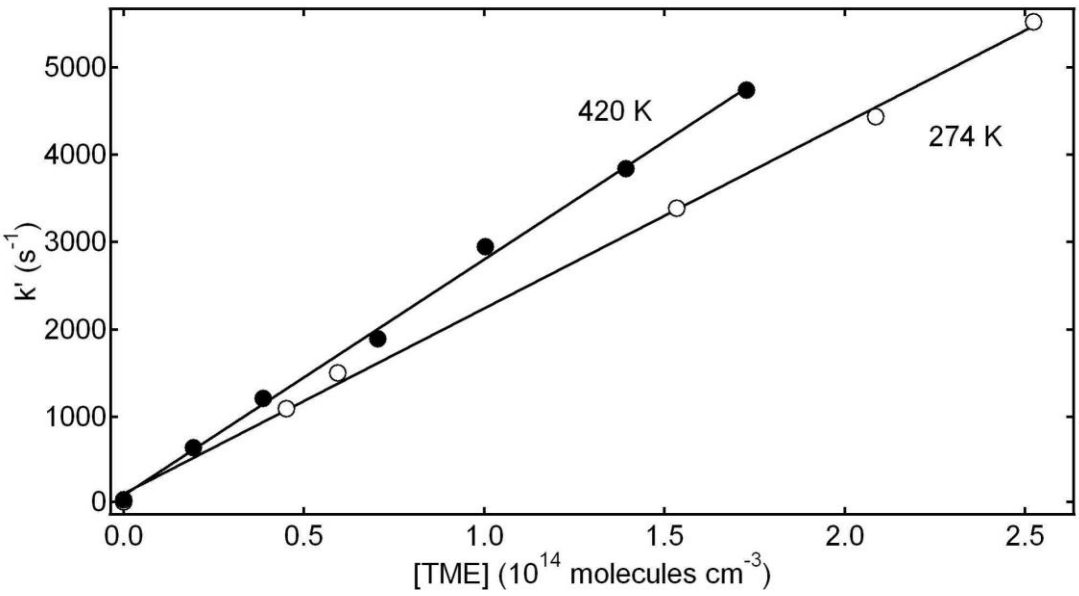

Figure 5.2. Typical plots of k′ versus [TME] for reaction (5.1a). Kinetic data obtained at 274 K (open circles) and 420 K (filled circles), P = 25 Torr. Solid lines are obtained from least-squares analyses and lead to the bimolecular rate coefficients given in Table 5.1.

Table 5.1. Summary of kinetic data at T ≥ 274 K for Br + TME. [a]

T	P	N[b]	$[CF_2Br_2]$	$[Br]_0$	$[TME]_{max}$	k'_{max} (s^{-1})	$k_{5.1a} \pm 2\sigma$[c]
274	25	5	6200	2.2	2200	5186	2.21 ± 0.16
274	25	5	5000	1.7	2500	5520	2.12 ± 0.09
274	200	4	6200	2.2	1490	3093	2.04 ± 0.04
298	25	6	7000	7.0	3420	7300	2.13 ± 0.11
298	700	5	4800	2.7	1350	2925	2.06 ± 0.07
344	50	5	6300	3.5	2350	5481	2.31 ± 0.02
420	25	5	5300	2.9	1930	4934	2.52 ± 0.06
420	25	6	4700	1.6	1730	4738	2.70 ± 0.11

[a] Units are T (K); P (Torr); k' (s^{-1}); $[CF_2Br_2]$, $[Br]_0$, (10^{11} per cm^3); $k_{5.1a}$ (10^{-11} cm^3 $molecule^{-1}$ s^{-1}); [TME] (10^{11} per cm^3); [b] N ≡ Number of determinations of a single pseudo-first order decay rate; [c]Uncertainties represent precision only.

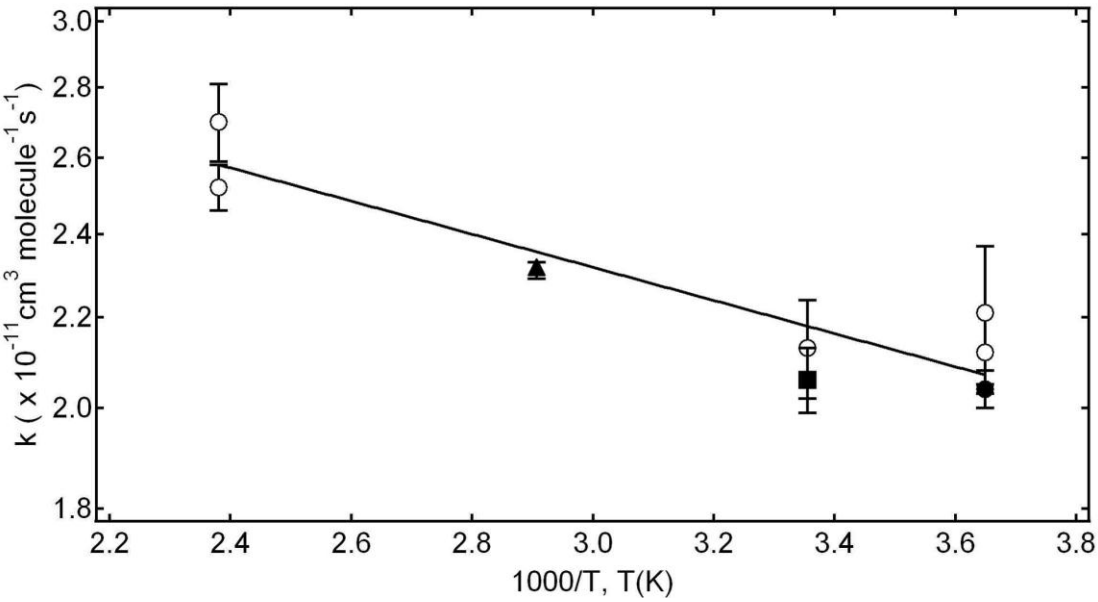

Figure 5.3. Arrhenius plot for the Br + TME H-abstraction reaction. The solid line is obtained from an unweighted least squares analysis and gives the following Arrhenius expression reported in the text. P = 25 Torr (open circles), 50 Torr (triangle), 200 Torr (filled circle), 700 Torr (square). Uncertainties are 2σ, precision only.

Br + TME at 203 K ≤ T ≤ 241 K

Over the temperature range 203 − 241 K, kinetic evidence for reversible addition of Br to TME was observed. The relevant kinetic scheme for analysis of this low temperature data includes reactions (5.1a), (5.1b), (−5.1b), (5.8), and (5.9).

Br−TME → loss by processes that do not regenerate Br atoms (5.9)

The rate equations for the above reaction scheme can be solved analytically and predict a double exponential functional form for the Br decay.

$$[S]_t / [S]_0 = [(Q + \lambda_1)\exp(\lambda_1 t) - (Q + \lambda_2)\exp(\lambda_2 t)] / (\lambda_1 - \lambda_2) \quad \text{(5-II)}$$

In equation (5-II), S_t and S_0 are the resonance fluorescence signal levels at times t and 0, and

$$Q = k_{-5.ib} + k_{5.9}, \quad \text{(5-III)}$$

$$-(\lambda_1 + \lambda_2) = Q + k_{5.8} + (k_{5.ia} + k_{5.ib})\,[TME], \quad \text{(5-IV)}$$

$$\lambda_1 \lambda_2 = Q\,(k_{5.8} + k_{5.ia}[TME]) + k_{5.9}\,k_{5.ib}\,[TME], \quad \text{(5-V)}$$

Observed Br temporal profiles for Br + TME are shown in Figure 5.4. The temporal profiles were fit to the double exponential equation (5-II) using a non-linear least squares method to obtain values for the fit parameters S_0, Q, λ_1, and λ_2. Rearrangement of equations (5-III) – (5-V) gives the following relationships for the rate coefficients of interest:

$$k_{5.ib} = -(Q + k_{5.8} + k_{5.ia}\,[TME] + \lambda_1 + \lambda_2) / [TME], \quad \text{(5-VI)}$$

$$k_{5.9} = \{\lambda_1\lambda_2 - Q\,(k_{5.8} + k_{5.ia}\,[TME])\} / (k_{5.ib})\,[TME], \quad \text{(5-VII)}$$

$$k_{-5.ib} = Q - k_{5.9} \quad \text{(5-VIII)}$$

The background Br atom loss rate ($k_{5.8}$) was directly measured by observing the RF decay in the absence of TME at each temperature and pressure. At 298 K, $k_{5.8}$ varied from 35 s^{-1} at 25 Torr to 11 s^{-1} at 700 Torr. Temperature dependent rate coefficients for the H-abstraction pathway ($k_{5.1a}(T)$) were obtained by extrapolation of the high-temperature (274 K $\leq$ T $\leq$ 420 K) kinetic data assuming Arrhenius behavior, i.e., a linear *ln* $k_{5.1a}$ vs. 1/T dependence from 274 K down to 203 K.

Experimental conditions and results of all Br + TME equilibration kinetics experiments are summarized in Table 5.2. The values of the equilibrium constants given in Table 5.2 have been derived from the following relationship

$$K_P = k_{5.ib} / (k_{-5.ib}RT) = K_c / (RT) \quad \text{(5-IX)}$$

The results at T = 212 ± 1 K and P = 25 and 700 Torr show that $k_{5.1b}$ and $k_{-5.1b}$ are dependent on pressure while K_P is not, which is expected for an addition/dissociation reaction. The observed pressure-independence of K_P increases confidence that the non-linear least squares fitting procedure is relatively free of systematic errors in the extracted rate coefficients. Examination of Table 5.2 shows that the precision of multiple determinations of $k_{5.ib}$ and $k_{-5.ib}$ at a given temperature and pressure is quite good, approximately ±5 % for $k_{5.ib}$ and ±20 % for $k_{-5.ib}$. We estimate the accuracies (95% confidence level) of reported $k_{5.ib}$ and $k_{-5.ib}$ values are ±15 % and ±25% respectively. Hence, a reasonable estimate for the accuracies of reported values for K_P is ±30 % (95% confidence level) over the full range of temperatures investigated.

A plot of *ln* K_P vs 1/T, i.e., a van't Hoff plot, is shown in Fig. 5.5. A linear least-squares analysis of the data gives the following expression:

$$ln\ K_P\ (atm^{-1}) = -(12.1 \pm 4.0) + (5690 \pm 860) / T \qquad \text{(Reactions} \pm 5.1b)$$

Uncertainties in the above expression are 2σ and represent the precision of the fit parameters in the van't Hoff analysis. As discussed later in this chapter, the slope and intercept of the van't Hoff plot are related to $\Delta_r H$ and $\Delta_r S$ for reaction (5.ib), respectively.

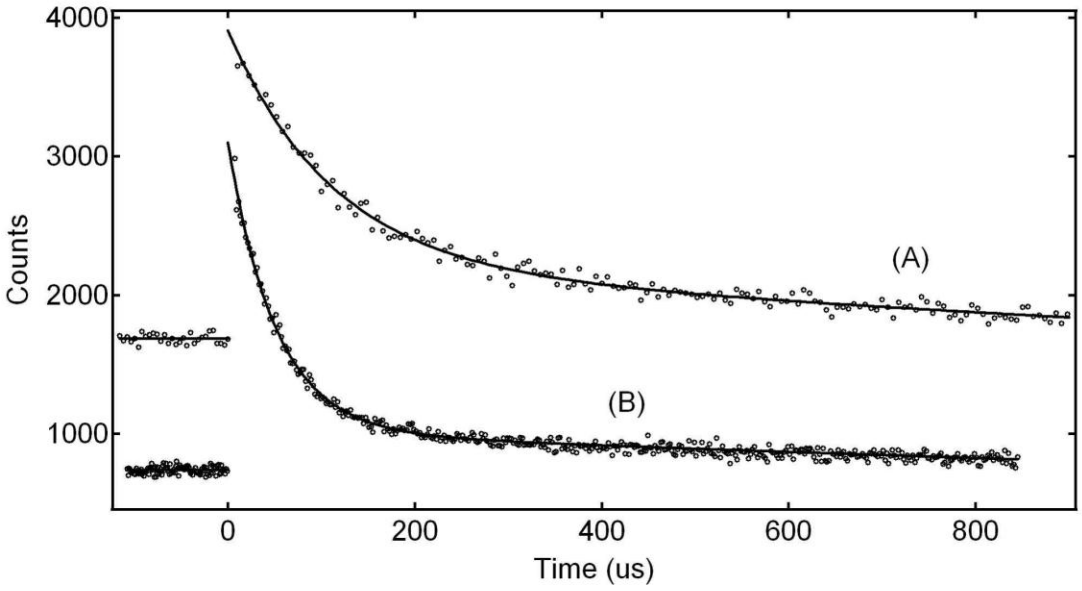

Figure 5.4. Typical resonance fluorescence Br temporal profiles observed over the range 203 ≤ T (K) ≤ 241. Experimental conditions: P = 25 Torr, T = 223 K, $[CF_2Br_2]$ (10^{14} molecules cm^{-3}) = (A) 7.0, (B) 7.3; $[Br]_0 \sim 3 \times 10^{11}$ atoms cm^{-3}; [TME] (10^{13} molecules cm^{-3}) = (A) 9.73, (B) 23.6. Solid lines through data at t > 0 are obtained from non-linear least squares fits to equation (II). Best fit parameters are (A): $S_0 = 2070$, $Q = 4660\ s^{-1}$, $\lambda_1 = -10400\ s^{-1}$, $\lambda_2 = -1680\ s^{-1}$; (B): $S_0 = 2340$, $Q = 4170\ s^{-1}$, $\lambda_1 = -19900\ s^{-1}$, $\lambda_2 = -1650\ s^{-1}$.

Table 5.2. Results of the Br + TME + N_2 ↔ Br−TME + N_2 equilibration kinetics experiments.[a]

T	P	Q	$-\lambda_1$	$-\lambda_2$	[TME]	$[CF_2Br_2]$	$[Br]_0$	$k_{5.1b}$	$k_{5.9}$	$k_{-5.1b}$	K_p
203	25	1110	13100	809	1310	5700	2.0	8.14	643	462	76.4
	25	898	6470	688	673	5600	2.0	7.66	553	345	97.4
	25	1500	3670	1080	339	5400	1.9	7.92	966	537	64.3
	25	1640	5330	1200	493	5600	2.0	8.25	1040	601	59.5
212	25	4080	15400	3070	1680	5800	2.1	6.91	2480	1600	18.7
	25	2490	8480	1610	910	5700	2.0	6.66	1290	1200	24.2
	25	2310	6540	1330	623	5200	1.9	7.22	1130	1180	26.1
	25	2120	4380	1050	362	5100	1.8	7.41	990	1130	28.0
211	100	2810	11500	1940	864	5600	2.0	10.6	1710	1100	38.8
	100	1840	5810	1030	400	5400	1.9	10.8	941	902	47.8
	100	1920	9330	1150	696	5300	1.9	10.6	991	928	45.8
	100	1570	6880	863	531	5100	1.8	9.92	732	835	48.1
212	200	2310	9810	1310	581	3600	1.0	13.4	1200	1120	46.8
	200	2270	13500	1300	817	3600	1.2	13.7	1140	1120	47.4
	200	2080	6930	1120	401	3700	1.2	13.1	1060	1020	50.1
	200	2330	7160	1210	404	1600	1.2	13.2	1170	1160	44.5
	700	5340	21200	2950	980	4700	1.3	17.5	2850	2490	26.6
	700	5070	11900	2720	493	4800	1.7	17.6	2950	2120	31.5
223	25	4080	7400	1190	537	8000	2.9	6.63	1100	2980	9.31
	25	4660	10400	1680	973	7000	2.5	5.87	1280	3380	7.46
	25	4040	14600	1650	1660	7800	2.8	5.58	1010	3040	7.99
	25	4170	19900	1650	2360	7300	2.6	5.60	895	3270	7.44
232	25	8340	22800	2590	2370	6400	2.3	5.38	1350	6990	3.26
	25	6170	11900	1760	1270	6400	1.8	4.04	877	5290	3.50
	25	7540	28800	2530	3650	6100	1.8	4.69	950	6590	3.12
	25	7630	24400	2480	3040	6000	1.7	4.49	940	6690	2.98
241	25	16200	28500	6180	3470	6100	2.2	3.43	3810	12400	1.30
	25	13200	18900	3210	1680	5800	2.1	3.43	2120	11000	1.46
	25	16200	21400	2370	1130	5600	2.0	4.88	2140	14000	1.47
	25	12200	14500	1410	650	5900	2.1	3.85	1460	10800	1.62

[a] Units are T (K); P (Torr);Q, λ_1, λ_2, $k_{5.9}$, $k_{-5.1b}$ (s^{-1}); $k_{5.1b}$ (10^{-11} cm^3 $molecule^{-1}$ s^{-1}); K_P (10^5 atm^{-1}); [TME], $[CF_2Br_2]$, $[Br]_0$ (10^{11} per cm^3).

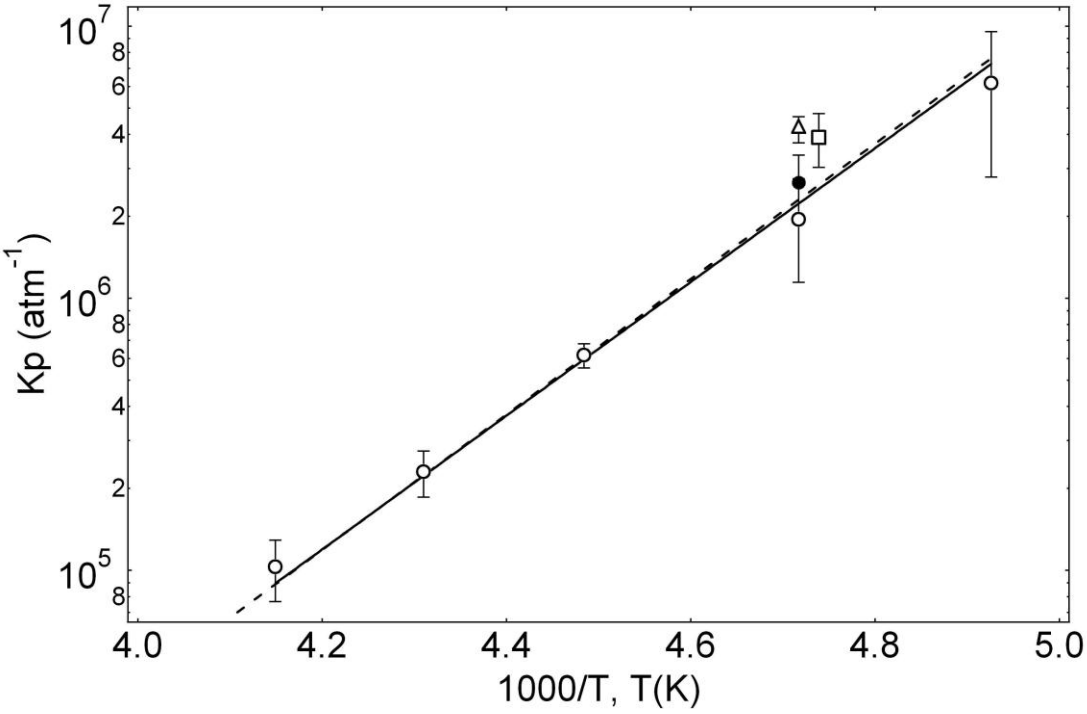

Figure 5.5. van't Hoff plot for the reversible addition reactions, Br + TME ↔ Br−TME. Solid line is obtained from least-squares analysis of *ln* K_P vs 1/T data and gives the second-law thermochemical parameters reported in Table 5.9. Data points are the average of all points at a specific T and P. Dashed line represents the results of the third law analysis. P = 25 Torr (open circles), 100 Torr (square), 200 Torr (triangle), 700 Torr (closed circle). Error bars on data points are 2σ, precision only.

Br + 1,3-butadiene at 271 K ≤ T ≤ 356 K

Over the temperature range 271 – 356 K, kinetic evidence for reversible addition of Br to 1,3-butadiene was observed. The relevant kinetic scheme for analysis of this equilibration data includes reactions (5.3a), (5.3b), (−5.3b), (5.8), and (5.9). The rate equations for the reaction scheme can be solved analytically and predict a double exponential functional form analogous to that shown in equations (5-II – 5-VIII) but with [TME] replaced by [1,3-butadiene], $k_{5.1a}$ replaced by $k_{5.3a}$, $k_{5.1b}$ replaced by $k_{5.3b}$, and $k_{-5.1b}$ replaced by $k_{-5.3b}$. Observed temporal profiles for Br + 1,3-butadiene over this temperature range were analogous to the Br + TME data (see Fig 5.4) obtained from 203 - 241 K. Experimental conditions and results of all equilibration kinetics experiments are summarized in Table 5.3. The equilibrium constants given in Table 5.3 have been derived from the relationship shown in equation (5-IX) with $k_{5.3b}$ replacing $k_{5.1b}$ and $k_{-5.3b}$ replacing $k_{-5.1b}$. The results at 298 ± 1 K show that $k_{5.3b}$ and $k_{-5.3b}$ are dependent on pressure while K_P is not, which is expected for an addition/dissociation reaction. The observed pressure-independence of K_P increases confidence that the non-linear least squares fitting procedure is relatively free of systematic errors in the extracted rate coefficients. Since the precision of multiple determinations of $k_{5.3b}$ and $k_{-5.3b}$ is quite good, approximately ±5% for $k_{5.3b}$ and ±20% for $k_{-5.3b}$. Hence, a reasonable estimate for the accuracies of reported values for K_p is ± 30% (95% confidence level) over the full range of temperature investigated.

Table 5.3. Results of the Br + 1,3-butadiene + N_2 ↔ Br−1,3-butadiene + N_2 equilibration kinetics experiments.[a]

T	P	Q	$-\lambda_1$	$-\lambda_2$	$[C_4H_6]$	$[CF_2Br_2]$	$[Br]_0$	$k_{5.3b}$	$k_{5.9}$	$k_{-5.3b}$	K_p
271	700	360	6690	192	376	962	1.7	1.30	197	163	21.6
		205	8490	55	465	910	1.4	1.35	56	149	24.5
		270	3550	111	212	913	1.4	1.20	115	155	21.0
		358	4980	180	288	933	1.4	1.26	186	171	19.8
283	100	416	7140	141	676	1960	.89	1.01	146	270	9.74
		297	4560	58	390	1990	.91	1.10	61	237	12.1
		354	6060	104	522	1940	.89	1.11	108	246	11.7
295	20	547	2330	211	365	1010	1.8	.405	242	305	3.30
		518	1560	182	206	1020	1.5	.436	225	293	3.71
		422	4090	81	670	1030	1.6	.418	86	336	3.09
		554	2870	178	430	1030	1.6	.431	200	353	3.03
297	50	709	1420	218	130	1410	4.3	.530	327	382	3.43
		979	3680	283	375	1460	4.0	.596	345	633	2.33
		811	2720	196	270	1430	3.9	.582	248	562	2.56
		724	5210	91	592	1410	3.4	.581	101	623	2.30
	100	1134	3280	147	202	1000	1.2	.851	203	930	2.25
		1114	4870	109	339	981	1.2	.856	134	980	2.15
		1203	4070	147	260	987	.90	.867	193	1010	2.12
		1099	5920	89	444	985	.96	.830	104	995	2.05
	200	1472	3970	238	195	986	1.5	1.05	339	1130	2.29
		1510	6570	200	361	1090	1.7	1.09	247	1260	2.13
		1480	5960	176	295	1050	1.6	1.12	223	1260	2.19
		1538	8060	168	451	1050	1.6	1.12	199	1340	2.05
		1532	4650	171	214	1030	1.3	1.15	236	1300	2.19
	400	1870	7620	188	315	1030	2.5	1.42	237	1630	2.13
		1836	7510	182	313	1060	2.7	1.41	229	1610	2.16
		1695	4700	177	173	939	1.7	1.38	255	1440	2.36
		1946	10400	206	458	981	1.8	1.42	244	1700	2.05
		1971	8880	216	378	1000	1.8	1.42	266	1710	2.04
	700	2144	10400	300	390	1060	3.5	1.64	362	1780	2.27
		1903	6100	201	214	1210	3.6	1.54	273	1630	2.33
		2068	12600	215	531	1180	3.6	1.53	249	1820	2.07
		1894	5150	195	169	1160	3.2	1.53	285	1610	2.34
311	25	1163	9050	182	1750	2230	1.1	.458	201	963	1.12
		1165	9290	145	1750	2270	1.1	.472	159	1010	1.11
	100	2281	16800	188	1920	1860	.85	.761	211	2070	.867
		2282	17200	180	1920	1860	.85	.785	201	2080	.890
		2223	9400	263	993	1960	.90	.736	329	1990	.871

Table 5.3. Cont'd.[a]

T	P	Q	$-\lambda_1$	$-\lambda_2$	$[C_4H_6]$	$[CF_2Br_2]$	$[Br]_0$	$k_{5.3b}$	$k_{5.9}$	$k_{-5.3b}$	K_p
311	250	3560	20600	129	1540	2930	1.3	1.12	153	3410	.773
		3430	19600	105	1530	2930	1.3	1.06	124	3300	.758
	500	4260	30900	144	2030	3810	1.9	1.32	161	4100	.759
	700	4610	37200	208	2060	4040	1.2	1.59	235	4380	.855
312	100	2190	4650	228	379	945	..86	.708	387	1800	.925
		2190	6400	209	604	1060	.97	.730	298	1890	.908
		2390	8160	236	771	1120	1.0	.778	217	2070	.884
		2110	5680	197	508	1130	1.0	.740	291	1820	.958
		2120	7130	230	671	1150	1.1	.751	321	1990	.885
		2450	10000	232	1010	1110	1.0	.772	295	2150	.843
327	100	5660	10500	267	943	1460	1.3	.546	534	5130	.239
		6140	17900	272	2070	1470	1.3	.585	398	5740	.229
		6030	16700	258	1830	1430	1.4	.596	387	5650	.237
		5910	13300	262	1330	1630	1.6	.579	445	5470	.238
343	25	5570	10700	175	2130	1080	.99	.249	316	5260	.101
		6350	20700	205	5800	1130	1.0	.251	275	6070	.088
		6160	14800	190	3380	1100	1.0	.259	294	5870	.095
		6490	19400	200	4830	1090	.99	.271	279	6210	.093
		5310	9450	150	1840	1080	.99	.232	287	5020	.099
356	25	10800	19100	190	4510	1310	1.2	.188	381	10400	.037
		11100	23500	200	6470	1370	1.3	.195	341	10800	.037
		9780	15500	163	3330	1350	1.2	.176	370	9410	.039
		11200	22300	207	5500	1320	1.2	.203	373	10900	.039
		9990	17500	163	4370	1350	1.2	.174	324	9670	.037

[a] Units are T (K); P (Torr); Q, λ_1, λ_2, $k_{5.9}$, $k_{-5.3b}$ (s^{-1}); $k_{5.3b}$ (10^{-10} cm^3 $molecule^{-1}$ s^{-1}); K_P (10^6 atm^{-1}); $[C_4H_6]$, $[CF_2Br_2]$, $[Br]_0$ (10^{11} per cm^3).

A plot of *ln* K_P vs 1/T, i.e., a van't Hoff plot, is shown in Fig. 5.7. A linear least-squares analysis of the data gives the following expression:

$$ln\ K_p = -(9.8 \pm 1.1) + (7270 \pm 180)/T \qquad \text{(Reactions} \pm 5.3b)$$

Uncertainties in the above expression are 2σ and represent the precision of the fit parameters in the van't Hoff analysis. As discussed below, the slope and intercept of the van't Hoff plot are related to $\Delta_r H$ and $\Delta_r S$ for reaction (5.3b), respectively.

Br + 1,3-butadiene at 227 K and 437 K

Attempts were made to evaluate $k_{5.3a}$. Extrapolations of reversible Br addition data mentioned above to T = 437 K, suggests the Br−1,3-butadiene adduct is extremely short-lived at this temperature. This would, allow for investigation of a potential H-abstraction channel. An experiment was conducted at 437 K and 25 Torr N_2 in an effort to determine $k_{5.3a}$, however, only an upper limit could be deduced as no reaction was observed.

$$k_{5.3a}(437\ K) < 5 \times 10^{-14}\ cm^3\ molecule^{-1}\ s^{-1}$$

Hence, $k_{5.3a}(T)$ was taken to be zero for analysis of the Br + 1,3-butadiene equilibration kinetics over the range 271−356 K.

Once the range of temperatures over which we could monitor Br + 1,3-butadiene equilibration kinetics on timescales of our experiments (10^{-5} – 10^{-2} s) was established, experiments were carried out at temperatures low enough that adduct dissociation would not impact kinetics on our timescales. Well-behaved pseudo-first-order Br atom kinetics were observed in studies carried out at 227 K. Figure 5.1 is a good illustration of what the decays looked like for Br + 1,3-butadiene at 227 K. The data are presented in Table 5.4 and from the table it can be seen that the rate coefficient, $k_{5.3b}(227\ K)$, increases with increasing pressure over the range 20 – 700 Torr. This behavior is consistent with the formation of a stable adduct being the dominant reaction channel at low temperature.

Table 5.4. Br + 1,3-butadiene at 227 K.[a]

P	# exp.	$[CF_2Br_2]$	$[Br]_0$	$[C_4H_6]_{max}$	k'_{max}	$k_{5.3b} \pm 2\sigma$
20	4	.96	.95	2.50	2579	1.02 ± .04
50	6	1.2	1.5	2.46	2873	1.19 ± .13
100	6	1.2	1.3	2.52	4011	1.58 ± .03
200	5	.89	.80	2.36	4316	1.86 ± .08
400	4	1.3	1.2	1.82	3757	2.08 ± .10
700	6	1.6	1.5	2.28	5042	2.14 ± .23

[a] Units: P (Torr); $[CF_2Br_2]$, [Br], $[C_4H_6] = 10^{11}$ molecule cm^{-3}; k' (s^{-1}); k_{ib} (10^{-10} cm^3 $molecule^{-1}$ s^{-1})

Br + isoprene kinetics at 273 K ≤ T ≤ 357 K

Over the temperature range 273 – 357 K, kinetic evidence for reversible addition of Br to isoprene was observed. The relevant kinetic scheme for analysis of this equilibration data includes reactions (5.5a), (5.5b), (−5.5b), (5.8), and (5.9). The rate equations can be solved analytically, and predict a double exponential functional form for the Br decay analogous to that shown in equations (5-II – 5-VIII) but with [TME] replaced by [isoprene], $k_{5.1a}$ replaced by $k_{5.5a}$, $k_{5.1b}$ replaced by $k_{5.5b}$, and $k_{-5.1b}$ replaced by $k_{-5.5b}$. Experimental conditions and results of all Br + isoprene equilibration kinetics experiments are summarized in Table 5.5. The values for equilibrium constants given in Table 5.5 have been derived from the relationship shown in equation (5-IX) with $k_{5.5b}$ replacing $k_{5.1b}$ and $k_{-5.5b}$ replacing $k_{-5.1b}$. Temperature dependent rate coefficients for the H-abstraction pathway ($k_{5.5a}(T)$) were obtained by extrapolation of the high-temperature (526 K ≤ T ≤ 673 K) kinetic data (see below) assuming Arrhenius behavior, i.e., a linear *ln* $k_{5.5a}$ vs. 1/T dependence from 357 K down to 273 K. The results at 298 (± 1) K and 330 K show that $k_{5.5b}$ and $k_{-5.5b}$ are dependent on pressure while K_P is independent of pressure, which is to be expected for an addition/dissociation reaction. This result

increases confidence that the non-linear least squares fitting procedure is relatively free of systematic errors in the extracted rate coefficients. Since the precision of multiple determinations of $k_{5.5b}$ and $k_{-5.5b}$ are quite good, we estimate that the absolute accuracies of reported $k_{5.5b}$, $k_{-5.5b}$, and K_p values are ± 15%, ± 25%, and ± 30%, respectively, over the full range of temperature and pressure spanned by the results given in Tables 5.5. A plot of *ln* K_P vs 1/T, i.e., a van't Hoff plot, is shown in Fig. 5.7. A linear least-squares analysis of the data gives the following expression:

$$ln\ K_P = -(10.7 \pm 0.6) + (7960 \pm 284)/T \qquad \text{(Reactions} \pm \text{5.5b)}$$

Errors in the above expression are 2σ and represent precision only. As discussed below, the slope of the van't Hoff plot is related to $\Delta_r H$ for the reaction (5.5b) while the intercept is related to $\Delta_r S$. $\Delta_r H(319)$ for Br + C_5H_8 ($K_P = 1.81 \pm 0.54$) × 10^6 atm^{-1}).

Br + isoprene at 526 K ≤ T ≤ 673 K

Well-behaved pseudo-first-order Br atom kinetics were observed in studies carried out at 526 K ≤ T ≤ 673 K. Observed Br atom decays from 526 – 673 K were found to be exponential and the pseudo-first-order Br atom decay rates were found to increase linearly with increasing isoprene concentration but were independent of laser photon fluence. Bimolecular rate coefficients obtained from the slopes of k′ vs. [isoprene] plots are summarized in Table 5.6. Observation of exponential decays, a linear increase of k′ with increasing [isoprene], and pressure independent bimolecular rate coefficients (Table 5.6) support the contention that the dominant reaction pathway at 526 K ≤ T ≤ 673 K is H-abstraction. Typical high temperature Br temporal profiles are

shown in Figure 5.8 and typical plots of k′ versus [isoprene] are shown in Figure 5.9. An Arrhenius plot describing T dependence of the H abstraction reaction is shown in Figure 5.10. The best fit Arrhenius expression is

$$k_{5.5a}(T) = (1.29 \pm 0.28) \times 10^{-11} \exp[(-2150 \pm 310) / T] \text{ cm}^3 \text{ molecule}^{-1} \text{ s}^{-1}$$

Uncertainties in the above expressions are 2σ and represent the precision of the Arrhenius parameters. We believe the largest systematic uncertainty in the determination of each bimolecular rate coefficient, $k_{5.5a}(P,T)$, lies in the determination of the reagent concentration in the reaction mixture; we estimate this uncertainty to be ± 10% independent of pressure and temperature. Since the precision of the $k_{5.5a}(P,T)$ values tabulated in Table 5.6 is quite good ($2\sigma \leq 9$ %), we conservatively estimate the accuracy of each reported value for $k_{5.5a}(T)$ to be ± 15%. The least endothermic H-transfer pathway involves abstraction of a methyl hydrogen [*Lou, 2007*] and this is almost certainly the reaction responsible for the observed reactivity at $526 \text{ K} \leq T \leq 673 \text{ K}$.

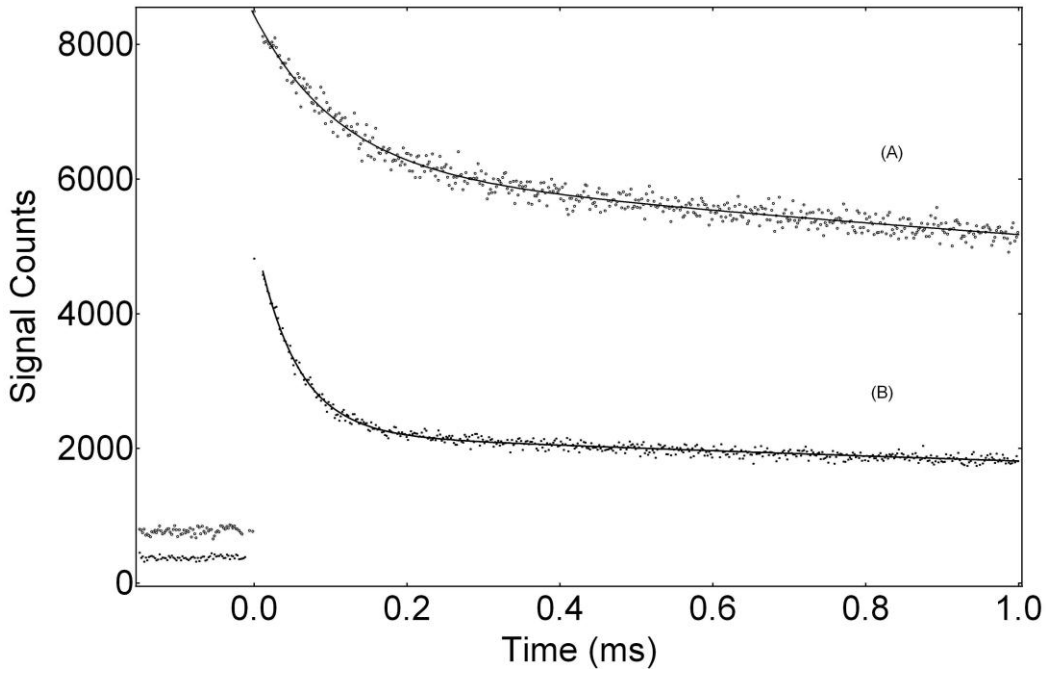

Figure 5.6 Typical Br atom temporal profiles observed at 273 K ≤ T ≤ 357 K for Br + isoprene. Experimental conditions: T = 346 K, P = 50 Torr N_2, $[Br]_0 \sim 3 \times 10^{11}$ atoms cm^{-3}; [isoprene] (in units of 10^{14} molecule cm^{-3}) = (A) 0.47, (B) 1.6. Solid lines through data at t > 0 are obtained from non-linear least-squares fits to equation (II). Best fit parameters (also shown in Table 2) are: (A) $S_0 = 4780$, $Q = 5884$, $\lambda_1 = -8479$, $\lambda_2 = -170$ and (B) $S_0 = 4783$, $Q = 7094$, $\lambda_1 = -18355$, $\lambda_2 = -227$. Trace (A) scaled by 2 for clarity.

Table 5.5. Results of the Br + Isoprene + N_2 ↔ Br−Isoprene + N_2 equilibration kinetics experiments.[a]

T	P	Q	$-\lambda_1$	$-\lambda_2$	[isoprene]	$[CF_2Br2]$	$[Br]_0$	$k_{5.5b}$	$k_{5.9}$	$k_{-5.5b}$	K_P
273	50	-61	22192	-102	1320	3400	2.9	1.68	-102	41	110
		-115	11186	-163	634	3500	3.7	1.75	-163	48	98.8
284	50	271	9401	149	628	3200	2.7	1.47	151	120	31.7
		623	17893	461	1200	3400	3.1	1.47	465	158	24.1
		354	4891	226	315	3500	3.2	1.50	231	123	31.7
		488	14253	333	958	3500	3.3	1.47	336	152	25.0
		245	3448	137	222	3600	3.3	1.50	141	104	37.1
298	20	522	15566	302	137	5200	5.5	1.12	305	216	12.7
		664	26033	391	2260	5200	5.5	1.14	395	270	10.4
	50	752	9258	380	696	5500	5.5	1.27	395	357	8.80
		771	14069	404	1130	4300	4.8	1.21	414	357	8.32
		681	13629	297	1130	4300	4.6	1.17	305	376	7.67
		578	6436	237	502	4200	4.9	1.21	249	330	9.01
		592	6393	254	501	4200	4.3	1.20	266	326	9.07
		788	11277	378	908	4100	4.3	1.19	391	397	7.40
		760	12714	381	1040	4100	4.8	1.19	392	368	7.94
	200	1384	39884	774	2270	3700	3.9	1.73	786	598	7.12
		823	11650	378	656	3700	3.9	1.71	392	430	9.77
		1351	22655	801	1030	3800	4.3	1.69	821	531	7.85
297	700	252	8343	376	404	5800	6.8	1.94	398	454	10.6
		600	4587	236	223	5800	6.0	1.89	255	345	13.5
		887	11633	422	601	5700	5.9	1.86	439	447	10.2
308	50	916	9395	237	830	3500	2.9	1.05	253	663	3.76
		1001	22735	270	2000	6500	3.2	1.10	279	723	3.62
		909	16713	218	1480	3500	3.4	1.08	226	683	3.77
		803	7004	174	585	3500	3.4	1.09	188	615	4.21
319	50	1551	8312	172	587	3300	3.1	1.18	200	1351	1.83
		1687	22539	195	1800	3300	2.8	1.17	206	1481	1.65
		1675	17126	213	1340	3300	3.1	1.17	229	1446	1.70
		1423	5931	180	396	3300	3.0	1.18	219	1204	2.05
330	50	3005	14287	209	1460	3200	3.0	0.79	253	2752	0.64
		2858	7254	236	578	3300	3.0	0.80	354	2504	0.71
		3038	16970	213	1800	3300	2.9	0.80	250	2788	0.63
		2885	10243	219	945	3400	3.0	0.80	286	2599	0.68
	700	4414	17611	254	899	4200	4.1	1.49	328	4086	0.81
		4477	17892	304	887	4100	4.5	1.55	392	4085	0.84
		4197	12086	297	549	4000	4.2	1.49	432	3765	0.88
		4491	22133	292	1200	4000	4.2	1.49	357	4134	0.80
		4396	21521	294	1170	4000	4.2	1.49	359	4037	0.82
346	50	6468	9285	166	471	3600	3.4	0.63	466	6002	0.20
		5884	8479	170	471	3600	3.4	0.58	470	5414	0.21
		6983	14806	216	140	3700	3.4	0.70	377	6606	0.21
		7094	18355	227	1620	3600	3.3	0.69	347	6747	0.20
		6029	9481	212	590	3600	3.3	0.62	511	5518	0.22

Table 5.5. Cont'd.[a]

T	P	Q	$-\lambda_1$	$-\lambda_2$	[isoprene]	$[CF_2Br2]$	$[Br]_0$	$k_{5.5b}$	$k_{5.9}$	$k_{-5.5b}$	K_P
348	50	7309	12844	203	803	1700	1.4	0.71	423	6886	0.22
		7532	11942	196	609	1800	1.4	0.75	468	7064	0.22
357	20	7693	14325	274	2000	3300	2.9	0.34	538	7154	0.099
		8346	19800	282	3280	3400	2.9	0.36	456	7891	0.093
		8159	17478	277	2560	3400	2.9	0.37	480	7669	0.10

[a] Units are T (K); P (Torr); Q, λ_1, λ_2, $k_{5.9}$, $k_{-5.5b}$ (s^{-1}); $k_{5.3b}$ (10^{-10} cm^3 $molecule^{-1}$ s^{-1}); K_P (10^6 atm^{-1}); [isoprene], $[CF_2Br_2]$, $[Br]_0$ (10^{11} cm^{-3}).

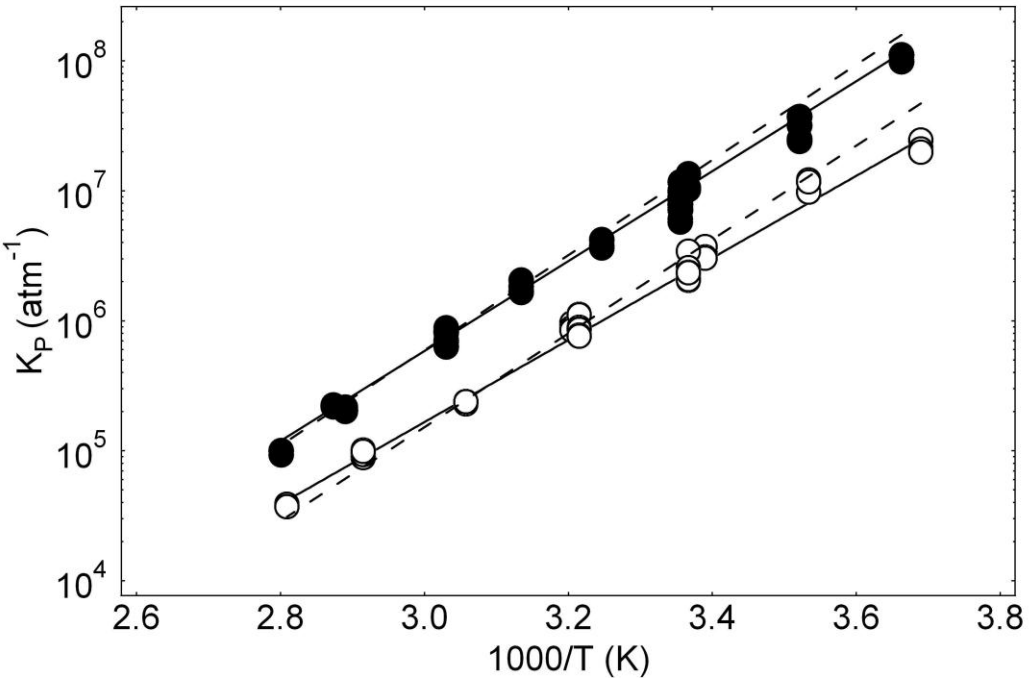

Figure 5.7 van't Hoff plots for Br + isoprene ↔ Br−isoprene and for Br + 1,3-butadiene ↔ Br−1,3-butadiene at 271 K ≤ T ≤ 357 K. Solid lines are obtained from least-squares analyses of the *ln* K_P vs 1/T data and give the second-law thermochemical parameters reported in Tables 5.9. All filled circles represent isoprene data while all open symbols represent 1,3-butadiene data. Dashed lines represent the results of the third-law analysis.

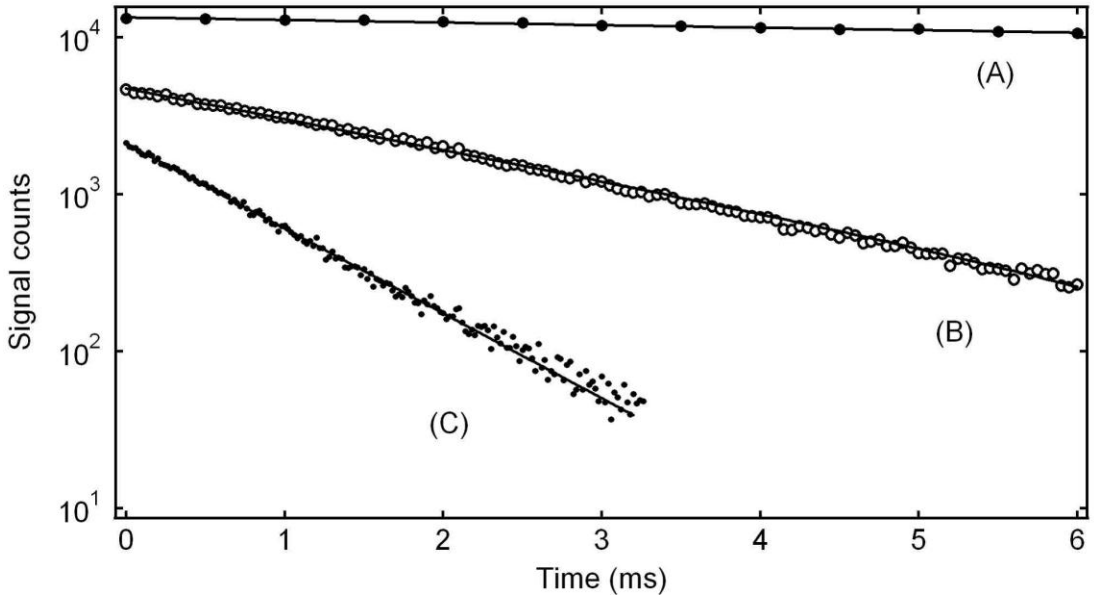

Figure 5.8 Typical resonance fluorescence temporal profiles observed in kinetic studies of reaction (5.5a). Experimental conditions: T = 610 K ; P = 50 Torr; $[CF_2Br_2]$ = 6 x 10^{14} molecule cm^{-3}, $[Br]_0 \sim 6 \times 10^{11}$ atoms cm^{-3}; [isoprene] (10^{15} molecule cm^{-3}) = (A) 0, (B) 1.25, (C) 3.35; number of laser shots averaged = (A) 50, (B) 500, (C) 1500. Solid lines are obtained from linear least-squares analyses and give the following pseudo-first-order decay rates in units of s^{-1}: (A) 35, (B) 480, (C) 1220 s^{-1}. Data were collected for 2000 channels with the multi channel scalar dwell time set to 500 μs (A), 50 μs (B), 20 μs (C). For clarity, traces were scaled by the following factors: (A) 3, (B) 2.

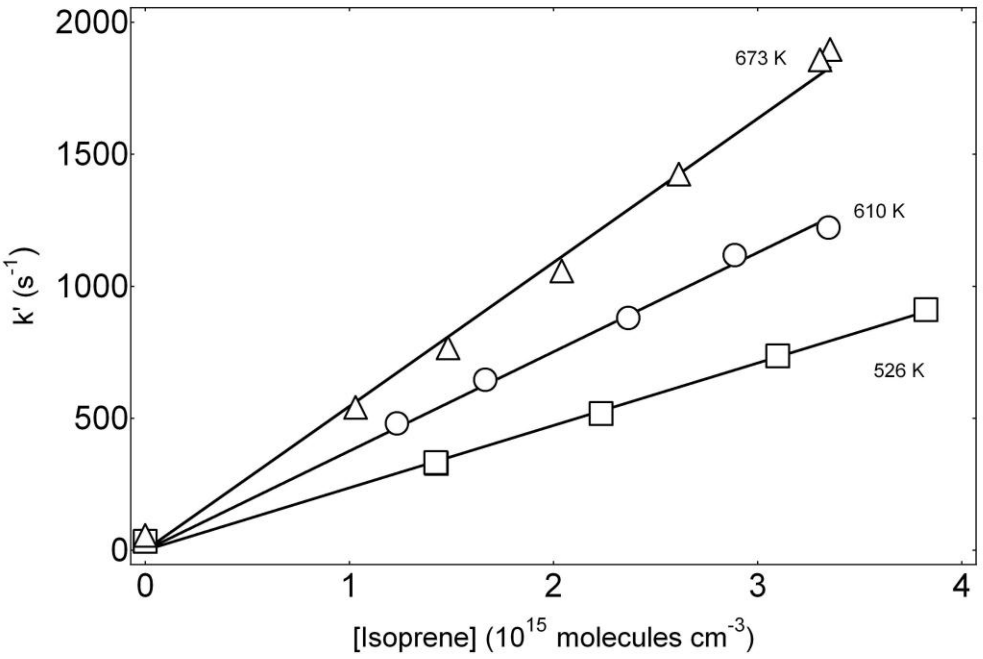

Figure 5.9 Plots of k′, the pseudo-first order Br atom decay rate, versus [isoprene] as a function of temperature. All data shown were obtained at P = 50 Torr. Solid lines are obtained from linear least-square analyses and the resulting bimolecular rate coefficients are listed in Table 5.6. k (526 K) = 2.28×10^{-13} molecule cm^{-3} s^{-1}, k (610 K) = 3.52×10^{-13} molecule cm^{-3} s^{-1}, k (673 K) = 5.39×10^{-13} molecule cm^{-3} s^{-1}. Extrapolated intercepts are (2 ± 28) s^{-1} at 526 K, (37 ± 61) s^{-1} at 610 K, and (−32 ± 65) at 673 K. Uncertainties are 2σ and represent precision only.

Table 5.6. Kinetic data for Br + isoprene (5.5a) from 526 - 673 K.[a]

T	P	N [b]	CF_2Br_2	$Br_{t=0}$	$C_5H_{8\ max}$	k'_{max}	$k \pm 2\sigma$ [c]
526	50	5	4.5	8.2	3.83	911	2.28 ± .18
555	50	5	5.4	4.7	3.72	1120	2.59 ± .23
582	50	5	4.3	3.9	3.21	1251	3.41 ± .22
610	50	5	6.0	6.1	3.35	1221	3.52 ± .19
646	25	5	6.2	5.1	3.42	1846	4.72 ± .16
650	150	5	6.8	5.9	3.79	1968	4.64 ± .25
673	50	6	6.3	6.7	3.35	1881	5.39 ± .45

[a]Concentrations (cm^{-3}): CF_2Br_2 (10^{14}), Br (10^{11}), isoprene (10^{15}). Units: k (10^{-13} $cm^3molecule^{-1}s^{-1}$), $k'(s^{-1})$; [b] N ≡ number of experiments; [c] Uncertainty is precision only.

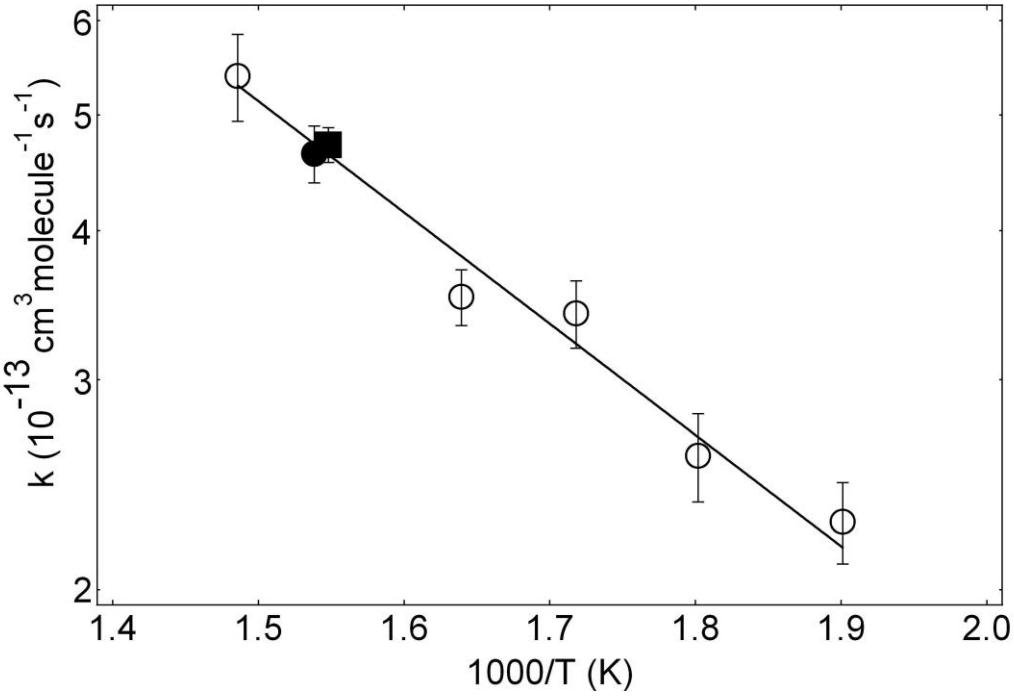

Figure 5.10 Arrhenius plot for the Br + Isoprene H abstraction reacation. The solid line is obtained from an unweighted linear least-squares analysis and gives the Arrhenius expression reported in the text. P = 25 Torr (closed square), 50 Torr (open symbols), 150 Torr (closed circle). Error bars are 2σ, precision only.

Br + Isoprene at 227 K

Well-behaved pseudo-first-order Br atom kinetics were observed in studies carried out at T = 227 K, where decomposition of the Br−isoprene adduct is too slow to impact observed kinetics. At this temperature, we were monitoring $k_{5.5}(P)$. Table 5.7 contains data over a wide range of pressures for the Br + isoprene reaction. The data suggests 700 Torr is near the high-Pressure limit for this reaction.

Table 5.7. Results for Br + isoprene at 227 K.[a]

P	# exp.	$[CF_2Br_2]$	$[Br]_0$	$[isoprene]_{max}$	k'_{max}	$k_{5.5} \pm 2\sigma$ [b]
20	5	7900	2.5	334	6756	1.99 ± .07
50	5	5900	1.8	434	8350	1.98 ± .12
100	5	7000	2.1	253	6011	2.39 ± .08
200	5	8200	2.5	250	6097	2.51 ± .20
400	5	8100	2.5	269	7166	2.67 ± .16
700	4	9600	2.9	436	11634	2.73 ± .17

[a] Units: P (Torr); $[CF_2Br_2]$, $[Br]_0$, $[isoprene]_{max}$ (10^{11} cm^{-3}); k'_{max} (s^{-1}); $k_{5.5}$ (10^{-10} cm^3 $molecule^{-1}$ s^{-1}). [b]Uncertainties are precision only.

Br−alkene adduct thermochemistry

Both second and third law methods were employed to evaluate the thermochemistry of the Br−alkene adducts. In the second law approach, the enthalpy and entropy changes associated with Br−alkene formation (5.1b, 5.3b, 5.5b) are evaluated from the van't Hoff plots shown in Figures 5.5 and 5.7. Since

$$ln\ K_p = (\Delta_r S / R) - (\Delta_r H / RT), \qquad (5\text{-X})$$

the enthalpy change is obtained from the slope of the van't Hoff plot while the entropy change is obtained from the intercept. At 223 K, near the midpoint of the experimental 1/T range for the Br + TME reaction, this second-law analysis gives the results $\Delta_r H$ =

-44.8 ± 6.2 kJ mol^{-1} and $\Delta_r S = -87 \pm 28$ J mol^{-1} K^{-1}. At 312 K, the midpoint of the experimental 1/T range for the Br + 1,3-butadiene reaction, this second-law analysis gives the results $\Delta_r H = -60.4 \pm 8.1$ kJ mol^{-1} and $\Delta_r S = -81.4 \pm 25$ J mol^{-1} K^{-1}. For Br + isoprene, the midpoint of the experimental 1/T range is 319 K, and this second-law analysis gives the results $\Delta_r H = -63.2 \pm 8$ kJ mol^{-1} and $\Delta_r S = -80.0 \pm 11$ J mol^{-1} K^{-1}, all uncertainties are 2σ and represent precision only.

In addition to the second-law analysis, we have carried out a third-law analyses where experimental values for K_P at the mid-points of the 1/T range investigated are employed in conjunction with a calculated entropy change to determine $\Delta_r H$. The experimental equilibrium constants used in the third law analyses are, in units of 10^5 atm^{-1}, 6.18 ± 1.8 at 223 K for Br−TME, 9.01 ± 2.7 at 312 K for Br−1,3-butadiene, and 18.1 ± 5.4 at 319 K for Br−isoprene. To evaluate $\Delta_r S$, absolute entropies as a function of temperature were obtained from the JANAF tables for Br [Chase *et al.,* 1985] and calculated using *ab initio* vibrational frequencies and moments of inertia for each alkene and each Br−alkene adduct; all vibrational frequencies and moments of inertia were obtained from electronic structure calculations carried out by our collaborator Michael L. McKee of Auburn University.

The geometry of each alkene and the Br−alkene adducts were determined by the G4 method [*Curtiss et al.,* 2007] using the Gaussian09 program [*Frisch et al.,* 2009]. The G4 method is a composite of several calculations and includes an extrapolation procedure and spin-orbit corrections for the bromine atom (−14.7 kJ mol^{-1}). The average absolute deviation from experiment for the G3/05 test set (454 experimental energies) is only 3.5 kJ/mol. Relevant parameters used in the calculations of absolute entropies and heat

capacity corrections are summarized in Table 5.8. Theoretical bond strengths are also tabulated in Table 5.9 and agree reasonably well with the experimental values.

In arriving at the above uncertainties in $\Delta_r S$, we assume that the frequencies of the three lowest frequency Br−alkene vibrations could differ from the values given in Table 5.8 by ± 25 cm^{-1}. Appropriate heat capacity corrections have been employed to obtain $\Delta_r H$ values at 298 and 0 K; the results are summarized in Table 5.9. The thermochemical parameters determined from the second- and third-law analyses agree within their combined uncertainties; however, the third-law uncertainties are smaller. Hence, we feel it appropriate to report the third-law results as the experimentally determined values for $\Delta_r H$(5.ib). In units of kJ/mol, $\Delta_r H$(5.1b): = −47.1 ± 3.0 at 0 K and −47.3 ± 3.0 at 298 K; $\Delta_r H$(5.3b): = −67.1 ± 4.5 at 0 K and −69.4 ± 4.0 at 298 K; $\Delta_r H$(5.5b): = −69.4 ± 4.0 at 0 K and −70.1 ± 4.0 at 298 K. Uncertainties are accuracy estimates at the 95% confidence level.

The dashed lines in Figures 5.5 and 5.7 are generated from equation (5-X) using third law values for $\Delta_r S$ and $\Delta_r H$. The mathematical expressions represented by the dashed lines are

$ln\ K_P\ (atm^{-1}) = -12.2 + 5750 / T$ (Br + TME, third law analysis)

$ln\ K_P\ (atm^{-1}) = -12.9 + 8310 / T$ (Br + 1,3-butadiene, third law analysis)

$ln\ K_P\ (atm^{-1}) = -12.0 + 8430 / T$ (Br + isoprene, third law analysis)

The values for $\Delta_r H$ obtained above can be used in conjunction with literature values for the standard enthalpies of formation of Br [*Chase et al., 1985*], TME [*Lias et al., 1988*], isoprene [*Fraser and Prosen, 1955*], and 1,3-butadiene [*Prosen and Maron, 1951*;

Prosen and Rossini, 1945] to deduce values for the standard enthalpy of formation of each Br−alkene adduct at 298 K, in units of kJ mol^{-1} $\Delta_f H_{298}$ (Br-TME) = −4.6 ± 7.3, $\Delta_f H_{298}$ (Br-1,3-butadiene) = 153.1 ± 7.3, and $\Delta_f H_{298}$ (Br-isoprene) = 117.5 ± 7.3.

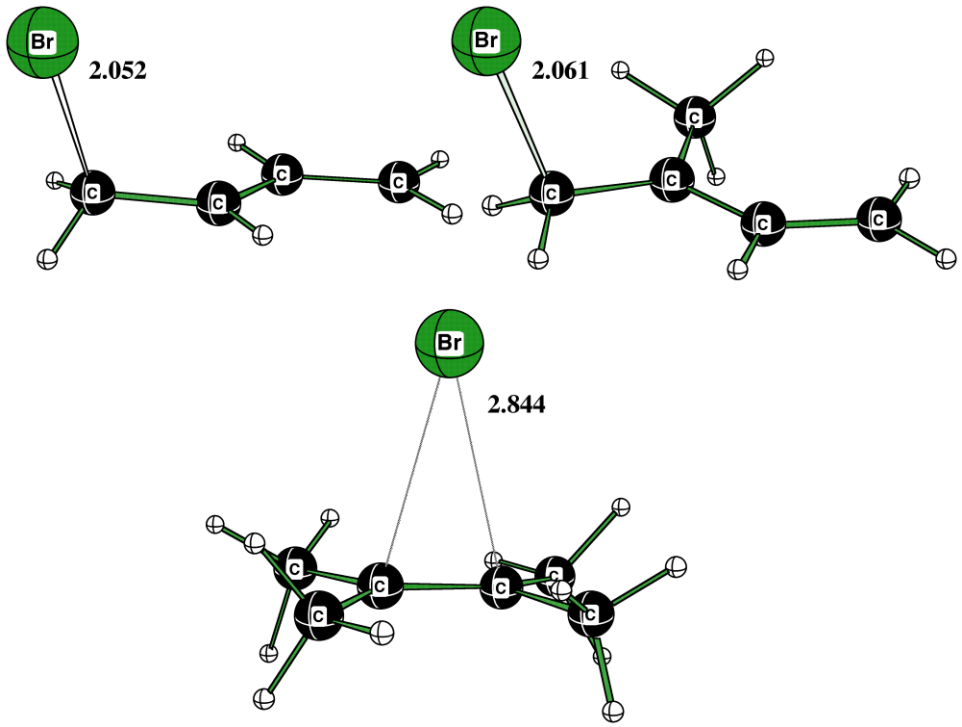

Figure 5.11. Lowest energy theoretical structures for each of the Br-alkene adducts. Top left: C1 symmetry structure of Br−1,3-butadiene; Top right: C1 symmetry structure of Br−isoprene; Bottom: The C_2 symmetry structure of Br−TME. The numbers represent the bond distances for each of the C−Br bonds in Angstroms.

Table 5.8. Summary of parameters used in calculations of absolute entropies and heat capacity corrections for each Br + alkene reaction.

	Br	TME	Br−TME
g_0	4	1	2
g_1	2		
$\Delta\varepsilon$ (cm-1)[a]	3685.24		
σ		4	2
Rot. Constants (GHz)[b]		4.48, 2.95, 1.86	1.86, 1.15, 1.02
Vib. Frequencies (cm^{-1}) [b, c]		**49**, **92**, **135**, 157, **173**, 343, 346, 410, 418, 493, 529, 688, 900, 946, 957, 976, 1021, 1057, 1096, 1108, 1157, 1195, 1271, 1401, 1408, 1414, 1434, 1469, 1475, 1478, 1491, 1495, 1499, 1502, 1505, 1742, 3010, 3012, 3016, 3021, 3050, 3051, 3054, 3054,	57, **92**, **99**, **101**, 111, 131, **144**, 158, 335, 362, 410, 414, 482, 490, 691, 897, 937, 948, 988, 994, 1049, 1078, 1085, 1180, 1194, 1292, 1401, 1401, 1405, 1416, 1454, 1462, 1465, 1475, 1483, 1488, 1502, 1508, 1612, 3016, 3017, 3024, 3025, 3089, 3090, 3099, 3099, 3154, 3156, 3168, 3169

		1,3-butadiene	Br−1,3-butadiene
g_0	4	1	2
g_1	2		
$\Delta\varepsilon/cm^{-1a}$	3685.24		
σ		2	1
Rot. Constants (GHz)[b]		42.5733, 4.4283, 4.0111	11.2616, 1.1249, 1.0741
Vib. Frequencies (cm^{-1}) [b]		176, 294, 514, 544, 788, 901, 937, 941, 1001, 1011, 1069, 1228, 1318, 1320, 1421, 1477, 1662, 1714, 3134, 3144, 3149, 3150, 3234, 3234	79, 152, 261, 280, 475, 506, 573, 801, 845, 855, 952, 1011, 1078, 1161, 1192, 1234, 1289, 1356, 1475, 1499, 1526, 3116, 3138, 3156, 3166, 3191, 3252

		isoprene	Br−isoprene
g_0	4	1	2
g_1	2		
$\Delta\varepsilon/cm^{-1a}$	3685.24		
σ		1	1
Rot. Constants (GHz)[b]		8.5477, 4.1750, 2.8544	4.9426, 1.0021, 0.9319
Vib. Frequencies (cm^{-1}) [b, c]		164, **209**, 277, 413, 426, 533, 649, 794, 796, 930, 937, 965, 1012, 1041, 1074, 1091, 1328, 1330, 1411, 1435, 1462, 1481, 1503, 1669, 1708, 3029, 3080, 3121, 3140, 3148, 3158, 3230, 3237	**37**, 66, 119, 215, 290, 345, 396, 489, 541, 633, 779, 842, 884, 984, 993, 1029, 1048, 1110, 1183, 1259, 1281, 1370, 1408, 1447, 1479, 1491, 1493, 1537, 3022, 3083, 3115, 3117, 3139, 3165, 3191, 3253

[a]$\Delta\varepsilon \equiv$ energy splitting between the lowest two electronic states; neither of the di-alkenes in question here has low-energy excited states and the adducts are assumed to have none. [b]Calculated values at the B3LYP/6-31G(2d,p) level of theory.[c] Frequencies shown in bold represent methyl torsions.

Table 5.9. Thermochemical parameters for Br + Alkene ↔ Br−Alkene.

T (K)	Method	$-\Delta_r H$ (kJ mol^{-1})	$-\Delta_r S$ (J mol^{-1} K^{-1})	$\Delta_f H$ (Br−alkene) [a], kJ mol^{-1}
		Br + TME→ Br−TME		
223	Second law	47.3 ± 7.1 [b]	100.4 ± 28 [b]	
	Third law	47.6 ± 3.0 [c]	102.8 ± 10.0 [c]	
0	Second law	46.7 ± 7.7 [b]		
	Third law	47.1 ± 3.0 [c]		
	G4 theory [d]	55.9 ± 3.5 [e]		
298	Second law	47.0 ± 7.2 [b]		
	Third law	47.3 ± 3.0 [c]	101.5 ± 10.0 [c]	−4.6 ± 7.3 [c]
	G4 theory [d]	56.1 ± 3.5 [e]		
		Br + 1,3-butadiene → Br−1,3-butadiene		
312	Second law	60.4 ± 7.0 [b]	81.4 ± 19.1 [b]	
	Third law	69.1 ± 4.0 [c]	107.6 ± 11.0 [c]	
0	Second law	58.3 ± 7.6 [b]		
	Third law	67.1 ± 4.5 [c]		
	G4 theory [d]	66.9 ± 3.5 [e]		
298	Second law	60.4 ± 7.0 [b]		
	Third law	69.2 ± 4.0 [c]	107.8 ± 11.0 [c]	153.1 ± 7.3 [c]
	G4 theory [d]	69.0 ± 3.5 [e]		
		Br + isoprene → Br−isoprene		
319	Second law	63.2 ± 8.0 [b]	80 ± 26 [b]	
	Third law	70.1 ± 4.0 [c]	99.9 ± 11.0 [c]	
0	Second law	62.5 ± 8.5 [b]		
	Third law	69.4 ± 4.0 [c]		
	G4 theory [d]	72.6 ± 3.5 [e]		
298	Second law	63.3 ± 8.0 [b]		
	Third law	70.1 ± 4.0 [c]	100.2 ± 11.0 [c]	117.5 ± 7.3 [c]
	G4 theory [d]	75.6 ± 3.5 [e]		

[a] Values are based on third law results; [b] Uncertainty is 2σ, precision only; [c] Uncertainty is estimated accuracy at the 95 % confidence level; [d] The level of optimization is B3LYP/6-31G(2df,p); [e] Uncertainty represents average deviation between experiment and theory for a test set of 454 chemical species, 34 of which are radicals.

Br−alkene + O_2 reactions

Observations of perturbation to "approach to equilibrium" kinetics upon addition of O_2 to CF_2Br_2/alkene/N_2 reaction mixtures allows the Br−alkene + O_2 rate coefficients, $k_{5.2}$, $k_{5.4}$, and $k_{5.6}$ to be evaluated. The data shown in figures 5.12 and 5.14 illustrate how the addition of O_2 perturbs the Br approach to equilibrium kinetic data. Rate coefficients, $k_i(P)$, (i = 5.2, 5.4, 5.6), are obtained from the slopes of $k_{5.9}$ vs. [O_2] plots as shown in Figure 5.13 and 5.15. The reactions (5.2, 5.4, and 5.6) compete with reactions (−5.1b, −5.3b, and −5.5b) respectively, for removal of the Br−alkene. Hence, the slow component of the double exponential decay increases with increasing [O_2]. If O_2 is added in sufficient excess the Br decay should become exponential, and the slope of a plot of the pseudo-first order Br decay rate vs. [alkene] should give the sum of the H-abstraction and forward addition rate coefficients, i.e., $k_{5.1a} + k_{5.1b}$ (for Br + TME), $k_{5.3a} + k_{5.3b}$ (for Br + 1,3-butadiene), and $k_{5.5a} + k_{5.5b}$ (for Br + isoprene). Table 5.10 summarizes the Br−alkene + O_2 results obtained under conditions where double exponential decays were observed, and Table 5.11 shows kinetic data for experiments where O_2 was added in sufficient excess that observed decays were exponential, i.e., Br loss is irreversible on the timescale of our experiments.

Br−TME + O_2 The values for $k_{5.1a} + k_{5.1b}$ obtained from the data summarized in Table 5.11 agree well with the sum of the $k_{5.1a}$ values obtained from extrapolation of high temperature data (Table 5.1) and $k_{5.1b}$ values reported in Table 5.2 for the Br + TME reaction. At 223 K, the Br−TME rate coefficient ($k_{5.2}$) increases with increasing N_2 pressure (25 – 200 Torr) from 3.9 to 5.5 × 10^{-12} cm^3 $molecule^{-1}$ s^{-1}.

Br−1,3-butadiene + O_2 For the Br + 1,3-butadiene reaction, the H-abstraction rate coefficient is negligible and values for $k_{5.3}$ shown in Table 5.11 agree well with values for $k_{5.3b}$ obtained from the non-exponential fits to equation (5-II) (see Table 5.3). At 311 K, $k_{5.4}$ is observed to increase with increasing pressure (25 – 700 Torr) from 3.2 to 4.7 × 10^{-13} cm^3 $molecule^{-1}$ s^{-1}. Figure 5.15 shows $k_{5.9}$ vs $[O_2]$ for the Br−1,3-butadiene + O_2 reaction.

Br−isoprene + O_2 Figure 5.14 illustrates the effect of increased $[O_2]$ on observed kinetics. Figure 5.15 shows $k_{5.9}$ vs $[O_2]$ as a function of P for the Br−isoprene + O_2 rate coefficient. The Br−C_5H_8 + O_2 rate has been determined to be independent of pressure from 50 to 700 Torr, $k_{5.6}$ = (2.94 ± .46) x 10^{-13} cm^3 $molecule^{-1}$ s^{-1}.

Table 5.10. Kinetic data for Br−alkene + O_2 reactions.[a]

T	P	N [b]	$[O_2]_{max}$	$[CF_2Br_2]$	$[Br]_0$	[TME]	k'_{max}	$k_{5.2} \pm 2\sigma$ [c]
223	200	6	7900	5200	4.0	1300	4600	47 ± 6
223	25	7	8000	5300	4.6	1550	3960	39 ± 5
						$[C_4H_6]$		$k_{5.4}$ [c]
311	25	8	54000	2250	1.1	174	1889	3.2 ± 0.3
	100	5	46000	1900	.90	990	1760	3.1 ± 0.1
	100	8	61000	1900	.89	193	2240	3.4 ± 0.3
	250	7	66000	2800	1.3	155	2930	4.1 ± 0.5
	500	5	89000	3700	1.9	205	4097	4.2 ± 0.7
	700	5	82000	2000	1.1	208	4190	4.7 ± 1.0
						$[C_5H_8]$		$k_{5.6}$ [c]
297	50	7	30000	2600	2.9	360	1280	3.11± 1.4
	50	7	74100	2400	2.5	560	2750	2.95± 0.68
	50	4	44300	2000	2.0	900	2240	4.07± 0.83
	50	5	27200	2000	2.2	300	880	2.61± 0.24
	700	5	45900	2100	2.6	500	1780	3.09 ± 0.74

[a] Units are T (K); P (Torr); k' (s^{-1}); $[O_2]$, $[CF_2Br_2]$, $[Br]_0$, [alkene] (10^{11} molecule cm^{-3}); $k_{5.2}$, $k_{5.4}$, and $k_{5.6}$ (10^{-13} cm^3 $molecule^{-1}$ s^{-1}); [b] N ≡ number of experiments; [c] Uncertainties are 2s, precision only.

Table 5.11. Kinetic data for excess O_2 experiments.[ab]

T	P	No. expts.	$[TME]_{max}$	k'_{max}	$k_{5.1}$ [c]
212	200	9	387	5240	14.0 ± 0.90
241	25	6	570	3580	6.24 ± 0.68
			[d] $[1,3\text{-butadiene}]_{max}$		$k_{5.3}$ [d]
300	700	5	780	12608	15.6 ± 1.6
283	100	5	350	3850	10.9 ± .70
			$[isoprene]_{max}$		$k_{5.5}$ [d]
298	5.5	5	430	2600	5.51 ± .22
298	10	5	380	3040	8.03 ± .16
298	10	5	420	3520	7.80 ± .63
298	10	3	360	2700	7.77 ± .29
298	20	7	260	2620	10.4 ± .57
298	50	5	260	4000	14.1 ± .56
298	50*	6	220	2800	12.6 ± .64
298	250	5	300	5010	17.1 ± .78
298	250	9	580	9750	16.4 ± .50
298	700	7	570	10500	18.3 ± .75

[a] $[O_2]$ concentrations were varied from 5 to 17 x 10^{16} molecules cm^{-3} for TME and butadiene reactions and $[O_2]$ = 1.1 – 3.2 x 10^{16} molecules cm^{-3} for isoprene reactions; [b] Units are T (K); P (Torr); k' (s^{-1}); $[alkene]_{max}$ (10^{11} molecule cm^{-3}), $[CF_2Br_2]$ = 2-6 x 10^{14} molecule cm^{-3}, $[Br]_0$ = 1-6 x 10^{11} molecule cm^{-3}; [c] $k_{5.i}$ (i=1,3,5): (10^{-11} cm^3 $molecule^{-1}$ s^{-1}); [d] Br + 1,3-butadiene experiments with excess O_2 were conducted to show that the rate coefficient was equal to the forward addition rate coefficient derived from the nonexponential fits; * Br_2 photolysis at 355 nm was employed as Br atom source.

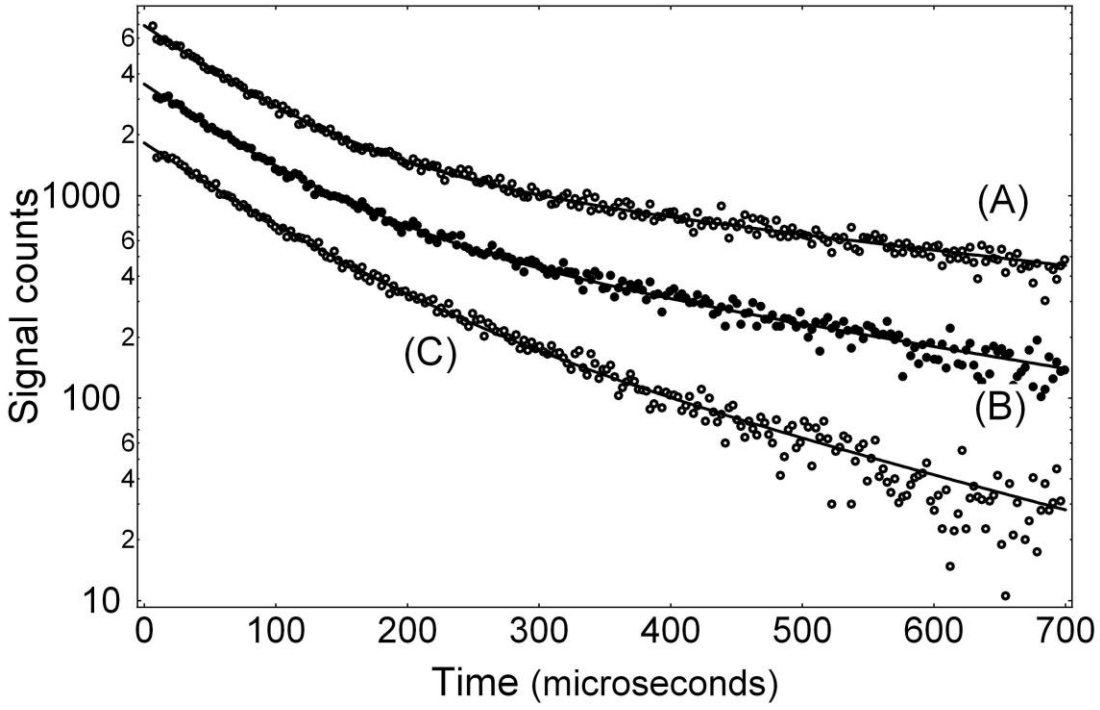

Figure 5.12. Typical data showing the dependence of observed resonance fluorescence temporal profiles on [O_2]. Experimental conditions: P = 25 Torr, T = 223 K. Concentrations in units of 10^{12} molecule cm^{-3}: [TME] = 160; [O_2] = (A) 0, (B) 210, (C) 690; [CF_2Br_2] = 535 ± 15; $[Br]_0$ ~ 0.4 ± 0.1. Solid lines are obtained from non-linear least squares fits to equation (II). Best fit parameters are (A): S_0 = 3560, Q = 4310 s^{-1}, λ_1 = −13100 s^{-1}, λ_2 = −1780 s^{-1}; (B): S_0 = 3570, Q = 5060 s^{-1}, λ_1 = −12800 s^{-1}, λ_2 = −2360 s^{-1}; (C): S_0 = 2610, Q = 6690 s^{-1}, λ_1 = −12400 s^{-1}, λ_2 = −4390 s^{-1}. For clarity, traces (A) and (C) are scaled by factors of 2 and 0.5, respectively.

We believe that the largest contributor to the intercepts of the plots shown in Figure 5.13 and 5.15 is reaction of Br−alkene with background O_2 in the reaction cell. For convenience of operation, the apparatus is assembled with significant amounts of Teflon tubing (somewhat permeable to O_2) as well as a number of valves and Cajon fittings that are susceptible to small leaks. Hence, some background O_2 in the reaction cell is expected. In studies (employing the same apparatus) of the kinetics of reversible addition of Cl atoms to CH_3I [*Ayhens et al., 1997*], CH_3CH_2I [*Orlando et al., 2005*], and $(CH_3)_2SO$ [*Nicovich et al., 2006*], where the formed adducts do not react with O_2 at measurable rates [*Dookwah-Roberts et al., 2008a; 2008b; Kleissas et al., 2007*], values of $k_{5.9}$ extracted from analysis of the double exponential decays are much smaller than those obtained in this study. The data shown in Figure 5.13 and 5.15 suggests that the mole fraction of O_2 in reaction mixtures where O_2 was not intentionally added to the mixture was typically around 10^{-4} (it appears to have varied over the approximate range 2×10^{-5} to 5×10^{-4}).

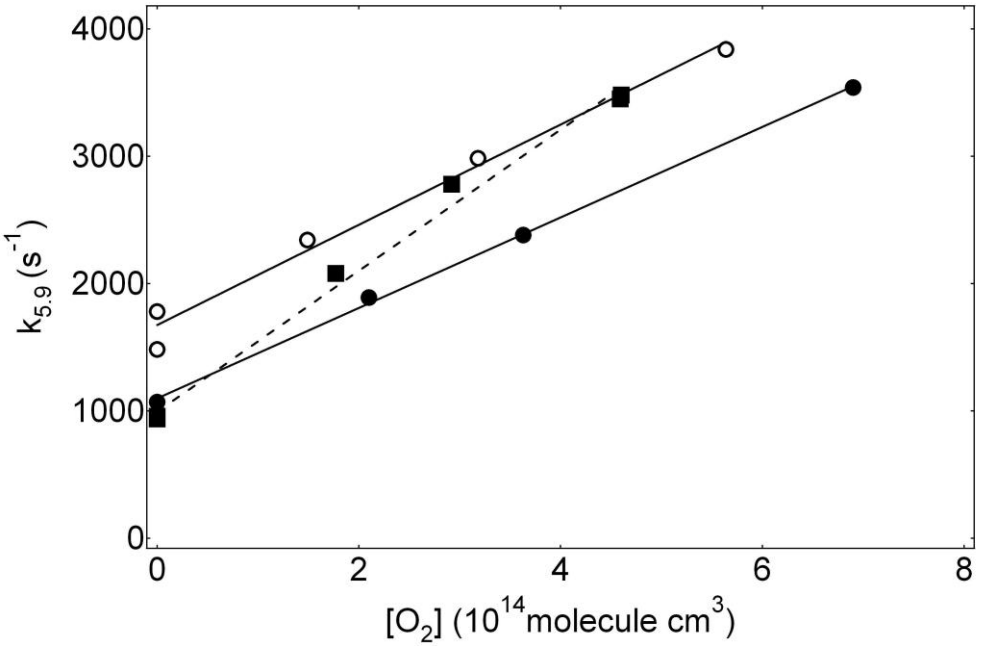

Figure 5.13. **Plots of $k_{5.9}$ versus [O_2] for data obtained at T = 223 K for Br + TME.** Circular points and solid lines represent data obtained at P = 25 Torr in two separate sets of experiments carried out on different days, whereas square-shaped points and the dashed line represent data obtained at P = 200 Torr. [TME] (10^{13} molecules cm^{-3}) = 5.3 (open circles), 16 (filled circles), 13 (squares). Lines are obtained from linear least-squares analyses and lead to the bimolecular rate coefficients given in Table 5.7.

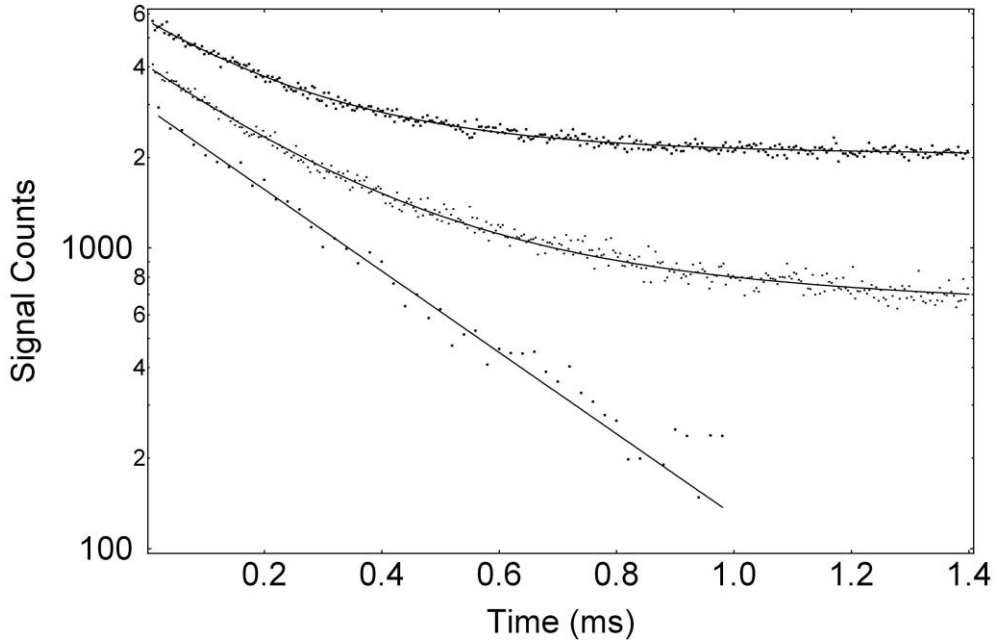

Figure 5.14 Typical data showing the dependence of observed resonance fluorescence temporal profiles on [O_2]. Experimental conditions: P = 50 Torr, T = 297 K. Concentrations in units of 10^{13} molecule cm^{-3}: [isoprene] 1.7; [O_2] (A) 0, (B) 150, (C) 1500; [CF_2Br_2] = 50; $[Br]_0 \sim .05$. Solid lines are obtained from non-linear least-squares fits to equation (II). Best fit parameters are: (A) $S_0 = 2057$, $Q = 681$, $\lambda_1 = -4081$, $\lambda_2 = -144$; (B) $S_0 = 2393$, $Q = 872$, $\lambda_1 = -3782$, $\lambda_2 = -457$. Trace (C) was exponential with a decay of 3100 s^{-1}. For clarity, traces (A) and (B) are scaled upwards by factors of 3 and 2, respectively.

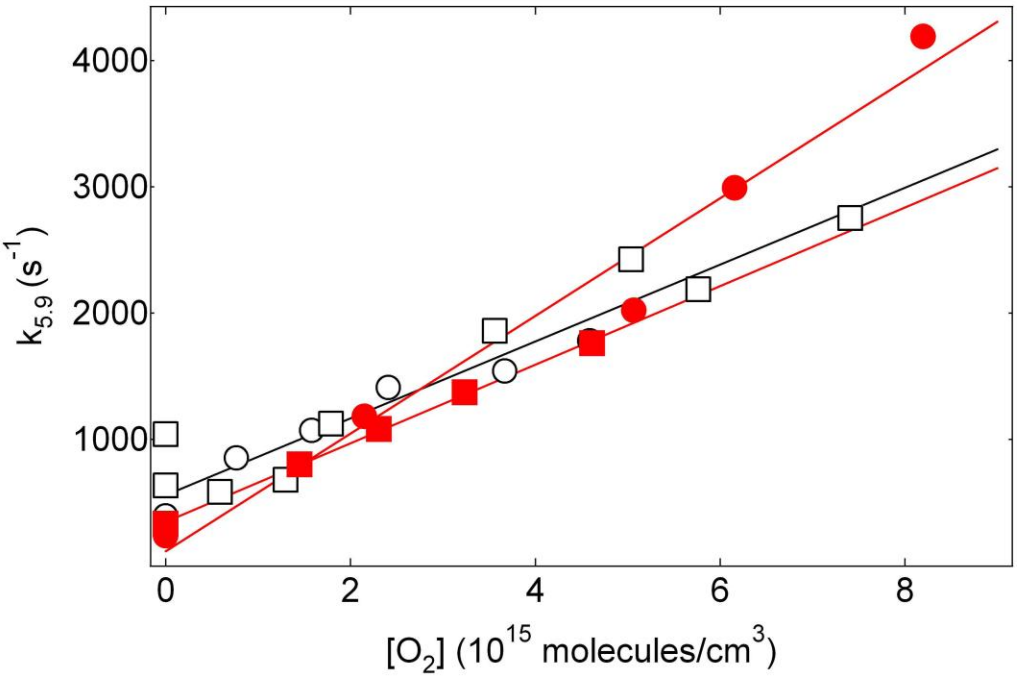

Figure 5.15. Plots of $k_{5.9}$, the pseudo-first order rate of loss of adduct that does not regenerate Br, versus [O_2] for Br−isoprene (black) and Br−1,3-butadiene (red). The rate constant for the Br−isoprene adduct reaction with O_2 at 298 K is (3.05 ± .48) × 10^{-13} independent of pressure (black open squares = 50 Torr and black open circles = 700 Torr), while the rate coefficient for the Br−1,3-butadiene adduct reaction with O_2 increases slightly (3.1-4.7 × 10^{-13}) with increasing P, data for T = 311 K, P = 100 (red filled squares) and P = 700 Torr (red filled circles) are shown here; additional Br−alkene + O_2 data can be found in Table 8. Solid lines are obtained from linear least-square analyses and give the resulting bimolecular rate coefficients.

Pressure Dependence of Br Association Reactions with 1,3-Butadiene and Isoprene

Experiments employing excess amounts of O_2 have been performed as a function of T and P. 298 K falloff curves (Fig 5.16) describing the pressure dependence of the overall Br + Isoprene (5.5a + 5.5b) and Br + 1,3-butadiene reactions (5.3a + 5.3b) have been derived by adding excess amounts of O_2; i.e., enough O_2 so that loss of Br was irreversible on the timescale of our experiments. Since the H-abstraction rate coefficients ($k_{5.3a}$ and $k_{5.5a}$) are negligibly slow at 298 K, these experiments are observing the kinetics of the association reactions (5.3b and 5.5b). The results were obtained by analyzing exponential decays that follow the relationship described by equation (5-I). Table 5.11 includes all data obtained in the presence of excess O_2. Rate coefficients were found to increase with increasing pressure at all temperatures investigated (see Tables 5.5, 5.4, and 5.11). To provide a parameterization that is convenient for representing pressure dependent kinetic data in atmospheric models and in Figure 5.16, the data were fit to the following expression [*Sander et al., 2011*].

$$k(M,T) = \left(\frac{k_0(T)[M]}{1 + \frac{k_0(T)[M]}{k_\infty(T)}} \right) 0.6^{\left\{1+\left[\log_{10}\left(\frac{k_0(T)[M]}{k_\infty(T)}\right)\right]^2\right\}^{-1}} \qquad \text{(5-XI)}$$

In eq 5-XI, k_0 and k_∞ are approximations to the low and high pressure limiting rate coefficients and 0.6 is a fixed value representing the broadening parameter, F_c; although F_c is dependent on both the identity of the bath gas and the temperature [*Troe, 1979; 1983; Luther and Troe, 1978*], assuming F_c=0.6 allows data to be fit well over the range of conditions typically encountered in the atmosphere [*Sander et al., 2011*]. The pressure

dependent data for Br + isoprene and Br + 1,3-butadiene at 298 K are plotted in Figures 6.4 and 6.5, respectively.

The temperature dependence the Br + isoprene association reaction at P = 50 Torr N_2 is best described by the following Arrhenius expression over the range 210 K ≤ T ≤ 298 K (see Figure 5.17)

$k_{5.5}(T) = (2.5 \pm 0.7) \times 10^{-11} \exp((505 \pm 74)/T)$ cm^3 molecule^{-1} s^{-1}

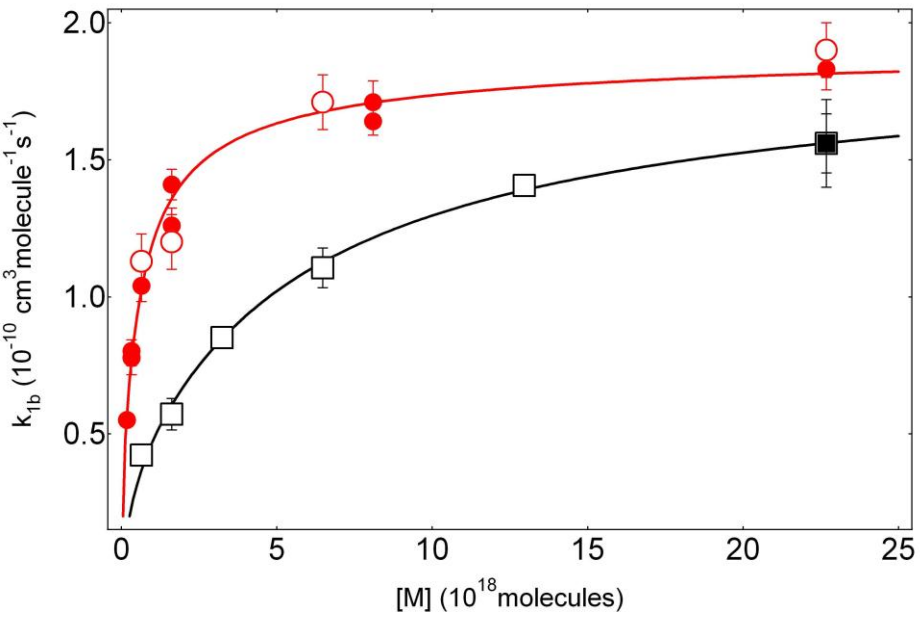

Figure 5.16. A falloff curve showing $k_{ib}(P)$ (i=3,5). Red circles represent Br + isoprene (5.5 – 700 Torr at 298 K with $[O_2]$ = 1.1-3.2 × 10^{16}, data is shown in Table 5.11) and black squares for Br + 1,3 butadiene (20-700 Torr at 298 K). Open symbols represent data points that represent the average of the 297 K forward rates found in Tables 5.3 and 5.5). Filled symbols represent data obtained by adding excess O_2 to the reaction mixture. Solid lines represents non-linear least squares fits to eq 5-XI.

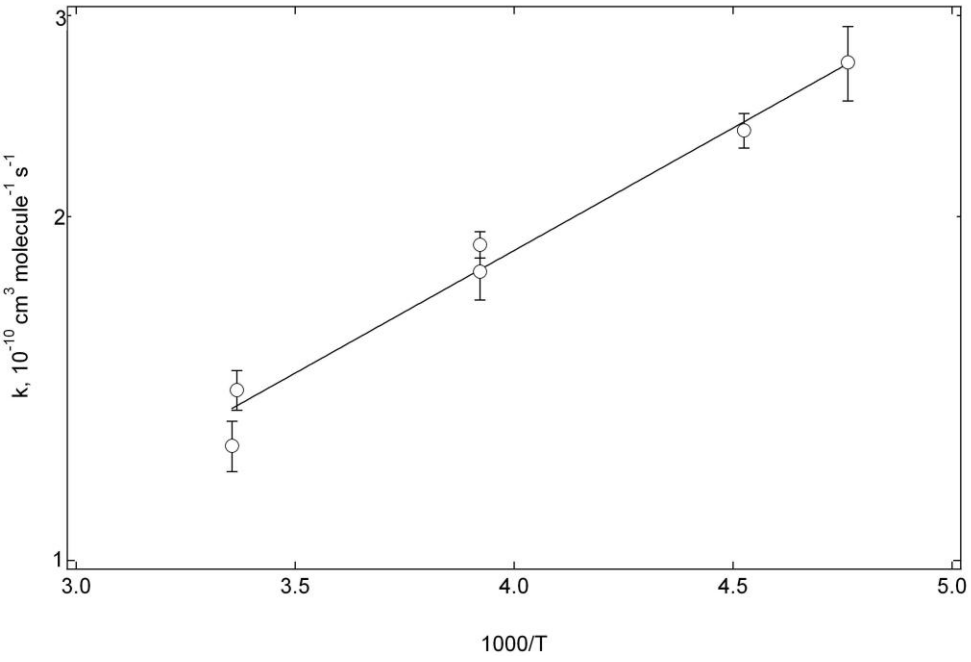

Figure 5.17. Arrhenius plot for $k_{5.5}$ (T) at 210 K ≤ T ≤ 298 K.
Experimental conditions: 50 Torr total pressure. $[O_2]$ = 0.65 – 3.4 x 10^{16} molecules cm^{-3}. Best fit expression is k = (2.48 ± 0.7) × 10^{-11} exp ((505 ± 74)/T) cm^3 $molecule^{-1}$ s^{-1}.

Literature Comparisons

Kinetics

Bierbach *et al.* [*1996*] report results from a relative rate study where several Br + alkene reactions were investigated at 298 K and 1000 mbar synthetic air. These researchers determined the overall rate coefficient for the Br-initiated oxidation of isoprene to be 7.4×10^{-11} cm^3 $molecule^{-1}$ s^{-1} with 1,3-butadiene as the competitor. They determined the rate coefficient for Br + 1,3-butadiene to be 5.75×10^{-11} cm^3 $molecule^{-1}$ s^{-1} where the reference reactant was TME. Bierbach *et al.* measured the rate coefficient for Br + TME to be 2.82×10^{-11} cm^3 $molecule^{-1}$ s^{-1}, using *trans*-2-butene as the reference reactant. They measured the Br + *trans*-2-butene rate coefficient to be 9.1×10^{-12} cm^3 $molecule^{-1}$ s^{-1} in a relative rate study using propene as the reference reactant. They measured the Br + propene rate coefficient to be 2.7×10^{-12} cm^3 $molecule^{-1}$ s^{-1} in a relative rate study using acetaldehyde as the reference reactant. The rate coefficient for Br + acetaldehyde, which has been measured absolutely, was assumed by Bierbach *et al.* to be 3.6×10^{-12} cm^3 $molecule^{-1}$ s^{-1}. The currently recommended Br + acetaldehyde rate coefficient is 3.9×10^{-12} cm^3 $molecule^{-1}$ s^{-1} [*Atkinson et al., 2006; Sander et al., 2011*], suggesting that all rate coefficients reported by Bierbach *et al.* should be scaled upward by a factor of 3.9/3.6 = 1.08. Our observed 298 K, 700 Torr rate coefficients, $k_{5.3}$ and $k_{5.5}$, are 1.56×10^{-10} cm^3 $molecule^{-1}$ s^{-1} and 1.83×10^{-10} cm^3 $molecule^{-1}$ s^{-1}, respectively. Although our experiments were not conducted in 1000 mbar air, our experiments conducted in the presence of O_2 indicate that less than 1 Torr of O_2 is needed to scavange all of the Br−alkene adduct formed by reactions 5.3 and 5.5. Hence, we feel we can directly compare our results with that from the Bierbach *et al.* results which were obtained in 1000 mbar air. While our new rate coefficients are significantly larger than

that reported by Bierbach *et al.,* a comparison of our "relative rates" for reactions 5.3 and 5.5 with the relative rates reported Bierbach *et al.* yields $k_{5.5}/k_{5.3} = 1.17$ and $k_{5.5}/k_{5.3} = 1.29$, respectively. Thus, our "relative rates" are in reasonable agreement with that from Bierbach *et al*. within combined experimental uncertainties.

Our data for the Br + TME reaction cannot be compared directly with that from Bierbach *et al.* [*1996*] due to experimental limitations on time resolution and Br atom detection sensitivity in the presence of large quantities of O_2. We were unable to quantitatively evaluate $k_{5.1b}$, $k_{-5.1b}$, and $k_{5.2}$ at the temperature, pressure, and $[O_2]$ employed by Bierbach *et al*. However, in an effort to assess the consistency of our results with those from Bierbach *et al.,* we can make several reasonable assumptions and extrapolations from our low temperature data to derive an estimate for $k_{5.1b}$ at T = 298 K and P = 700 Torr.

If we assume that in the experiments of Bierbach *et al*., TME regeneration could not occur following conversion of Br−TME to a peroxy radical via reaction (2) then the Br + TME rate coefficient measured by Bierbach *et al.,* k_{Bier}, can be expressed in terms of the rate coefficients for elementary steps as follows:

$$k_{Bier} = k_{5.1a} + k_{1b} (1+X)^{-1}, \qquad \text{(5-XII)}$$

$$X = k_{-5.1b} (k_2 [O_2])^{-1}. \qquad \text{(5-XIII)}$$

Under the experimental conditions employed by Bierbach *et al.,* $[O_2] = 5.08 \times 10^{18}$ molecule cm^{-3}. The scaled Br + TME rate coefficient reported by Bierbach *et al.*, 3.05×10^{-11} cm^3 $molecule^{-1}$ s^{-1}, is a factor of 1.4 faster than our reported value for the H-abstraction rate coefficient, $k_{5.1a}$(298 K).

The following reasonable extrapolations of our low temperature data seem to suggest a lack of consistency between our results and those of Bierbach *et al.* We have directly measured $k_{5.1b}$(212 K, 700 Torr) to be 1.75×10^{-10} cm^3 molecule^{-1} s^{-1}, and the pressure dependence of $k_{5.1b}$ at this temperature indicates that 700 Torr is near the high pressure limit (see Table 5.2). Typically, rate coefficients for association reactions such as reaction (5.1b) do decrease with increasing temperature, but it seems unlikely that $k_{5.1b}$ at P = 1 bar would decrease by more than a factor of 5 between 212 K and 298 K; hence, our results suggest that $k_{5.1b}$(298 K, 1 bar) > 3.5×10^{-11} cm^3 molecule^{-1} s^{-1}. Additionally, in order to compare our data with the data reported by Bierbach *et al.* we must consider the competition between adduct reaction with O_2 and adduct unimolecular decomposition. Based on our low temperature measurements of the Br−TME + O_2 rate coefficient ($k_{5.2}$), we estimate $k_{5.2}$(298 K, 1 bar) = $(5 \pm 2) \times 10^{-12}$ cm^3 molecule^{-1} s^{-1}, so $k_{5.2}[O_2] = (2.5 \pm 1.0) \times 10^7$ s^{-1} under the experimental conditions employed by Bierbach *et al.* [*1996*]. Using an equilibrium constant obtained from equation (X), the third law values for $\Delta_r H$(298 K) and $\Delta_r S$(298 K), and an estimate of the minimum $k_{5.1b}$ obtained as described above, we estimate $k_{-5.1b} \leq 1.0 \times 10^6$ s^{-1}. Thus, our results suggest that *at least* 93% of Br−TME is scavenged by O_2 under the experimental conditions employed by Bierbach et al.; this implies that $k_{Bier} \geq 6 \times 10^{-11}$ cm^3 molecule^{-1} s^{-1}, i.e., *at least* a factor of 2 larger than the value reported by Bierbach *et al.* [*1996*]. It is worth noting that the analysis described above is based on the assumption that the Br−TME + O_2 reaction is irreversible with regards to regeneration of TME under both our experimental conditions and those of Bierbach *et al.*

The one additional experimentally reported rate coefficient for the Br + TME reaction [*Bedjanian et al., 2000*] can be compared directly with our data. By monitoring the appearance of HBr in experiments carried out at 1 Torr total pressure in He bath gas, Bedjanian *et al.* obtained the following Arrhenius expression for the H-abstraction reaction; $k_{5.1a} = (2.4 \pm 0.6) \times 10^{-11} \exp\{(-75 \pm 130)/T\}$ (233-320 K) in reasonable agreement with the Arrhenius expression obtained in this study.

Thermochemistry

Bedjanian *et al*. [*2000*] have determined the temperature dependence of the product of the equilibrium constant for Br−TME formation/dissociation and the rate coefficient for Br−TME reaction with Br_2, from which they deduce the enthalpy change associated with Br−TME formation to be −41±9 kJ/mol, in reasonable agreement with the second (47.0 kJ/mol) and third law values (47.3 kJ/mol) for $\Delta_r H$ obtained in this study. There are no reported bond strengths which we can compare our results for Br−1,3-butadiene or Br−isoprene. However, the Br−1,3-butadiene and Br−isoprene adducts characterized in this study are much more strongly bound, 69.2 and 70.2 kJ/mol respectively, than other Br−alkene adducts for which literature results are available [*Barnes et al., 1989; Frisch et al., 2009; Chase et al., 1985; Lias et al., 1988; Atkinson, 2006; Ferrell, 1998*]. The increased stability can be attributed to the allyl-resonance stabilization effect as the result of conjugated double bonds, i.e., 298 K C−Br bond strengths in Br−isoprene and Br−1,3-butadiene are ~70 kJ/mol whereas 298 K C−Br bond strengths for Br−MVK (MVK ≡ methyl vinyl ketone) [*Huskey, 2008*], Br−TME, and Br−ethylene [*Ferrell, 1998*] are 49, 47, and 29 kJ/mol, respectively.

Implications for Atmospheric Chemistry

Our findings suggest that the Br + olefin reactions are significantly faster under atmospheric conditions than previously thought. Examination of the effect of added O_2 on Br atom kinetics under conditions where reversible adduct formation is observed allows rate coefficients for the Br−olefin + O_2 reactions to be determined. Results from the Br−olefin + O_2 experiments provide further evidence of the effect of allyl-resonance stabilized bromoalkyl radicals. The rate coefficient for the Br−TME + O_2 reaction is ~ 10 times larger than the rate coefficients for the Br−isoprene + O_2 and Br−1,3-butadiene + O_2 reactions. Our results suggest that, for the bromoalkyl radicals investigated in this study (Br−isoprene, Br−1,3-butadiene, and Br−TME), bromoalkyl radical reaction with O_2 occurs considerably more rapidly under atmospheric conditions than bromoalkyl radical unimolecular decomposition. Hence, the near gas kinetic addition reactions appear to control the rate of olefin loss by reaction with Br in the atmosphere.

Table 5.12 shows a comparison of the lifetimes of each alkene towards oxidation by various species. While such comparisons are difficult to make due to the dependence on oxidant concentrations employed in each lifetime calculations, the table helps to illustrate the impact that Br kinetics *could* have on the alkenes of interest. A few highlights from the data in the table include (i) NO_3 will dominate TME chemistry at night, however, during the daytime hours Br chemistry could play an important part in the oxidation of TME in certain environments, (ii) the Br reaction could play a role as a significant loss pathway for isoprene and 1,3-butadiene in environments where [Br] are sufficiently high enough. This could especially be important in the case of isoprene given that isoprene is so prevalent in our atmosphere.

Table 5.12. Estimated atmospheric lifetimes for each alkene with X (= OH, NO_3, O_3, Cl, or Br).

k(cm^3 $molec^{-1}$ s^{-1})		X[a]	τ (297 K)	τ (212 K)	297 K	212 K
TME						
297 K	212 K		Clean enviromnemt		References for k_x	
1.1×10^{-10}	1.1×10^{-10}	OH	2.5 hrs.	2.5 hrs	(1)	See note[b]
5.7×10^{-11}		NO_3	35 s		(2)	
1.1×10^{-15}	7.3×10^{-16}	O_3	15 min.	23 min.	(3), (4)	
1.2×10^{-10}	1.8×10^{-10}	Br	10 min.	7 min.	This work	
1,3-butadiene						
6.7×10^{-11}	1.0×10^{-10}	OH	4.1 hrs.	2.8 hrs.	(5)	
1.0×10^{-13}		NO_3	5.5 hrs.		(6)	
6.5×10^{-18}	5.5×10^{-19}	O_3	1.8 d	21 d	(7)	
1.6×10^{-10}	[c] 2.0×10^{-10}	Br	7.4 min	6 min	This work	
Isoprene						
1.0×10^{-10}	1.6×10^{-10}	OH	2.8 hrs.	1.7 hrs.	(8)	
7.3×10^{-13}	4.0×10^{-13}	NO_3	46 min.	1.4 hrs	(8)	
1.3×10^{-17}	9.2×10^{-19}	O_3	21 hrs	12.6 d	(8)	
3.6×10^{-10}	3.6×10^{-10}	Cl	7.7 hrs.	7.7 hrs.	Our work (Ch. 4 of this thesis)	
1.8×10^{-10}	2.7×10^{-10}	Br	6.6 min.	4.4 min.	This work	

[a]Estimated concentrations (molecule cm^{-3}): [Br]=1.4×10^7 [Boudries and Bottenheim, 2000]; [OH] = 1×10^6 (global avg.) [Seinfeld and Pandis, 2006]; [NO_3] = 5×10^8 (12 hr nighttime avg.)[Atkinson, 1997]; [O_3] = 1×10^{12} [Seinfeld and Pandis, 2006]; [Cl] = 1×10^5 [Wingenter, 2005]; [b]k_{OH}(T) not known, we assumed no T dependence; [c] estimate based on our direct measurement of $k_{5.3}$(227 K) = 2.1×10^{-10}. References: (1) Atkinson and Aschman, 1984, (2) Atkinson, 1997, (3) Huie and Herron, 1975, (4) Drozd et al., 2011, (5) Atkinson, 1986, (6) Atkinson, 1991, (7) Bahta et al., 1984, (8) Sander et al., 2011.

CHAPTER 6

THE REACTIONS OF ATOMIC CHLORINE WITH DIMETHYL SULFIDE AND DIMETHYL SELENIDE: H-ABSTRACTION AND REVERSIBLE ADDITION CHANNELS OBSERVED

Introduction

Dimethylsulfide (DMS) constitutes roughly half of all biogenic sulfur emissions to the atmosphere [*Bates et al., 1994*]. DMS is emitted in large quantities from the oceans as a result of biological activity in seawater, and its oxidation products, mainly sulfur dioxide and methane sulfonic acid, are thought to play an important role in particle formation and growth in the marine environment [*Charlson et al., 1987; Andreae et al., 1994*]. The formation of aerosols can have significant impact on the Earth's radiation budget by serving as cloud condensation nuclei (CCN). Non-sea-salt aerosols are a major source of CCN in the marine boundary layer (MBL), and the primary component of non-sea-salt aerosol in the (MBL) is sulfate which results from gas phase oxidation of DMS [*Andreae et al., 1994*].

Similar to its analog DMS, dimethyl selenide (DMSe) is found to be the most abundant volatile Se species in the atmosphere and in surface seawater. As a result of the geochemical and physiochemical similarities between selenium and sulfur, the atmospheric oxidation mechanisms of DMS and DMSe are presumed to be quite similar. It has been thought that DMSe is produced via a similar pathway to DMS in

cocolithophorid, which is the most widespread species of plankton in the ocean [*Armoroux et al., 2001*]. Although DMSe exists in much lower abundance than DMS, their concentrations have been found to be linked in marine environments. Despite this linkage, DMS chemistry has been the subject of many studies while the chemistry of DMSe has hardly been studied at all.

It is well established that the oxidation of DMS is initiated by reaction with OH, BrO, and NO_3, however, there is also evidence that Cl atoms may play an important role as an oxidant for DMS in some locales [*Urbanski and Wine, 1999*]. It has been reported that levels of Cl atoms in the marine boundary layer can be 1-10% of OH levels [*Wingenter et al., 2005*], and recent published work suggests a significant Cl production rate even in the middle of the continental United States [*Thornton et al., 2010*]. Furthermore, recent laboratory and theoretical research has shown that the heterogeneous reaction of N_2O_5 with HCl may represent a significant source of tropospheric $ClNO_x$ species that can readily undergo photolysis to produce Cl atoms [*Raff et al., 2009*]. Depending on the relative rate coefficients for OH and Cl (Cl reactions are often faster than the corresponding OH reactions) and depending on local Cl concentrations, Cl reactions could be competitive with OH reaction as an atmospheric loss process for DMS and/or DMSe.

While there have been numerous laboratory [*Urbanski and Wine, 1999; Stickel et al., 1992; Diaz-de-Mera et al., 2002; Butkovskaya et al., 1994; Kinnison et al., 1996; Langer et al., 1996; Arsene et al., 2005; Zhao et al., 1996; Nielson et al., 1990*] and theoretical [*Resende and DeAlmeida, 1997; Enami et al., 2004; Thompson et al., 2002; Wilson and Hirst, 1997; McKee, 1993*] studies pertaining to the Cl + DMS reaction,

quantitative assessment of the role of Cl as a DMS oxidant in the marine boundary layer is currently not possible because (i) Cl mixing ratios are not well established and (ii) as a result of disagreements in published laboratory studies, neither the rate nor the mechanism of the Cl + DMS reaction is well-established.

There has been increased uncertainty with regard to the fate of the Cl−DMS adduct, under conditions relevant to the atmosphere. It has been reported that dissociation channels to yield CH_3 + CH_3SCl or CH_3S + CH_3Cl are very minor pathways [*Langer et al., 1996; Zhao et al., 1996*]. Several groups have investigated the interaction (or lack thereof) between the adduct and O_2, and there is considerable disagreement [*Urbanski and Wine, 1999; Kinnison et al., 1996; Arsene et al., 2005; Enami et al., 2004; Thompson et al., 2002*]. Urbanski and Wine [*1999*] used LFP/UV absorption spectroscopy to observe the DMS−Cl adduct; no reaction was observed between the adduct and O_2. In fact, an upper limit was determined for the reaction ($< 4 \times 10^{-18}$ cm^3 $molecule^{-1}$ s^{-1}) at 298 K. Recent work by Enami *et al.* [*2004*] supports the notion that the atmospheric fate of the DMS−Cl adduct does not include reaction with O_2, however, Thompson *et al.* [*2002*] point out that reaction with O_2 could be competitive with the decomposition channel even if the rate constant for the reaction (DMS−Cl + O_2) is as slow as ~ 10^{-22} cm^3 $molecule^{-1}$ s^{-1}. Thompson *et al.* used variational RRKM theory to predict the thermal decomposition rate of the stabilized adduct, and a value of 0.02 s^{-1} was obtained. DMS−Cl absorbs near UV radiation very strongly [*Urbanski and Wine, 1999; Enami et al., 2004*], suggesting that photolysis could also be an important atmospheric loss pathway.

As mentioned above, publications describing kinetic and mechanistic studies of atmospheric DMSe reactions are extremely limited [*Atkinson et al., 1990; Thompson et al. 2002; Tuazon et al., 1996*]. Atkinson *et al.* [*1990*] investigated the reactions of DMSe with OH, O_3, and NO_3 at 296 K and 1 atm air using a relative rate technique and reported rate coefficients (in units of cm^3 $molecule^{-1}$ s^{-1}) of 6.78×10^{-11}, 6.80×10^{-17}, and 1.4×10^{-11}, respectively. The rate coefficients above are at least an order of magnitude faster than the corresponding rate coefficients for OH, O_3, and NO_3 reactions with DMS at 296 K, 1 atm air [*Sander et al., 2011*]. It is worth noting that DMSe oxidation products are likely to be much less volatile than the analogous DMS products, allowing them to potentially play a significant role in aerosol formation and/or growth.

In this study, we couple 248 nm laser flash photolysis of Cl_2CO with monitoring of Cl by time-resolved atomic resonance fluorescence spectroscopy to investigate Cl + DMS and Cl + DMSe kinetics over a wide range of temperature and pressure. The high and low pressure limit rate coefficients are established over the range of temperatures studied. The results allow rate coefficients for the elementary reactions listed below to be evaluated.

$$Cl + CH_3SCH_3 \rightarrow CH_3SCH_2 + HCl \qquad (6.1a)$$

$$Cl + CH_3SCH_3 + M \leftrightarrow CH_3S(Cl)CH_3 + M \qquad (6.1b, -6.1b)$$

$$Cl + CH_3SeCH_3 \rightarrow CH_3SeCH_2 + HCl \qquad (6.2a)$$

$$Cl + CH_3SeCH_3 + M \leftrightarrow CH_3Se(Cl)CH_3 + M \qquad (6.2b, -6.2b)$$

In addition, the Cl−S and Cl−Se bond strengths in DMS−Cl and DMSe−Cl are evaluated based on direct measurements of $k_{6.ib}$ and $k_{-6.ib}$ (i=1,2). The new kinetic and

thermochemical data allow adduct lifetimes toward unimolecular decomposition under atmospheric conditions to be evaluated based on experimental data for the first time. Our results are compared with the literature data described above and the potential importance of Cl-initiated oxidation as an atmospheric sink for DMS and DMSe is assessed.

Experimental Details

Chlorine atom kinetics in the presence of a range of concentrations of DMS and DMSe over a range of temperature and pressure were investigated using the LFP−RF technique described in Chapter 2. Features of the method that are specific to this study and, therefore, are not discussed in Chapter 2 are addressed below.

Cl_2CO was chosen as the photolyte for our experiments in part because molecular chlorine is known to react with DMS [*Barnes et al., 2006*].

$$Cl_2CO + h\nu\ (248\ nm) \rightarrow 2Cl + CO \qquad (6.3)$$

A Lamda Physik Compex 102 KrF eximer laser served as the 248 nm light source (pulse width was ~25 ns). Fluences employed in the study ranged from 3 to 12 mJ cm^{-2} $pulse^{-1}$ and the laser repetition rate was varied over the range 2−10 Hz. Typical reaction mixtures contained (3−15) × 10^{14} molecules cm^{-3} Cl_2CO and $[Cl]_0$ was typically in the range (1−7) × 10^{11} atoms cm^{-3}. For each measured chlorine atom decay, signals from a large number of laser shots were averaged to obtain a well-defined temporal profile.

Experiments were performed over the temperature range 238–423 K for Cl + DMS and 236–640 K for Cl + DMSe. Total pressure was varied over the range 1−700 Torr. For the high pressure experiments (P > 1 Torr) phosgene and DMS were introduced into the reaction cell from 12-L pyrex bulbs containing dilute mixtures of

phosgene or DMS with N_2 and all gas flows were measured using calibrated mass flow meters. Experiments at 1 Torr total pressure were conducted using both N_2 and He as bath gas, while experiments at all other pressures employed N_2 as the bath gas. Additionally, in the case of the 1 Torr experiments, conditions were such that half of the Cl_2CO flow into the reaction cell came from a bulb containing ~2 % mixing ratio of Cl_2CO in He, while the other half of the flow into the cell came from bulbs containing known mixing ratios of DMS or DMSe in He. The contents of each bulb were measured frequently by UV photometry at 228.8 nm (Cd lamp). The absorption cross sections at 228.8 nm employed to determine the bulb concentrations were, in units of 10^{-20} cm^2, 116 for DMS, 700 for DMSe.

The gases used in this study were as follows: N_2 (99.999%, Air Gas), He (99.999%, Air Gas), CO_2 (99.99%, Air Gas), Cl_2CO (99.0 %, Matheson Trigas,). For Cl_2CO and CO_2 the stated purity refers to the liquid phase in a high-pressure gas cylinder. The liquid chemicals used in this study were as follows: DMS (99.0 %, Sigma-Aldrich), DMSe (99%, Alpha Aesar). N_2, He, and CO_2 were used as supplied, while Cl_2CO, DMS and DMSe were degassed repeatedly at 77 K, then diluted in N_2 or He and stored in pyrex bulbs (1 or 12 L), from which it was flowed into the reaction cell.

Results and Discussion

All experiments were carried out under pseudo-first-order conditions with $[DMS(e)] >> [Cl]_0$; DMS(e) ≡ 'DMS *or* DMSe'. Thus, in the absence of secondary reactions that enhance or deplete the Cl concentration, the Cl temporal profile following the laser flash would be described by the relationship

$$ln\{[Cl]_0/[Cl]_t\} = ln\{S_0/S_t\} = (k_{6.i}[DMS(e)] + k_{6.4})t = k't \qquad (i=1,2) \qquad (6\text{-I})$$

In equation (6-I), S_0 is the Cl fluorescence signal at a time immediately after the laser fires, S_t, is the Cl fluorescence signal at time t, $k_{6.1}$ is the overall rate coefficient for loss of Cl by all *irreversible* Cl + DMS reaction channels, $k_{6.2}$ is the overall rate coefficient for loss of Cl by all *irreversible* Cl + DMSe reaction channels, and $k_{6.4}$ is the rate coefficient for the following reaction:

$$Cl \rightarrow \text{Reaction with background impurities and/or loss by diffusion from detector field of view} \qquad (6.4)$$

The bimolecular rate coefficients of interest, $k_{6.i}(P,T)$, are determined from the slopes of k′ vs [DMS(e)] plots for data obtained at constant T and P. We have been able to evaluate rate coefficients for H-abstraction, adduct formation, and adduct dissociation. In addition, the bond dissociation enthalpy for the addition reaction has been evaluated. Prior to this study, there has been no experimental data published on the bond strengths of the DMS−Cl or DMSe−Cl adducts. Since the Cl + DMS(e) reaction mechanisms vary with temperature and pressure, each regime is discussed separately.

Experiments at P = 1 Torr He

We expect data obtained at P = 1 Torr He to be attributed to the H-abstraction reaction. To this end we will be able to directly compare our results with data reported by Diaz de Mera *et al.* [*2002*], also obtained at P = 1 Torr He. Well-behaved pseudo-first-order Cl atom kinetics were observed in studies carried out at 223 K < T < 640 K and 1 Torr He bath gas, i.e., Cl temporal profiles were exponential and observed first order decay rates were found to increase linearly with increasing [DMS(e)]. Observed

kinetics were found to be independent of laser photon fluence variations and variations in photolyte concentrations. The kinetic observations are consistent with the behavior predicted by equation (6-I), and this evidence strongly supports the contention that reactions (6.i) and (6.4) are the only processes that significantly affect the post-laser-flash Cl time history. Typical data are shown in Figures 6.1 and 6.2, and measured bimolecular rate coefficients, $k_{6.ia}(P,T)$, are summarized in Table 6.1.

The background Cl atom loss rate ($k_{6.4}$) was measured directly at each temperature and pressure. Of note are the large values for $k_{6.4}$ found at P = 1 Torr He (see Figure 2). For the 1 Torr He experiments $k_{6.4}$ varied from 900 s^{-1} (at 220 K) to 3000 s^{-1} (at 640 K). A negative temperature dependence is observed over a range of temperatures (223-423 K) as bimolecular rate coefficients were obtained from the slopes of k′ vs. [DMS(e)] plots. Arrhenius plots for reactions 6.1a and 6.2a are shown in Figure 6.3. Also shown in Figure 6.3 are the 1 Torr He data reported by Diaz-Mera *et al.* [*2002*]. The following best fit Arrhenius expressions are derived from a linear least-squares analysis of the *ln* k_{ia} versus T^{-1} data:

$$k_{6.1a}(T) = (8.0 \pm 1.8) \times 10^{-11} \exp[+(310 \pm 51)/T] \text{ cm}^3 \text{ molecule}^{-1} \text{ s}^{-1}$$

$$k_{6.2a}(T) = (1.4 \pm 0.2) \times 10^{-10} \exp[+(220 \pm 24)/T] \text{ cm}^3 \text{ molecule}^{-1} \text{ s}^{-1}$$

Uncertainties in the above expressions are 2σ and represent the precision of the Arrhenius parameters. The largest systematic uncertainty in the determination of each bimolecular rate coefficient, $k_{6.i}(P,T)$ (i=1,2), lies in the determination of the reagent concentration in the reaction mixture; we estimate this uncertainty to be ± 10% independent of pressure and temperature. Since the precision of the $k_{6.i}(P,T)$ values tabulated in Tables 6.1 and

6.2 are quite good ($2\sigma \leq 10\%$), we conservatively estimate the accuracy of each reported value for $k_{6.i}(T)$ (i = 1, 2) to be ± 15%.

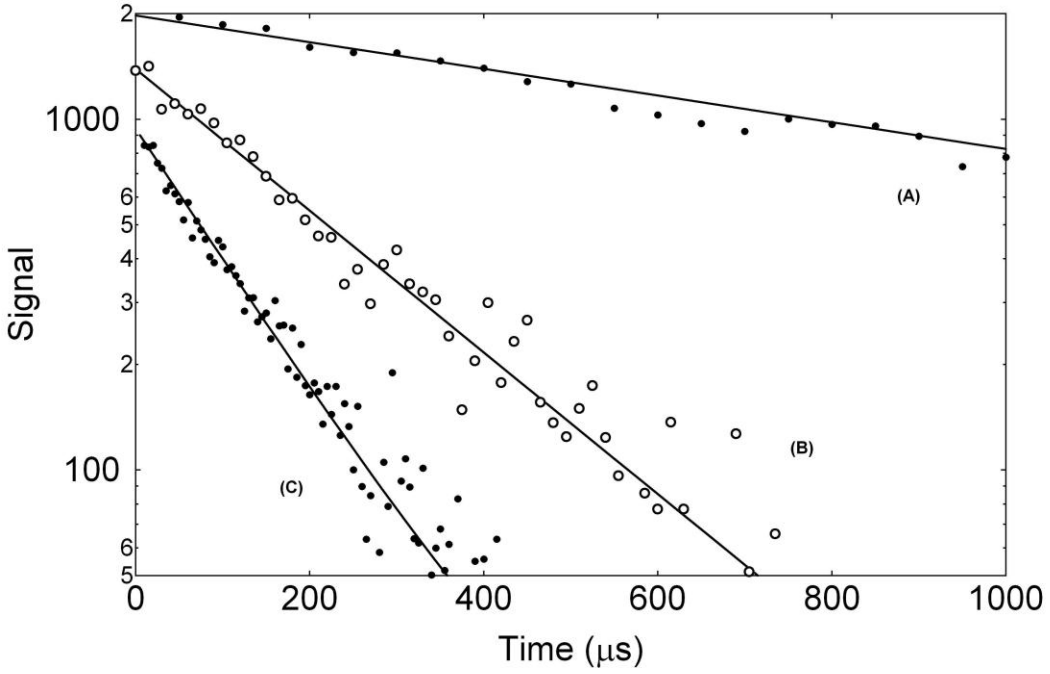

Figure 6.1 Typical Cl atom temporal profiles observed at P = 1 Torr He. Experimental conditions: T = 239 K; $[Cl_2CO]$ = 4 x 10^{14} molecules cm^{-3}; $[Cl]_0$ = 5 x 10^{11} atoms cm^{-3}; [DMS] in units of 10^{13} molecules cm^{-3} = (a) 0, (b) 1.20, (c) 2.35. Lines are obtained from least-squares analyses and give the following pseudo-first-order decay rates in units of s^{-1}: (a) 990, (b) 4600, (c) 7700.

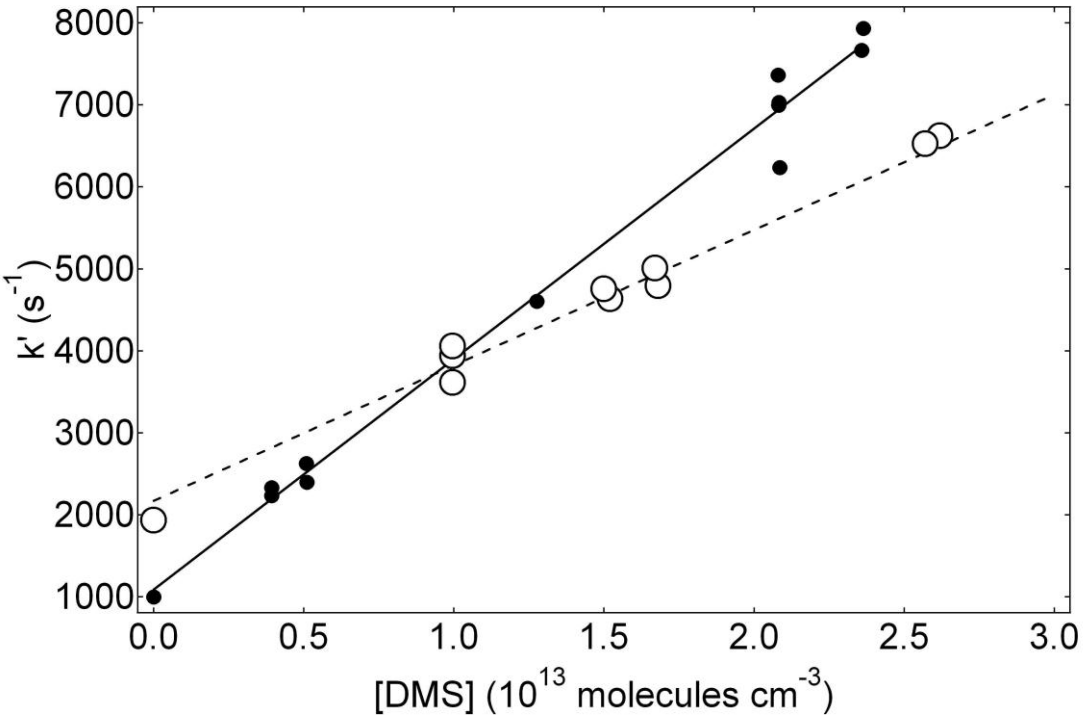

Figure 6.2 Plots of k′, the pseudo-first-order Cl atom decay rate, versus [DMS] for data obtained at 298 K. Lines are obtained from linear least squares analyses, and the resulting bimolecular rate coefficients, i.e., the slopes of the data are listed in Table 6.1. Open circles represent data obtained at 1 Torr He and filled circles represent data obtained at 500 Torr N_2.

Table 6.1. Summary of Kinetic Data at P = 1 Torr He for the Cl + DMS Reaction at 423 K ≥ T ≥ 223 K and Cl + DMSe at 640 K ≥ T ≥ 236 K.[a]

T	N	$[Cl_2CO]$	$[Cl]_0$	$[DMS]_{max}$	$k_{6.4}$	k'_{max}	$k_{6.1a} \pm 2\sigma$
223	10	6000	3	950	600	33000	3.34 ± .19
238	11	3700	3.5	230	1000	7700	2.75 ± .18
250	10	6000	3	840	900	22000	2.68 ± .12
299	10	6000	3	190	1400	5900	2.17 ± .07
298	12	5000	5	860	1910	20000	2.34 ± .15
352	10	4000	3	600	1800	12000	1.76 ± .14
357	12	4000	3	600	1800	12000	1.83 ± .11
357	19	2000	2	160	1900	5300	2.01 ± .14
423	6	4000	4	500	2200	10000	1.65 ± .05
T	no.of expts	$[Cl_2CO]$	$[Cl]_0$	$[DMSe]_{max}$		k'_{max}	$k_{6.2a} \pm 2\sigma$
236	12	4300	3.5	690	940	25000	3.50 ± .07
299	12	3400	3.5	550	1600	15990	2.78 ± .13
401	12	2500	2.6	400	2000	3300	2.32 ± .10
498	8	2000	1.8	330	2100	3300	2.15 ± .13
640	10	1600	1.6	260	3000	3600	2.03 ± .15

[a] Units: T(K); P(Torr); concentrations $[COCl_2]$, $[Cl]_0$, [DMS(e)]: (10^{11} cm^{-3}) ; $k'_{max}(s^{-1})$; $k_{6.ia}(10^{-10}$ cm^3 $molecule^{-1}$ s^{-1}). N ≡ number of measurements of a single qseudo-first-order Cl decay rate. Uncertainties represent precision only.

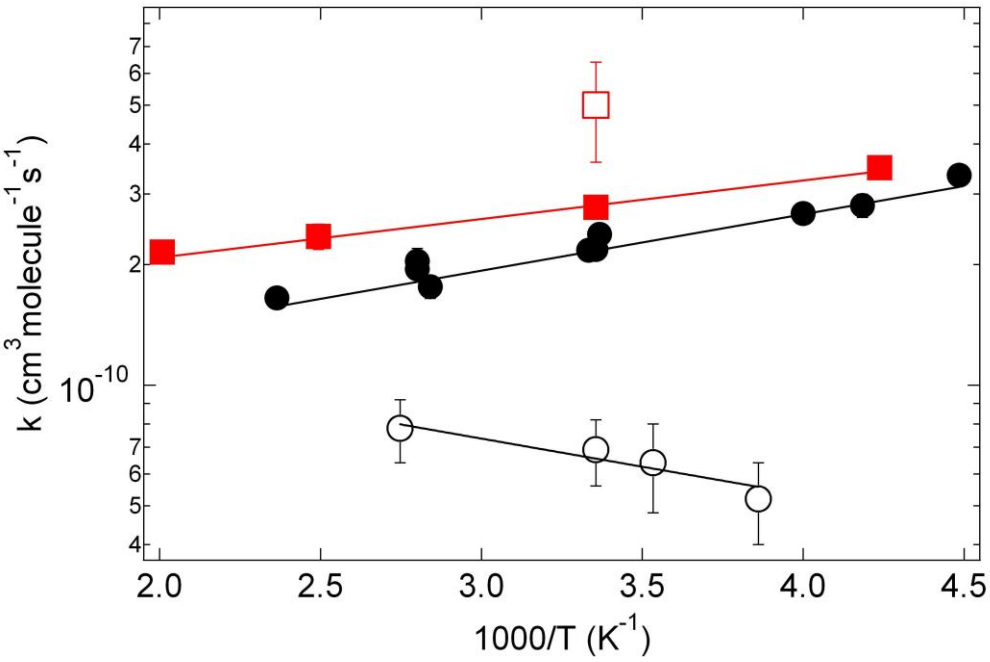

Figure 6.3. **Arrhenius plots for Cl + DMS (black circles) and Cl + DMSe (red squares) H-abstraction reactions.** The solid lines are obtained from an unweighted linear least-squares analysis and give the Arrhenius expressions reported in the text. Uncertainties are 2σ, precision only. Closed symbols represent our work, while open symbols are taken from Diaz de Mera *et al.*[*2002*] (Cl + DMS) and Thompson *et al.*[*2002*] (Cl + DMSe).

Table 6.2. Summary of Kinetic Data for Cl + DMS at 357 ≥ T ≥ 238 K.

T	P	N	$[Cl_2CO]$	$[Cl]_0$	$[DMS]_{max}$	k'_{max}	$k_{6.1} \pm 2\sigma$
238	1	10	4000	3	370	10000	2.52 ± .01
	1	10	4000	3	370	10000	2.63 ± .01
	3	10	10000	3	1000	30000	2.80 ± .16
	10	5	6000	3	180	5200	2.94 ± .09
	20	6	6000	3	160	5100	3.01 ± .19
	50	6	6000	3	160	5700	3.53 ± .18
	100	6	6000	3	140	5400	3.82 ± .23
	200	7	6000	3	160	6600	3.89 ± .09
	400	8	6000	3	170	6200	3.82 ± .17
	500	6	6000	3	160	6700	3.93 ± .47
298	1	12	3000	4	300	7600	2.31 ± .07
	3	10	9000	10	850	20000	2.41 ± .08
	10	7	5000	2	130	3700	2.67 ± .21
	20	5	3000-10000	1-6	200	6000	2.91 ± .12
	50	7	5000	2	140	4500	3.09 ± .20
	100	7	5000	2	130	4400	3.26 ± .10
	300	6	5500	3	110	4100	3.59 ± .23
	400	4	5000	2	130	4500	3.32 ± .47
	500	8	5500	3	160	5800	3.55 ± .19
357	1	10	3000	2	170	4300	2.07 ±.01
	3	10	9000	4	500	10500	1.93 ± .06
	10	6	10000	5	110	2700	2.26 ± .16
	20	5	10000	5	130	3300	2.45 ± .07
	50	6	10000	5	130	3300	2.49 ± .16
	100	6	10000	5	120	3600	2.69 ± .06
	200	6	10000	4	140	4300	3.04 ± .14
	400	8	10000	5	120	4000	3.17 ± .16
	500	6	10000	4	130	4000	3.13 ± .19

Units: T(K); P(Torr); concentrations $[COCl_2]$, $[Cl]_0$, [DMS]: (10^{11} cm^{-3}) ; $k'_{max}(s^{-1})$; $k_{6.1}(10^{-10}$ cm^3 $molecule^{-1}$ s^{-1}). N ≡ number of measurements of a single qseudo-first-order Cl decay rate. Uncertainties represent precision only. ~ 4 x 10^{15} CO_2 cm^{-3} was added to promote more rapid equilibration of the $Cl(^2P_{3/2,1/2})$ spin−orbit states.

Table 6.3. Summary of Kinetic Data for Cl + DMSe at 401 K ≥ T ≥ 236 K.[a]

T	P	N	$[Cl_2CO]$	$[Cl]_0$	$[DMSe]_{max}$	k'_{max}	$K_{6.2} \pm 2\sigma$
236	10	5	1500	2.2	57.5	2219	3.63 ± .24
	20	5	2400	2.6	63.4	2454	3.71 ± .17
	50	8	3200	3.5	110	4172	3.89 ± .29
	100	5	4500	7.0	105	4181	3.85 ± .17
	300	8	3500	3.5	252	9836	3.79 ± .11
	500	7	3900	4.3	195	7386	3.80 ± .13
299	2.5	5	1600	1.9	150	4659	2.95 ± .15
	2.5	5	2000	3.5	165	4615	2.71 ± .17
	5	5	1200	3.0	230	6818	2.89 ± .21
	5	5	2300	2.2	180	5133	2.84 ± .20
	7.5	5	1900	1.9	185	5449	2.97 ± .17
	10	5	1700	3.3	188	5802	3.01 ± .19
	15	5	2300	2.2	193	5904	2.94 ± .28
	20	5	1700	3.7	222	6805	3.23 ± .18
	20	5	2300	2.2	225	6810	3.02 ± .17
	25	5	2200	3.7	178	5396	3.08 ± .27
	30	5	2300	3.6	211	6705	3.16 ± .11
	35	5	1500	3.5	233	7655	3.40 ± .15
	35	5	2200	1.9	176	5632	3.24 ± .25
	100	5	2300	3.6	120	3689	3.26 ± .24
	200	5	2300	4.0	128	3913	3.46 ± .14
	300	5	4000	6.1	135	4579	3.37 ± .11
	500	5	4000	6.1	114	3967	3.44 ± .19
	700	5	4000	6.1	101	3490	3.43 ± .29
401	20	5	1900	2.0	143	3603	2.53 ± .11
	50	5	3300	1.5	117	3443	2.80 ± .11
	100	7	3000	3.8	182	5278	2.91 ± .19
	300	5	3300	6.5	173	5662	3.25 ± .19
	500	5	3500	4.4	183	5954	3.35 ± .25
	700	5	2700	2.4	90.2	2956	3.33 ± .29

[a] Units: T(K); P(Torr); concentrations(molec cm^{-3}) $[Cl_2CO]$, $[Cl]_0$, [DMSe]: (10^{11} cm^{-3}); $k'_{max}(s^{-1})$; $k_{6.2}(10^{-10}$ cm^3 $molecule^{-1}$ $s^{-1})$; N ≡ number of measurements of a single pseudo-first-order Cl decay rate. Uncertainties represent precision only.

Pressure Dependent Channel

Experiments were performed over the temperature ranges 220 – 421 K for Cl + DMS and from 236 – 640 K for Cl + DMSe. Total pressure varied from 1 Torr to 700 Torr N_2. Rate coefficients were found to increase with increasing pressure at all temperatures investigated (see Tables 6.2 and 6.3). To provide a parameterization that is convenient for representing pressure dependent kinetic data in atmospheric models and in Figures 6.4 and 6.5, the data were fit to the following expression [*Sander et al., 2011*].

$$k(M,T) = \left(\frac{k_0(T)[M]}{1 + \frac{k_0(T)[M]}{k_\infty(T)}} \right) 0.6^{\left\{1+\left[\log_{10}\left(\frac{k_0(T)[M]}{k_\infty(T)}\right)\right]^2\right\}^{-1}} \qquad \text{(6-II)}$$

In eq 6-II, k_0 and k_∞ are approximations to the low and high pressure limiting rate coefficients and 0.6 is a fixed value representing the broadening parameter, F_c; although F_c is dependent on both the identity of the bath gas and the temperature [*Troe, 1979; 1983; Luther and Troe, 1978*], assuming F_c=0.6 allows data to be fit well over the range of conditions typically encountered in the atmosphere [*Sander et al., 2011*]. The pressure dependent data for Cl + DMS and Cl + DMSe at 298 K are plotted in Figures 6.4 and 6.5, respectively. The solid lines in these figures are best fits of the data to the sum of a pressure independent rate coefficient (H-abstraction) and a pressure dependent rate coefficient using eq 6-II to represent the pressure dependent component. The dashed lines in the figures show the pressure dependent and pressure independent components. It should be noted that in Figures 6.4 and 6.5 the 1 Torr He data are are plotted as 0.5 Torr N_2 because low pressure limit rate coefficients for association reactions are typically a factor of two slower in He than in N_2 at a given total pressure. The data indicate that

the H-abstraction channel accounts for approximately 60% (Cl + DMS) and 80% (Cl + DMSe) of the total rate coefficient at 298 K and 1 atm N_2.

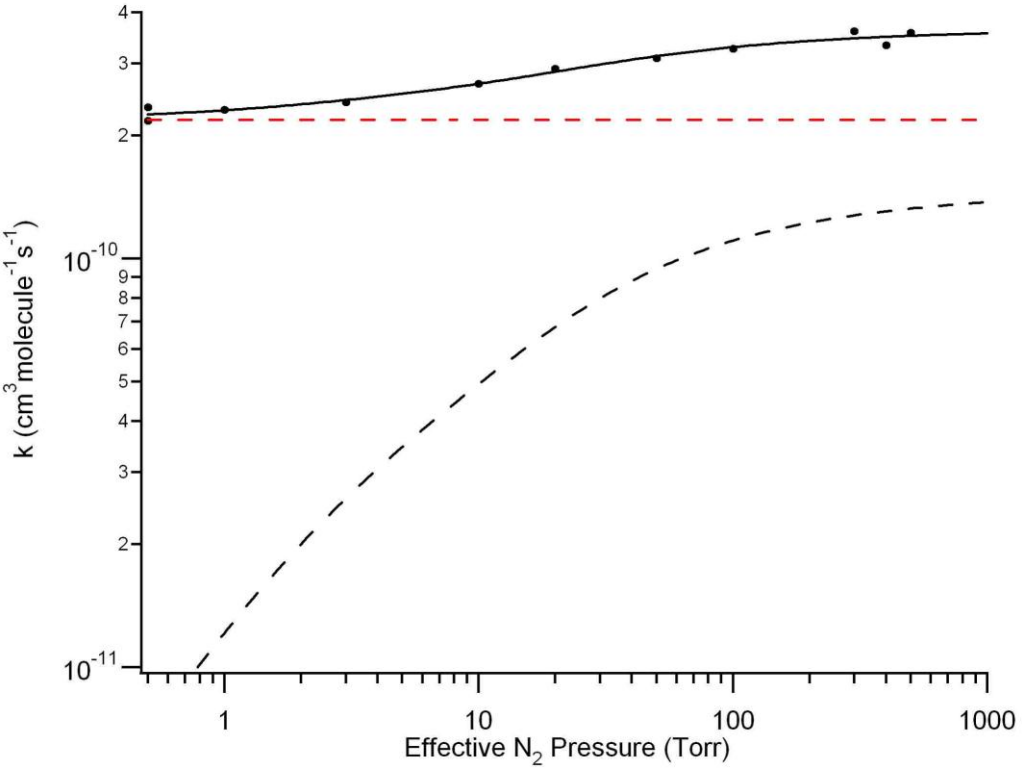

Figure 6.4 Data shown for Cl + DMS at 298 K as a function of P. Dotted line represents the addition channel; solid line represents total rate constant as a function of pressure; dotted horizontal (red) line represents $k_{6.1a}$. Note: 1 Torr He data plotted as 0.5 Torr N_2.

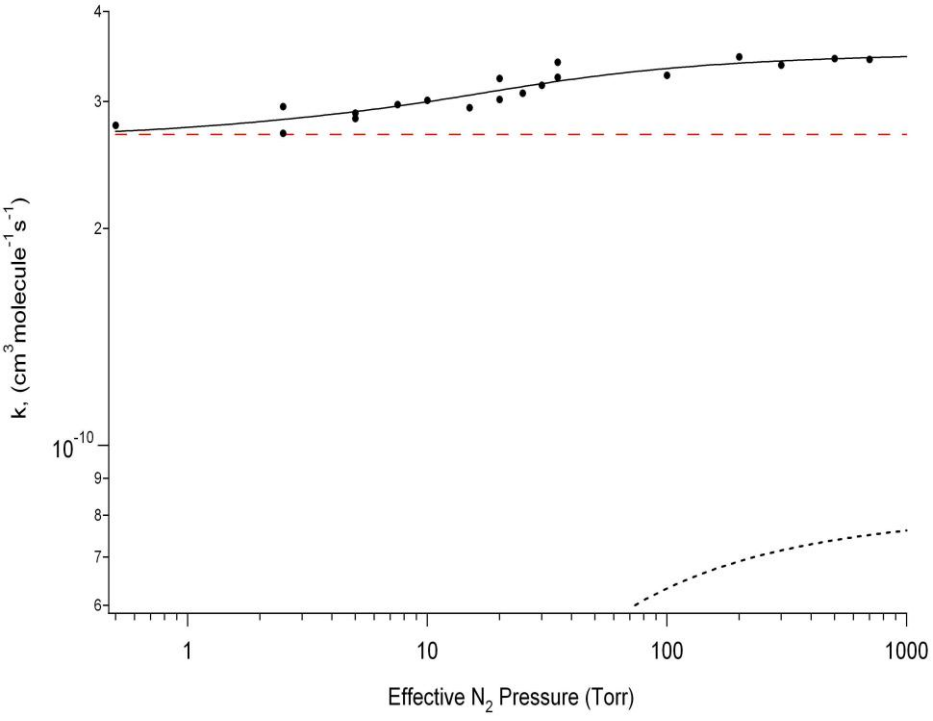

Figure 6.5 Data shown for Cl + DMSe at 299 K as a function of P. Dotted line represents the addition channel; solid line represents total rate constant as a function of pressure; dotted horizontal (red) line represents $k_{6.2a}$. Note: 1 Torr He data plotted as 0.5 Torr N_2.

High Temperature Equilibration Kinetics

At temperatures around 420 K and high pressures (around 500 Torr N_2), kinetic evidence for reversible addition of Cl to DMS was observed, and at 492 K similar evidence was observed for Cl + DMSe. The relevant kinetic scheme for analysis of this "approach to equilibrium" data includes reactions (6.ia), (6.ib), (−6.ib), (6.4), and (6.5), where i = 1 for Cl + DMS and i = 2 for Cl + DMSe.

$CH_3S(e)(Cl)CH_3 \rightarrow$ loss by processes that do not regenerate Cl atoms (6.5)

The rate equations for the above reaction schemes can be solved analytically, and predict double exponential functional forms for the Cl decay:

$$[S]_t/[S]_0 = [(Q + \lambda_1)\exp(\lambda_1 t) - (Q + \lambda_2)\exp(\lambda_2 t)] / (\lambda_1 - \lambda_2) \quad \text{(6-III)}$$

In equation (6-III), S_t and S_0 are the resonance fluorescence signal levels at times t and 0, and

$$Q = k_{-6.ib} + k_{6.5}, \quad \text{(6-IV)}$$

$$-(\lambda_1 + \lambda_2) = Q + k_{6.4} + (k_{6.ia} + k_{6.ib})[DMS] \quad \text{(6-V)}$$

$$\lambda_1\lambda_2 = Q(k_{6.4} + k_{6.ia}[DMS]) + k_{6.5}k_{6.ib}[DMS] \quad \text{(6-VI)}$$

A typical observed Cl temporal profile is shown in Figure 6.6. The temporal profiles were fit to the double exponential equation (6-III) using a non-linear least squares method to obtain values for the fit parameters S_0, Q, λ_1, and λ_2. Rearrangement of equations (6-IV) – (6-VI) gives relationships for the rate coefficients of interest:

$$k_{ib} = -(Q + k_{6.4} + k_{6.ia}[DMS] + \lambda_1 + \lambda_2) / [DMS] \quad \text{(6-VII)}$$

$$k_{6.5} = \{\lambda_1\lambda_2 - Q(k_{6.4} + k_{6.ia}[DMS])\} / k_{6.ib}[DMS] \quad (6\text{-VIII})$$

$$k_{-6.ib} = Q - k_{6.5} \quad (6\text{-IX})$$

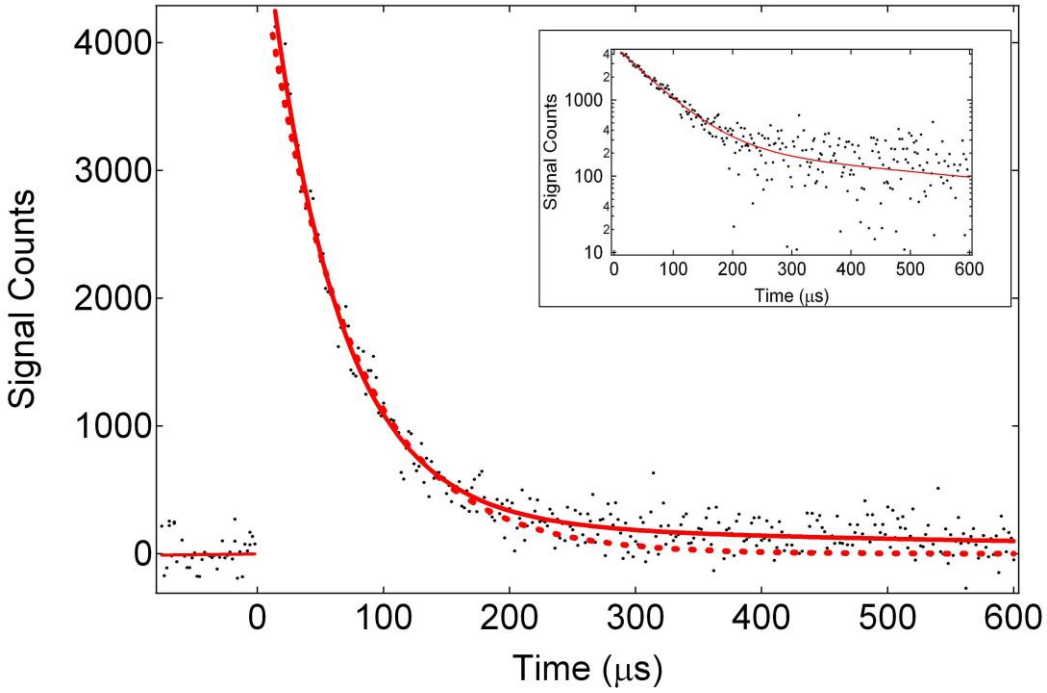

Figure 6.6. **Typical approach to equilibrium kinetic data for Cl + DMS.** Experimental conditions: T = 421 K, P = 500 Torr N_2, [Cl] ~ 5 × 10^{11} atom cm, [DMS] = 7.1 × 10^{13} molec cm^{-3}. Solid line represents best fit to equation 6-III; the best fit parameters are S_0 = 5200, Q = 2480 s^{-1}, λ_1 = −17700 s^{-1}, λ_2 = −1660 s^{-1}. Dashed line represents best fit to a single exponential decay. Photolysis laser fired at time = 0.

The background Cl atom loss rate ($k_{6.4}$) was directly measured by observing the RF decay in the absence of DMS(e) at each temperature and pressure. At 421 K and 500 Torr, $k_{6.4} \sim 20\ s^{-1}$, and at 492 K, 500 Torr, $k_{6.4} \sim 30\ s^{-1}$. Experimental conditions and results of all equilibration kinetics experiments are summarized in Tables 6.4 and 6.5. The values of the equilibrium constants given in the tables have been derived from the following relationship

$$K_P = k_{6.ib} / (k_{-6.ib}\, RT) = K_c / (RT) \qquad (6\text{-X})$$

The fact that the H-abstraction channel is such a large fraction of the total reaction inhibits our ability to observe equilibration, i.e., in order to observe double exponential decays where the long-time decay rate is significantly slower than the short time decay rate, it is necessary to drive the Cl ↔ DMS(e)−Cl equilibrium very far toward DMS(e)−Cl. Further complicating matters is the strong temperature dependence of k_{-ib}. Because we were limited in our ability to observe equilibrium conditions, our efforts concentrated on experimental conditions where optimal data could be obtained (421 K for DMS and 492 K for DMSe). We estimate the accuracies (95% confidence level) of $k_{6.ib}$ and $k_{-6.ib}$ to be ±20% and ±30%, respectively (i = 1, 2). Hence, a reasonable estimate for the accuracies of reported values for K_P is ± 35% at the 95% confidence level.

Ideally, we would like to obtain values for K_P over a wide range of temperature and extract $\Delta_r H$ and $\Delta_r S$ from the slope and intercept of a van't Hoff plot (*ln* K_P vs 1/T), however, due to the limitations noted above we were forced to rely on data at a single temperature for each reaction. Thus, values for the adduct bond strength are derived by

using a third-law method. The enthalpy change for each reaction is obtained from the relationship

$$ln\ K_P = (\Delta_r S / R) - (\Delta_r H / RT) \qquad (6\text{-XI})$$

The experimental values for K_P are $(6.82 \pm 2.39) \times 10^5$ atm^{-1} at 421 K (Cl + DMS) and $(1.66 \pm 0.58) \times 10^5$ atm^{-1} at 492 K (Cl + DMSe). These experimental values were employed in conjunction with calculated entropy changes for each reaction to determine $\Delta_r H_{6.1b}$(421 K) and $\Delta_r H_{6.2b}$(492 K). To evaluate $\Delta_r S$ for reactions (6.1b and 6.2b), absolute entropies as a function of temperature were obtained from the JANAF tables for Cl and calculated using ab initio vibrational frequencies and moments of inertia for DMS(e) and DMS(e)−Cl. Relevant parameters used in the calculations of absolute entropies and heat capacity corrections are summarized in Table 6.6. The electronic structure calculations were carried out by our collaborator, Michael L. McKee of Auburn University. Geometries were determined by the G4 method [*Curtiss et al., 2007*] using the Gaussian 09 program [*Frisch et al., 2009*]. The G4 level is a composite of several calculations starting with geometries and frequencies at the B3LYP/6-31G(2df,p) level. Theoretical values for enthalpy of binding at 298K for DMS−Cl and DMSe−Cl are found to be 85.4±3.5 and 101.7±3.5 kJ/mol, respectively. The uncertainty is based on the average deviation from experiment in a test set of 454 chemical species, 34 of which are radicals [*Curtiss et al., 2007*]; the calculations include a spin orbit correction for atoms which is 3.52 kJ/mol for Cl (^{2}P) [*Curtiss et al., 2007*]. Figure 6.7 shows the optimized B3LYP/GTBas3 structures for DMS−Cl and DMSe−Cl.

Table 6.4. Results for Cl + DMS + N_2 ↔ DMS−Cl + N_2 at T = 421 K.[a]

P	Q	$-\lambda_1$	$-\lambda_2$	[DMS]	$[Cl_2CO]$	$[Cl]_0$	$k_{6.1b}$	$k_{6.5}$	$k_{-6.1b}$	K_P
700	4388	2865	19855	647	7750	1.2	1.24	1450	2940	7.36
700	4492	3077	15270	492	7750	1.2	1.22	1950	2550	8.36
700	6205	3509	12934	354	7750	1.2	1.29	2230	3980	5.66
500	4227	7499	2137	195	4500	2.8	1.24	1402	2820	7.82
500	4952	11711	2987	376	12000	7.7	1.08	1683	3270	5.87
500	2694	5624	1692	198	12000	7.7	.803	843	1850	7.69
500	3525	11187	2426	410	15000	6.5	.872	1170	2360	6.44
500	4179	6603	2441	198	15000	6.5	.845	1660	2520	5.84
500	3497	14812	2494	551	11500	4.7	.914	1943	2253	7.06
500	3079	12465	2090	449	11700	4.8	.963	929	2150	7.79
500	2800	10191	1760	366	11600	4.7	.899	468	2332	6.71
500	2476	17729	1662	715	11600	4.7	.777	242	2234	6.05
500	2990	23068	1928	879	11600	4.7	.915	338	2650	6.00

[a] Units: P (Torr); Q, λ_1, λ_2, $k_{6.5}$, $k_{-6.1b}$ (s^{-1}); [DMS], $[Cl_2CO]$, $[Cl]_0$ (10^{11} cm^{-3}); $k_{6.1b}$ (10^{-10} cm^3 $molec^{-1}$ s^{-1}); K_P (atm^{-1}); $k_{6.1a}$ = 1.58 x 10^{-10} cm^3 $molec^{-1}$ s^{-1}.

Table 6.5. Results for Cl + DMSe + N_2 ↔ DMSe−Cl + N_2 at T = 492 K and P = 500 Torr.[a]

Q	$-\lambda_1$	$-\lambda_2$	[DMSe]	$[Cl_2CO]$	$[Cl]_0$	$k_{6.2b}$	$k_{6.5}$	$k_{-6.2b}$	K_P
4806	13774	3575	457	3500	6	5.61	506	4300	1.95
5266	19711	3965	667	3500	6	5.77	388	4880	1.77
3780	20732	2940	749	3500	6	4.75	-223	4000	1.77
6301	28763	4948	997	3500	6	5.69	943	5360	1.58
5386	27950	4334	1010	3500	6	4.72	436	4950	1.42
4564	35418	3359	1250	3500	6	5.54	-800	5360	1.54
7365	36941	5928	1280	3500	6	5.89	1740	5630	1.56

[a] Units: P (Torr); Q, λ_1, λ_2, $k_{6.5}$, $k_{-6.2b}$ (s^{-1}); [DMSe], $[Cl_2CO]$, $[Cl]_0$ (10^{11} cm^{-3}); $k_{6.2b}$ (10^{-11} cm^3 $molec^{-1}$ s^{-1}); K_P (atm^{-1}); $k_{6.2a}$ = 2.18 x 10^{-10} cm^3 $molec^{-1}$ s^{-1}.

The ab initio frequencies and rotational constants obtained by McKee are in good agreement with theoretical literature values [*Resende and DeAlmeida, 1997; Enami et al., 2004; Thompson et al., 2002; Wilson and Hirst, 1997*]. It should be noted that internal rotations of the methyl groups were treated as vibrations in all calculations described above.

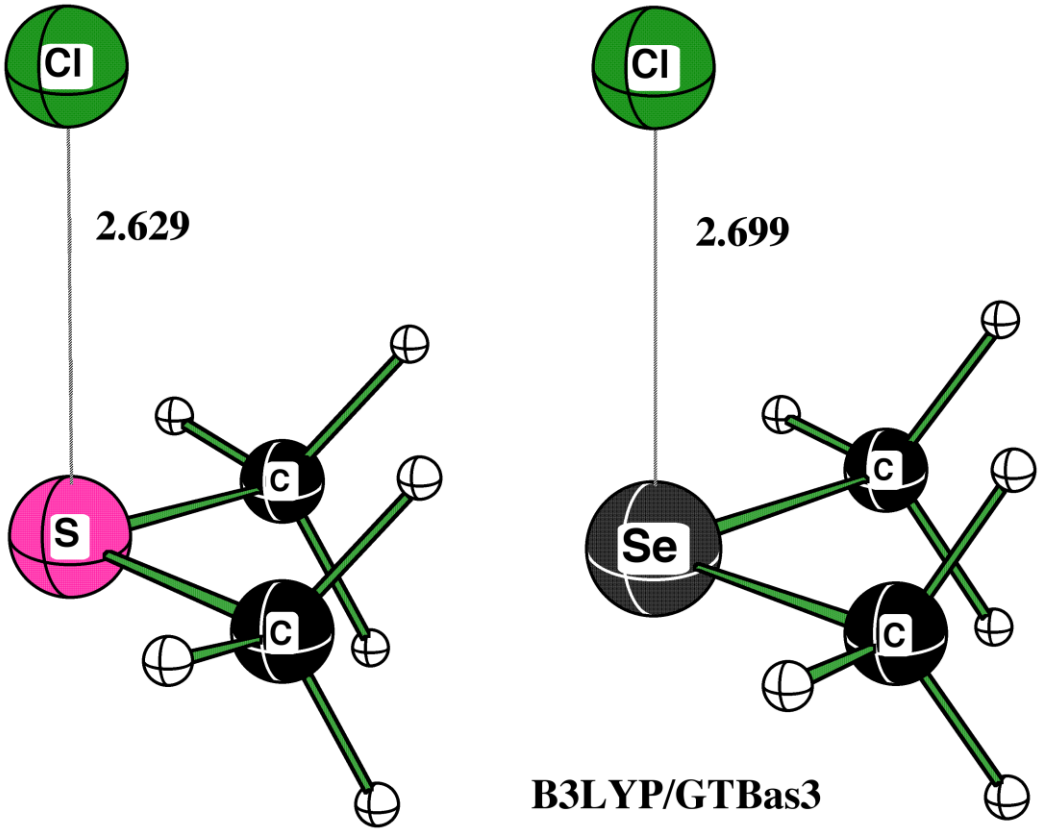

Figure 6.7 Theoretical structures of DMS−Cl and DMSe−Cl adducts. Numerical values represent bond lengths in Angstroms.

Cl−DMS Thermochemistry

The third-law analysis gives the following results, Cl + DMS (421 K): $\Delta_r S = -100 \pm 10$ J mol^{-1} K^{-1} and $\Delta_r H = -89.3 \pm 2.9$ kJ/mol; Cl + DMSe (492 K): $\Delta_r S = -99 \pm 10$ J mol^{-1} K^{-1} and $\Delta_r H = -98.1 \pm 3.6$ kJ/mol; the uncertainties we report reflect an estimate of our imperfect knowledge of the input data needed to calculate absolute entropies (particularly the low frequency DMS(e)−Cl vibrations) as well as the estimated uncertainty in the experimental values for K_P at each temperature. In arriving at the above uncertainties in $\Delta_r S$, we assume that the frequencies of the three lowest frequency DMS(e)−Cl vibrations could differ from the values given in Table 6.6 by ± 25 cm^{-1}. Appropriate heat capacity corrections have been employed to obtain the following $\Delta_r H$ values at 298 K and 0 K (units are kJ/mol): $\Delta_r H_{298}$(1b) = −89.6, $\Delta_r H_0$(1b) = −88.4 and $\Delta_r H_{298}$(2b) = −98.5, $\Delta_r H_0$(2b) = −97.6. Uncertainties are accuracy estimates at the 95 % confidence level. All results are summarized in Table 6.7. Theoretical bond strengths are also tabulated in Table 6.7 and agree reasonably well with the experimental values. The van't Hoff expressions that represent our third-law analyses are given below:

$$ln\ K_P\ (atm^{-1}) = -(12.0 \pm 1.2) + (10770 \pm 1940) / T \qquad \text{Cl + DMS}$$

$$ln\ K_P\ (atm^{-1}) = -(12.0 \pm 1.2) + (11850 \pm 2120) / T \qquad \text{Cl + DMSe}$$

The values for $\Delta_r H$ obtained above can be used in conjunction with literature values for the standard enthalpies of formation of Cl [*Chase et al., 1985*] and DMS [*Voronkov et al., 1989; McCullough et al., 1957*] to deduce a value for the standard enthalpy of formation of Cl−DMS at 298 K, $\Delta_f H_{298} = -5.8 + 7.0$ kJ mol^{-1}. To our knowledge, the standard

enthalpy of formation is not known for DMSe, which prevents us from deducing a value for the standard enthalpy of formation of DMSe−Cl.

Table 6.6. Summary of parameters used in calculations of absolute entropies and heat capacity corrections for Cl + DMS and Cl + DMSe.

	Cl	DMS	DMS−Cl
g_0	4	1	2
g_1	2		
$\Delta\varepsilon$ (cm-1)[a]	882.36		
σ		2	1
Rot. Constants (GHz)[b]		17.77, 7.44, 5.62	5.79, 2.58, 2.12
Vib. Frequencies (cm^{-1}) [b, c]		**184**, **187**, 257, 687, 739, 909, 948, 984, 1050, 1338, 1363, 1462, 1472, 1479, 1487, 3035, 3038, 3113, 3119, 3137, 3138	98, 149, **166**, **172**, 245, 270, 683, 735, 919, 940, 968, 1057, 1334, 1356, 1451, 1458, 1463, 1470, 3053, 3054, 3148, 3151, 3166, 3167
		DMSe	DMSe−Cl
g_0	4	1	2
g_1	2		
$\Delta\varepsilon$ (cm-1)[a]	882.36		
σ		2	1
Rot. Constants (GHz)[b]		11.27, 6.73, 4.45	4.54, 2.09, 1.84
Vib. Frequencies (cm^{-1}) [b, c]		146, 158, 206, 581, 596, 857, 897, 924, 977, 1297, 1319, 1460, 1469, 1475, 1481, 3055, 3058, 3148, 3153, 3156, 3156	84, 130, **138**, **146**, 206, 214, 584, 601, 872, 895, 913, 990, 1296, 1315, 1449, 1457, 1459, 1468, 3064, 3066, 3169, 3170, 3182, 3183

[a]$\Delta\varepsilon \equiv$ energy splitting between the lowest two electronic states; DMS(e) has no low-energy excited states and the adducts are assumed to have none. [b]Calculated values at the B3LYP/GTBas3 level of theory. [c] Frequencies in bold print represent methyl torsions.

Table 6.7. Thermochemical parameters for Cl + DMS ↔ DMS−Cl and Cl + DMSe ↔ DMSe−Cl. [a]

	T (K)	Method	$-\Delta_r H$ (kJ mol^{-1})	$-\Delta_r S$ (J mol^{-1} K^{-1})	$\Delta_f H$ (Adduct) [a], kJ mol^{-1}
DMS	421	Third law	89.3 ± 2.9 [c]	100.1 ± 10 [c]	
	0	Third law	88.4 ± 2.9 [c]		
		G4 theory [d]	84.2 ± 3.5 [e]		
	298	Third law	89.6 ± 2.9 [c]	100.8 ± 10 [c]	−5.8 ± 7.0 [c]
		G4 theory [d]	85.4 ± 3.5 [e]		
DMSe	492	Third law	98.1 ± 3.6 [c]	99.4 ± 10.0 [c]	
	0	Third law	97.6 ± 3.6 [c]		
		G4 theory [d]	100.8 ± 3.5 [e]		
	298	Third law	98.5 ± 3.6 [c]	100.3 ± 10.0 [c]	N/A
		G4 theory [d]	101.7 ± 3.5 [e]		

[a] Values are based on third law results; [b] Uncertainty is 2σ, precision only; [c] Uncertainty is estimated accuracy at the 95 % confidence level; [d] The level of optimization is B3LYP/6-31G(2df,p), also note G4 calculations include spin orbit corrections for atoms; [e] Uncertainty represents average deviation between experiment and theory for a test set of 454 chemical species, 34 of which are radicals.

Literature Comparisons

Cl + DMS. It has previously been established that the Cl + DMS reaction proceeds through 2 different channels, a pressure-dependent addition channel and a pressure-independent H-abstraction channel [*Stickel et al., 1992*]. High pressure values for the room temperature rate coefficient reported in this study agree well with the literature (Table 6.8). However, there are some inconsistencies with regard to the temperature dependence at both high [*Stickel et al., 1992; Kinnison et al., 1996; Arsene et al., 2005; Zhao et al., 1996*] and low [*Stickel et al., 1992; Diaz de Mera et al., 2002*] pressures. Enami *et al.* [*2004*] and Stickel et al. [*1992*] show results for the pressure dependence (obtained by different methods) of the reaction which are in reasonable agreement. Our low pressure data agrees well with the results reported by Stickel *et al.* [*1992*] but disagree significantly with the results ($k_{6.1a}(T) = (2.0 \pm 1.2) \exp[-(332 \pm 173/T)]$ cm^3 $molecule^{-1}$ s^{-1}) reported by Diaz de Mera *et al.* [*2002*]. Both Arrhenius plots are shown and the discrepancy in the data can be seen in Figure 6.3. Diaz-de-Mera *et al.* [*2002*] report a rate constant in 1 Torr He that is over a factor of 2 lower than that reported by Stickel *et al.*[*1992*] at 3 Torr N_2. In addition, Diaz de Mera *et al.* report a small positive activation energy, while multiple research groups have reported a negative temperature dependence for the reaction [*Stickel et al., 1992; Arsene et al., 2005; Enami et al., 2004*]. New data reported herein includes experiments conducted in 1 Torr He bath gas as a function of temperature to more accurately determine the magnitude and T-dependence of the H-abstraction rate coefficient ($k_{6.1a}$). Our results are in strong disagreement with the results of Diaz de Mera *et al.* [*2002*] regarding both the magnitude and T-dependence of $k_{6.1a}$. Diaz de Mera employed a discharge flow (DF) − mass

spectrometry (MS) technique to obtain rate coefficients at P = 0.5-1 Torr He. Table 6.8 summarizes all available kinetic data along with all previously published experimentally determined rate coefficients for the reaction over the full range of pressures.

Table 6.8: Previously Reported Kinetic Data for Cl + DMS.[a]

$k_{6.1}$ (297 K)	A	E/R	P	Method	Reference
3.3 ± 0.5			700, N_2	LFP-RF	Stickel *et al.,* 1992
1.8 ± 0.5			3.1, N_2		
0.69 ± .13	2.0×10^{-10}	332	1, He	DF-MS	Diaz de Mera *et al.,* 2002
2.2 ± 0.2	8.0×10^{-11}	−310	1, He	LFP-RF	This work.
3.55 ± .19			500, N_2	LFP-RF	This work.
3.22 ± 0.3			740, N_2	Relative Rate	Nielsen *et al.,* 1990
3.61 ± .21			760, N_2	Relative Rate	Kinnison *et al.,* 1996
3.15 ± .33	4.2×10^{-13}	−1968	760, N_2	Relative Rate	Arsene *et al.,* 2005
4.03 ± .17			760, Air	Relative Rate	Kinnison *et al.,* 1996
3.6 ± .0.2			760, N_2	CRDS[b]	Enami *et al.,* 2004
3.82 ± .36			760, Air	Relative Rate	Arsene *et al.,* 2005

[a]Units: $k_{6.1}$ (10^{-10} $cm^3 molec^{-1} s^{-1}$); A (cm^3 $molecule^{-1}$ s^{-1}); E/R (K); P (Torr). [b]CRDS ≡ Cavity Ring-Down Spectroscopy.

The binding energy of DMS–Cl has been the subject of several theoretical investigations; however, no experimental results for the S–Cl bond strength have been reported until this work. An *ab initio* study by Enami *et al.* [*2004*] suggests that DMS–Cl is bound by 74.0 kJ/mol, in agreement with Wilson and Hirst [*Wilson and Hirst*, 1997] but significantly higher than earlier calculations by McKee [*1993*] and Resende and De Almeida [*1997*]. A recent theoretical study by Thompson et al. [*2002*] suggests an even larger bond strength for DMS–Cl, 97.0 kJ/mol. Results from our laboratory support an

S−Cl bond energy near the high end of the range of theoretical estimates summarized in Table 6.9.

Table 6.9: Calculated 298 K Bond Strengths for the Cl−DMS adduct

ΔH (kJ/mol)	Literature
80.9	Wilson and Hirst, 1997
51	Mckee, 1993
58.6	Resende, DeAlmeda, 1997
74	Enami et al., 2004
97	Thompson et al., 2002
85.4	Laine et al., 2011c

Cl + DMSe

There is only one experimental kinetic study reported in the literature for the Cl + DMSe reaction [*Thompson et al., 2002*]. The 298 K rate coefficient obtained from this work is considerably smaller than that reported by Thompson *et al.*, who carried out a discharge flow study at P = 1.5 Torr He and found $k_{6.2} = (5.0 \pm 1.4) \times 10^{-10}$ cm^3 $molecule^{-1}$ s^{-1}. There has been no experimental data reported on the bond strength of the DMSe−Cl adduct.

In addition to their experimental work, Thompson *et al.* [*2002*] also carried out a theoretical investigation that addressed the DMSe−Cl bond strength and unimolecular decomposition products. The theoretical 298 K bond strength reported by Thompson *et al.* is −111.4 kJ/mol which is somewhat higher than the experimental and theoretical values reported in this study. Thompson *et al.* employed variational RRKM theory to investigate adduct unimolecular decomposition and suggest that instead of being stabilized or decomposing back to the starting compounds, the adduct $CH_3Se(Cl)CH_3$ predominantly fragments to $CH_3SeCl + CH_3$ under atmospheric conditions, a process that does not occur [*Zhao et al., 1996*] for $CH_3S(Cl)CH_3$ due to unfavorable energetics

[*Thompson et al., 2002*]. This difference in the adduct decay mechanism of DMS–Cl and DMSe–Cl, if correct, implies an enhanced contribution of Cl reaction as a DMSe removal mechanism in marine environments since there would be no DMSe regeneration from the adduct. However, our results are not consistent with the prediction of Thompson *et al.* as we see evidence for a long-lived DMSe−Cl adduct.

Implications for Atmospheric Chemistry

Table 6.10 shows lifetimes toward unimolecular decomposition computed for DMS−Cl and DMSe−Cl over the atmospheric temperature range. The lifetimes (k_{-ib}^{-1}) are obtained using equilibrium constants and values for $k_{ib}(T)$ that are based on the results reported in this study. These lifetimes are sufficiently long that pathways other than unimolecular decomposition, i.e., photochemical loss [*Urbanski and Wine, 1999*] and/or slow reaction with O_2, are likely to be important.

It appears that the Cl + DMS reaction is fast enough to compete with other DMS loss processes in some atmospheric environments. Although the kinetic database is extremely limited for radical reactions with DMSe, it appears unlikely that reaction with Cl would be an important contributor towards DMSe loss in the atmosphere. Table 6.11 shows estimated characteristic times for loss of DMS and DMSe with regard to several different oxidants.

Table 6.10. Atmospheric lifetime calculations for DMS−Cl and DMSe−Cl. [a]

T	$\Delta_r H$	K_p	K_{ib}	k_{-ib}	T
		DMS−Cl			
298.15	−89.4	2.5×10^{10}	1.4	.140	0.12
273	−89.4	6.9×10^{11}	1.4	.00549	3
225	−89.5	3.6×10^{15}	1.3	1.17×10^{-6}	11,000
		DMSe−Cl			
298.15	−98.5	1.2×10^{12}	0.6	.0012	13
273	−98.5	4.5×10^{13}	0.6	3.57×10^{-5}	450
225	−98.4	4.8×10^{17}	0.3	2.03×10^{-9}	3,700,000

[a] Units: T(K); ΔS (J/mol); $\Delta_r H$ (kJ/mol); K_P (atm^{-1}); k_{ib} (10^{-10} cm^3 molecule s^{-1}); k_{-ib} (s^{-1}); τ (minutes).

Table 6.11. Estimated atmospheric lifetimes for DMS and DMSe with regard to several oxidants, X (= OH, NO_3, O_3, Cl, Br, BrO, and IO).

k(cm^3 $molec^{-1}$ s^{-1})		X[a]	τ (297 K)	τ (230 K)	297 K	230 K
DMS						
297 K	230 K		Clean enviromnemt		References for k_x	
6.7×10^{-12}	4.7×10^{-11}	OH	41 hr	6 hr	(1)	
1.1×10^{-12}	1.9×10^{-12}	NO_3	30 min	17 min	(1)	
$< 1.5 \times 10^{-19}$		O_3	> 77 d		(1)	
3.4×10^{-13}	8.7×10^{-13}	BrO	≥ 1.1 hr	≥ 27 min	(1)	
1.7×10^{-14}	4.0×10^{-15}	IO	≥ 4.5 d	≥ 19 d		
3.6×10^{-10}	3.9×10^{-10}	Cl	8 hr	7 hr	This work	
DMSe						
6.8×10^{-11}		OH	4 hr		(2)	
1.4×10^{-11}		NO_3	2.4 min		(2)	
6.8×10^{-17}		O_3	4 hr		(2)	
3.5×10^{-10}	3.8×10^{-10}	Cl	8 hr	7 hr	This work	

[a]Estimated concentrations (molecule cm^{-3}): [OH] = 1×10^6 (global avg.) [Seinfeld and Pandis, 2006]; [NO_3] = 5×10^8 (12 hr nighttime avg.)[Atkinson, 1997]; [O_3] = 1×10^{12} [Seinfeld and Pandis, 2006]; [BrO] = ≤ 7×10^8 [Platt and Honninger]; [IO] = ≤ 1.5×10^8 [Platt and Honninger]; [Cl] = 1×10^5 [Wingenter, 2005]. References: (1) Sander *et al.*, 2011; (2) Atkinson *et al.*, 1990.

Chapter 7

CONCLUSIONS AND FUTURE WORK

This dissertation reports studies of some gas phase halogen atom reactions that are of potential importance in atmospheric chemistry. Laser flash photolysis (LFP) was employed to initiate radical reactions. LFP was coupled with time-resolved atomic resonance fluorescence (RF) spectroscopy to monitor the time-dependent concentrations of either an atomic reactant or product. The new kinetic information facilitates a better understanding of the roles of the studied reactions in atmospheric chemistry.

Rate coefficients as well as branching ratios for β-hydrogen abstraction are determined for Cl reactions with bromoethane, *n*-bromopropane, and 1,2-dibromoethane as a function of temperature by monitoring the appearance of Br that is rapidly eliminated from the products of the β-hydrogen abstraction reactions. We have carried out the first temperature dependent study of these reactions as well as the first absolute rate coefficient measurements at any temperature. Rate coefficients for reactions of Cl atoms with CH_3CH_2Br and $CH_3CH_2CH_2Br$ are substantially faster than the corresponding OH rate coefficients (factors of 30-90 depending on temperature and the identity of R−Br), so it seems likely that the Cl reaction makes a significant contribution to the tropospheric degradation of these compounds. As a result, the ozone depletion potentials of CH_3CH_2Br and $CH_3CH_2CH_2Br$ may be smaller than current estimates suggest. The rate coefficient for the reaction of Cl atoms with CH_2BrCH_2Br is at most a factor of 5-6 faster than the corresponding OH reaction at tropospheric temperatures, so reaction with Cl is

probably only a very minor contributor to the tropospheric degradation of this alkyl bromide.

The kinetics and thermochemistry of the isoprene reaction with Cl has been investigated. Prior to this work, there had only been one temperature dependent study of the Cl + isoprene reaction. Our 298 K data is near the low end of the range of the reported literature values, and our T-dependent result does not agree with the lone previous study [*Bedjanian et al., 1998*]. Our temperature dependent results indicate that the Cl + isoprene reaction is ~ 2.5 times faster than OH + isoprene at 230 K, whereas the previous temperature dependent result suggests the Cl reaction to be ~ 5 times faster than the OH reaction at this temperature. The new result lessens the likelihood that the Cl reaction could compete with the OH reaction in the atmosphere. In addition, this study reports the first experimental determination of the Cl-isoprene bond strength as well as the first investigation of Cl + isoprene kinetics at temperatures above 320 K.

We have investigated the kinetics of Br reactions with three olefins over a wide range of temperature, pressure, and $[O_2]$. The results allow rate coefficients for elementary steps in the expected atmospheric reaction mechanisms for the Br-initiated oxidation of olefins to be evaluated more directly than in previous studies of any Br + olefin reaction. The results presented herein indicate that the 298 K rate coefficients for Br + isoprene, 1,3-butadiene, and 2,3-dimethyl-2-butene are significantly faster than previous published work suggests [*Bierbach et al., 1996*]. Reasons for the discrepancy are not clearly understood at this time. Bond dissociation enthalpies for Br + isoprene and 1,3-butadiene have been determined for the first time, and the results suggest the C−Br bonds in Br−isoprene and Br−1,3-butadiene are stronger than any C−Br bond

strength previously reported for any bromoalkyl radical. The increased stability can be attributed to the allyl-resonance stabilization effect as the result of conjugated double bonds, i.e., C−Br bond strengths in Br−isoprene and Br−1,3-butadiene are ~70 kJ/mol whereas C−Br bond strengths Br−TME and Br−ethylene [*Ferrell, 1998*] are 47 and 29 kJ/mol, respectively. Examination of the effect of added O_2 on Br kinetics under conditions where reversible adduct formation is observed allows rate coefficients for the Br−olefin + O_2 reactions to be determined. Results from the Br−olefin + O_2 experiments provide further evidence of the effect of allyl-resonance stabilized bromoalkyl radicals. The rate coefficient for the Br−TME + O_2 reaction is ~ 10 times larger than the rate coefficients for the Br−isoprene + O_2 and Br−1,3-butadiene + O_2 reactions. Our results suggest that, for the bromoalkyl radicals investigated in this study (Br−isoprene, Br−1,3-butadiene, and Br−TME), bromoalkyl radical reaction with O_2 occurs considerably more rapidly under atmospheric conditions than bromoalkyl radical unimolecular decomposition. Hence, the near gas kinetic addition reactions appear to control the rate of olefin loss by reaction with Br in the atmosphere.

Reactions of Cl atoms with DMS and DMSe have been investigated. The Cl + DMS reaction has been studied extensively. Our 700 Torr, 298 K results agree well with several other experimental studies performed using a variety of techniques [*Enami et al., 2004; Arsene et al., 2005; Kinnison et al., 1996; Stickel et al., 1992; Nielsen et al., 1990*], however, our H-abstraction rate coefficient is a factor of 3 larger than the lone H-abstraction rate coefficient reported in the literature [*Diaz-de-Mara et al., 2002*]. We also report the first experimentally determined bond dissociation enthalpy for the Cl−DMS adduct, which is near the high end of the range of theoretical estimates.

The rate coefficient for the Cl + DMSe reaction at 298 K is found to be significantly slower than the lone previous experimental study [*Thompson et al., 2002*]. Kinetic data, as well as the experimental bond dissociation enthalpy over the relevant range of atmospheric temperatures and pressures, are reported for the first time.

The 298 K high and low pressure limits for the association rate coefficients have been established for both Cl + DMS and Cl + DMSe. We observe evidence for a long-lived Cl−DMSe adduct which argues against a published theoretical prediction [*Thompson et al., 2002*] that this adduct rapidly decomposes to CH_3 + CH_3SeCl. The new kinetic and thermochemical data allow adduct lifetimes toward unimolecular decomposition under atmospheric conditions to be evaluated based on experimental data for the first time.

The studies described in this dissertation can be followed by some future work. As discussed in Chapter 1, chlorine atom chemistry can compete with OH as an important oxidant in marine and coastal environments. Furthermore, based on recent findings of significant levels of $ClNO_2$(g) in Colorado, far removed from any marine environments, Cl chemistry could potentially play an important role in terrestrial environments [*Thornton et al., 2010*]. However, the kinetic database for gas phase reactions of Cl with volatile organic compounds is still limited [*Atkinson et al., 2006; Sander et al., 2011*], especially for some biogenic organic compounds that are thought to be abundant in coastal and/or marine regions and play important roles in impacting regional air quality and/or aerosol formation [*Atkinson and Arey, 2003* and the references therein]. Many Cl reactions can proceed via both H-abstraction and addition pathways and, as a result, display complex temperature and pressure dependences. Temperature

dependences of both rates and mechanisms are needed information for evaluating the atmospheric fates of these organic compounds as well as for understanding the ensuing chemistry.

Given that our Br + olefin results do not agree with those from Bierbach *et al.* [*1996*], it would be helpful to have absolute rate coefficient determinations for all of the olefins studied in the chain of Br + olefin reactions investigated by Bierbach *et al.* in their relative rate study. The Br + olefin + O_2 experiments confirm that the bromoalkyl radicals studied undergo reaction with O_2, however, the LFP-RF experiments described herein do not provide insight into the subsequent chemistry of the resulting peroxy radical. In order to explain the large discrepancy between our Br + olefin results and those from Bierbach et al. [*1996*], the subsequent chemistry following Br−olefin reaction with O_2, i.e., the fate of the bromoperoxy radical, should be explored. This explanation could lead to determination of the "effective" atmospheric rate coefficient for the Br + olefin reactions of interest.

Kinetic data and mechanistic information for DMSe reactions with a variety of important atmospheric oxidants (OH, BrO, NO_3, O_3) are necessary to facilitate a comprehensive understanding of DMSe oxidation process in its transport from marine to terrestrial environments. There has only been one published study (298 K) on the reactions of DMSe with OH, NO_3, or O_3 [*Atkinson et al., 1990*]. The limited kinetic data available for the above DMSe reactions suggests these reactions are significantly faster than the corresponding reactions with DMS. The BrO reaction with DMS plays an important role in atmospheric DMS oxidation, and published studies indicate there could potentially be a pressure dependence for the reaction [*Ingham et al.*, 1999; *Nakano et al.*,

2001; *Read et al.*, 2008]. Thus, further work towards the potential pressure dependence for the BrO + DMS reaction is needed. In addition, it is necessary to evaluate the kinetics of BrO + DMSe in order to accurately assess the fate of DMSe in the atmosphere. Because DMSe oxidation products are expected to partition primarily to the condensed phase, investigations of the aqueous phase transformations of these species are needed in order to develop a complete understanding of the atmospheric cycling of selenium.

REFERENCES

Abbatt, J.P.D. (1994), Heterogeneous reaction of HOBr with HBr and HCl on ice surfaces at 228 K, *Geophys. Res. Lett.*, 21, 665-668.

Abbatt, J.P.D. and J.B. Nowak, (1997), Heterogeneous interactions of HBr and HOCl with cold sulfuric acid solutions: Implications for Arctic boundary layer bromine chemistry, *J. Phys. Chem. A,* 101, 2131-2137.

Adams, J.W.; N.S. Holmes, J.N. Crowley, (2002), Uptake and reaction of HOBr on frozen and dry salt surfaces, *Atmos. Chem. Phys*., 2, 79-91.

Agency for Toxic Substances and Disease Registry (ATSDR) (1992a), Toxicological profile for 1,3-butadiene, Department of Health and Human Services, Public Health Service., Atlanta, GA: U.S.

Albaladejo, J.; Notario, A.; Cuevas, C. A.; Ballesteros, B.; Martinez, E. (2003) A pulsed laser photolysis–resonance fluorescence kinetic study of the atmospheric Cl atom-initiated oxidation of propene and a series of 3-halopropenes at room temperature, *J. Atmos. Chem.*, *45*, 35-50.

Amouroux, D., and O. F. X. Donard (1996), Maritime emission of selenium to the atmosphere in eastern Mediterranean seas, *Geophys. Res. Lett.*, *23*(14), 1777-1780.

Amouroux, D.; Liss, P. S.; Tessier, E.; Hamren-Larsson, M.; Donard, O. F. X. (2001), Role of oceans as biogenic sources of selenium, *Earth and Planet. Sci. Lett.*, *189*, 277-283.

Andreae, M.O. and H. Raemdonck (1983), Dimethyl sulfide in the surface ocean and the marine atmosphere-a global view, *Science*, 221, 4612, 744-747.

Andreae, M.O. and W.R. Barnard (1984), The marine chemistry of dimethylsulfide, *Marine Chem.*, 14, 3, 267-279.

Andreae, M. O.; Andreae, T. W.; Schebeske, G. (1994) Biogenic sulfur emissions and aerosols over the tropical South Atlantic 1. Dimethylsulfide in sea water and in the atmospheric boundary layer, *J. Geophys. Res., 99*, D11, 22819.

Andreae, M.O. (1990), Ocean-atmosphere interactions in the global biogeochemical sulfur cycle, *Marine Chem.*, 30, 1-29.

Andreae, M. O.; Talbot, R.; Andreae, T. W.; Harriss, R. (1988), Formic and acetic acid over the central Amazon region, Brazil 1. dry season, *J. Geophys. Res., 93*, 1616.

Anthony, L.M. and Roscoe, J.M. (2004) A kinetic analysis of the effect of O_2 on the reactions of atomic bromine with some hydrocarbons and ethers, *J. Phys. Chem. A*, 108, 7535.

Ariya, P. A., Niki, H., Harris, G. W., Anlauf, K. G., Worthy, D. E. (1999), Polar sunrise experiment 1995: hydrocarbon measurements and tropospheric Cl and Br-atoms chemistry, *Atmos. Environ.*, *33*(6), 931-938.

Arnold, S. R., Spracklen, D. V., Williams, J., Yasaa, N., Sciare, J., Bonsang, B., Gros, V., Peeken, I., Lewis, A. C., Alvain, S., and Moulin, C. (2009) Evaluation of the global oceanic isoprene source and its impacts on marine organic carbon aerosol, *Atmos. Chem. Phys.*, 9, 1253.

Arsene, C.; Barnes, I.; Becker, K. H.; Benter, T. (2005) Gas-phase reaction of Cl with dimethyl sulfide: Temperature and oxygen partial pressure dependence of the rate coefficient, *International Journal of Chemical Kinetics*, *37*, 66.

Ashworth, S.H.; B.J. Allan, J.M.C. Plane, (2002), High resolution spectroscopy of the OIO radical: implications for the ozone depletion potential of iodine in the marine boundary layer, *Geophys. Res. Lett*., 29, 1456, doi:10.1029/2001GL013851.

Atkinson, R. (1991) Kinetics and mechanisms of the gas-phase reactions of the NO_3 radical with organic compounds, J. Phys. Chem. Ref. Data, 20, 459.

Atkinson, R.; Aschmann, S. M.; Hasegawa, D.; Thompson-Eagle, E. T.; Frankenberger Jr., W. T. (1990), Kinetics of the atmospherically important reactions of dimethyl selenide, *Environ. Sci. Technol.*, *24*(9), 1326-1332.

Atkinson, R. and Aschmann, S. M. (1990) Rate constants for the gas-phase reactions of the OH radical with the cresols and dimethylphenols at 296 ± 2 K, *Int. J. Chem. Kinet.*, 22, 59.

Atkinson, R.; Aschmann, S. M.; Pitts, J. N. (1988) Rate constants for the gas phase reactions of the nitrate radical with a series of organic compounds at 296 K, *J. Phys. Chem.*, 92, 3454.

Atkinson, R.; Aschmann, S.M.; Winer, A.M.; Pitts, J.N., Jr. (1984) Kinetics of the gas-phase reactions of NO_3 radicals with a series of dialkenes, cycloalkenes, and monoterpenes at 295 ± 1 K, Environ. Sci. Technol., 18, 370.

Atkinson, R. and Aschmann, S. M. (1984) Rate constants for the reaction of hydroxyl radicals with a series of alkenes and kialkenes at 295 K, *Int. J. Chem. Kinet.*, 16, 1175.

Atkinson, R. (1986) Kinetics and mechanisms of the gas phase reactions of the hydroxyl radical with organic compounds under atmospheric conditions, *Chem. Rev.*, 86, 1, 69-201.

Atkinson, R., and J. Arey (2003), Gas-phase tropospheric chemistry of biogenic volatile organic compounds: a review, *Atmos. Environ.*, *37 Suppl.*(2), S197-S219.

Atkinson, R.; Plum, C.N.; Carter, W.P.L.; Winer, A.M.; Pitts, J.N., Jr. (1984) Rate constants for the gas-phase reactions of nitrate radicals with a series of organics in air at 298 ± 1 K, *J. Phys. Chem.*, 88, 2361.

Atkinson, R.; Baulch, D.L.; Cox, R.A.; Hampson, R.F.; Kerr, J.A.; Rossi, M.J.; Troe, J. (1997), Evaluated kinetic and photochemical data for atmospheric chemistry: Supplement VI-IUPAC subcommittee on gas kinetic data evaluation for atmospheric chemistry, *J. Phys. Chem. Ref. Data*, 26, 6, 1329-1499.

Atkinson, R.; Baulch, D. L.; Cox, R. A.; Crowley, J. N.; Hampson, R. F.; Hynes, R. G.; Jenkin, M. E.; Rossi, M. J.; Troe, J. (2004), Evaluated kinetic and photochemical data for atmospheric chemistry: Volume I - gas phase reactions of O_x, HO_x, NO_x and SO_x species, *Atmos. Chem. Phys.*, *4*(6), 1461-1738.

Atkinson, R., Baulch, D. L., Cox, R. A., Crowley, J. N., Hampson, R. F., Hynes, R. G., Jenkin, M. E., Rossi, M. J., Troe, J. (2006), Evaluated kinetic and photochemical data for atmospheric chemistry: Volume II - gas phase reactions of organic species, *Atmos. Chem. Phys.*, *6*(11), 3625-4055.

Atkinson, R.; Baulch, D. L.; Cox, R. A.; Crowley, J. N.; Hampson, R. F.; Hynes, R. G.; Jenkin, M. E.; Rossi, M. J.; Troe, J. (2007), Evaluated kinetic and photochemical data for atmospheric chemistry: Volume III - gas phase reactions of inorganic halogens, *Atmos. Chem. Phys.*, *7*(4), 981-1191.

Atkinson, R.**;** Baulch, D. L.; Cox, R. A.; Crowley, J. N.; Hampson, R. F.; Hynes, R. G.; Jenkin, M. E.; Rossi, M. J.; Troe, J.; Wallington, T. J. (2008), Evaluated kinetic and photochemical data for atmospheric chemistry: Volume IV – gas phase reactions of organic halogen species, *Atmos. Chem. Phys.*, *8*(15), 4141-4496.

Ayers, G.P.; J.M. Cainey, H. Granek, C. Leck, (1996), Dimethylsulfide oxidation and the ratio of methanesulfonate to non sea-salt sulfate in the marine aerosol, *J. Atmos. Chem.*, 25, 3, 307-325.

Ayhens, Y.V.; Nicovich, J.M.; McKee, M.L.; Wine, P.H. (1997), Kinetic and mechanistic study of the reaction of atomic chlorine with methyl iodide over the temperature range 218-694 K, *J. Phys. Chem. A*, 101, 9382-9390.

Bahta, A.; R. Simonaitis, J. Heicklen (1984), Reactions of ozone with olefins: ethylene, allene, 1,3-butadiene, and trans-1,3-pentadiene, *Int. J. Chem. Kinet*., 16, 10, 1227-1246.

Barnes, I., Hjorth, J., and Mihalopoulos, N. (2006), Dimethyl sulfide and dimethyl sulfoxide and their oxidation in the atmosphere, *Chem. Rev., 106*(3), 940-975.

Barnes, I.; Bastian, V.; Becker, K.H.; Overath, R.; Tong, Z. (1989), Rate constants for the reactions of Br atoms with a series of alkanes, alkenes, and alkynes in the presence of O_2, *Int. J. Chem. Kinet.,* 21, 499.

Barrie, L. A.; Bottenheim, J. W.; Schnell, R. C.; Crutzen, P. J.; Rasmussen, R. A. (1988), Ozone destruction and photochemical reactions at polar sunrise in the lower Arctic atmosphere, *Nature*, *334*(6178), 138-141.

Bates, T.S.; J.A. Calhoun, P.K. Quinn, (1992), Variations in the methanesulfonate to sulfate molar ratio in submicrometer marine aerosol particles over the south pacific ocean, *J. Geophys. Res. Atmos*., 97, D9, 9859-9865.

Bates, T. S.; R.P. Kiene, G.V. Wolfe, P.A. Matrai, F.P. Chavez, K.R. Buck, B.W. Blomquist, R.L. Cunel (1994), The cycling of sulfur in surface seawater of the northeast Pacific, *Geophysical Research*, *99*, 7835-7843.

Beavington, F.; P.A. Cawse, A. Wakenshaw (2004), Comparative studies of atmospheric trace elements: improvements in air quality near a copper smelter, *Sci. Total Environ.*, *332*(1-3), 39-49.

Bedjanian, Y.; G. Laverdet, G. Le Bras (1998), Low pressure study of the reaction of Cl atoms with isoprene, *J. Phys. Chem. A* 102, 953.

Bedjanian, Y.; G. Poulet, G. LeBras (2000), Low pressure study of the reactions of Br atoms with alkenes. 3. Reactions with 2-methyl-2-butene, 2,3-dimethyl-2-butene, and 1-hexene, *J. Phys. Chem. A*, 104, 577.

Bedjanian, Y.; G. Poulet, G. LeBras (1999), Low pressure study of the reactions of Br atoms with alkenes. 2. Reactions with ethene and trans-2-butene, *J. Phys. Chem. A*, 103, 4026.

Bedjanian, Y.; G. Poulet, G. LeBras (1998), Low pressure study of the reactions of Br atoms with alkenes. 1. Reactions with propene, *J. Phys. Chem. A*, 102, 5867.

Bierbach, A.; I. Barnes, K.H. Becker (1996), Rate coefficients for the gas phase reactions of bromine radicals with a series of alkenes, dienes, and aromatic hydrocarbons at 298 K, *Int. J. Chem. Kinet.,* 28, 565.

Bilde, M.; J. Sehested, O.J. Nielsen, T.J. Wallington, R.J. Meagher, M.E. McIntosh, C.A. Piety, J.M. Nicovich, P.H. Wine (1997), Kinetics and mechanism of the gas phase reaction of atomic chlorine with CH_2ICl at 206-432 K *J. Phys. Chem. A, 101*, 8035-8041.

Bottenheim, J. W.; L.A. Barrie, E. Atlas, L.E. Heidt, H. Niki, R.A. Rasmussen, P.B. Shepson (1990), Depletion of lower tropospheric ozone during arctic spring: the Polar Sunrise Experiment, *J. Geophys. Res.*, *95*, 18555-18568.

Boudries, H., and J. W. Bottenheim (2000), Cl and Br atom concentrations during a surface boundary layer ozone depletion event in the Canadian high arctic, *Geophys. Res. Lett.*, *27*(4), 517-520.

Brasseur, G. P.; J.J. Orlando, G.S. Tyndall (1999), *Atmospheric Chemistry and Global Change*, Oxford Unveristy Press, New York.

Brauers, T.; U. Aschmutat, U. Brandenburger, H.P. Dorn, M. Hausmann, M. Hessling, A. Hofzumahaus, F. Holland, C. Plass-Dulmer, D.H. Ehhalt (1996), Intercomparison of tropospheric OH radical mesurements by multiple folded long path laser absorption and laser induced fluorescence, *Geophys. Res. Lett.* 23, 2545.

Brioude, J.; R.W. Portmann, J.S. Daniel, O.R. Cooper, G.J. Frost, K.H. Rosenlof, C. Ranier, A.R. Ravishankara, S.A. Montzka, A. Stohl (2010), Variations in ozone depletion potentials of very short lived substances with season and emission region, *Geophys. Res. Lett.*, 37, L19804.

Brown, S.S.; J.A. De Gouw, C. Warneke, T.B. Ryerson, W.P. Dube, E. Atlas, R.J. Weber, R.E. Peltier, J.A. Neuman, J.M. Roberts, A. Swanson, F. Flocke, S.A. McKeen, J. Brioude, R. Sommariva, M. Trainer, F.C. Fehsenfeld, and A.R. Ravishankara (2009), Nocturnal isoprene oxidation over the Northeast United States in summer and its impact on reactive nitrogen partitioning and secondary organic aerosol, *Atmos. Chem. Phys.*, 9, 3027-3042.

Canosa-Mas, C. E., H.R. Hutton-Squire, M.D. King, D.J. Stewart, K.C. Thompson, R.P. Wayne (1999), Laboratory kinetic studies of the reactions of Cl atoms with species of biogenic origin: Delta(3)-carene, isoprene, methacrolein, and methyl vinyl ketone, *J. Atmos. Chem.* 34, 163.

Carpenter, L. J. (2003), Iodine in the marine boundary layer, *Chem. Rev.*, *103*(12), 4953-4962.

Chameides, W. L., and D. D. Davis (1980), Iodine: its possible role in tropospheric photochemistry, *J. Geophys. Res.*, *85*, 7383-7398.

Chameides, W.L., F. Fehsenfeld, M.O. Rogers, C. Cardelino, J. Martinez, D. Parrish, W. Lonneman, D.R. Lawson, R.A. Rasmussen, P. Zimmerman, J. Greenberg, P. Middleton, T. Wang (1992), Ozone precursor relationships in the ambient atmosphere, *J. Geophys. Res.*, 97, 6037-6055.

Chang, S., E. McDonald-Buller, Y. Kimura, G. Yarwood, J. Neece, M. Russell, P. Tanaka, D. Allen, (2002), Sensitivity of urban ozone formation to chlorine emission estimates, *Atmos. Environ.*, *36*(32), 4991-5003.

Charlson, R. J., J.E. Lovelock, M.O. Andreae, S.G. Warren, (1987), Oceanic phytoplankton, atmospheric sulphur, cloud albedo and climate, *Nature*, *326*(6114), 655-661.

Chase, M. W., C.A. Davies, J.R. Downey, D.J. Frurip, R.A. McDonald, and A.N. Syverud (1985a), JANAF thermochemical tables - 3rd edition, *J. Phys. Chem. Ref. Data*, *14*, 927-1856.

Chase, M. W., C.A. Davies, J.R. Downey, D.J. Frurip, R.A. McDonald, and A.N. Syverud (1985b), JANAF thermochemical tables - 3rd edition.1. AL-CO, *J. Phys. Chem. Ref. Data*, *14*, 1-926.

Chichinin, A. I. (1993), Measurement of $Cl(^2P_{1/2})$ quantum yield for the photodissociation of NOCl, ICl, PCl_3, Cl_2O and $COCl_2$, *Chem. Phys. Lett.*, *209*(5,6), 459-463.

Chichinin, A. I. (1996), Study of elementary processes with participation of $Cl(^2P_{1/2})$ atoms by the laser magnetic resonance method, *Khim. Phys.* 15, 49.

Chichinin, A. I. (1997), Collisions of $O(^1D)$ with HCl, Cl_2, and $COCl_2$: total quenching, channel specific rate constants, and yields of $Cl(^2P_{1/2})$, *J. Chem. Phys.*, *106*(3), 1057-1062.

Christiansen, C. J. and J.S. Fransisco (2009), Atmospheric oxidation mechanism of 1,2-dibromoethane, *J. Phys. Chem. A*, 113, 7189.

Class, T. H. and K. Ballschmiter (1988), Chemistry of organic traces in air. VIII: Sources and distribution of bromo- and bromochloromethanes in marine air and surface water of the Atlantic Ocean, *J. Atmos. Chem.* 6, 35-46.

Cohen, N. and S.W. Benson (1987), Transition state theory calculations for the reactions of OH with haloalkanes, *J. Phys. Chem.*, 91, 162.

Crowley, J.N., M. Ammann, R.A. Cox, R.H. Hynes, M.E. Jenkin, A. Mellouki, M.J. Rossi, J. Troe, T.J. Wallington (2010), Evaluated kinetic and photochemical data for atmospheric chemistry: Volume V - heterogeneous reactions on solid substrates, *Atmos. Chem. Phys.*, 10, 18, 9059-9223.

Curtiss, L.A.; P.C. Redfern, K. Raghavachari (2007), Gaussian-4 theory, *J. Chem. Phys.*, 126, 084108.

Daniel, J. S., S. Solomon, R. W. Portmann, R. R. Garcia, (1999), Stratospheric ozone destruction: the importance of bromine relative to chlorine, *J. Geophys. Res., [Atmospheres] 104*(D19), 23871-23880.

Daykin, E. P., and P. H. Wine (1990), A study of the reactions of NO_3 radicals with organic sulfides: reactivity trend at 298 K, *Int. J. Chem. Kinet.*, *22*, 1083-1094.

Diaz-de-Mera, Y.; A. Aranda, D. Rodriguez, R. Lopez, B. Cabanas, E. Martinez (2002), Gas-Phase Reactions of Chlorine Atoms and ClO Radicals with Dimethyl Sulfide. Rate Coefficients and Temperature Dependences, *J. Phys. Chem. A, 106*, 8627.

Donaghy, T.; I. Shanahan, M. Hande, S. Fitzpatrick (1993), Rate constants and atmospheric lifetimes for the reactions of OH radicals and Cl atoms with haloalkanes, *Int. J. Chem. Kinet.*, 25, 73.

Donovan, R.J. and D. Husain, (1966), Electronically excited Bromine atoms: spin orbit relaxation, *Trans. Faraday Soc.*, 62, 2987.

Dookwah-Roberts, V. (2008a), Spectroscopy and kinetics of weakly bound gas phase adducts of atmospheric interest, Dissertation, Georgia Institute of Technology, Atlanta, GA.

Dookwah-Roberts, V., J.M. Nicovich, P.H. Wine (2008b), Spectroscopic and kinetic study of the gas-phase CH_3I–Cl and C_2H_5–Cl adducts, *J. Phys. Chem. A*, *112*(39), 9535-9543.

Eldred, R. A. (1997), Comparison of selenium and sulphur at remote sites throughout the United States, *J. Air Waste Manag. Assoc.*, *47*(2), 204-211.

Enami, S.; Y. Nakano, S. Hashimoto, M. Kawasaki, S. Aloisio, and J.S. Francisco (2004), Reactions of Cl atoms with dimethyl sulfide: a theoretical calculation and an experimental study with cavity ring-down spectroscopy, *J. Phys. Chem. A*, *108*(39), 7785-7789.

Fan, S.M. and D.J. Jacob, (1992), Surface ozone depletion in Arctic spring sustained by bromine reactions on aerosols, *Nature*, 359, 522-524.

Fantechi, G.; N.R. Jensen, O. Saastad, J. Hjorth, J. Peeters (1998), Reactions of Cl atoms with selected VOCs: Kinetics, products, and mechanisms, *J. Atmos. Chem.* 31, 247.

Ferrell, V.M. (1998) Experimental studies of the kinetics and thermochemistry of the reactions Br + ethylene and Br + ethane, Thesis, Georgia Institute of Technology.

Fickert, S.; J.W. Adams, J.N. Crowley, (1999), Activation of Br_2 and BrCl via uptake of HOBr onto aqueous salt solutions, *J. Geophys. Res*., 104, 23719-23727.

Finlayson-Pitts, B.J. (2010), Halogens in the troposphere, *Anal. Chem.*, 82, 770-776.

Finlayson-Pitts, B. J.; C.J. Keoshian, B. Buehler, A.A. Ezell (1999) Kinetics of reaction of chlorine atoms with some biogenic organics, *Int. J. Chem. Kinet.*, 31, 491.

Finlayson-Pitts, B. J.; M.J. Ezell, J.N. Pitts Jr. (1989), Formation of chemically active chlorine compounds by reactions of atmospheric NaCl particles with gaseous N_2O_5 and $ClONO_2$, *Nature*, *337*(19), 241-244.

Finlayson-Pitts, B. J., and J. N. Pitts Jr. (2000), *Chemistry of the Upper and Lower Atmosphere*, Academic Press, San Diego, p 146.

Finlayson-Pitts, B. J. (2003), The tropospheric chemistry of sea salt: a molecular-level view of the chemistry of NaCl and NaBr, *Chem. Rev.*, *103*, 4801-4822.

Finley, B. D., and E. S. Saltzman (2006), Measurement of Cl_2 in coastal urban air, *Geophys. Res. Lett.*, *33*, L11809, doi: 11810.11029/12006GL025799.

Finley, B. D., and E. S. Saltzman (2008), Observations of Cl_2, Br_2, and I_2 in coastal marine air, *J. Geophys. Res.*, *113*(D21), D21301 doi:21310.21029/22008JD010269.

Fordyce, F. M.; Z. Guangdi, K. Green, L. Xinping (1999), Soil, grain and water chemistry in relation to human selenium-responsive diseases in Enshi District, China, *Applied Geochemistry*, *15*(1), 117-132.

Foster, K.L.; R.A. Plastridge, J.W. Bottenheim, P.B. Shepson, B.J. Finlayson-Pitts, C.W. Spicer, (2001), The role of Br_2 and BrCl in surface ozone destruction at polar sunrise, *Science*, 291, 471-474.

Fraser, F.M.; E.J. Prosen (1955), Heats of combustion and isomerization of six pentadienes and spiropentane, *J. Res. NBS*, 54, 143-148.

Frinak, E.K. and J. P. D. Abbatt (2006), Br_2 production from the heterogeneous reaction of gas-phase OH with aqueous salt solutions: impacts of acidity, halide concentration, and organic surfactants, *J. Phys. Chem. A*, *110*(35), 10456-10464.

Frisch, M.J.; G.W. Trucks, J.R. Cheeseman, G. Scalmani, M. Caricato, H.P. Hratchian, X. Li, V. Barone, J. Bloino, G. Zheng, T. Vreven, J.A. Montgomery, G.A. Petersson, G.E. Scuseria, H.B. Schlegel, H. Nakatsuji, A.F. Izmaylov, R.L. Martin, J.L. Sonnenberg, J.E. Peralta, J.J. Heyd, E. Brothers, F. Ogliaro, M. Bearpark, M.A. Robb, B. Mennucci, K.N. Kudin, V.N. Staroverov, R. Kobayashi, J. Normand, A. Rendell, R. Gomperts, V.G. Zakrzewski, M. Hada, M. Ehara, K. Toyota, R. Fukuda, J. Hasegawa, M. Ishida, T. Nakajima, Y. Honda, O. Kitao, H. Nakai, (2009)Gaussian 09; Gaussian, Inc.: Wallingford, CT.

Gantt, B.; N. Meskhidze, D. Kamykowski (2009), A new physically-based quantification of marine isoprene and primary organic aerosol emissions, *Atmos. Chem. Phys.*, 9, 4915.

Gantt, B.; N. Meskhidze, Y. Zhang, J. Xu (2010), The effect of marine isoprene emissions on secondary organic aerosol and ozone formation in the coastal United States, *Atmos. Environ.*, 44, 115.

Gilles, M.K.; J.B. Burkholder, T. Gierczak, P. Marshall, A.R. Ravishankara (2002), Rate coefficient and product branching measurements for the reaction of OH plus bromopropane from 230 to 360 K, *J. Phys. Chem. A*, 106, 5358.

Herndon, S.C.; T. Gierzak, R.K. Talukdar, A.R. Ravishankara (2001), Kinetics of the reactions of OH with several alkyl halides, *Phys. Chem. Chem. Phys.*, 3, 4529.

Heverly-Coulson, G.S.; R.J. Boyd (2011), Systematic study of the performance of density functional theory methods for prediction of energies and geometries of organoselenium compounds, *J. Phys. Chem. A*, 115, 4827-4831.

Hoffmann, T.; C.D. O'Dowd, J.H. Seinfeld (2001), Iodine oxide homogeneous nucleation: an explanation for coastal new particle production, *Geophys. Res. Lett.*, *28*(10), 1949-1952.

Howard, C.J. and K.M. Evenson (1976) Rate constants for reactions of OH with ethane and some halogen substituted ethanes at 296 K, *J. Chem. Phys.*, 64, 4303.

Huff, A.K. and J.P.D. Abbatt, (2000), Gas phase Br_2 production in heterogeneous reactions of Cl_2, HOCl, and BrCl with halide-ice surfaces, *J. Phys. Chem. A*, 104, 7284-7293.

Huff, A.K. and J.P.D. Abbatt, (2002), Kinetics and product yields in the heterogeneous reactions of HOBr with ice surfaces containing NaBr and NaCl, *J. Phys. Chem. A*, 106, 5279-5287.

Huskey, D.T. (2008), A temperature and pressure dependent kinetics study of the gas phase reactions of bromine and chlorine atoms with methylvinyl ketone, Thesis, Georgia Institute of Technology.

Hynes, A.J.; P.H. Wine, D.H. Semmes (1986), Kinetics and mechanism of hydroxyl reactions with organic sulfides, *J. Phys. Chem.*, *90*(17), 4148-4156.

Ingham, T.; M. Cameron, J.N. Crowley, (2000), Photodissociation of IO (355nm) and OIO (532nm): Quantum Yields for $O(^3P)$/I Production, *J. Phys. Chem. A*, 104, 8001-8010.

Ingham, T.; D. Bauer, R. Sander, P.J. Crutzen, J.N. Crowley (1999), Kinetics and products of the reactions BrO + DMS and Br + DMS at 298 K, *J. Phys. Chem. A*, *103*(36), 7199-7209.

Jacob, D.J. (1999), *Introduction to Atmospheric Chemistry*, Princeton University Press, Princeton.

Jammoul, A.; S. Dumas, B. D'Anna, C. George (2009), Photoinduced oxidation of sea salt halides by aromatic ketones: a source of halogenated radicals, *Atmos. Chem. Phys.*, *9*(13), 4229-4237.

Jefferson, A.; J.M. Nicovich, P.H. Wine (1994), Temperature-dependent kinetics studies of the reactions $Br(^2P_{3/2})$ + CH_3SCH_3 ↔ CH_3SCH_2 + HBr. Heat of formation of the CH_3SCH_2 radical, *J. Phys. Chem.*, *98*(29), 7128-7135.

Jobson, B.T.; H. Niki, Y. Yokouchi, J. Bottenheim, F. Hopper, R. Leaitch (1994), Measurements of C2-C6 hydrocarbons during the Polar Sunrise 1992 Experiment: evidence for Cl atom and Br atom chemistry, *J. Geophys. Res.*, *99*(D12), 25355-25368.

Johnson, R.O., G.P. Perram, and W.B. Roh. (1996), Spin-orbit relaxation kinetics of excited bromine atoms, *J. Chem. Phys.*, 104, 7052-7058.

Kagawa, M.; Y. Ishizaka, K. Ohta (2003), Sources of sulfate in winter aerosols over the Sea of Japan, as inferred from selenium composition, *Atmos. Environ.*, *37*(12), 1593-1600.

Keene, W.C., Stutz, Jochen; Pszenny, Alexander A. P.; Maben, John R.; Fischer, Emily V.; Smith, Allen M.; von Glasow, Roland; Pechtl, Susanne; Sive, Barkley C.; Varner, Ruth K. (2007), Inorganic chlorine and bromine in coastal New England air during summer, *J. Geophys. Res.*, *112*, D10S12, doi: 10.1029/2006jd007689.

Kinnison, D.J.; W. Mengon, J.A. Kerr (1996), Rate coefficients for the room temperature reaction of Cl atoms with dimethyl sulfide and related alkyl sulfides, *J. Chem. Soc.-Faraday Trans.*, *92*, 369.

Kirchner, U.; T. Benter, R.N. Schindler, (1997), Experimental verification of gas phase bromine enrichment in reactions of HOBr with sea salt doped ice surfaces, *Ber. Bunsenges. Phys. Chem.*, 101, 975-977.

Kleissas, K.M.; J.M. Nicovich, P.H. Wine (2007), Spectroscopy and kinetics of the gas phase addition complex of atomic chlorine with dimethyl sulfoxide, *J. Photochem. Photobiol. A: Chem.*, *187*(1), 1-9.

Knipping, E.M., and D. Dabdub (2003), Impact of chlorine emissions from sea-salt aerosol on coastal urban ozone, *Environ. Sci. Technol.*, *37*, 275-284.

Knipping, E.M.; M.J. Lakin, K.L. Foster, P. Jungwirth, D.J. Tobias, R.B. Gerber, D. Dabdub, B.J. Finlayson-Pitts (2000), Experiments and simulations of ion-enhanced interfacial chemistry on aqueous NaCl aerosols, *Science*, 288, 301-306.

Koch, W. and M.C. Holthausen (2000), *A Chemist's Guide to Density Functional Theory*, Wiley-VCH, Weinheim.

Kozlov, S. N.; V.L. Orkin, R.E. Huie, M.J. Kurylo (2003), OH reactivity and UV spectra of propane, n-propyl bromide, and isopropyl bromide, *J. Phys. Chem. A*, 107, 1333.

Laine, P.L.; J.M. Nicovich, P.H. Wine (2011a), Kinetic and Mechanistic Study of of the Reactions of Atomic Chlorine with CH_3CH_2Br, $CH_3CH_2CH_2Br$, and CH_2BrCH_2Br, *J. Phys. Chem. A*, 115, 1658-1666.

Laine, P.L.; Y.S. Sohn, J.M. Nicovich, M.L. McKee, P.H. Wine (2011b) Kinetics of Elementary steps in the reaction of atomic bromine with 2,3-dimethyl-2-butene under atmospheric conditions, *Int. J. Chem. Kinet.*, Published online for early viewing, DOI 10.1002/kin.20608.

Laine, P.L.; J. M. Nicovich, M.L. McKee, P.H. Wine (2011c) Manuscript in preparation.

Langer, S.; B.T. McGovney, B.J. Finlayson-Pitts, R.M. Moore (1996), The dimethyl sulfide reaction with atomic chlorine and its implications for the budget of methyl chloride, *Geophys. Res. Lett., 23,* 1661.

Laskin, A.; H. Wang, W.H. Robertson, J.P. Cowin, M.J. Ezell, B.J. Finlayson-Pitts (2006), A new approach to determining gas-particle reaction probabilities and application to the heterogeneous reaction of deliquesced sodium chloride particles with gas-phase hydroxyl radicals, *J. Phys. Chem. A,* 110, 10619-10627.

Law, K.S.; Sturges, W. T. (lead authors); Blake, D. R.; Blake, N. J.; Burkholder, J. B.; Butler, J. H.; Cox, R. A.; Haynes, P. H.; Ko, M. K. W.; Kreher, K.; Mari, C.; Pfeilsticker, K.; Plane, J. M. C.; Salawitch, R. J.; Schiller, C.; Sinnhuber, B.-M.; von Glasow, R.; Warwick, N. J.; Wuebbles, D. J.; Yvon-Lewis, S. A. (2006), Halogenated Very Short-Lived Substances. In Scientific Assessment of Ozone Depletion: 2006; Global Ozone Research and Monitoring Project-Report No. 50; World Meteorological Organization: Geneva, Switzerland, 2007; Chapter 2, 572.

Lawler, M.J.; B.D. Finley, W.C. Keene, A.A.P. Pszenny, K.A. Read, R. von Glasow, E.S. Saltzman (2009), Pollution-enhanced reactive chlorine chemistry in the eastern tropical Atlantic boundary layer, *Geophys. Res. Lett., 36,* L08810, doi: 08810.01029/02008GL036666.

Leu, M.-T. (1988a), Laboratory studies of sticking coefficients and heterogeneous reactions important in the Antarctic stratosphere, *Geophys. Res. Lett., 15*(1), 17-20.

Leu, M.-T. (1988b), Heterogeneous reactions of N_2O_5 with H_2O and HCl on ice surfaces: implications for Antarctic ozone depletion, *Geophys. Res. Lett., 15*(8), 851-854.

Liakakou, E.; M. Vrekoussis, B. Bonsang, C. Donousis, M. Kanakidou, N. Mihalopoulos (2007), Isoprene above the Eastern Mediterranean: Seasonal variation and contribution to the oxidation capacity of the atmosphere, *Atmos. Environ.* 41, 1002.

Liao, J.; H. Sihler, L.G. Huey, J.A. Neuman, D.J. Tanner, U. Friess, U. Platt, F.M. Flocke, J.J. Orlando, P.B. Shepson, H.J. Beine, A.J. Weinheimer, S.J. Sjostedt, J.B. Nowak, D.J. Knapp, R.M. Staebler, W. Zheng, R. Sander, S.R. Hall, K. Ullmann (2011a), A comparison of Arctic BrO measurements by chemical ionization mass spectrometry and long path-differential optical absorption spectroscopy, *J. Geophys. Res,* 116, D00R02, doi:10.1029/2010JD014788, 14pp.

Liao, J.; L.G. Huey, D.J. Tanner, F.M. Flocke, J.J. Orlando, J.A. Neuman, J.B. Nowak, A.J. Weinheimer, S.R. Hall, J.N. Smith, A. Fried, R.M. Staebler, Y. Wang, J.-H. Koo, C.A. Cantrell, P. Weibring, J. Walega, D.J. Knapp, P.B. Shepson, C.R. Stephens (2011b) Observed and modeled inorganic bromine (HOBr, BrO, and Br_2) speciation at Barrow, AK in spring 2009, *Submitted to J. Geophys. Res. in September 2011.*

Lias, S.G.; J.E. Bartmess, J.F. Liebman, J.L. Holmes, R.D. Levin, W.G. Mallard (1988) Gas-phase ion and neutral thermochemistry, *J. Phys. Chem. Ref. Data,* 17, 1-861.

Liss, P.S. (2007), Trace gas emissions from the marine biosphere, *Phil. Trans. Roy. Soc.* 365, 1697.

Lou, Y.R. (2007) Comprehensive Handbook of Chemical Bond Energies, CRC Press, New York.

Lurmann, F.W. and H.H. Main (1992), Analysis of the Ambient VOC data Collected in the Southern California Air Quality Study, Final Report, ARB Contract A832-130, California Air Resources Board, Sacramento, CA.

Luther, K. and J. Troe (1978), *Intl. Symp. Combust., [Proc.]*, 17th, 535.

Martinez-Aviles, M.; C.M. Rosado-Reyes, J.S. Fransisco (2007), Atmospheric oxidation mechanism of bromoethane, *J. Phys. Chem. A*, 111, 11652.

Martinez-Aviles, M.; C.M. Rosado-Reyes, J.S. Fransisco (2008a), Hydroxyl radical initiated oxidation mechanism of bromopropane, *J. Phys. Chem. A*, 112, 7930.

Martinez-Aviles, M.; S. Yang, J.S. Fransisco (2008b), Structure and vibrational spectra of bromine reservoir species from the atmospheric oxidations of bromoethane and bromopropane, *Mol. Phys*., 106, 299.

Matsumi, Y.; K. Izumi, V. Skorokhdov, M. Kawasaki, N.J. Tanaka (1997), Reaction and quenching of $Cl(^2P_j)$ atoms in collisions with methane and deuterated methanes, *J. Phys. Chem. A*, 101, 1216.

Maul, C.; T. Haas, K.H. Gericke, F.J. Comes (1995), Spin selectivity in the ultraviolet photodissociation of phosgene, *J. Chem. Phys.*, *102*(8), 3238-3247.

McConnell, J.C.; G.S. Henderson, L. Barrie., J. Bottenheim, H. Niki, C.H. Langford, E.M.J. Templeton, (1992), Photochemical bromine production implicated in Arctic boundary-layer ozone depletion, *Nature*, 355, 150-152.

McCullough, J.P.; W.N. Hubbard, F.R. Frow, I.A. Hossenlopp, G. Waddington (1957), Ethanethiol and 2-thiapropane: Heats of formation and isomerization; the chemical thermodynamic properties from 0 to 1000 K, *J. Am. Chem. Soc.*, 79, 561-566.

McElroy, M. B., R.J. Salawitch, S.C. Wofsy, J.A. Logan (1986), Reductions of Antarctic ozone due to synergistic interactions of chlorine and bromine, *Nature*, *321*(19), 759-762.

McEwen, D.J. (1966), Automobile exhaust hydrocarbon analysis by gas chromatography, *Anal. Chem.*, 38, 1047.

McKee, M. L. (1993), Computational study of addition and abstraction reactions between hydroxyl radical and dimethyl sulfide: a difficult case, *J. Phys. Chem.*, *97*(42), 10971-10976.

Meller, R.; D. Boglu, G.K. Moortgat (1991), Kinetics and Mechanisms for the Reactions of Halogenated Organic Compounds in the Troposphere. Proceedings of the STEP-HALOCSIDE/AFEAS Workshop, Dublin, Ireland, pp 110-115.

Molina, M.J., and F. S. Rowland (1974), Stratospheric sink for chlorofluoromethanes: chlorine atom catalysed destruction of ozone, *Nature, 249*, 810-812.

Molina, M.J., T.L. Tso, L.T. Molina, F.C.Y. Wang (1987), Antarctic stratospheric chemistry of chlorine nitrate, hydrogen chloride, and ice: release of active chlorine, *Science, 238*, 1253-1257.

Moore, R.M.; D.E. Oram, S.A. Penkett (1994), Production of isoprene by marine phytoplankton cultures, *Geophys. Res. Lett.*, 21, 23, 2507-2510.

Mosher, B.W. and R.A. Duce (1987), A global atmospheric selenium budget, *J. Geophys. Res., 92*(D11), 13289-13298.

Nakano, Y.; M. Goto, S. Hashimoto, M. Kawasaki, T.J. Wallington (2001), Cavity ring-down spectroscopic study of the reactions of Br atoms and BrO radicals with dimethyl sulfide, *J. Phys. Chem. A, 105*(49), 11045-11050.

Nelson Jr., D. D.; J.C. Wormhoudt, M.S. Zahniser, C.E. Kolb, M.K.W. Ko, D.K. Weisenstein (1997), OH reaction kinetics and atmospheric impacts of 1-bromopropane, *J. Phys. Chem. A*, 101, 4987.

Nicovich, J.M.; C.J. Shackelford, P.H. Wine (1990), Kinetics of the Br_2–CH_3CHO photochemical chain reaction, *J. Photochem. Photobiol. A: Chem., 51*, 141-153.

Nicovich, J.M.; C.A. van Dijk, K.D. Kreutter, P.H. Wine (1991), Kinetics of the reactions of alkyl radicals with HBr and DBr, *J. Phys. Chem.*, 95, 9890.

Nicovich, J.M.; K.D. Kreutter, C.A. van Dijk, P.H. Wine (1992), Temperature dependent kinetics studies of the reactions Br + H_2S reversible SH + HBr, and Br + CH_3SH reversible CH_3S + HBr-heats of formation of SH and CH_3S Radicals, *J. Phys. Chem.*, 96, 2518.

Nicovich, J.M.; K.D. Kreutter, P.H. Wine (1990), Kinetics and thermochemistry of ClCO formation from the Cl + CO association reaction, *J. Chem. Phys.*, 92, 3539.

Nicovich, J.M.; S. Wang, P.H. Wine (1995), Kinetics of the reactions of atomic chlorine with H_2S, D_2S, CH_3SH, and CD_3SD, *Int. J. Chem. Kinet., 27*, 359-368.

Nicovich, J.M., S.Wang, M.L. McKee, P.H. Wine (1996), Kinetics and thermochemistry of the $Cl(^2P_J)$ + C_2Cl_4 association reaction *J. Phys. Chem., 100*, 680-688.

Nicovich, J.M.; Parthasarathy, S.; Pope, F.D.; Pegus, A.T.; McKee, M.L.; Wine, P.H. (2006), Kinetics, mechanism, and thermochemistry of the gas phase reaction of atomic chlorine with dimethyl sulfoxide, *J. Phys. Chem. A, 110*, 6874-6885.

Nielsen, O.J.; H.W. Sidebottom, L. Nelson, O. Rattigan, J.J. Treacy, D.J. Ofarrell (1990) Rate constants for the reactions of OH radicals and chlorine atoms with diethyl sulfide, dipropyl sulfide, and dibutyl sulfide, *Int. J. Chem. Kinet.*, *22*, 603-612.

Notario, A.; G. Le Bras, A. Mellouki (1997), Kinetics of Cl atom reactions with butadienes including isoprene, *Chem. Phys. Lett.* 281, 421.

O'Dowd, C.D., J.L. Jimenez, R. Bahreini, R.C. Flagan, J.H. Seinfeld, K. Hameri, L. Pirjola, M. Kulmala, S.G. Jennings, T. Hoffman (2002), Marine aerosol formation from biogenic iodine emissions, *Nature*, *417*(6889), 632-636.

Orlando, J.J. (1999), Temperature dependence of the rate coefficients for the reaction of chlorine atoms with chloromethanes, *Int. J. Chem. Kinet.*, *31*, 515-524.

Orlando, J.J. and G.S. Tyndall (2002), Oxidation mechanisms for ethyl chloride and ethyl bromide under atmospheric conditions, *J. Phys. Chem. A*, 106, 312.

Orlando, J.J.; G.S. Tyndall, E.C. Apel, D.D. Reimer, S.E. Paulson (2003), Rate coefficients and mechanisms of the reaction of Cl-atoms with a series of unsaturated hydrocarbons under atmospheric conditions, 35, 334.

Orlando, J.J.; C.A. Piety, J.M. Nicovich, M.L. McKee, P.H. Wine (2005) Rates and mechanisms for the reactions of chlorine atoms with iodoethane and 2-iodopropane, *J. Phys. Chem. A*, 109, 6659-6675.

Park, M.S.; T.K. Kim, S.H. Lee, K.H. Jung, H.R. Volpp, J. Wolfrum (2001), Avoided curve crossing between the A1 and B1 states in CF_2Br_2 photolysis at 234 and 265 nm, *J. Phys. Chem. A*, 105, 5606-5612.

Pechtl, S.; E.R. Lovejoy, J.B. Burkholder, R. von Glasow (2006), Modeling the possible role of iodine oxides in atmospheric new particle formation, *Atmos. Chem. Phys.*, *6*, 505-523.

Pechtl, S. and R. von Glasow (2007), Reactive chlorine in the marine boundary layer in the outflow of polluted continental air: a model study, *Geophys. Res. Lett.*, *34*(11), 5.

Piety, C.A., R. Soller, J.M. Nicovich, M.L. McKee, P.H. Wine (1998), Kinetic and mechanistic study of the reaction of atomic chlorine with methyl bromide over an extended temperature range, *Chem. Phys.*, *231*, 155-169.

Pilling, M.J.; Seakins, P. W. Reaction Kinetics; Oxford University Press: New York, 2005; pp 198-200.

Platt, U. (1995) The chemistry of halogen compounds in the Arctic troposphere, in Tropospheric Oxidation Mechanisms, K.H. Becker ed., European Commission, Report EUR 16171 EN, Luxembourg, pp. 9-20.

Platt, U. and C. Janssen, (1995), Observation and role of the free radicals NO3, ClO, BrO, and IO in the troposphere, *Faraday Discuss.*, *100*, 175-198.

Platt, U. and E. Lehrer, (1996), Arctic tropospheric ozone chemistry, ARCTOC, Final report of the EU-Project No. EV5V-CT93-0318.

Platt, U.; G. Honninger (2003) The role of halogen species in the troposphere, *Chemosphere*, 32, 325-338.

Prinn, R.G., J. Huang, R.F. Weiss, D.M. Cunnold, P.J. Fraser, P.G. Simmonds, A. McCulloch, C. Harth, P. Salameh, S. O'Doherty, R.H.J. Wang, L. Porter, B.R. Miller (2001), Evidence for Substantial Variations of Atmospheric Hydroxyl Radicals in the Past Two Decades *Science*, *292*, 1882-1888.

Pszenny, A.A.P.; W.C. Keene, D.J. Jacob (1993), Evidence of inorganic chlorine gases other than hydrogen chloride in marine surface air, *Geophys. Res. Lett.*, *20*(8), 699-702.

Qiu, L.X.; S.H. Shi, S.B. Xing, X.G. Chen (1992), Rate constants for the reactions of hydroxyl with five halogen substituted ethanes from 292 to 366 K, *J. Phys. Chem.*, 96, 685.

Raff, J.D.; B. Njegic, W.L. Chang, M.S. Gordon, D. Dabdub, R.B. Gerber, B.J. Finlayson- Pitts (2009), Chlorine activation indoors and outdoors via surface mediated reactions of nitrogen oxides with hydrogen chloride, *Proc. Natl. Acad. Sci.* U.S.A., 106, 13639–13647.

Ragains, M.L. and B.J. Finlayson Pitts (1997), Kinetics and mechanism of the reaction of Cl atoms with 2-methyl-1,3-butadiene (isoprene) at 298 K, *J. Phys. Chem. A* 101, 1509.

Ramacher, B.; J.J. Orlando, G.S. Tyndall (2001), Temperature dependent rate coefficient measurements for the reaction of bromine atoms with trichloroethene, ethene, acetylene, and tetrachloroethene in air, *Int. J. Chem. Kinet.*, 33, 198.

Ramacher, B.; J. Rudolph, R.J. Koppmann, (1997), Hydrocarbon measurements in the spring arctic troposphere during the ARCTOC 95 campaign, *Tellus*., 49B, 607.

Rayman, M.P. (2000), The importance of selenium to human health, *Lancet*, *356*(9225), 233-241.

Read, K.A., A.C. Lewis, S. Baugitte, A.M. Rankin, R.A. Salmon, E.W. Wolff, A. Saiz-Lopez, W.J. Bloss, D.E. Heard, J.D. Lee, J.M.C. Plane (2008), DMS and MSA measurements in the Antarctic boundary layer: impact of BrO on MSA production, *Atmos. Chem. Phys.*, *8*(11), 2985-2997.

Reeser, D.I., A. Jammoul, D. Clifford, M. Brigante, B. D'Anna, C. George, D.J. Donaldson (2009), Photoenhanced reaction of ozone with chlorophyll at the seawater surface, *J. Phys. Chem. C*, *113*(6), 2071-2077.

Resende, S.M., and W. B. De Almeida (1997), Theoretical study of the atmospheric reaction between dimethyl sulfide and chlorine atoms, *J. Phys. Chem. A, 101*(50), 9738-9744.

Rosado-Reyes, C.M.; M. Martinez-Aviles, J.S. Francisco, In Advances in Quantum Chemistry; Goodsite, M. E., Johnson, M. S., Eds.; Elsevier: New York, 2008; Vol. 55, pp 215-244.

Ross, H.B. (1984), *Atmospheric selenium*, CM-66, Institute of Meteorology, Stockholm University.

Sander, S.P., J.P.D. Abbatt, J.R. Barker, J.B. Burkholder, R.R. Friedl, D.M. Golden, R.E. Huie, C.E. Kolb, M.J. Kurylo, G.K. Moortgat, V.L. Orkin and P.H. Wine, Chemical Kinetics and Photochemical Data for Use in Atmospheric Studies, Evaluation No. 17, JPL Publication 10-6, Jet Propulsion Laboratory, Pasadena, CA, 2011. http://jpldataeval.jpl.nasa.gov/.

Sauer, C.G., I. Barnes, K.H. Becker (1999), FT-TR kinetic and product study of the Br radical initiated oxidation of alpha, beta unsaturated organic carbonyl compounds, *Atmos. Environ., 33*, 2969.

Seinfeld, J.H., and S. N. Pandis (2006), *Atmospheric Chemistry and Physics: From Air Pollution to Climate Change*, Wiley, New York.

Singh, H.B. and J.F. Kasting (1988), Chlorine-hydrocarbon photochemistry in the marine troposphere and lower stratosphere, *J. Atmos. Chem.* 7, 261.

Singh, H.B., A.N. Thakur, Y.E. Chen, M. Kanakidou (1996), Tetrachloroethylene as an indicator of low Cl atom concentrations in the troposphere, *Geophys. Res. Lett., 23*(12), 1529-1532.

Singh, H.B., Y. Chen, A. Tabazadeh, Y. Fukui, I. Bey, R. Yantosca, D. Jacob, F. Arnold, K. Wohlfrom, E. Atlas, F. Flocke, K. Blake, N. Blake, B. Heikes, J. Snow, R. Talbot, G. Gregory, G. Sachse, S. Vay, Y. Kondo (2000), Distribution and fate of selected oxygenated organic species in the troposphere and lower stratosphere over the Atlantic, *J. Geophys. Res., 105*(D3), 3795-3805.

Singh, H.B., Y. Chen, A. Staudt, D. Jacob, D. Blake, B. Heikes, J. Snow (2001), Evidence from the Pacific troposphere for large global sources of oxygenated organic compounds, *Nature, 410*, 1078-1081.

Sinha, V.; J. Williams, M. Meyerhofer, U. Riebesell, A.I. Paulino, A. Larsen (2007), Air-sea fluxes of methanol, acetone, acetaldehyde, isoprene, and DMS from a Norwegian fjord following a phytoplankton bloom in a mesocosm experiment, *Atmos Chem. Phys.* 7, 739.

Simpson, W.R.; R. von Glasow, K. Riedel, P. Anderson, P. Ariya, J. Bottenheim, J. Burrows, L.J. Carpenter, U. Frieβ, M.E. Goodsite, D. Heard, M.Hutterli, H.-W. Jacobi, L.

Kaleschke, B. Neff, J. Plane, U. Platt, A. Richter, H. Roscoe, R. Sander, P. Shepson, J. Sodeau, A. Steffen, T. Wagner, E. Wolff, (2007), Halogens and their role in polar boundary-layer ozone depletion, *Atmos. Chem. Phys.*, 7, 4375-4418.

Solberg, S.; O. Hermansen, E. Joranger, S.F. Schmidbauer, O. Hov (1994), Tropical O_3 depletion in the Arctic during Spring measurements on the Zeppelin mountain on Spitsbergen, NILU Report OR 27/94: ISBN 82-425-0575-6.

Solomon, S., R.R. Garcia, F.S. Rowland, D.J. Wuebbles (1986), On the depletion of Antarctic ozone, *Nature, 321*(19), 755-758.

Solomon, S.; G.R. Rolando, A.R. Ravishankara (1994), On the role of iodine in ozone depletion, *J. Geophys. Res. [Atmospheres]*, 99(D10), 20491-20499.

Sotnichenko, S.A.; V.C. Bokun, A.I. Nadkhin (1988), Collisional quenching of chlorine ($^2P_{1/2}$) by H_2, D_2, CO, O_2, N_2 and CO_2, *Chem. Phys. Lett.*, *153*(6), 560-568.

Spicer, C.W.; E.G. Chapman, B.J. Finlayson-Pitts, R.A. Plastridge, J.M. Hubbe, J.D. Fast, C.M. Berkowitz (1998), Unexpectedly high concentrations of molecular chlorine in coastal air, *Nature, 394*, 353-356.

Spiro, P.A.; D.J. Jacob, J.A. Logan, (1992), Global inventory of sulfur emissions with 1 degrees-x1-degrees resolution, *J. Geophys. Res. Atoms.*, 97, D5, 6023-6036.

Stickel, R.E.; J.M. Nicovich, S. Wang, Z. Zhao, P.H. Wine (1992), Kinetic and mechanistic study of the reaction of atomic chlorine with dimethyl sulfide, *J. Phys. Chem.*, *96*, 9875-9883.

Sturges, W.T; G.F. Cota, P.T. Buckley, (1992), Bromoform emission from Arctic ice algae, *Nature, 358*, 660.

Sturges, W.T. and G.E. Shaw (1993a), Halogens in aerosols in central Alaska, *Atmos. Environ., 27A*, 2969.

Sturges, W.T.; R.C. Schnell, G.S. Dutton, S.R. Garcia, J.A. Lind (1993b), Spring measurements of tropospheric bromine at Barrow, Alaska, *Geophys. Res. Lett.*, 20, 201.

Stutz, J.; M.J. Ezell, A.A. Ezell, B.J. Finlayson-Pitts (1998), Rate constants and kinetic isotope effects in the reactions of atomic chlorine with n-butane and simple alkenes at room temperature, *J. Phys. Chem. A* 102, 8510.

Suh, I. and R. Zhang (2000), Kinetic studies of isoprene reactions initiated by chlorine atoms, *J. Phys. Chem. A* 104, 6590.

Tang, T. and J.C. McConnell (1996), Autocatalytic release of bromine from arctic snow pack during polar sunrise, *Geophys. Res. Lett., 23*, 2633-2636.

Teton, S.; A. El Boudali, A. Mellouki (1996), Rate constants for the reactions of OH radicals with 1- and 2-bromopropane, *J. Chim. Phys.*, 93, 274.

Thompson, K.C.; C.E. Canosa-Mas, R.P. Wayne (2002), Kinetics and mechanism of the reaction between atomic chlorine and dimethyl selenide; comparison with the reaction between atomic chlorine and dimethyl sulfide, *Phys. Chem. Chem. Phys.*, *4*, 4133-4139.

Thornton, J.A.; J.P. Kercher, T.P. Riedel, N.L. Wagner, J. Cozic, J.S. Holloway, W.P. Dube, G.M. Wolfe, P.K. Quinn, A.M. Middlebrook, B. Alexander, S.S. Brown (2010), A large atomic chlorine source inferred from mid-continental reactive nitrogen chemistry, *Nature*, 464, 271.

Tolbert, M.A., M.J. Rossi, R. Malhotra, D.M. Golden (1987), Reaction of chlorine nitrate with hydrogen chloride and water at Antarctic stratospheric temperatures, *Science*, *238*, 1258-1260.

Tolbert, M.A., M.J. Rossi, D.M. Golden (1988a), Antarctic ozone depletion chemistry: reactions of N_2O_5 with H_2O and HCl on ice surfaces, *Science*, *240*, 1018-1021.

Tolbert, M.A., M.J. Rossi, D.M. Golden (1988b), Heterogeneous interactions of chlorine nitrate, hydrogen chloride, and nitric acid with sulfuric acid surfaces at stratospheric temperatures, *Geophys. Res. Lett.*, *15*(8), 847-850.

Troe, J., (1979), Predictive possibilities of unimolecular rate theory, *J. Phys. Chem.*, 83, 114-126.

Troe, J., (1983), Theory of thermal unimolecular reactions in the fall-off range. 1. Strong collision rate constants, *Ber. Bunsenges. Phys. Chem.*, 87, 161-169.

Tuazon, E.C.; R.M. Rael, W.T. Frankenberger Jr. (1996), Gas phase reactions of dimethyl selenide with ozone and the hydroxyl and nitrate radicals, *Atmos. Environ.* 30, 1221-1232.

Turner, S.M. and P.S. Liss, (1985), Measurements of various sulfur gases in a coastal marine environment, *J. Atmos. Chem.*, 2, 3, 223-232.

Tyndall, G.S. and A. R. Ravishankara (1989), Kinetics and mechanism of the reactions of CH_3S with O_2 and NO_2 at 298 K, *J. Phys. Chem.*, *93*, 2426-2435.

Tyndall, G.S.; J.J. Orlando, C.S. Kegleyowen (1995), Rate coefficients for quenching of $Cl(^2P_{1/2})$ by various atmospheric gases, *J. Chem. Soc. Faraday Trans.*, *91*, 3055-3061.

Tyndall, G.S., J.J. Orlando, T.J. Wallington, M. Dill, E.W. Kaiser (1997), Kinetics and mechanisms of the reactions of chlorine atoms with ethane, propane, and *n*-butane, *Int. J. Chem. Kinet.*, *29*, 43-55.

Urbanski, S.P. and P. H. Wine (1999), Spectroscopic and kinetic study of the $Cl–S(CH_3)_2$ adduct, *J. Phys. Chem. A*, *103*(50), 10935-10944.

Uthman, A.P.; P.J. Demlein, T.D. Allston, M.C. Withiam, M.J. McClements, G.A. Takacs (1978), Photoabsorption spectra of gaseous methyl bromide, ethylene dibromide, nitrosyl bromide, thionyl chloride, and sulfuryl chloride, *J. Phys. Chem.*, 82, 2252.

Vogt, R.; P.J. Crutzen, R. Sander, (1996), A mechanism for halogen release from sea-salt aerosol in the remote marine boundary layer, *Nature*, *383*, 327-330.

Voronkov, M.G.; V.A. Klyuchnikov, S.N. Kolabin, G.N. Shvets, P.I. Varusin, E.N. Deryagina, N.A. Korchevin, S.I. Tsvetnitskaya (1989), Thermochemical properties of diorganyl chalcogenides and dichalcogenides RM_nR(M = S, Se, Te; n = 1,2)., *Dokl. Phys. Chem. (Engl. Transl.)*, 307, 650-653.

Wen, H. and J. Carignan (2007), Reviews on atmospheric selenium: emissions, speciation and fate, *Atmos. Environ.*, *41*, 7151-7165.

Wennberg, P. (1999) Bromine explosion, *Nature*, 397, 299-301.

Wilber, C.G. (1980), Toxicology of selenium: a review, *Clin. Toxicol.*, *17*, 171-230.

Wilson, C. and D. M. Hirst (1997), Ab initio study of the reaction of chlorine atoms with H_2S, CH_3SH, CH_3SCH_3 and CS_2, *J. Chem. Soc. Faraday Trans.*, *93*, 2831-2837.

Wine, P.H., et al. (1993), The tropospheric chemistry of ozone in the polar regions, in *NATO ASI Series, Series I: Global Environmental Change Vol. 7*, edited by H. Niki and K. H. Becker, pp. 385-395.

Wine, P.H.; J.M. Nicovich (2012), Atmospheric radical chemistry, in *Encyclopedia of Radicals in Chemistry, Biology, and materials*, Ed. by Chryssostomos Chatgilialoglu and Armido Studer, John Wiley & Sons, Ltd. ISBN: 978-0-470-97125-3.

Wingenter, Oliver W.; Kubo, Michael K.; Blake, Nicola J.; Smith, Tyrrel, W., Jr.; Blake, Donald R.; Rowland, F. Sherwood. (1996), Hydrocarbon and halocarbon measurements as photochemical and dynamical indicators of atmospheric hydroxyl, atomic chlorine, and vertical mixing obtained during Lagrangian flights, *J. Geophys. Res.*, *101*(D2), 4331-4340.

Wingenter, Oliver W.; Sive, Barkley C.; Blake, Nicola J.; Blake, Donald R.; Rowland, F. Sherwood. (2005), Atomic chlorine concentrations derived from ethane and hydroxyl measurements over the equatorial Pacific Ocean: implication for dimethyl sulfide and bromine monoxide., *J. Geophys. Res.*, *110*, D20308, doi: 20310.21029/22005JD005875.

WMO (World Meteorological Organization) (2007), *Scientific Assessment of Ozone Depletion: 2007, Global Ozone Research and Monitoring Project – Report No. 50*, Geneva, Switzerland.

WMO (World Meteorological Organization) (2010), *Scientific Assessment of Ozone Depletion: 2010, Global Ozone Research and Monitoring Project – Report No. 52*, Geneva, Switzerland, 2011.

Wolfsy, S.C., M.B. Mcelroy, Y.L. Yung (1975), Chemistry of atmospheric bromine, *Geophys. Res. Lett.*, *2*(6), 215-218.

Wuebbles, D.J.; A.K. Jain, K.O. Patten (1998), Evaluation of ozone depletion potentials for chlorobromomethane and 1-bromopropane, *Atmos. Environ.*, 32, 107.

Xing, S.; S. Shi, L. Qiu (1992), Kinetics studies of reactions of OH radicals with four haloethanes part I. Experiment and BEBO calculation, *Int. J. Chem. Kinet.*,, 24, 1.

Xing, J.H., K. Takahashi, M.D. Hurley, T.J. Wallington (2009), Kinetics of the reaction of chlorine atoms with isoprene at 297 ± 2 K, *Chem. Phys. Lett.*, 472, 39-43.

Yang, X., R.A. Cox, N.J. Warwick, J.A. Pyle, G.D. Carver, F.M. O'Connor, N.H. Savage (2005), Tropospheric bromine chemistry and its impacts on ozone: a model study, *J. Geophys. Res. Atmos.*, *110*, D23311, 18 PP., doi: 23310.21029/22005JD006244.

Yung, Y.L., J.P. Pinto, R.T. Watson, S.P. Sander (1980), Atmospheric bromine and ozone perturbations in the lower stratosphere, *J. Atmos. Sci.*, *37*(2), 339-353.

Zhang, L.; W. Fuss, K.L. Kompa (1990), Bond selective photodissociation of CBr, CI in $BrC_2H_4C_2F_4Br$, $IC_2H_4C_2F_4I$, *Chem. Phys.* 1990, 144, 289.

Zhao, Z., R.E. Stickel, P.H. Wine (1996), Branching ratios for methyl elimination in the reactions of OD radicals and Cl atoms with CH_3SCH_3, *Chem. Phys. Lett.*, *251*, 59-66.

Zeng, T. (2005), Three-dimensional model analysis of tropospheric photochemicalprocesses in the Arctic and northern mid-latitudes, Ph.D. Thesis, Georgia Inst. of Technol., Atlanta, Ga.